BOND STRENGTH OF ASTM A615 GRADE 100 REINFORCEMENT FOR BEAMS

by

Rebecca Glucksman

A Thesis

Submitted to the Faculty of Purdue University

In Partial Fulfillment of the Requirements for the degree of

Master of Science in Civil Engineering

Lyles School of Civil Engineering

West Lafayette, Indiana

December 2018

THE PURDUE UNIVERSITY GRADUATE SCHOOL
STATEMENT OF COMMITTEE APPROVAL

Dr. Robert Frosch, Chair
Lyles School of Civil Engineering
Dr. Santiago Pujol
Lyles School of Civil Engineering
Dr. Christopher Williams
Lyles School of Civil Engineering

Approved by:

Dr. Dulcy Abraham
Head of the Graduate Program

To Franklin

ACKNOWLEDGMENTS

I would like to start off by thanking my advisor, Dr. Robert Frosch, for his support throughout this journey. His attention to detail and support throughout the process encouraged me to produce my best work and develop into a better engineer. Under his guidance, I gained invaluable knowledge that I will be able to carry through the rest of my career. I would also like to thank Dr. Christopher Williams and Dr. Santiago Pujol for serving on my thesis committee. Their thoughtful advice helped to not only strengthen this work, but my technical writing skills.

This study was sponsored by the Charles Pankow Foundation with materials generously donated from Harris Rebar, Nucor Steel, and Dayton Superior. Without their financial support and resources, I would have never had the opportunity to learn so much from my work on this project. Their contributions are greatly appreciated.

I am grateful for the support provided by the Bowen Laboratory staff members: Harry Tidrick, Kevin Brower, and Molly Stetler. Without them, completing my thesis would not be possible. I would also like to thank all my colleagues who helped with advice or manual labor. Without you, I would have never been able to complete my project. You all have been a truly invaluable resource.

Finally, I would never have been able to come this far without the support of my parents or my boyfriend, Danny White. Thank you for always believing in me and providing words of encouragement.

TABLE OF CONTENTS

LIST OF TABLES

LIST OF FIGURES

ABSTRACT

Author: Glucksman, Rebecca, L. MSCE
Institution: Purdue University
Degree Received: December 2018
Title: Bond Strength of ASTM A615 Grade 100 Reinforcement for Beams
Major Professor: Robert Frosch

In the past decade, high-strength reinforcement (f_y > 60 ksi) has become more prevalent and more widely accepted. Building codes such as ACI 318-14 do not address the use of high-strength reinforcement for proper development and splicing of reinforcement. Furthermore, research on development of high-strength reinforcement is limited. The objective of the study is to develop a suitable expression for the development and splicing of high-strength reinforcement. Of particular interest is evaluating the influence of splice length and confinement on bond strength as well as evaluating the effectiveness of high-strength transverse reinforcement on bond strength. The study tested 22 large-scale concrete beams reinforced with ASTM A615 Grade 100 deformed steel bars: 11 specimens without transverse reinforcement within the splice region (unconfined) and 11 specimens with transverse reinforcement within the splice region (confined). Splice lengths varied from 40 bar diameters to 120 bar diameters, which are some of the largest ever tested. The effect of the test variables which were systematically studied, found that splice strength is nonlinearly related with splice length and can be represented by a power equation. Furthermore, it was found that high-strength transverse reinforcement does not improve bond strength compared with the use of Grade 60 transverse reinforcement. Considering the test results and review of historical test results, an analytical investigation was conducted which developed a simple expression for estimating the capacity of both unconfined and confined beams. The results are compared with the current building code design expressions as well as other proposed bond strength equations. The research conducted here provides the basis for development of a design expression that will allow for the incorporation of high-strength reinforcement in future building codes.

1. INTRODUCTION

1.1 History of High-Strength Reinforcement

In the past decade, high-strength reinforcement (f_y > 60 ksi) has become more prevalent and widely accepted. Building codes such as ACI 318-14 (ACI Committee 318 2014) lack adequate guidance for the use of high-strength reinforcement. In 2004, ASTM A1035 was developed and addressed the use of Grade 100 bars. Grade 120 bars were added in 2007. In 2009, ASTM A615 was expanded to include provisions for Grade 80 reinforcement. Because of increasing use, in 2014, the Applied Technology Council (ATC) developed a "roadmap" for the adoption of high-strength reinforcement (ATC 115). With the expansion of these standards, high-strength reinforcement is becoming more readily available and used. Additionally, Grade 100 reinforcing bars have been approved for use in column reinforcement by the New York City Department of Buildings (ATC 2014).

1.2 Advantages of High-Strength Reinforcement

The use of Grade 80, Grade 100, and Grade 120 reinforcement is being considered specifically for gravity, wind, and seismic loading (ATC 2014). The benefits of using high-strength reinforcement include reducing congestion within members, allowing better consolidation, and speeding up construction time (ATC 2014).

Because of the cost premium associated with high-strength reinforcement, there is a need for an overall reduction in the volume of reinforcement to allow for overall project savings. As a result, cost effectiveness of high-strength reinforcement is dependent on minimum spacing, minimum reinforcement ratios, and other detailing requirements specified in ACI 318 (ATC 2014). Although longer splice lengths may be required, using less reinforcement at larger spacings means that construction and cost efficiencies are achieved through lower placement costs, less congestion, and better consolidation of the concrete during placement. According to a cost study reported in the National Institute for Standards and Technology GCR 14-917-30 (NIST 2014), it was determined that cost savings associated with the substitution of Grade 80 reinforcement for Grade 60 reinforcement was approximately 4% of the cost of the concrete structure (ATC 2014).

1.3 Bar Development

In reinforced concrete structures, bars must be properly developed to take advantage of their strengths and to avoid (brittle) bond failures. Stresses must be transferred from the steel reinforcement to the surrounding concrete to ensure a safe design. Stress is transferred between the steel bars and concrete by three mechanisms: chemical adhesion, friction, and mechanical interlock (Tepfers 1973). Stresses are first transferred through chemical adhesion. As the bar slips, surface adhesion is lost, and force is transferred through friction arising from roughness of the concrete interface and bearing against bar deformations. After initial slip of the bar, most of the force is transferred by bearing of the reinforcement ribs against the concrete (ACI Committee 408 2003, Orangun et al. 1977). Friction also transfers force as demonstrated by the lower bond capacities of bars with no deformations and bars with epoxy coatings, which have lower coefficients of friction (ACI Committee 408 2003). These friction and bearing forces are balanced by compressive and shear stresses in the surrounding concrete (Tepfers 1973). The compressive stresses in the surrounding concrete serve to tighten the concrete around the reinforcing bar, thus increasing frictional resistance. Tensile forces are also caused by the inclined force exerted by the bar deformation on the concrete. The radial component of this force causes splitting of the surrounding concrete at failure (Tepfers 1973). The forces acting on the reinforcing bar and concrete are shown in Figure 1.1.

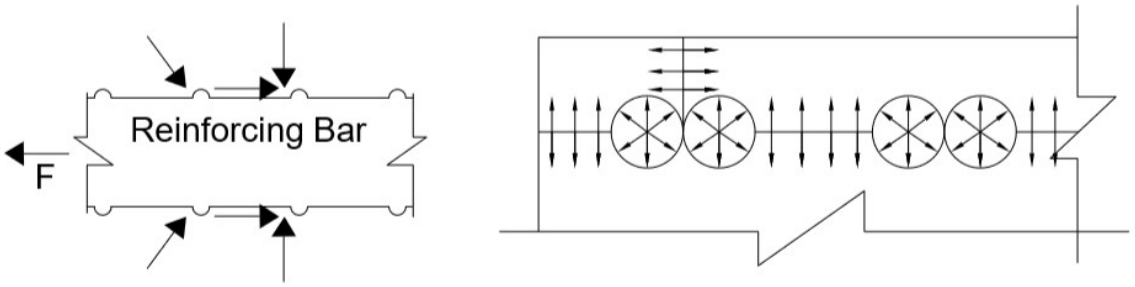

a) Compressive Forces on Longitudinal Bar **b) Tensile Forces on Concrete**

Figure 1.1: Forces Acting on Reinforcement and Concrete

The capacity of the concrete to resist splitting is dependent on the tensile strength of the concrete (Orangun et al. 1977). If concrete cover and spacing between bars is small, splitting cracks can eventually cause a splitting failure (Tepfers 1973).

1.4 Nonuniform Bond Stress

Although it is more convenient to treat bond stress as if it were uniform over the splice length (ACI Committee 408 2003), bond stresses over the development length are not uniform (Kluge and Tuma 1945). Axial tensile stress in the reinforcement varies from high values at cracks to lower values between cracks where the concrete shares the tensile resistance with the reinforcing steel. While assuming a linear relationship of bar force development is conservative for shorter splice lengths, the assumption becomes unconservative with increasing splice length (ACI Committee 408 2003).

Failures start at the end of the splice where there is the highest bond force per unit length (ACI Committee 408 2003) and the strain is the largest. As the relative deformation capacity between the reinforcing bar and concrete exceeds the deformation corresponding to the peak bond strength, local bond damage occurs, which causes the bond stress to decrease (Hwang & Yi 2017). The use of transverse reinforcement has been shown to reduce the variation of stress along splices (Ferguson & Krishnaswamy 1971).

1.5 Factors Influencing Bond Behavior

The different variables that impact bond behavior are described in the following sections.

1.5.1 Casting Position

Top casting, defined in ACI 318-14 as placing more than 12 in. of fresh concrete below the bars, has been shown to reduce bond strength by 3-8% (Chinn, Ferguson, & Thompson 1955). This phenomenon is likely because of bleeding and settlement of the concrete below the bars (Zuo & Darwin 1998). The larger the depth of concrete below the bar, the larger the settlement and accumulation of bleed water. As the concrete settles, it leaves a void beneath the rigid reinforcing bars. The effects of settlement and bleeding on bond strength are magnified by a higher concrete slump and decreased top cover. Good vibration of the concrete helps to combat the effects of settlement and bleeding by restoring uniformity within the concrete and removing trapped air (ACI Committee 408 2003).

1.5.2 Bar Size

According to Mathey and Watstein (1961), bond strength has been shown to decrease with an increase in bar diameter for a consistent splice length to bar diameter (l_s/d_b) ratio. For specimens with comparable l_s/d_b and cover in terms of bar diameter, #3 bars showed a 19% increase in bond strength compared with the #6 bars, while the #11 bars showed a 16% decrease in bond strength (Chinn et al. 1955).

1.5.3 Splice Length

Although splice strength increases with increasing splice length, the effectiveness of increasing the splice length decreases as the length increases. Mathey and Watstein (1961) have shown that the unit bond strength decreases with increasing splice length for a bar of a given size. Canbay and Frosch (2005) have found the influence of a steel splice length to be proportional to the square root. Therefore, doubling the splice length from 18 to 36 in. results in a 41% increase in bar stress. Studies conducted by Chinn et al. (1955) show that compared with an 11-in. splice length of #6 bars, a 16-in. splice length (45% increase) was 19-28% stronger, while a 24-in. splice length (118% increase) was 60-80% stronger.

1.5.4 Concrete Strength

The tensile and bearing strength of the concrete impacts the bond strength (ACI Committee 408 2003). The currently accepted relationship between concrete and bond strength is represented by the square root of the concrete compressive strength (Ferguson and Thompson 1962). Esfahani and Rangan (1998) observed that the extent of crushing in front of the ribs, and thus the bond strength, was dependent on the concrete strength. In specimens with normal strength concrete, concrete crushing occurred regardless of the size of the concrete cover. For 7250 psi concrete, concrete crushing only occurred for large covers, and for 10,880 psi concrete, no concrete crushing occurred. Because of the reduced crushing in high-strength concrete, local slip was reduced (Zuo & Darwin 1998). When crushing occurred in front of the ribs, fewer ribs participated in resisting the applied forces in the bars. When crushing around the bar

deformations was coupled with a smaller concrete cover, the result was a splitting failure in concrete prior to achieving a uniform bond stress distribution (Zuo & Darwin 1998).

Additionally, increasing the coarse aggregate content increased the splice strength. For specimens without transverse reinforcement within the splice length, increasing the coarse aggregate content produced a higher splice strength characterized by $f_c'^{0.25}$. Likewise, for specimens with transverse reinforcement within the splice length, increasing the coarse aggregate content produced a higher splice strength characterized by $f_c'^{0.75}$ (Zuo & Darwin 1998).

1.5.5 Concrete Cover and Bar Spacing

Concrete cover and bar spacing determine the type of bond failure and influence bond behavior of the specimen. Chamberlin (1956) and Orangun et al. (1977) found that increasing the side cover (c_{so}) or clear spacing ($2c_{si}$) also increased splice strength. Thompson et al. (1975) found that increasing the ratio of clear cover to clear spacing ($c_{so}/2c_{si}$) could provide a 10% increase in splice strength.

In experiments conducted by Chinn et al. (1955), doubling the cover from 0.75 in. to 1.50 in. increased the strength of shorter splices by 7-15%. Chinn et al. (1955) found that increasing the concrete cover increased the splice strength, but only for shorter splices. The same trend between concrete cover and splice strength was also observed for both uncoated black bars and epoxy-coated bars (Hadje-Ghaffari et al. 1994).

1.5.6 Transverse Reinforcement (Confinement)

The use of transverse reinforcement has been shown to increase splice strength (Chinn et al. 1955). Transverse reinforcement has also been found to cause a more ductile failure than comparable unconfined specimens (Ferguson & Krishnaswamy 1971). The use of transverse reinforcement allows larger deformations of the longitudinal reinforcement prior to failure by minimizing the distress caused by concrete splitting (Zekany, Neumann, Jirsa, & Breen 1981). Transverse reinforcement adds to bond strength by resisting tension where the concrete has split

(Ferguson & Krishnaswamy 1971) and decreasing the effective crack length between bars (ACI Committee 408 2003). In this way, the transverse reinforcement helps to slow the spread of splitting (Ferguson & Krishnaswamy 1971). Transverse reinforcement has been shown to be more effective for larger bars as larger bars induce higher strains and stresses when they slip (ACI Committee 408 2003). The use of transverse reinforcement in MMFX specimens (ASTM A1035) allowed the failure stresses in #8 and #11 bars to increase to an average of 150 ksi (Seliem et al. 2007), enabling the full capability of the high-strength reinforcement to be utilized (Seliem et al. 2007).

Thompson et al. (1975) corroborated that transverse reinforcement resists tension by noticing an increase in strain in the transverse reinforcement after cracking of concrete in the plane of the splice. It was also observed that strain in the transverse reinforcement increased before failure of the specimen. Additionally, the strain in the stirrups located closest to the ends of the splice seemed to have the highest strains (Thompson et al. 1975). In fact, tests conducted by Azizinamini et al. (1999) showed that the strain in stirrups located at the ends of splices can reach their yield strength. Sim (2014) made a similar observation that transverse reinforcement located closest to the ends of the splice proved to be the most effective.

1.5.7 Relative Rib Area

The relative rib area, R_r, for ribbed steel reinforcing bars is calculated using the expression specified in ACI 408R-03 Section 6.6 (Equation 1-1). Figure 1.2 shows the variables used to calculate R_r.

$$R_r = \left(\frac{h_r}{s_r}\right)\left(1 - \frac{\sum gaps}{p}\right) \qquad (1\text{-}1)$$

$$where\ h_r = \frac{\frac{a_1 + a_5}{2} + a_2 + a_3 + a_4}{4}$$

where:

$\sum gaps$ = *sum of gaps between ends of transverse deformations, plus the width of any continuous longitudinal lines used to represent the grade of the bar multiplied by the ratio of the height of the line, h_r, in.*

h_r = *average height of deformations (ACI 408R-03 Section 6.6.1), in.*

p = *nominal perimeter of bar, in.*

s_r = *average spacing of deformations, in.*

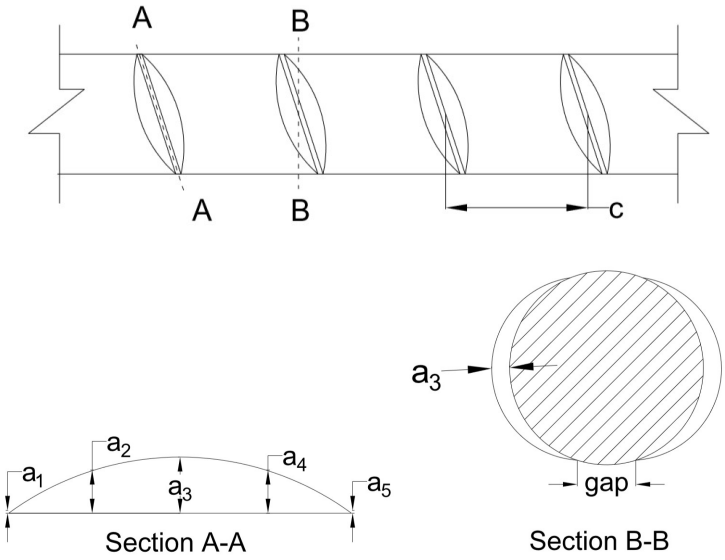

Figure 1.2: Relative Rib Area Calculation

Zuo and Darwin (1998) found that splice strength is not affected by the relative rib area, R_r, for bars not confined by transverse reinforcement. For splices confined by transverse reinforcement, results show an increase in splice strength with an increase in bar size and R_r (Zuo & Darwin 1998).

1.6 Failure Modes

Bond failures can occur in two ways: bar pullout or concrete splitting. A splitting failure occurs if the concrete cover and/or spacing of the bars are small enough for a splitting plane to develop (Tepfers 1993). If the concrete cover, bar spacing, and transverse reinforcement are sufficient, but the development length is not, the specimen will fail in a pullout mode. A pullout failure

occurs when concrete splitting is prevented, but the splice length is inadequate to develop the forces.

Splitting failures occur in three ways: side splitting, face splitting, and face and side splitting. According to Tepfers (1973), splitting failures depend on whether the bottom clear cover, c_b, is smaller than either the concrete side cover, c_{so}, or ½ of the bar clear spacing, c_{si} (Figure 1.3). If c_{so} or c_{si} is smaller than c_b, the splitting crack forms through the side cover or between the reinforcing bars (side splitting, as shown in Figure 1.3(a)). If c_b is smaller than c_{so} and c_{si}, the splitting crack occurs through the cover to the tension face (face splitting, as shown in Figure 1.3(b)). Cracks initiate at the end of the splice, where the bond stress is the highest, and propagate towards the center.

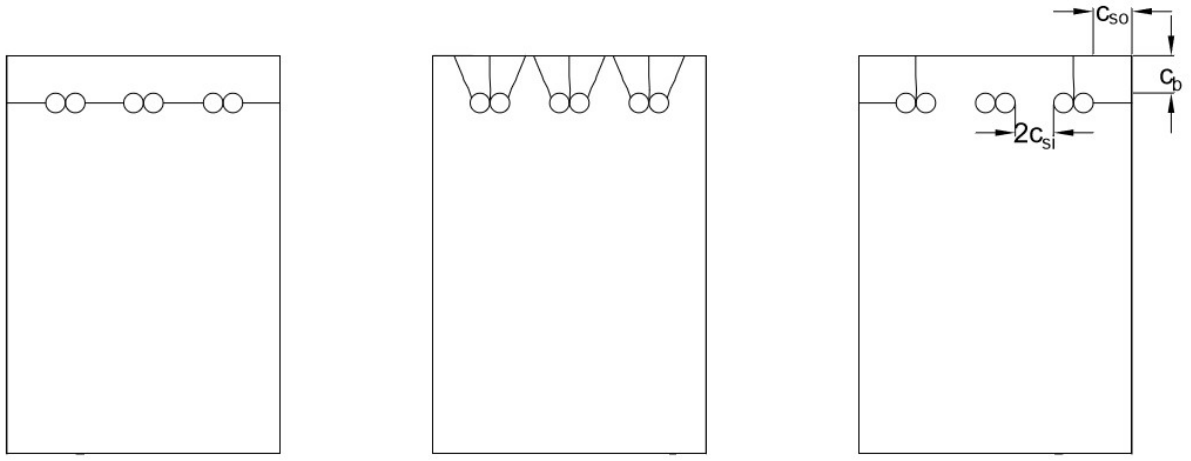

a) Side Splitting **b) Face Splitting** **c) Face and Side Splitting**

Figure 1.3: Splitting Cracks

For face and side splitting (Figure 1.3(c)), initial splitting occurs in the clear cover over the splices on the sides. If the distances between the reinforcing bars are large, and the concrete side cover is smaller than the bottom cover, the side cover will longitudinally crack. When the ultimate tensile stress of the concrete is reached, a block of concrete bordering the edge lap splices will spall off due to the failure of the bottom cover (Tepfers 1973).

1.7 Past High-Strength Reinforcement Research

Limited splice tests have been conducted using high strength reinforcement, and these tests used ASTM A1035 (MMFX) rather than ASTM A615. The two materials have similar stress-strain curves, but the shape of the post-yield response is different. Past research has been conducted comparing the splice strength of MMFX bars to conventional Grade 60 bars and determining the reliability of the current code equations. Ansley (2002) first evaluated this reinforcement and tested four pairs of beam-splice specimens to compare the impact of replacing Grade 60 reinforcement with MMFX. He warned of "blind substitution" of MMFX for Grade 60 because although the strength of the beam was increased, the ductility of the beam was inadequate. Ansley also concluded that the use of reinforcing bars, like MMFX, without a well-defined yield point needs to be addressed before adoption. In 2006, El-Hacha et al. (2006) tested eight beam-splice specimens reinforced with MMFX. He found that the bond behavior of Grade 60 specimens and MMFX specimens was similar up to the proportional limit of 80 ksi, however, at higher stress levels, the bond strength of MMFX changes. El-Hacha et al. (2006) also concluded that the ACI 318-02 equation was unconservative for use with MMFX. Extensive research was conducted at the University of Kansas, North Carolina State University, and the University of Texas at Austin. Sixty-nine beam-splice specimens were tested, of which 64 specimens failed in bond (Briggs 2008). Based on their tests, they also concluded that ACI 318-05 is unconservative and recommended a high-strength reinforcement factor of 1.48 to be used with bar stresses above 80 ksi, however, they concluded that ACI 408R-03, with φ=0.82, is safe for use with high-strength reinforcement. They also recommended the use of confining transverse reinforcement as it increased the splice strength and beam deformation capacity. Currently, high-strength reinforcement splice tests have been conducted using specimens with splice lengths ranging from 10 to 91 in. Of the tests, only confined specimens failed in flexure. Additionally, all the unconfined specimens failed in bond before yield, except for one of El-Hacha's specimens which failed at the yield stress calculated from the 0.2% offset method. Although limited research has been conducted on the splice strength of high-strength reinforcement, no known splice research has been conducted using ASTM A615 Grade 100 bars.

1.8 Objective and Scope

Research evaluating the development length of high-strength reinforcement (f_y > 60 ksi) is limited. Therefore, the objective of this research program is to assist in the development of an analysis expression for the development and splicing of high-strength reinforcement. Research is focused on the following:

- Evaluating the influence of splice length on bond strength
- Evaluating the influence of transverse reinforcement on bond strength
- Evaluating the effectiveness of high-strength (100 ksi) transverse reinforcement on bond strength

2. EXPERIMENTAL PROGRAM

2.1 Introduction

Twenty-two beams with tension lap splices were tested to evaluate the effect of splice length, transverse reinforcement, and bar spacing on bond strength. The beams were constructed in four series.

2.2 Specimen Design

The specimens were designed to investigate the bond behavior of high-strength steel reinforced concrete beams. Grade 100 longitudinal bars were used for all specimens. Each of the specimens was designed to fail in bond when tested in four-point bending. The concrete strength targeted for these specimens was 5,000 psi.

All specimens were rectangular in cross section with a height of 20 in. Three #8 Grade 100 longitudinal bars were spliced at midspan, in a region of constant moment. Cross sectional details for both unconfined and confined specimens are shown in Figure 2.1. Unconfined specimens are defined as having no transverse reinforcement in the splice region, while confined specimens are defined as having transverse reinforcement in the splice region. Confinement configurations and splice lengths were varied to determine the effect of these variables on the capacity of the splice.

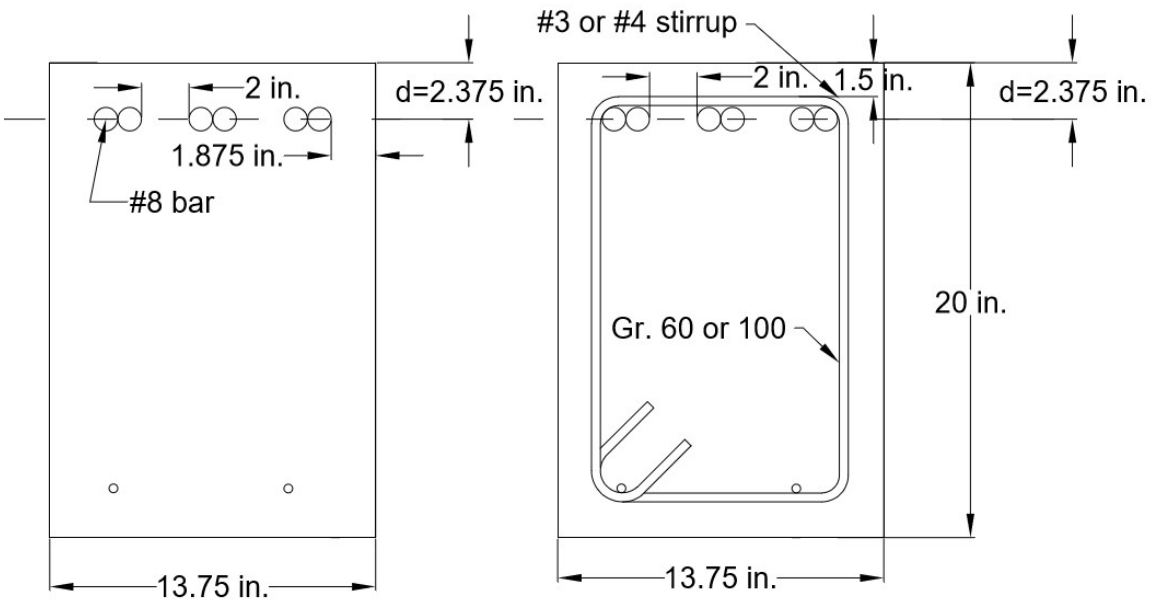

Figure 2.1: Typical Cross Section

The specimens with transverse reinforcement had a cover of 1-$^1/_2$ in. (the minimum cover specified by ACI 318-14 for beams). To keep the effective depth the same for all specimens, the cover for specimens without transverse reinforcement was designed to be 1-$^7/_8$ in. It is important to keep the effective depth constant to eliminate the effect of this variable from the study.

Nineteen out of 22 specimens had a 2-in. clear spacing between longitudinal bars. This resulted in the confined specimens, with a minimum clear side cover of 1-$^1/_2$ in., having an overall beam width of 13-$^3/_4$ in. The confined and unconfined specimens were designed to have the same width. The 2-in. clear spacing between longitudinal bars was selected as it represented a lower bound dimension for a typical beam design. Three specimens had 1-in. clear spacing between longitudinal bars. The 1-in. clear spacing is the minimum clear spacing specified in ACI 318-14 Section 25.2. The specimens with a 1-in. spacing represent the worst-case scenario for bar spacing. As-built dimensions are provided in Appendix A.

Confined specimens were designed with varied spacings, grades, and sizes of transverse reinforcement in the splice region. Both #3 and #4 stirrups were used, however, the width of the

specimen and effective depth remained the same. Additionally, both Grade 60 and Grade 100 stirrups were used to understand the influence of transverse reinforcement yield strength.

The length of the beam was controlled by two factors: the longest splice length to be tested and the spacing of tie-down holes in the Bowen Laboratory strong floor. The longest splice length was selected as 120 in. According to St. Venant's principle, stresses because of bending, approach a linear distribution at a distance equal to the overall height of the specimen. To be conservative, the supports were placed at least 1.5 times the overall height of the specimen away from the end of the 120 in. splice. This distance was rounded to 36 in. so that the loading points would line up with the holes in the strong floor. Although the length of the splice varied from specimen to specimen, the length of the beam was maintained constant for all specimens so that the same test setup could be used, as well as to allow for a direct comparison between results.

The specimens were tested in four-point bending as this method of testing produces a realistic stress-state in the region of the bars. Additionally, the majority of data used to establish current design provisions for development and lap splice lengths were tested in four-point bending (ACI Committee 408 2003). A constant shear region of 4 ft was selected, and the load was placed 1 ft from the end of the beam. The shear regions of the beam were reinforced with #4 Grade 60 stirrups at 4-$^1/_4$ in. center-to-center. These stirrups were included to prevent failure outside the constant moment region. The specimens were designed for the load to be applied downward to each end of the beam so that the top of the specimen was in tension. This loading allowed for easier crack mapping and measuring of crack widths. Although the specimens were tested with the reinforcement near the top face, all specimens were cast with reinforcement near the bottom face. Therefore, the beams were flipped prior to testing. This was done because casting position has been shown to influence the bond strength of the specimen, and elimination of this factor was desired. Figure 2.2 shows the test setup used for the testing of all the beams. Two #3 longitudinal bars were included on the compression side of the specimen to assist with fabrication and to prevent the specimen from falling in the case of a brittle failure.

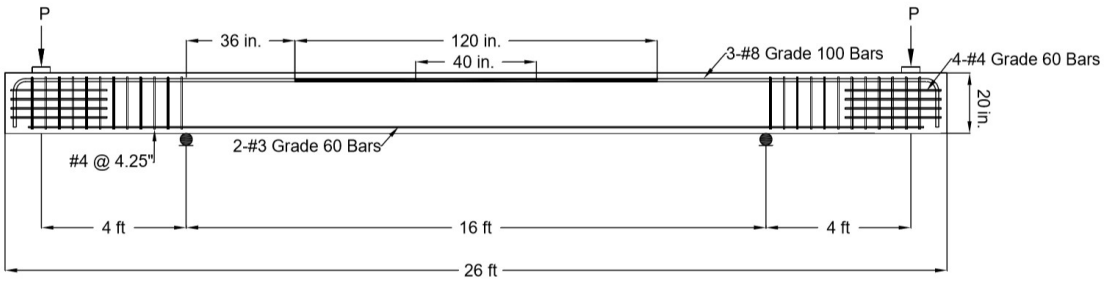

a) Unconfined

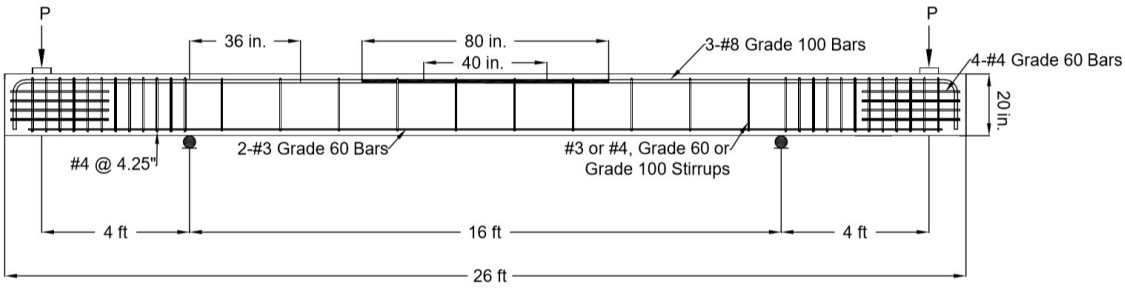

b) Confined

Figure 2.2: Typical Specimen Configuration

2.3 Test Variables

The variables studied included splice length, spacing of bars, grade of transverse reinforcement, and transverse reinforcement spacing. Each of the experimental variables is described in detail in Table 2.1.

The concrete mix was maintained constant throughout all specimens. Additionally, the bar cover and bar spacing were also constant in the majority of specimens. All specimens had #8 Grade 100 longitudinal bars from the same heat and had an effective depth, d, of 17-$^5/_8$ in.

Specimens are labeled using the following notation:
Unconfined Specimens:
U (Unconfined) - Splice length (d_b) – Target 28-day concrete compressive strength (f'_c)
Ex: U-60-5

Confined Specimens:
C (Confined), Stirrup bar size (#)/ Grade of transverse reinforcement (ksi) - Splice length (d_b) – Target 28-day concrete compressive strength (f'_c) - Effective stress provided by transverse reinforcement (psi)
Ex: C3/60-60-5-100

Term 1: Presence of transverse reinforcement in the splice region: U (no transverse reinforcement), C (transverse reinforcement). For confined specimens, the transverse reinforcement bar size and grade of reinforcement directly follows.

Term 2: Splice length (d_b)

Term 3: Target 28-day compressive strength of concrete (f'_c). A letter following this term indicates a duplicate specimen.

Term 4: For confined specimens, the effective stress provided by the transverse reinforcement, represented in psi (See Section 2.3.4). For unconfined specimens, "M" indicates minimum clear spacing provided between bars (1 in. clear).

Table 2.1: Specimen Variables

Series	Specimen Name	Splice Length (d_b)	Target Concrete Strength (ksi)	Bar Spacing (d_b)	Trans. Reinf. Bar Size (#)	Trans. Reinf. Gr. (ksi)	Spacing of Trans. Reinf. (in.)
I	U-40-5	40	5	2	-	-	-
	U-60-5	60	5	2	-	-	-
	U-80-5	80	5	2	-	-	-
	U-100-5	100	5	2	-	-	-
	U-120-5	120	5	2	-	-	-
	U-80-5-M	80	5	1	-	-	-
	U-100-5-M	100	5	1	-	-	-
	U-120-5-M	120	5	1	-	-	-
II	C3/60-60-5-50	60	5	2	3	60	19
	C3/60-60-5-100	60	5	2	3	60	9.5
	C3/60-60-5-150	60	5	2	3	60	6.375
	C3/60-60-5-200	60	5	2	3	60	4.75
	C4/60-60-5-100	60	5	2	4	60	9.5
	C3/100-60-5-100	60	5	2	3	100	9.5
	C4/60-60-5-150	60	5	2	4	60	6.375
	C3/100-60-5-150	60	5	2	3	100	6.375
III	C3/60-80-5-50	80	5	2	3	60	19
	C3/60-80-5-100	80	5	2	3	60	9.5
	C3/60-80-5-150	80	5	2	3	60	6.375
	C3/60-80-5-200	80	5	2	3	60	4.75
	C4/60-80-5-100	80	5	2	4	60	9.5
	C3/100-80-5-100	80	5	2	3	100	9.5
	C4/60-80-5-150	80	5	2	4	60	6.375
	C3/100-80-5-150	80	5	2	3	100	6.375
IV	U-40-5a	40	5	2	3	-	-
	U-60-5a	60	5	2	3	-	-
	U-70-5	70	5	2	3	-	-
	C3/60/2-40-5-50	40	5	2	3	60	19
	C3/60/3-40-5-50	40	5	2	3	60	19
	C3/100/3-40-5-50	40	5	2	3	100	19
	C3/60-40-5-100	40	5	2	3	60	9.5
	C3/100-40-5-100	40	5	2	3	100	9.5

2.3.1 Splice Length

Mathey and Watstein (1961) have shown that the relationship between splice length and bar stress is not linear. Because of the lack of data for longer splice lengths (longer than $40d_b$), longer splice lengths that would be required for high-strength reinforcement were of primary interest in this study.

Splice lengths were varied as follows:

Unconfined Specimens: $40d_b$ to $120d_b$

Confined Specimens: $40d_b$ to $80d_b$

2.3.2 Spacing of Bars

Increasing the clear spacing between bars and the concrete clear cover to the bar have both been shown to increase the splice strength. Additionally, concrete clear cover and clear spacing dimensions are important in determining the mode of failure. The clear spacing between spliced bars, based on a typical beam design, was selected as 2 in. for 19 of 22 specimens. To evaluate the lower limit allowed by the code, three specimens (designated by the ID "M") included a clear spacing of 1 in. between bars. For these specimens, the specimen width was correspondingly reduced (Figure 2.3), while the side cover remained constant.

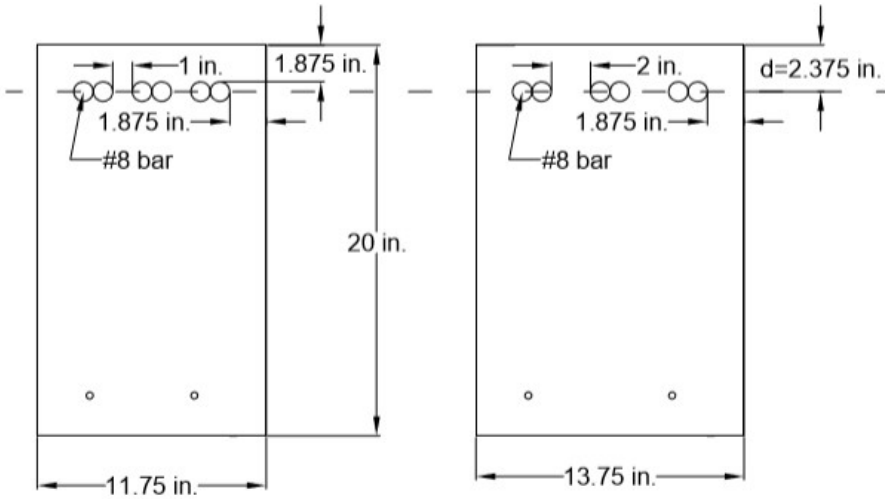

a) 2-in. Clear Spacing **b) 1-in. Clear Spacing ("M" Spacing)**

Figure 2.3: Minimum Cover Cross Section

2.3.3 Transverse Reinforcement Grade

There has been debate whether it is beneficial to use high-strength transverse reinforcement to increase splice strength. It has been reported (ACI 318-14 Section R25.4.2.3, Azizinamini et al. 1995) that transverse reinforcement rarely reaches yield prior to a brittle failure, even for Grade 60 reinforcement. To investigate the effectiveness of high-strength transverse reinforcement, comparable specimens were built with either Grade 60 or Grade 100 transverse reinforcement in the splice region. The same size stirrups and spacings were used so that the effect of the grade of transverse reinforcement could be directly compared.

2.3.4 Transverse Reinforcement Spacing

Transverse reinforcement has been shown to improve the ductility and strength of splices. This study attempts to quantify the increase in splice strength with a given area of transverse reinforcement. The study varied the spacing of the transverse reinforcement from 4-$^{3}/_{4}$ in. to 19 in. In addition to evaluating spacings, two specimens were designed with the same stirrup spacing, but a different number of stirrups within the splice region. Specimen C3/60/3-40-5-50 contained three stirrups in the splice region, whereas Specimen C3/60/2-40-5-50 contained only two stirrups. The purpose of these specimens was to investigate if the location of the stirrups within the splice region affected the bond strength of the specimen.

A minimum amount of shear reinforcement is required by the building code (ACI 318-14). Both a minimum spacing ($^{d}/_{2}$, ACI 318-14 Table 10.7.6.5.2) and a minimum area (ACI 318-14 Equation 10.6.2.2) are specified.

The spacing of transverse reinforcement in this study was selected based on the minimum area requirements, which typically produce the largest spacing. Based on Equation 10.6.2.2.b in ACI 318-14, which provides for a minimum effective stress of 50 psi, the effective stress that the transverse reinforcement provides was calculated to determine the various spacings of the stirrups within the splice region. The effective stresses selected were 50, 100, 150, and 200 psi.

$$50\frac{b_w s}{f_{yt}} = A_{v,min} \qquad \text{(ACI 318-14 Equation 10.6.2.2.b)}$$

The spacings calculated for these effective pressures are based on a beam width (b_w) of 13-$^3/_4$ in., a transverse reinforcement area ($A_{v,min}$) of 0.22 in^2 (2-legged #3 stirrup), and transverse reinforcement yield strength (f_{yt}) of 60 ksi. The "effective pressure" coefficient in ACI 318-14 Equation 10.5.2.2.b was varied in 50 psi increments to calculate spacings at consistent intervals. The calculated spacings for each of the four confinement cases are shown below.

$A_{v,min} = 0.11\ in.^2 * 2 = 0.22\ in.^2$ (two stirrup legs)

50 psi: $s = \frac{A_{v,min} f_{yt}}{50 b_w} = \frac{(0.22\ in.^2)(60\ ksi)}{(50\ psi)(13.75\ in.)} = 19.2\ in. \rightarrow 19\ in.$

100 psi: $s = \frac{(0.22\ in.^2)(60\ ksi)}{(100\ psi)(13.75\ in.)} = 9.6\ in. \rightarrow 9.5\ in.$

150 psi: $s = \frac{(0.22\ in.^2)(60\ ksi)}{(150\ psi)(13.75\ in.)} = 6.4\ in. \rightarrow 6.375\ in.$

200 psi: $s = \frac{(0.22\ in.^2)(60\ ksi)}{(200\ psi)(13.75\ in.)} = 4.8\ in. \rightarrow 4.75\ in.$

The spacings were maintained for #4 stirrups and Grade 100 stirrups, regardless of the actual effective pressure that would be calculated. The spacings were maintained to directly compare results.

2.4 Materials

2.4.1 Steel Reinforcement

ASTM A615 deformed steel bars were exclusively used in the testing program. All reinforcing bars were manufactured and fabricated at Nucor Kankakee. Bars of each size were obtained from the same heat to ensure consistent material properties. A minimum of three bar coupons were tested for each bar type and size.

2.4.1.1 Longitudinal Bars

Figure 2.4 shows the bar mark for the longitudinal bars used during testing. Testing was conducted using a 220-kip MTS universal testing machine according to ASTM E8 (Figure 2.5).

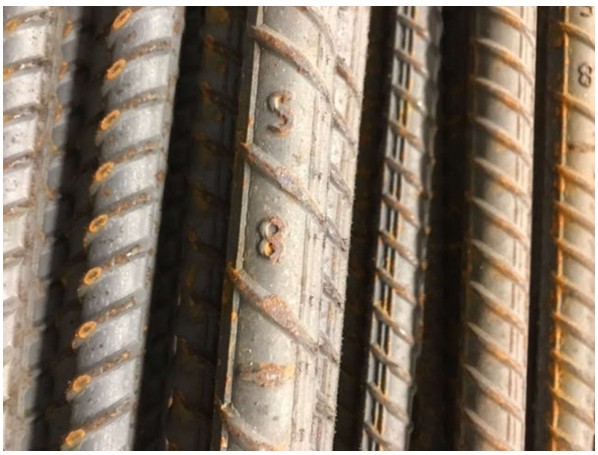

Figure 2.4: Bar Mark for Longitudinal Bars

Figure 2.5: Testing of #8 Bars

To determine the stress-strain response, the test machine measured the load applied while an Epsilon 2-in. extensometer measured strain during testing. Stress was calculated by dividing the measured load by the nominal bar area. A representative stress-strain curve is shown in Figures 2.6 and 2.7. The elastic limit of the #8 bars was measured as 87 ksi (Figure 2.7). In addition, the yield strength of the #8 bars using the 0.2% offset method was determined to be 108 ksi (Figure 2.7). The strength of the #8 Grade 100 bars was measured as 140 ksi, and the elongation at failure, 11% (Figure 2.6). The material properties of the Grade 100 #8 longitudinal bars are

summarized in Table 2.2. The stress-strain curves for the longitudinal bars tested are provided in Appendix B.

Table 2.2: Material Properties of Longitudinal Reinforcement

Bar Size	Grade (ksi)	Elastic Limit Stress (ksi)	Yield Stress 0.2% Offset (ksi)	Ultimate Strength (ksi)	Elongation at Failure
#8	100	87	108	140	11%

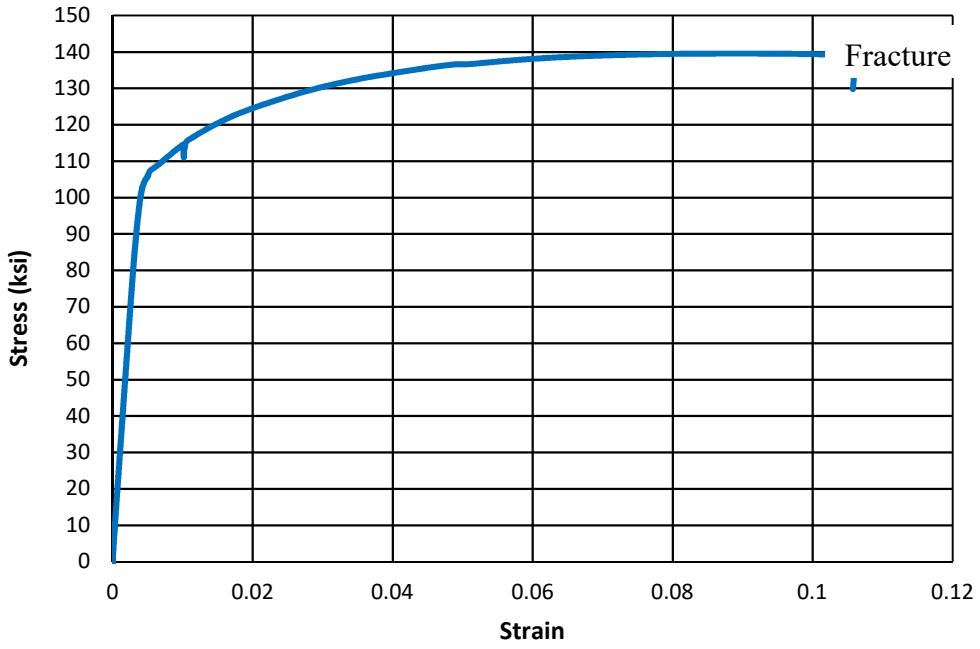

Figure 2.6: Stress-Strain Curve of Representative #8 Grade 100 Bar

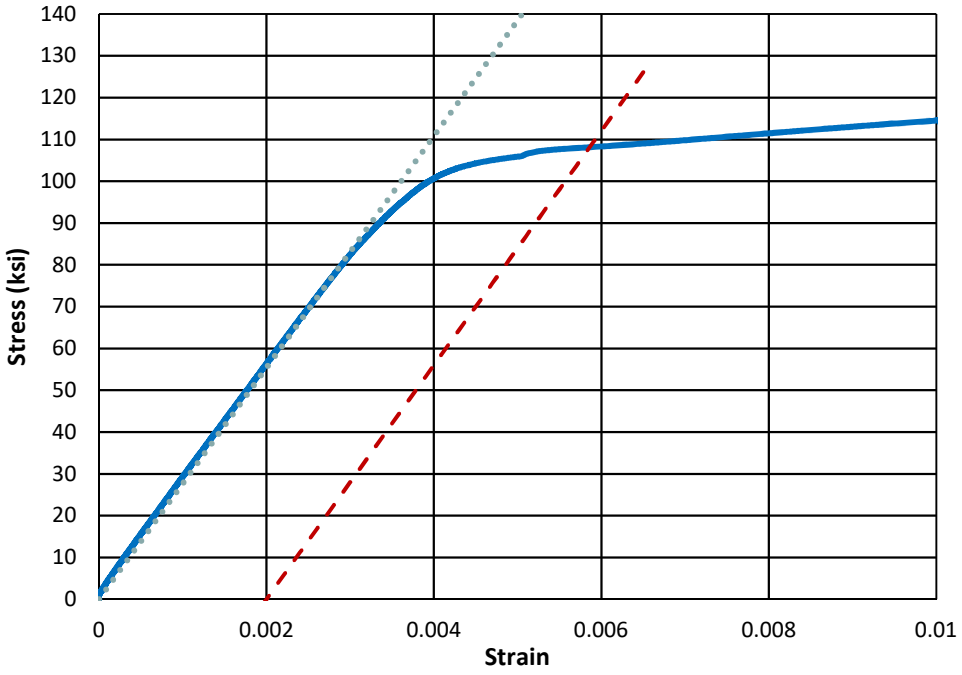

Figure 2.7: Linear Limit and Yield Strength, #8 Grade 100 Bar

To measure the elongation at failure, the bars were marked with a punch before testing at approximately 4-in. increments. The spacing of the punches was measured using a micrometer before and after testing to determine the failure strain. No failures occurred at the location of a punch. Additionally, the use of a breakaway extensometer allowed the strain at failure to be captured. The relative rib area for the longitudinal bars is 0.098, calculated according to Equation 1-1.

2.4.1.2 Transverse Reinforcement

Both Grade 60 and Grade 100 ASTM A615 steel were used as transverse reinforcement. In addition to varying the grade of steel, both #3 and #4 stirrups were used. All stirrups were fabricated from straight bars rather than coils to minimize residual stresses caused from bending and unbending the coil. A minimum of three samples for each bar size and grade were tested in a 120-kip Baldwin universal testing machine in accordance with ASTM E8. The testing machine measured the stress, while an Epsilon 2-in. extensometer measured the strain during testing.

To determine the elongation at failure, the bars were marked with a punch and measured before and after testing. None of the specimens had the location of rupture coincide with one of the punches. Additionally, the use of a breakaway extensometer allowed the strain at failure to be captured. Representative stress-strain curves for each type of transverse reinforcement used are shown in Figures 2.8 through 2.10. The mean yield and elongation properties at failure are summarized in Table 2.3. The stress-strain curves for the transverse reinforcement tested are provided in Appendix B.

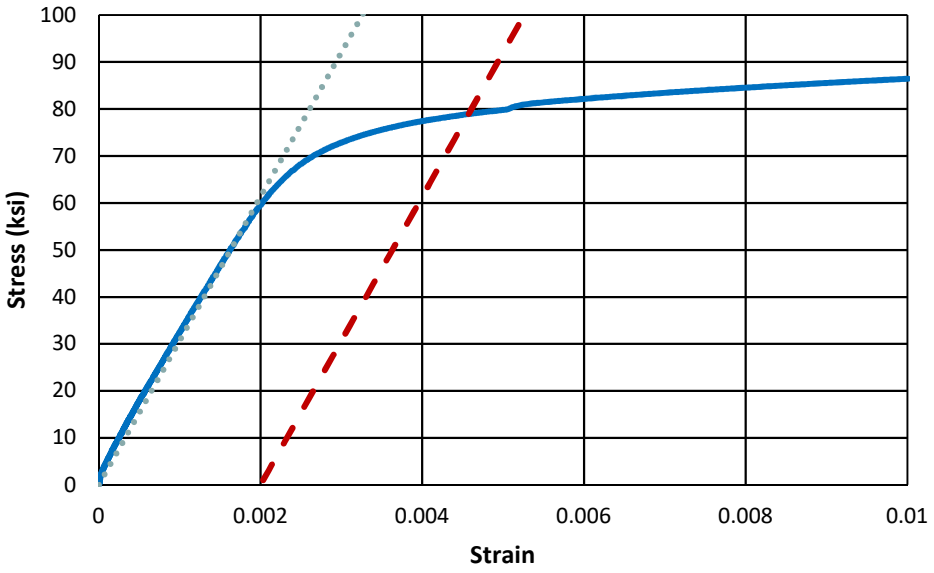

Figure 2.8: Linear Limit and Yield Strength, #3 Grade 60 Bar

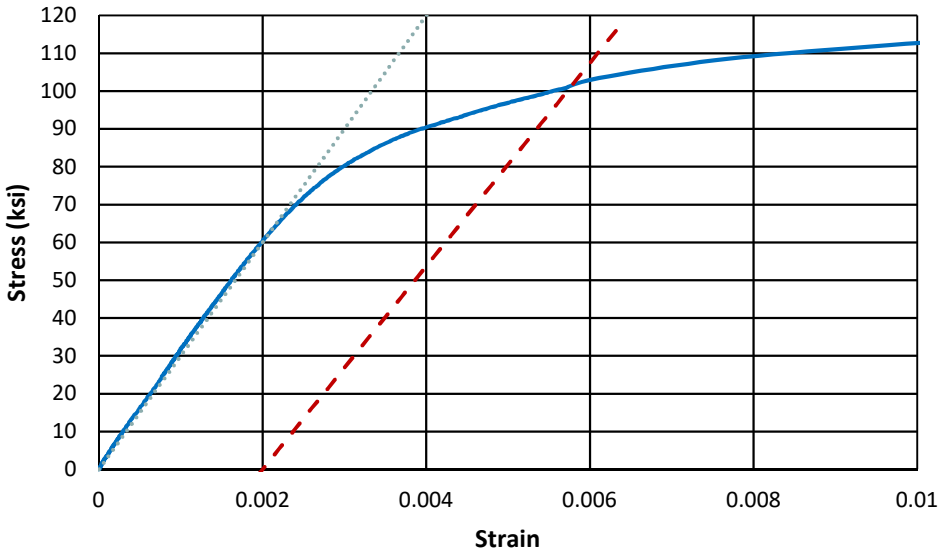

Figure 2.9: Linear Limit and Yield Strength, #3 Grade 100 Bar

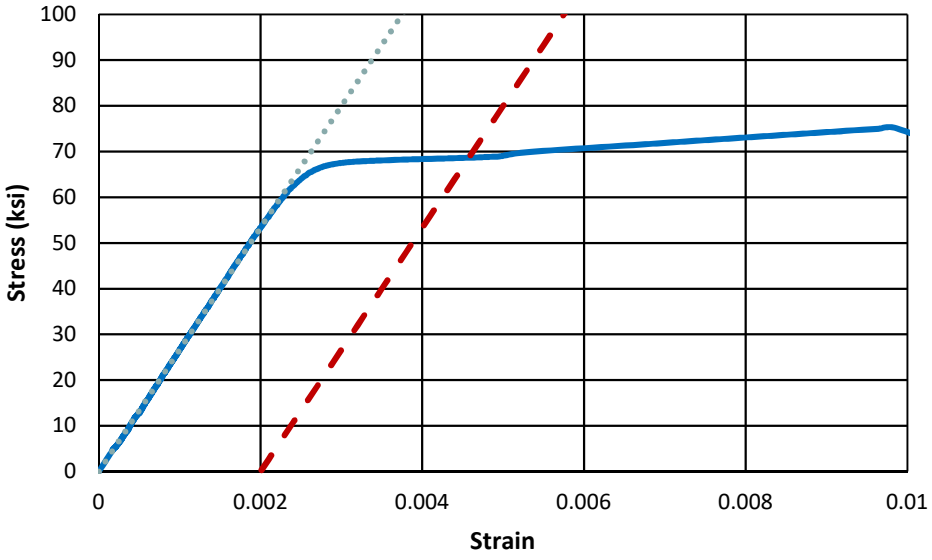

Figure 2.10: Linear Limit and Yield Strength, #4 Grade 60 Bar

Table 2.3: Material Properties of Transverse Reinforcement

Bar Size	Grade (ksi)	Elastic Limit Stress (ksi)	Yield Stress 0.2% Offset (ksi)	Ultimate Strength (ksi)	Elongation at Failure
#3	60	62	79	101	11%
	100	72	102	138	8%
#4	60	65	69	105	12%

2.4.2 Concrete Strength

Concrete was provided by Irving Materials Inc. (IMI), a ready-mix supplier in West Lafayette, Indiana. The selected mixes were based on previous batch statistics provided by IMI and a target 28-day strength of 5,000 psi. After the first series (Mix 4101CC) provided lower strengths than desired, the mix design was changed to 4601CC. Concrete mix 4601CC provided strengths that were much higher. For the remainder of the series, mix 4101CC was used.

All specimens in the same series were cast with the same mix design. Both concrete mixes were non-air entrained containing ¾" crushed limestone aggregate. Details of the two mix designs are provided in Table 2.4. Actual mix quantities for each series are provided in Appendix C.

Table 2.4: Concrete Mix Design per Cubic Yard

	Mix Design I 4101CC	Mix Design II 4601CC
Nominal Strength (psi)	4000	4500
Type I Cement (lb/cy)	517	564
#8 Limestone (lb/cy)	1875	1850
Fine Aggregate (lb/cy)	1475	1450
Water (lb/cy)	249.9	249.9
Mid-Range Water Reducer (oz/cy)	20.7	11.3
Series	I, III, and IV	II
Slump (in.)	6	6

Concrete strength was determined using 6x12 in. cylinders that were cured and cast in the same conditions as the specimens. Differences in concrete strengths between series occurred because

of time of year, water added, and mix design. Compressive and tensile strengths were determined from testing in a 600-kip Forney testing machine according to ASTM C39 and ASTM C496, respectively. Loading was applied at 35 psi/sec for the compression tests and 2.5 psi/sec for the split tensile tests. The test setup for the compression and split tensile tests are shown in Figure 2.11. The elastic modulus test was also conducted using the 600-kip Forney testing machine. Load was applied at 35 psi/sec in accordance with ASTM C469.

Two trucks were required for casting of each series. To minimize the number of cylinders required, only cylinders from Truck 1 were tested at 7 and 14 days. Cylinders were tested at 28 days, the first day of testing, and the last day of testing of each series for each of the two trucks. At 28 days, the first day of testing, and the last day of testing, three cylinders from each truck were tested for each compression and split tensile test. Additionally, the modulus of elasticity test was conducted on either the first or last day of testing for the series. The results from the cylinder tests conducted on days 7, 14, and 28 days, and the first and last days of testing are summarized in Table 2.5. The strength gain of the different concrete series over time is shown in Figure 2.12.

a) Compression **b) Split Cylinder**

Figure 2.11: Concrete Cylinder Testing

Table 2.5: Concrete Strengths

Series	Truck	Day	f_c (psi)	f_t (psi)	E_c (ksi)
I	1	7	3980	-	-
		14	4350	-	-
		28	4530	490	-
		180	4780	450	3000
		189	4830	470	4000
	2	28	4470	460	-
		56	4660	460	4400
		177	4600	460	-
II	1	10	5680	-	-
		14	5830	-	-
		28	6450	570	-
		100	7250	560	4600
		103	7400	560	-
	2	28	6360	560	-
		107	7400	530	-
		110	7400	590	4900
III	1	7	4510	-	-
		14	5660	-	-
		28	6090	530	-
		38	6310	530	5500
	2	28	6960	610	
IV	1	7	4810	-	-
		14	5360	-	-
		28	5910	460	5100
		48	6110	510	5100
	2	28	6530	500	-
		49	6510	500	5000
		51	6520	520	5000

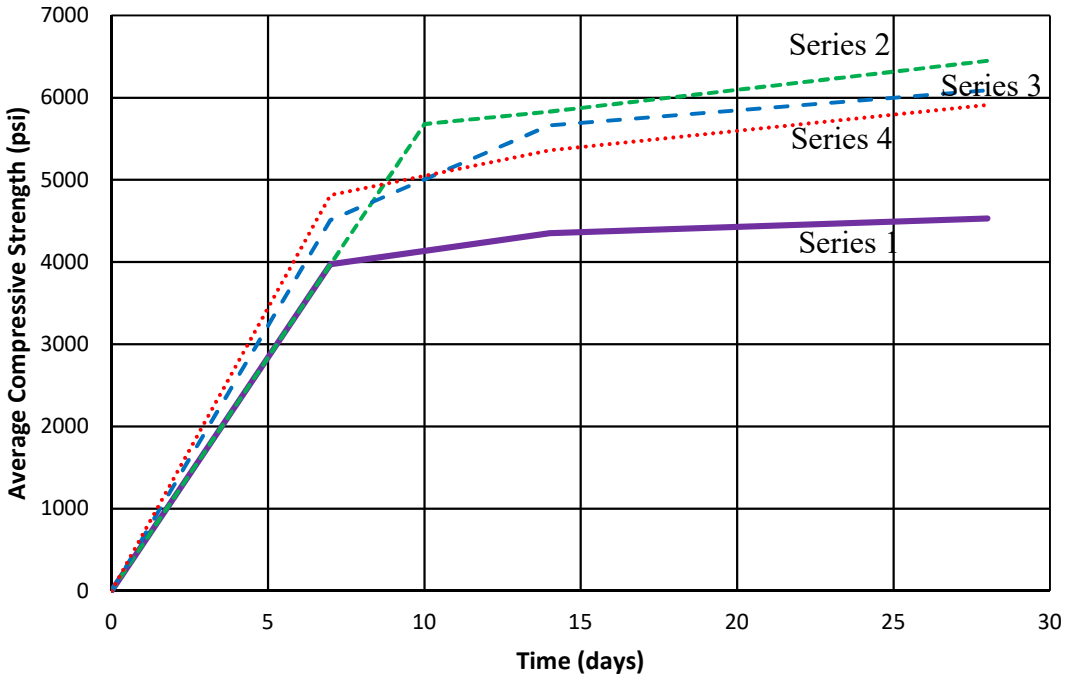

Figure 2.12: Concrete Compressive Strength Gain

2.5 Specimen Construction

2.5.1 Fabrication of Formwork

All series used the same set of wooden formwork. To conserve space and materials, the forms were designed and constructed so that two specimens could be cast side-by-side. Four sets of forms were built so that eight specimens could be cast at once. To build the side forms, stud wall like structures were built out of 2x4s and sheathed with ¾" HDO plywood (Figure 2.13). HDO plywood has a resin coating that allows the forms to be reused multiple times. To ensure that the top of the forms did not bulge during casting, a ¼" threaded rod was used in conjunction with wedges at seven points along the beam as shown in Figure 2.14. To prevent the threaded rod from bonding to the concrete, $^{3}/_{8}$" PEX pipe was used as a barrier between the concrete and threaded rod so that the threaded rod could be pulled out of the specimen after casting. Both the side forms and end forms were secured to the platform using lag screws for ease of removal.

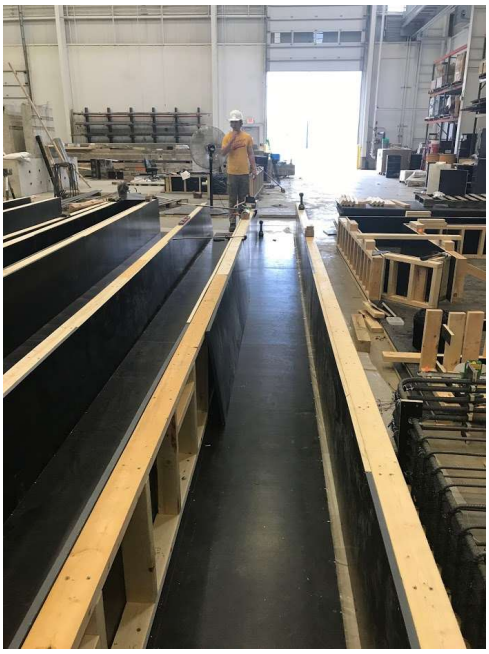

Figure 2.13: Center Side Form

Figure 2.14: Completed Formwork

2.5.2 Construction of Reinforcement Cages

The reinforcement cages contained longitudinal reinforcement both on the tension and compression faces of the specimen (Figure 2.2). All specimens also contained stirrups in the shear span to prevent failure outside of the splice region. The number of stirrups in the splice region varied according to the specimen. The cages were constructed on top of the forms and then lowered with two overhead gentry cranes. Stirrups were secured to the #3 compression bars

and the #8 longitudinal bars using metal rebar ties. The 1-$^{7}/_{8}$" concrete cover to the bars from the bottom of the forms was maintained using 2" plastic chairs with $^{1}/_{8}$" tips that were ground off. The longitudinal bars were tied to the chairs to ensure the spacing between bars remained during casting. Spacer wheels were used on the ends to ensure that appropriate side cover was maintained (Figure 2.15). Lifting inserts were tied to the stirrups with metal ties approximately 5 ft from the ends of the beam. The location of the lifting inserts was controlled by the minimum 19 ft spacing required to use two overhead cranes simultaneously and the cracking moment of the beam. An unconfined and a confined lap splice are shown in Figure 2.16.

Figure 2.15: Reinforcing Cages Inside Forms

a) Unconfined Lap Splice (Left: U-60-5, Right: U-40-5)

b) Confined Lap Splice (Left: C3/60-60-5-100, Right: C3/60-60-5-150)

Figure 2.16: Lap Splice Construction

2.6 Casting, Curing, and Storage

Specimens in each series were cast at the same time. Because of the volume of concrete required to cast eight beams at once, two trucks were required. For the first three series, four specimens were cast from the first truck and four specimens from the second truck. For the fourth series, five specimens were cast from the first truck and three from the second truck. Appendix C indicates the specific truck from which each specimen was cast. The slump was checked upon arrival of the concrete truck. The design slump was 6 in. If the slump was less than the 1 in. tolerance, water was added to the mixture, and the slump test repeated. Once the mix was accepted, the concrete was transported from the ready-mix truck to the forms using a bucket and overhead crane as shown in Figure 2.17.

The beams were cast in two lifts, alternating specimens on either side of the center form to ensure that the center form did not tilt because of the pressure of the concrete on one side. After each lift, the beams were vibrated to ensure that the concrete was properly consolidated.

Figure 2.17: Casting Procedure for Specimens

From each truck, 6x12 in. cylinders were cast in plastic molds simultaneously with the beams in accordance with ASTM C192. The cylinders were consolidated with a mechanical vibrator after each of the two lifts (Figure 2.18). The cylinders were also finished, cured, and stored in the same manner as the beams to ensure a reliable representation of strength. After allowing the concrete to set, the specimens were covered with wet burlap and plastic sheeting for moist curing. Once a day, for the next six days, the burlap on the specimens was watered to maintain moist curing. On day seven after casting, the cylinder molds, burlap, and forms were removed. The beams were stored inside of Bowen Laboratory until testing. The beams were flipped using a crane prior to installation in the test setup so that the bottom-cast bars were in the top testing position.

Figure 2.18: Making of Cylinders

2.7 Test Setup and Procedure

The beams were tested in four-point bending. Two equal, concentrated loads were applied 1 ft from each end of the beam with hydraulic rams connected to a single pump (Figure 2.19).

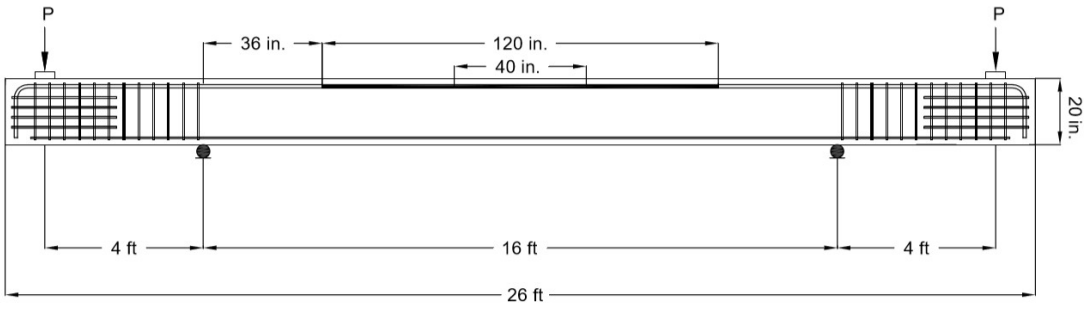

Figure 2.19: Test Setup

Concrete supports with either pin or roller supports were spaced 4 ft from the loading point. The beam was loaded in 5-kip increments. At each load step, the specimen was crack mapped, and crack widths were measured using an Edmund Direct 50x microscope. The specimen was crack mapped and crack widths were measured until it was deemed unsafe to approach the beam. Because these specimens contained some of the longest lap splices that have ever been tested, there was concern regarding maintaining verticality of the load. Different iterations of the test setup were explored as discussed in the following sections.

2.7.1 First Test Setup

The first test setup used a pin support on top of the concrete beam to allow the load to be applied vertically as the end of the beam deflected downwards. The pin support was made from a 1-$^1/_4$" steel roller and two 1" x 6" x 18" grooved steel plates. The groove was ¼" deep and 1-$^1/_8$" wide to allow the roller to fit partially within the groove. The pin did not work in the way intended, and the loading rods bent as the end deflection of the beam increased. For Specimen U-40-5, the pin beneath the HSS cross beam was removed to finish the test. Two Enerpac 30-ton hydraulic rams were placed on each of the 1-in. Dywidag bars to apply load to the specimen.

The beam was supported by a pin-roller support condition. The pin support was made from a 1-$^1/_4$" steel roller and two grooved steel plates, while the roller support was made from a 1-$^1/_4$" steel roller and two flat steel plates. This setup was only used for U-40-5 as the loads and deflections were small enough that the Dywidag bars used in the test setup did not yield during testing. The first iteration of test setup is shown in Figure 2.20.

Figure 2.20: First Test Setup (U-40-5)

2.7.2 Second Test Setup

The second iteration of the test setup included a frame and the same pin-roller support conditions described in Section 2.7.1. The second test setup was only used to fail Specimens U-60-5 and U-80-5. The same 1-in. Dywidag bars and 30-ton hydraulic rams were used along with the rollers

described in Section 2.7.1, placed under and the same HSS cross beam used in the first test setup. To stabilize the system and to prevent bending of the Dywidag bars with the deflection of the end of the beam, the hydraulic rams pushed against two HSS cross beams that transferred the load to two 1-$^1/_4$" in. Dywidag bars. This test setup configuration is shown in Figure 2.21.

Figure 2.21: Second Test Setup (U-60-5)

The second test setup worked well for lower loads. When higher loads were reached while testing U-80-5, the Dywidag bars yielded suddenly as shown in Figure 2.22. This behavior was attributed to a lack of centering on the pin under the HSS section. The setup was fixed and Specimen U-80-5 was failed using the same setup. While testing Specimen U-100-5, the second test setup failed again. This failure was because the top of the beam expanded as more cracks developed and opened on the tension face. The pin support on the top of the beam allowed rotation, but did not allow translation, forcing all displacement to one side of the specimen.

Figure 2.22: Dywidag Bars Yielding in Testing of U-80-5

2.7.3 Third Test Setup

The setup that was used to fail all specimens except for U-40-5, U-60-5, and U-80-5 (as previously discussed) is shown in Figure 2.23. Cross beams composed of two back-to-back channels and two 1-in. plates were used to suspend a 100-ton Enerpac hydraulic ram. With only one point of loading rather than two, the system could rotate even without a saddle bearing or pin support.

Figure 2.23: Third Test Setup (U-100-5-M)

Additionally, the support conditions were changed from pin-roller to roller-roller to allow for the equal expansion of the top of the specimen (and contraction of the bottom of the beam) at both supports. As shown in Figure 2.24, the rollers allowed for the translation that was required during testing. With two rollers as opposed to one, translation at the loading points was minimized as both ends could translate equally.

Figure 2.24: Roller-Roller Support (U-120-5-M)

2.7.4 Instrumentation Layout

Four Lebow 50-kip load cells (two on each end of the beam) were used to measure the load applied to the beam. String potentiometers with a stroke of 10 in. were used to measure the deflection under each load and at midspan. Two string potentiometers were used at midspan, one on each side face of the beam. Only one string potentiometer was used at each end (load point), and they were placed at the center of the bottom face. For Specimens U-40-5, U-60-5, and U-80-5, LVDTs were used to measure settlement at the pin support. The support settlements were shown to be negligible from the LVDT readings at the supports taken from the first three tests. With the pin support being changed to a roller, the LVDTs were eliminated because of the LVDT rods shearing when the beam failed suddenly. The instrumentation layouts for the various test setups are shown in Figure 2.25.

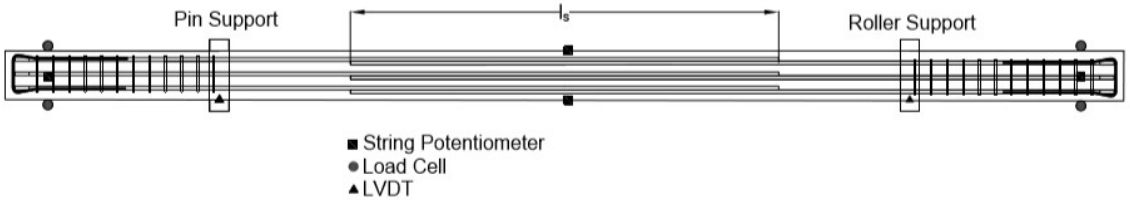

a) First Test Setup

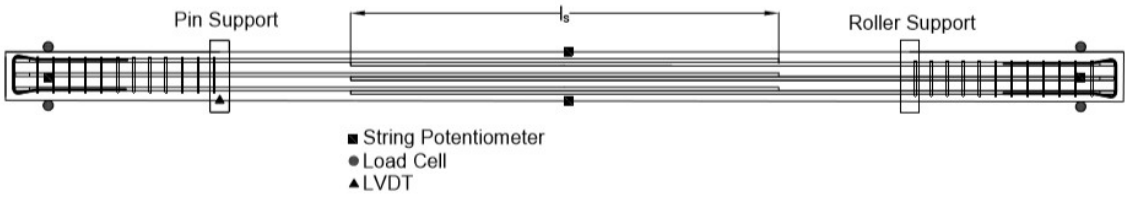

b) Second Test Setup

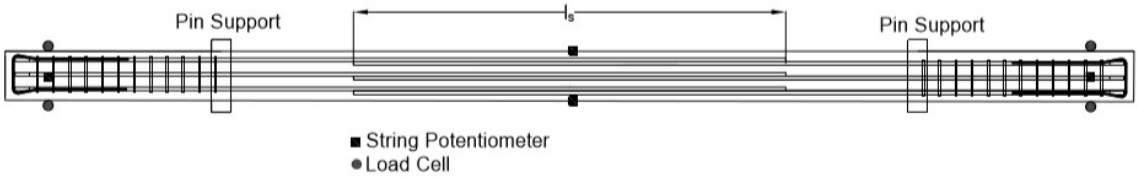

c) Third Test Setup

Figure 2.25: Instrumentation Layout

3. EXPERIMENTAL RESULTS

3.1 Introduction

The experimental results from each test are presented to evaluate the effects of the test variables on the behavior of the specimen and the bond strength of the splice. The failure mechanisms and cracking behavior of the specimen will be presented with an emphasis on failure modes and crack patterns. This chapter presents load-deflection response, crack width measurements, and observations made regarding crack patterns.

3.2 Test Results

A summary of the test results for each specimen are provided in Table 3.1 and the load-deflection responses are provided in Appendix D. The load at each end of the beam was measured using four load cells. The maximum average load from the two ends of the beam is defined as P_{ult}. The loads were averaged as they were approximately equal at each end. The loads measured at each end were within 2% of each other. The moment within the splice region, M_{ult}, is calculated by multiplying P_{ult} by the distance between the load and the support (4 ft). The bar stress, f_s, was calculated assuming a nonlinear stress distribution in the concrete. The compressive strength of the concrete was characterized by the Hognestad curve described by Equation 3-1. The tensile strength of the concrete was assumed to be zero. Nominal dimensions were used for all calculations.

$$f_c = f'_c \left[\frac{2\varepsilon}{\varepsilon_0} - \left(\frac{\varepsilon}{\varepsilon_0}\right)^2\right] \quad (3\text{-}1)$$

where:

ε= *concrete strain*

ε_0= *concrete strain at* f'_c

f'_c= *compressive strength of concrete, psi*

The concrete strength of the specimen was taken as the average of the first and last day of testing for the two trucks. This was done so that all specimens in a series could be compared.

Differences in concrete strengths between the first and last day of testing and each of the two trucks were within the acceptable variation of concrete tests.

The stress, f_s, was also calculated assuming a linear stress distribution in the concrete. This value is presented for comparison purposes. In general, the computed stresses are similar. For this study, the stresses considering the more accurate representation of the concrete stress-strain relationship were used. Both the self-weight of the beam and the contribution of compression steel were ignored in the calculation of bar stress as they were found to be negligible.

The specimens that experienced a splice failure and had a bar stress beyond the linear-elastic limit are indicated by an asterisk (*), while the specimens with a bar stress beyond the yield stress calculated according to the 0.2% offset method are indicated by a cross (†) in Table 3.1. The bar stress at failure and the corresponding location on the longitudinal bar stress-strain curve is shown for each specimen in Appendix D. It is observed that unconfined specimens fail in bond as soon as the stress-strain curve starts to become inelastic. For confined specimens, the bond failure occurs after more bar deformation occurs. The specimens that failed in flexure are indicated by double asterisks (**) in Table 3.1.

The specimens that were built, but not tested would have experienced a flexural failure based on the results of specimens with less transverse reinforcement and/or a shorter splice length. A flexural failure did not provide useful data in terms of quantifying the increase in splice strength because of different variables.

Table 3.1: Specimen Results

Series	Specimen	Test Age (days)	f_c (psi)	P_{ult} (kip)	M_{ult} (kip-ft)	Linear f_s (ksi)	Hognestad f_s (ksi)
I	U-40-5	56	4740	44.9	180	57.7	58.1
	U-60-5	112	4740	52.7	211	67.8	68.4
	U-80-5	146	4740	77.6	310	99.8	102.2*
	U-100-5	157	4740	78.7	315	101.2	103.7*
	U-120-5	186	4740	78.6	314	101.1	103.5*
	U-80-5-M	180	4740	73.3	293	95.0	97.6*
	U-100-5-M	187	4740	73.2	293	94.9	97.5*
	U-120-5-M	189	4740	71.8	287	93.0	95.5*
II	C3/60-60-5-50	100	7360	80.4	322	102.3	103.3*
	C3/60-60-5-100	101	7360	85.9	344	109.3	110.5†**
	C3/60-60-5-150	103	7360	85.1	340	108.3	109.4†**
	C3/60-60-5-200	NOT TESTED					
	C4/60-60-5-100	107	7360	84.7	339	107.8	108.9†**
	C4/60-60-5-150	NOT TESTED					
	C3/100-60-5-100	110	7360	86.3	345	109.8	111.0†**
	C3/100-60-5-150	NOT TESTED					
III	C3/60-80-5-50	38	6310	79.4	318	100.4	101.9**
	C3/60-80-5-100	NOT TESTED					
	C3/60-80-5-150						
	C3/60-80-5-200						
	C4/60-80-5-100						
	C4/60-80-5-150						
	C3/100-80-5-100						
	C3/100-80-5-150						
IV	U-40-5a	43	6260	54.6	218	69.3	69.8
	U-60-5a	28	6260	69.3	277	88.0	88.9*
	U-70-5	31	6260	73.8	295	93.7	94.9*
	C3/60/2-40-5-50	48	6260	63.9	256	81.1	81.8
	C3/60/3-40-5-50	44	6260	70.0	280	88.9	89.8*
	C3/100/3-40-5-50	49	6260	66.4	266	84.3	85.0
	C3/60-40-5-100	49	6260	71.4	286	90.7	91.7*
	C3/100-40-5-100	51	6260	72.5	290	92.1	93.2*

** beyond linear- elastic limit*

†beyond yield stress

***failed in flexure*

3.3 Behavior

3.3.1 Load-Deflection Response

The load-deflection response can be divided into three sections, and an example response is shown in Figure 3.1. The first section is linear. This response occurs until cracking. All beams exhibited approximately the same stiffness in this section of response, indicating that the stiffness of the beam at this point is primarily controlled by the concrete and behavior of the concrete remains elastic. The second section of response occurs after reaching the modulus of rupture of the concrete, resulting in flexural cracking. In this stage, stiffness is a function of the axial stiffness of the reinforcing bars, which is based on the modulus of elasticity and area of the bars. Because all the bars are the same throughout all specimens, the slopes in this stage of response are also similar. The final stage of the response represents yielding of the bars. At this point in the curve, deflection increased with relatively small increases in load. Specimens failed before yielding for 18 of 22 specimens. Therefore, the third stage of response does not occur in these specimens. The load-deflection response for all specimens is provided in Appendix D.

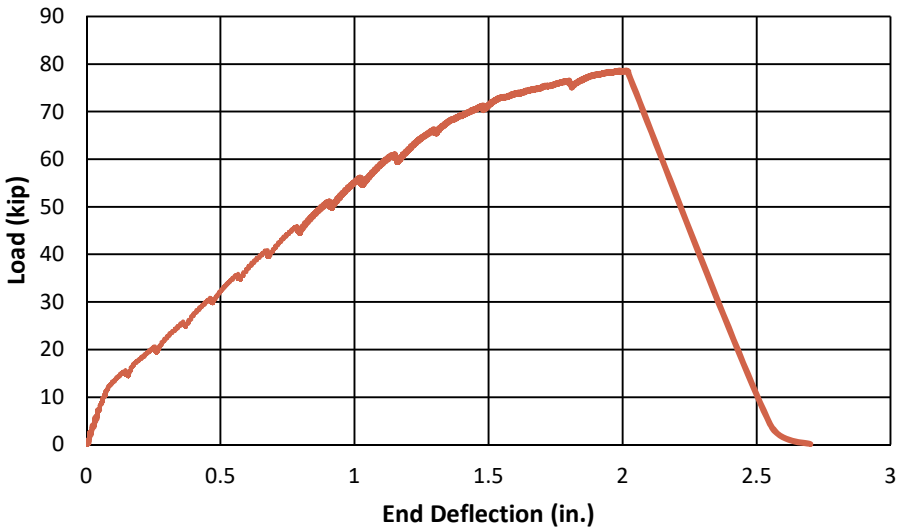

Figure 3.1: Representative Load Deflection Response (U-120-5)

3.3.2 Loading and Cracking of the Specimen

3.3.2.1 Flexural Cracking

Beyond a certain loading point, the full flexural cracking pattern developed and longitudinal cracks in the splice region became more prevalent. Across all specimens, regardless of spacing between bars, confinement, or splice length, propagation of the flexural cracks stopped at the beam's neutral axis as shown by the red lines drawn in Figure 3.2 (the red lines are an estimate of the neutral axis based on the cracking profile). The neutral axis at failure varied from 5 in. to 6.5 in. from the bottom of the specimen depending on the stress in the bars, the concrete strength, and the beam width.

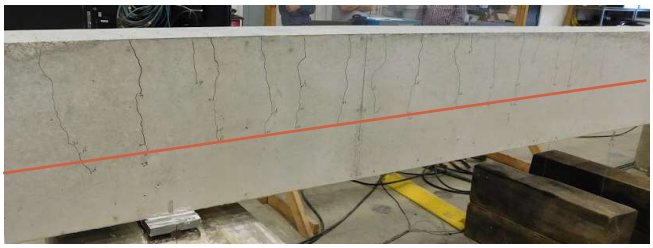

a) Specimen U-40-5

b) Specimen U-100-5

c) Specimen C3/100-40-5-100

Figure 3.2: Flexural Cracking

For unconfined specimens, flexural cracking developed across the entire depth of the beam at failure. After failure, large cracks through the entire beam section were observed emanating from the end of the splice (Figure 3.3). Only for the longest unconfined specimen, U-120-5, was a flexural crack also located at midspan (Figure 3.3(b)).

a) Specimen U-40-5a

b) Specimen U-120-5

Figure 3.3: Spacing of Cracks in Unconfined Specimens

For confined specimens, wide cracks emanating from the end of the splice were also observed. However, within the splice region, wide flexural cracks corresponding approximately to the location of the stirrups were also observed. Figure 3.4 shows two specimens with the same splice length, concrete strength, stirrup grade, stirrup size, and stirrup spacing. The only difference is that C3/60/3-40-5-50 (Figure 3.4(a)) has three stirrups within the splice region

whereas C3/60/2-40-5-50 (Figure 3.4(b)) only has two stirrups. As shown in Figure 3.4, the locations of the cracks align with the locations of the stirrups (indicated by the red lines).

a) Specimen C3/60/3-40-5-50

a) Specimen C3/60/2-40-5-50

b) Specimen C3/60-60-5-50

Figure 3.4: Spacing of Cracks in 50 psi Specimens

Beams with different stirrup spacings and different splice lengths exhibited this same behavior as shown in Figure 3.5. Figure 3.5 has stirrups spaced at 9-½ in., instead of the 19 in. shown in Figure 3.4.

a) Specimen C3/100-40-5-100

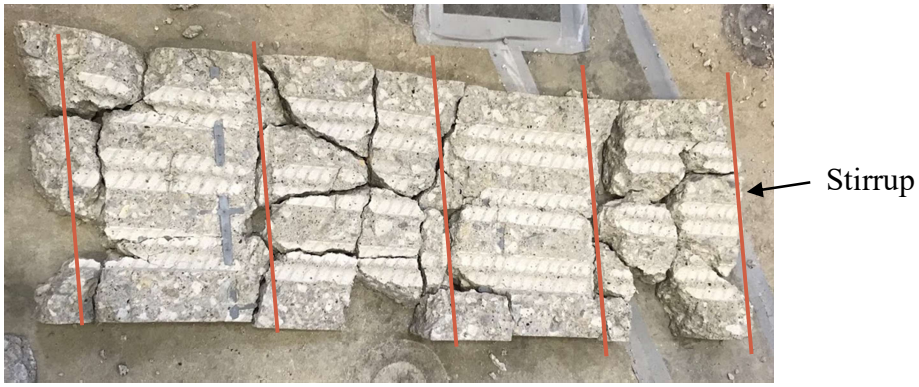

b) Specimen C3/60-40-5-100

Figure 3.5: Spacing of Cracks in 100 psi Specimen

The failure mechanism of the beams progressed in a similar manner. At 15 kips, flexural cracks developed at a consistent spacing along the length of the beam. As the load increased, more flexural cracks appeared, and the length of the flexural cracks increased until the neutral axis was reached. Between 30 and 40 kips, longitudinal cracks started to develop along the tension face

near the ends of the splice. As additional load was applied to the beam, the longitudinal cracks lengthened towards the center of the splice, connecting flexural cracks. The longitudinal cracking continued to lengthen toward the center of the splice until the beam failed suddenly. Typically, longitudinal cracking began at the end of the splice length and propagated towards the center of the splice. This behavior was observed in both unconfined and confined specimens as shown in Figures 3.6 and 3.7, respectively. For unconfined specimens, horizontal cracking also occurred along the side face. The beams that failed in flexure exhibited similar behavior; however, the beam failed in flexure near the support before the longitudinal cracking fully propagated to cause splice failure.

Figure 3.6(b) shows flexural cracks along the side of the beam that approached the neutral axis as the load increased. Longitudinal cracking became more extensive as loading increased up to failure (Figures 3.6(b) and 3.6(c)).

In Figure 3.7, the end of the splice is indicated by the star, circled in blue. As shown in Figure 3.7(a) for a $40d_b$ splice, longitudinal cracking propagated about 7 in. from the end of the splice towards the center of the beam at 50 kips for the 40-in. splice. The longitudinal cracking was even longer (10 in.) in the $60d_b$ splice. Although longitudinal cracking was observed in all specimens on the top face, longitudinal cracks on the side faces were evident for only a few of the confined specimens.

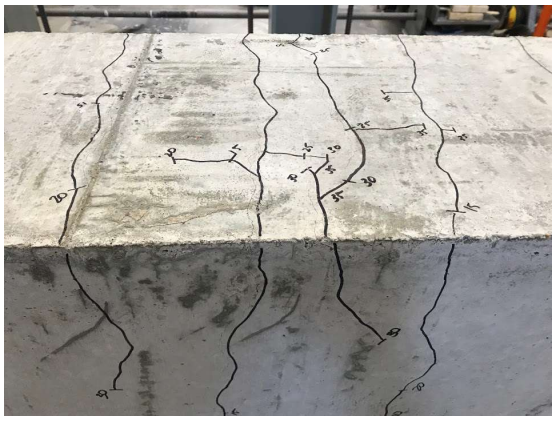

a) Tension and Side Faces of Specimen U-40-5a

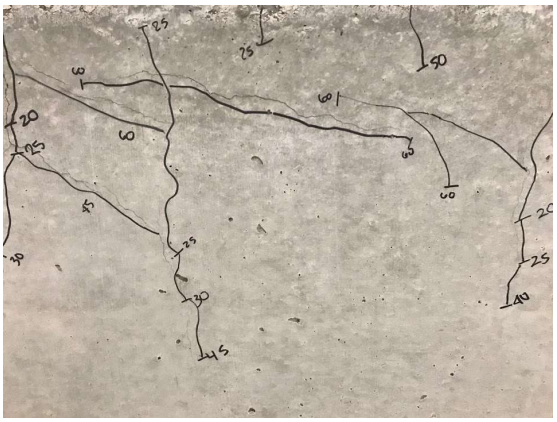

b) Side Face of Specimen U-120-5

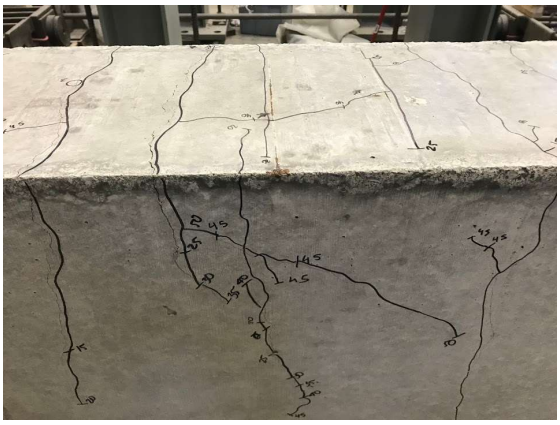

c) Tension and Side Faces of Specimen U-120-5-M

Figure 3.6: Longitudinal Cracking in Unconfined Specimens

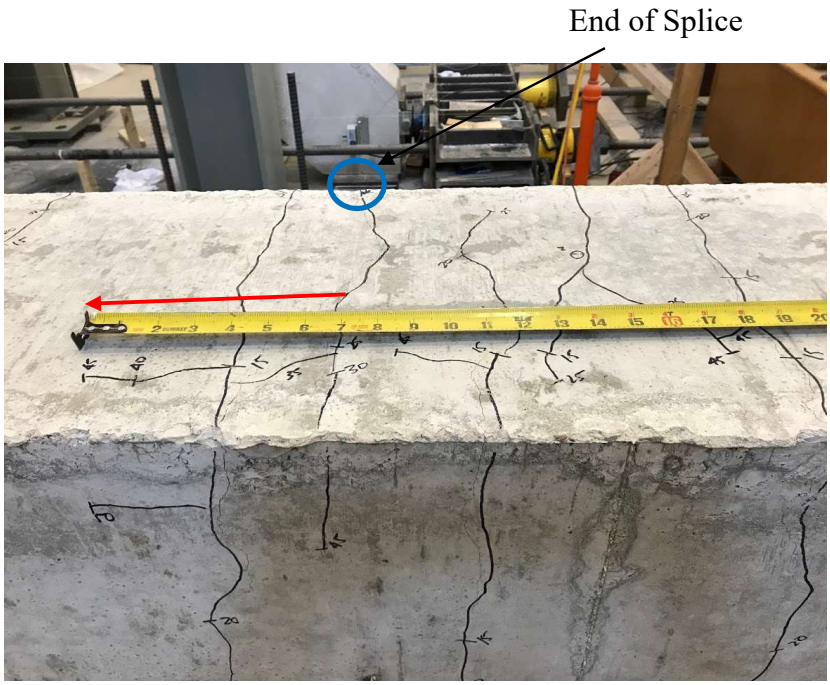

a) Tension Face of Specimen C3/60/3-40-5-50

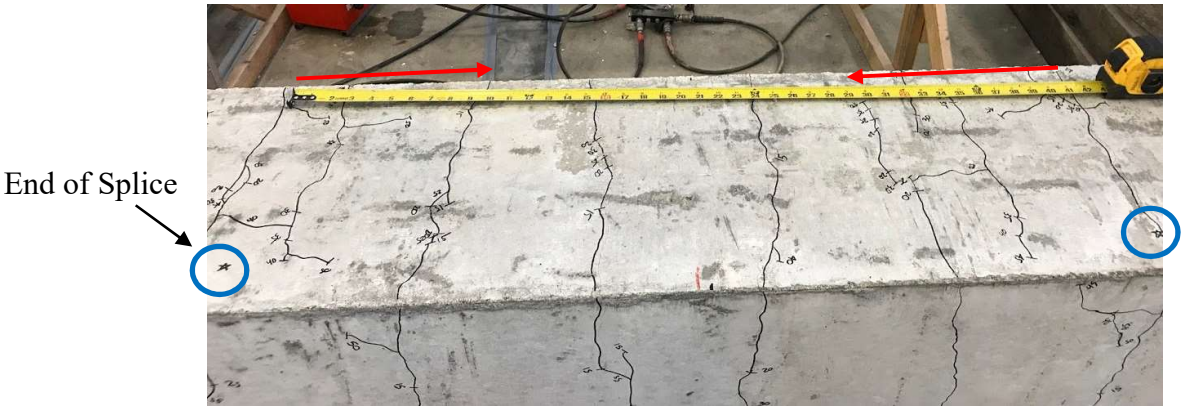

b) Tension Face of Specimen C3/60-60-5-100

Figure 3.7: Longitudinal Cracking in Confined Specimens

3.4 Failure Mode

Bond failures have been observed to be initiated by small internal cracks that exist immediately adjacent to the reinforcing bar because of concrete shrinkage that occurs during curing (ACI 408 Committee 2003). The cracks are considered to act as points of crack initiation at relatively low loads. Small splitting cracks begin to develop from the internal cracks formed in front of the ribs. As loading continues, longer longitudinal splitting cracks form (Goto 1971). In regions where transverse reinforcement is limited, splitting cracks open. As the load applied continues to

increase, the concrete in front of the reinforcing bar ribs may crush as the bar moves. The specimens that failed in bond seemed to exhibit this progression of behavior.

3.4.1 Unconfined

All the unconfined specimens failed in a brittle manner because of splice failure. Even the specimen with a $120d_b$ splice exhibited this failure mode. After an unconfined specimen failed, the #3 bars in the bottom of the specimen prevented the beam from completely collapsing. In general, the entire top cover split off the beam at the instant of failure (Figure 3.87).

3.4.2 Confined

Depending on the level of confinement, two different failure modes developed. For low levels of confinement, a splice failure with splitting occurred (Figure 3.9).

As confinement increased, a flexural failure occurred (Figure 3.10). A flexural failure occurs when the strength of the splice exceeds the strength of the beam. Instead of failing in bond within the splice region, the beam failed in compression near one of the supports. With 100 psi of transverse reinforcement in the splice region, the $60d_b$ splice failed in flexure. For an $80d_b$ splice, 50 psi of transverse reinforcement was sufficient to result in a flexural failure.

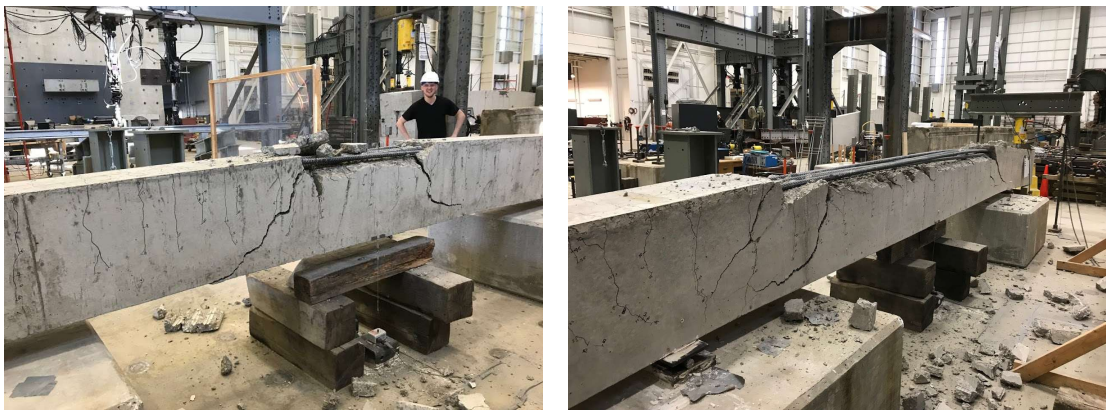

a) U-40-5a **b) U-120-5**

Figure 3.8: Typical Unconfined Specimen Failure

Figure 3.9: Typical Confined Specimen Failure (C3/60-40-5-100)

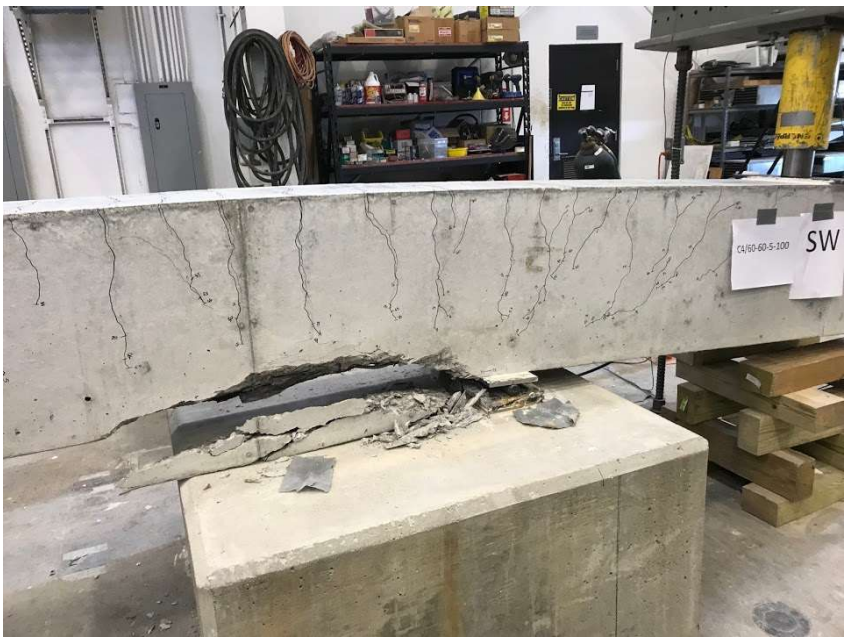

Figure 3.10: Flexural Failure (C4/60-60-5-100)

3.5 Crack Widths

Cracks were monitored over the course of testing. A specific location of four cracks in each specimen on the beam face were selected to enable consistent monitoring (Figure 3.11). At each load step, the crack width at the same location was measured with an Edmund Direct 50X microscope. All cracks selected were located outside of the splice length, but between the supports, in the constant moment region where stress is constant. Two cracks were located north of the end of the splice, and two cracks were located south of the end of the splice. As shown in Figures 3.12(a) and 3.12(b), as the load increased, there was an approximately linear increase in crack width, for both average and maximum crack widths. On average, maximum crack widths were 1.28 times the average crack width (Figure 3.13). The difference remains consistent throughout the range of bar stresses. Appendix E provides detailed information regarding location and crack widths for each specimen.

Figure 3.11: Example Crack

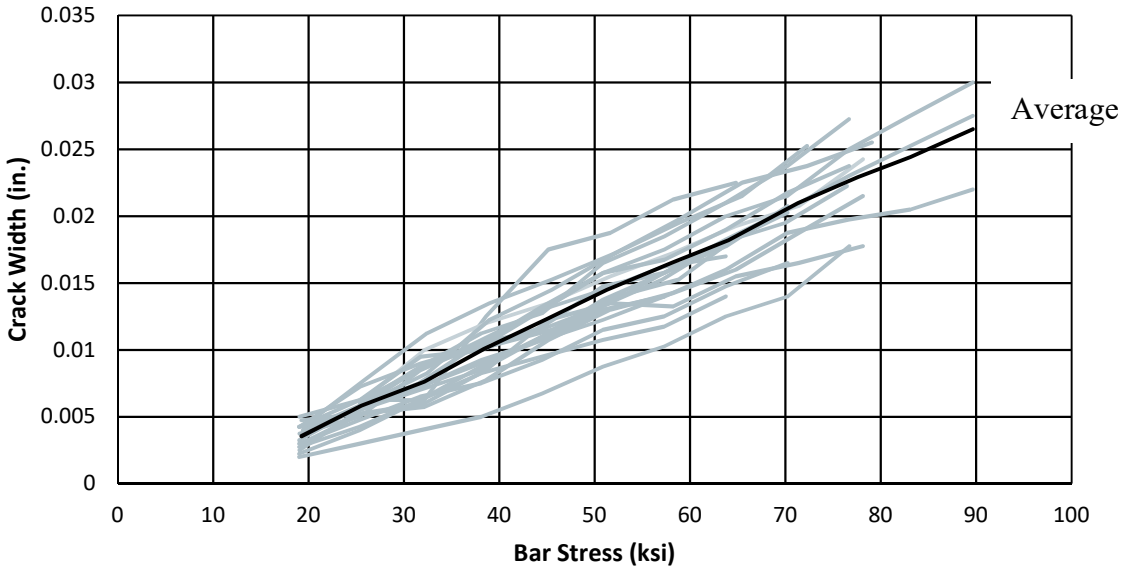

a) Average Crack Widths

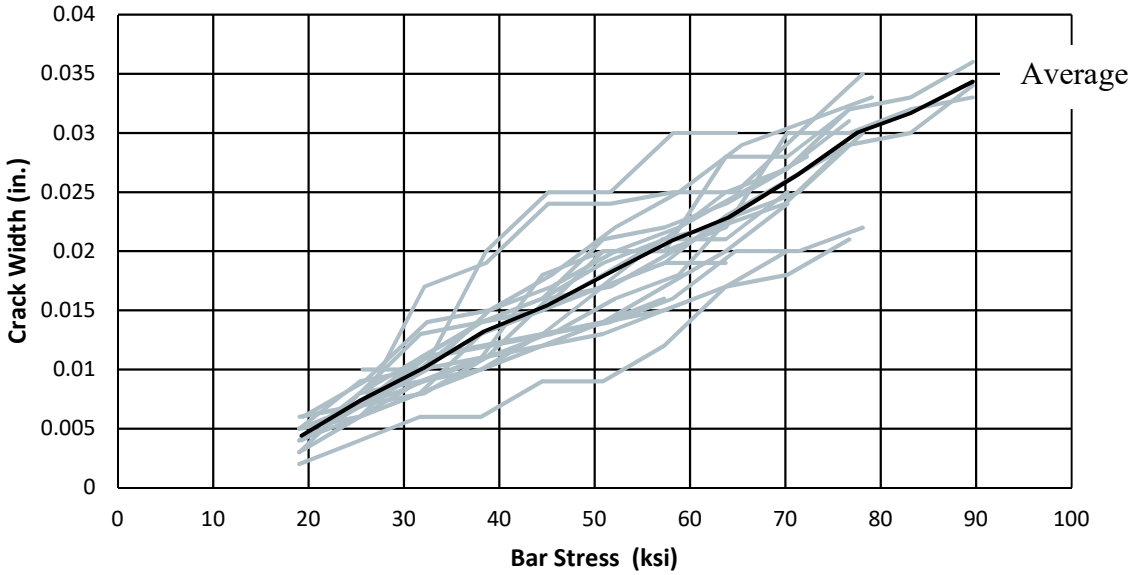

b) Maximum Crack Widths

Figure 3.12: Crack Width Measurements

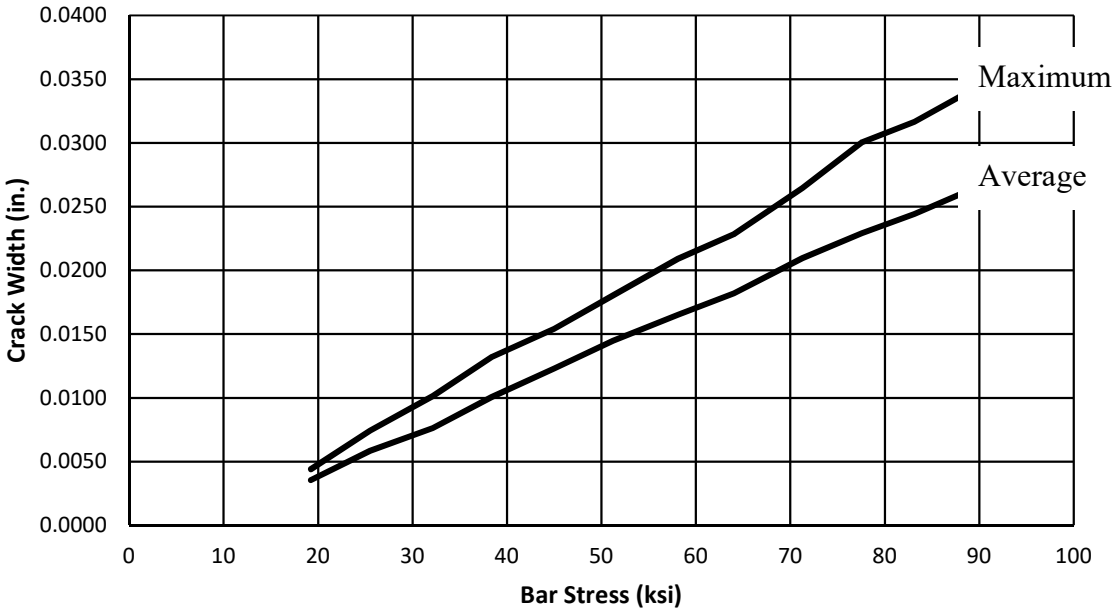

Figure 3.13: Comparison of Average and Maximum Crack Widths

4. DATA ANALYSIS

4.1 Introduction

Equations developed by past researchers along with code equations are evaluated for their appropriateness for use with high-strength reinforcement.

4.2 Bond Strength

4.2.1 ACI 318-14

Equation 25.4.2.3a in ACI 318-14 provides an equation used by designers for determining the development lengths of deformed bars. This equation was derived from the work of Orangun et al. (1977). Orangun et al. used an empirical approach rather than a theoretical approach because of the complications Ferguson and Krishnaswamy (1971) experienced while approximating the inclined force caused by the bearing of the bar deformations on the concrete. If splice failure occurs following the appearance of longitudinal cracks whether at the sides or on the tension face, only the influence of cover or spacing of the bars is of interest. Orangun's tests indicated that the average bond stress ($u = d_b f_s / 4 l_s$) for a splice in a constant moment region without transverse reinforcement was controlled by the tensile strength of the concrete (proportional to $\sqrt{f_c'}$), cover, diameter of the bar, and splice length. The constants in the equation were developed from a nonlinear regression analysis of the results of 62 beams tested by Chinn et al. (1955), Ferguson and Breen (1965), Chamberlin (1958), and Ferguson and Krishnaswamy (1971).

Because it is more practical to calculate the splice length rather than the average bond stress, the equations developed from the nonlinear regression analysis were rearranged to solve for the splice length. The work of Orangun et al. forms the basis of Equation 25.4.2.3a currently in ACI 318-14 (Equation 4-1).

$$l_d = \left[\frac{3}{40}\frac{f_y}{\lambda\sqrt{f_c'}}\frac{\Psi_t\Psi_e\Psi_s}{\left(\frac{c_b + K_{tr}}{d_b}\right)}\right]d_b \qquad (4\text{-}1)$$
$$where\ \left(\frac{c_b + K_{tr}}{d_b}\right) \leq 2.5$$

where:

A_{tr}= *total cross-sectional area of all transverse reinforcement within spacing, s, that crosses the potential plane of splitting through the reinforcement being developed, in.*

c_b= *factor that represents the least of the side cover, concrete cover to the bar (in both cases measured to the center of the bar), or one-half the center-to-center spacing of the bars*

d_b= *bar diameter, in.*

f_c'=*specified compressive strength of concrete, psi*

f_y= *specified yield strength of reinforcement, psi*

$K_{tr} = \frac{40A_{tr}}{sn}$, *transverse reinforcement index*

l_d=*development length in tension of deformed bar, in.*

n= *number of bars being spliced or developed along the plane of splitting*

s= *spacing of transverse reinforcement, in.*

Ψ_e=*coating factor (1.5 for epoxy-coated reinforcement with cover less than $3d_b$ or clear spacing less than $6d_b$; 1.2 for other epoxy-coated reinforcement; 1.0 for uncoated reinforcement); with $\Psi_t\Psi_e \leq 1.7$*

Ψ_s= *reinforcement size factor (0.8 for No. 6 and smaller bars; 1.0 for No. 7 and larger bars)*

Ψ_t= *reinforcement location factor (1.3 for reinforcement placed so that more than 12 in. of fresh concrete is cast below the development length or splice; 1.0 for other reinforcement)*

λ= *lightweight aggregate concrete factor (1.3 for lightweight concrete; 1.0 for normalweight concrete;* $\frac{f_{ct}}{6.7\sqrt{f_c'}} \leq 1.0$ *for lightweight concrete with split cylinder strength, f_{ct}, specified)*

Figure 4.1 compares the bar stress calculated based on Equation 4-1 from ACI 318-14 (f_{calc}) to the bar stress calculated according to the moment curvature method (f_{test}), and based on the maximum average load, P_{ult}. A f_{test}/f_{calc} ratio above 1.0 is conservative, meaning that the bar stress calculated was lower than the bar stress obtained during testing. The value of 1.0, which divides conservative values from unconservative values is represented by the thick black line in

Figure 4.1. The yellow bars in Figure 4.1 indicate those specimens which had a bar stress at failure beyond the elastic limit of the longitudinal bars (Section 2.4.1.1). These specimens are different because evaluation of bond strength is of most interest in the elastic region. Post elastic limit behavior means that the bars are yielding.

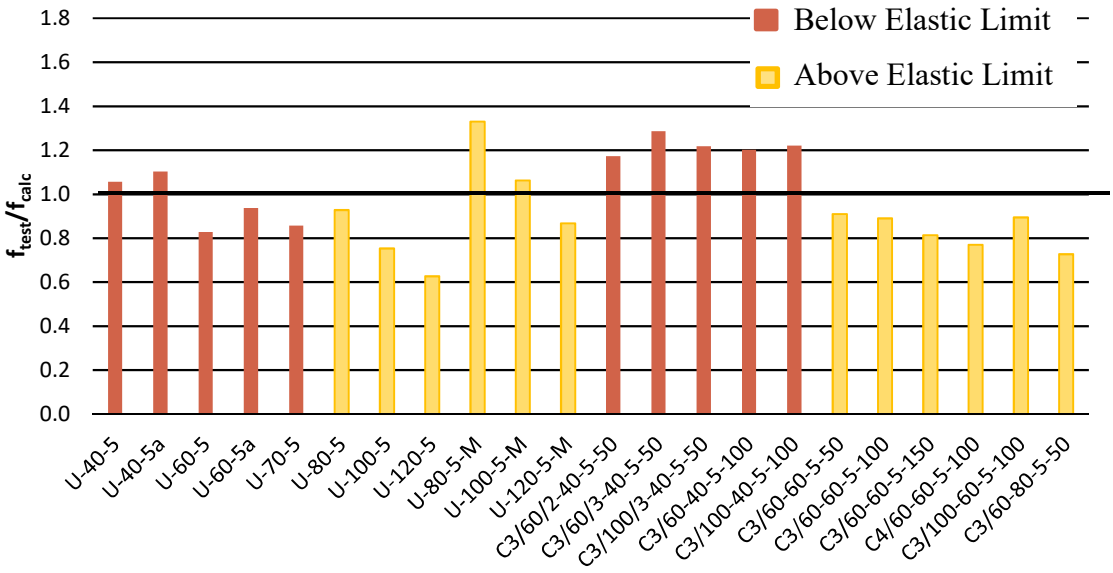

Figure 4.1: Comparison of Strength Calculations for Equation 4-1

As seen from Figure 4.1, bar stresses for unconfined specimens with bar lengths longer than $40d_b$ were unconservative when calculated according to ACI 318-14. Another interesting observation is that the equation underpredicted the stress by 33% for Specimen U-80-5-M even though the specimen had reached its elastic limit. ACI 318-14 equation reliably predicted the strength of the $40d_b$ specimens. This may be a result of the equation being largely based on data with splice lengths less than $40d_b$ resulting in lower failure stresses.

4.2.2 ACI 408R-03

The equation developed by ACI Committee 408 (ACI 408R-03) is based on the work by Zuo and Darwin (1998, 2000). Zuo and Darwin expanded the work of Darwin, Zuo, Tholen, and Idun (1996) by increasing the number of specimens in the database to include 171 unconfined and 196 confined bottom-cast splice test specimens. Zuo and Darwin (1998, 2000) investigated the effects of the c_{max}/c_{min} ratio, the relative rib area, and the fourth root of the concrete compressive

strength, instead of the square root (ACI Committee 408 2003). The empirical, best-fit equations from Zuo and Darwin (1998, 2000) were converted into design expressions which incorporated strength reduction factors, φ, to ensure a lower probability of failure. The φ-factor used for bond depends on the φ-factor used for tension, as well as the other load factors used in the analysis. Factors for bond were based on a Monte Carlo analysis conducted for various φ-factors for tension and load combinations (Table 4.1) (ACI Committee 408 2003). Equations 4-2 and 4-3 were developed by the ACI 408 Committee, with corresponding φ-factors. It should be noted that Equation 4-2 is intended for use with ACI 318-14 considering the load combination (1.2D+1.6L) and the φ-factor for tension (0.9).

Table 4.1: φ-Factors for Tension and Load Combinations

$\varphi_{tension}$	Load Combination	φ_{bond}
0.9	1.2D+1.6L	0.82
0.9	1.4D+1.7L	0.92
0.8	1.2D+1.6L	0.92

$$For\ \varphi = 0.82, \frac{l_d}{d_b} = \frac{\left(\frac{f_y}{f'^{1/4}_c} - 1970\omega\right)\alpha\beta\lambda}{62\left(\frac{c\omega + K_{tr}}{d_b}\right)} \tag{4-2}$$

$$For\ \varphi = 0.92, \frac{l_d}{d_b} = \frac{\left(\frac{f_y}{f'^{1/4}_c} - 2210\omega\right)\alpha\beta\lambda}{70.2\left(\frac{c\omega + K_{tr}}{d_b}\right)} \tag{4-3}$$

$$where\ \frac{c\omega + K_{tr}}{d_b} \leq 4.0$$

where:

A_{tr} = *total cross-sectional area of all transverse reinforcement within spacing, s, that crosses the potential plane of splitting through the reinforcement being development, in.*

c = *spacing or cover dimension,* $c_{min} + 0.5d_b$, *in.*

c_b = *bottom cover, in.*

c_s = *minimum (*c_{so}, c_{si}*+0.25 in.), in.*

c_{si} = *half of bar clear spacing, in.*

c_{so}= *side cover, in.*

c_{max}= *maximum(c_b,c_s), in.*

c_{min}= *minimum(c_b,c_s), in.*

d_b= *bar diameter, in.*

f_c'=*specified compressive strength of concrete, psi*

f_y= *specified yield strength of reinforcement, psi*

K_{tr}= *transverse reinforcement index,* $\left(\frac{0.52 t_r t_d A_{tr}}{sn}\right) f_c'^{1/2}$ *or* $\left(\frac{0.5 t_d A_{tr}}{sn}\right) f_c'^{1/2}$ *for conventional reinforcement corresponding to an R_r value of 0.0727*

l_d= *development length in tension of deformed bar, in.*

n= *number of bars being spliced or developed along the plane of splitting*

s= *spacing of transverse reinforcement, in.*

t_d=*term representing the effect of bar size on T_s, $0.78d_b+0.22$*

t_r= *term representing the effect of relative rib area on Ts, $9.6R_r+0.28 \leq 1.72$*

T_s= *steel contribution to total bond force, the additional bond strength provided by the transverse steel*

R_r=*relative rib area of reinforcement*

α=*reinforcement location factor (1.3 for reinforcement placed so that more than 12 in. of fresh concrete is cast below the development length or splice; 1.0 for other reinforcement)*

β=*coating factor (1.5 for epoxy-coated reinforcement with cover less than 3db or clear spacing less than 6db; 1.2 for other epoxy-coated reinforcement; 1.0 for uncoated reinforcement); with $\alpha\beta \leq 1.7$*

λ= *lightweight aggregate concrete factor (1.3 for lightweight concrete; 1.0 for normalweight concrete;* $\frac{6.7\sqrt{f_c'}}{f_{ct}} \geq 1.0$ *for lightweight concrete with split cylinder strength, f_{ct}, specified)*

$$\omega = 0.1\frac{c_{max}}{c_{min}} + 0.9 \leq 1.25$$

Figure 4.2 compares the bar stress calculated according to ACI 408R-03 (f_{calc}) to the bar stress determined from the maximum average load (f_{test}).

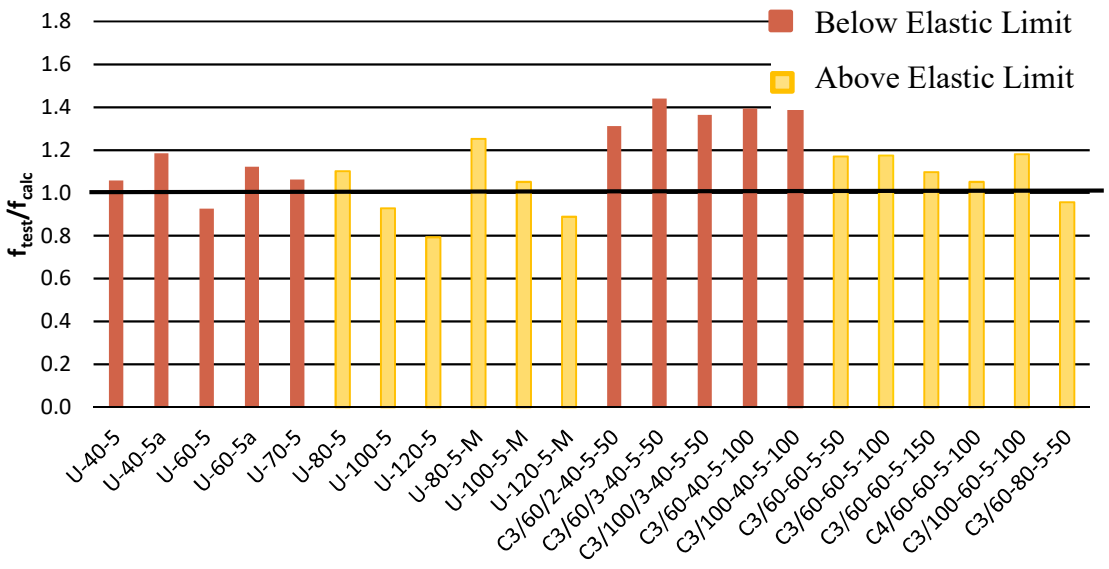

Figure 4.2: Comparison of Strength Calculations for Equation 4-2

As seen from Figure 4.2, most of the specimens were conservatively predicted using Equation 4-2. Specimen U-80-5-M was conservative, although it reached its elastic limit. Equation 4-2 only underpredicted the bar stress by 25% compared with the 33% ACI 318-14 underpredicted the bar stress. Another observation is that Equation 4-2 underpredicted the bar stress for the confined $40d_b$ specimens by as much as 44%.

Equation 4-3 yielded similar trends, except that the equation was less conservative (Figure 4.3) as expected because of the increased φ-factor. More of the test results yielded unconservative results when compared with Equation 4-3 instead of Equation 4-2. Although ACI 408R-03 predicts the strength better than ACI 318-14, it still yields unconservative results for longer splice lengths and is conservative for short splices with confinement.

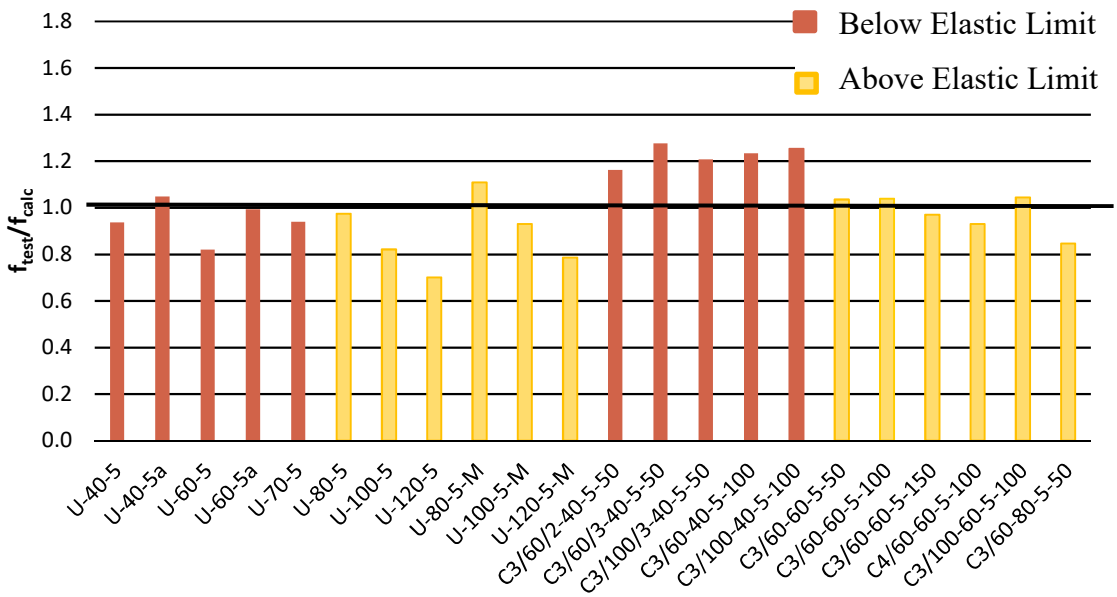

Figure 4.3: Comparison of Strength Calculations for Equation 4-3

4.2.3 Proposal CB 603

The current ACI 318-14 design expression for calculating development and splice lengths of straight bars (Equation 4-1) limits the reinforcement yield strength to 80 ksi and the value of $\sqrt{f_c'}$ to 100 if the compressive strength of the concrete exceeds 10 ksi. Using recent tests from Seliem et al. (2009) and results from the ACI 408 database, an equation was developed that could account for a larger range of material properties. The equation is primarily based on the equation from ACI 408. The proposed ACI 318 equation (CB 603) uses variables already defined in ACI 318-14 and recalculates the constants (m_1 and m_2) to better represent the trends of the expanded database (Equation 4-4).

$$\frac{l_d}{d_b} = \frac{\left(\frac{f_y}{\varphi {f_c'}^{0.25}} - m_2\right)\Psi_t\Psi_e}{m_1\lambda\left(\frac{c_b\omega + K_{tr}}{d_b}\right)} \tag{4-4}$$

Instead of using the equation for ω defined in ACI 408 (Equation 4-2 and Equation 4-3) that is based on the bar spacing and cover, a simplified definition is adopted. When the clear spacing of longitudinal reinforcement is at least six times the concrete clear cover and the clear side cover is

at least three times the concrete clear cover, normal to the plane, ω=1.25, otherwise, ω=1.0. Additionally, as defined in ACI 408-03, the confinement term, $(c_b\omega+K_{tr})/d_b$ has a limit of 4. The simplified definition for K_{tr} used in ACI 318-14 is used for this proposed equation. Equation 4-4 is simplified further by introducing the modification factor, Ψ_y, shown in Equation 4-5.

$$\Psi_y = \left(1 - m_2 \frac{\varphi {f_c'}^{0.25}}{f_y}\right) \tag{4-5}$$

Substituting the modification factor, Ψ_y (shown in Equation 4-5), Equation 4-4 becomes 4-6.

$$\frac{l_d}{d_b} = \frac{\left(\frac{f_y}{\varphi {f_c'}^{0.25}}\right)\Psi_t\Psi_e\Psi_y}{m_1\lambda\left(\frac{c_b\omega + K_{tr}}{d_b}\right)} \tag{4-6}$$

The equation can be simplified even further by dropping the f_c' term in the Ψ_y equation (Equation 4-5). Equation 4-5 can be simplified to Equation 4-7.

$$\Psi_y = \left(1 - \frac{\varphi m_3}{f_y}\right) \tag{4-7}$$

The constants m_1 and m_3 were derived by minimizing the square of the differences between the measured and calculated bar stresses. Substituting the coefficients and φ-factor, Equations 4-6 and 4-7 become 4-8 and 4-9 respectively.

$$\frac{l_d}{d_b} = \frac{\left(\frac{f_y}{{f_c'}^{0.25}}\right)\Psi_t\Psi_e\Psi_y}{58.4\lambda\left(\frac{c_b\omega + K_{tr}}{d_b}\right)} \tag{4-8}$$

$$\Psi_y = \left(1 - \frac{20{,}600}{f_y}\right) \tag{4-9}$$

For convenience, Ψ_y can be made to equal 1.0 when f_y=60,000 psi. Equations 4-8 and 4-9 become Equation 4-10.

$$l_d = \left(\frac{1}{90} \frac{f_y}{\lambda {f_c'}^{0.25}} \frac{\Psi_t \Psi_e \Psi_y}{\left(\frac{c_b \omega + K_{tr}}{d_b} \right)} \right) d_b \qquad (4\text{-}10)$$

$$where\ \Psi_y = \left(1.5 - \frac{30{,}000}{f_y} \right) \geq 0.75$$

$$\left(\frac{c_b \omega + K_{tr}}{d_b} \right) \leq 4$$

where:

A_{tr} = *total cross-sectional area of all transverse reinforcement within spacing, s, that crosses the potential plane of splitting through the reinforcement being development, in.*

c_b = *factor that represents the least of the side cover, concrete cover to the bar (in both cases measured to the center of the bar), or one-half the center-to-center spacing of the bars*

c_c = *clear bottom cover of reinforcement, in.*

d_b = *bar diameter, in.*

f_c' =*specified compressive strength of concrete up to 16,000 psi, psi*

f_y = *specified yield strength of reinforcement, psi*

$K_{tr} = \frac{40A_{tr}}{sn}$, *transverse reinforcement index*

l_d = *development length in tension of deformed bar, in.*

n = *number of bars being spliced or developed along the plane of splitting*

s = *spacing of transverse reinforcement, in.*

Ψ_e =*coating factor (1.5 for epoxy-coated reinforcement with cover less than $3d_b$ or clear spacing less than $6d_b$; 1.2 for other epoxy-coated reinforcement; 1.0 for uncoated reinforcement); with $\Psi_t \Psi_e \leq 1.7$*

Ψ_t = *reinforcement location factor (1.3 for reinforcement placed so that more than 12 in. of fresh concrete is cast below the development length or splice; 1.0 for other reinforcement)*

Ψ_y = *factor used to modify development length based on yield strength of reinforcement*

λ = *lightweight aggregate concrete factor (1.3 for lightweight concrete; 1.0 for normalweight concrete; $\frac{f_{ct}}{6.7\sqrt{f_c'}} \leq 1.0$ for lightweight concrete with split cylinder strength, f_{ct}, specified)*

$\omega = 1.25\ if\ 2c_{si} \geq 6c_C\ AND\ c_{si} \geq 3c_c; 1.0\ otherwise$

Figure 4.4 compares the bar stress calculated according to Equation 4-10 (f_{calc}) to the bar stress determined from the maximum average load (f_{test}).

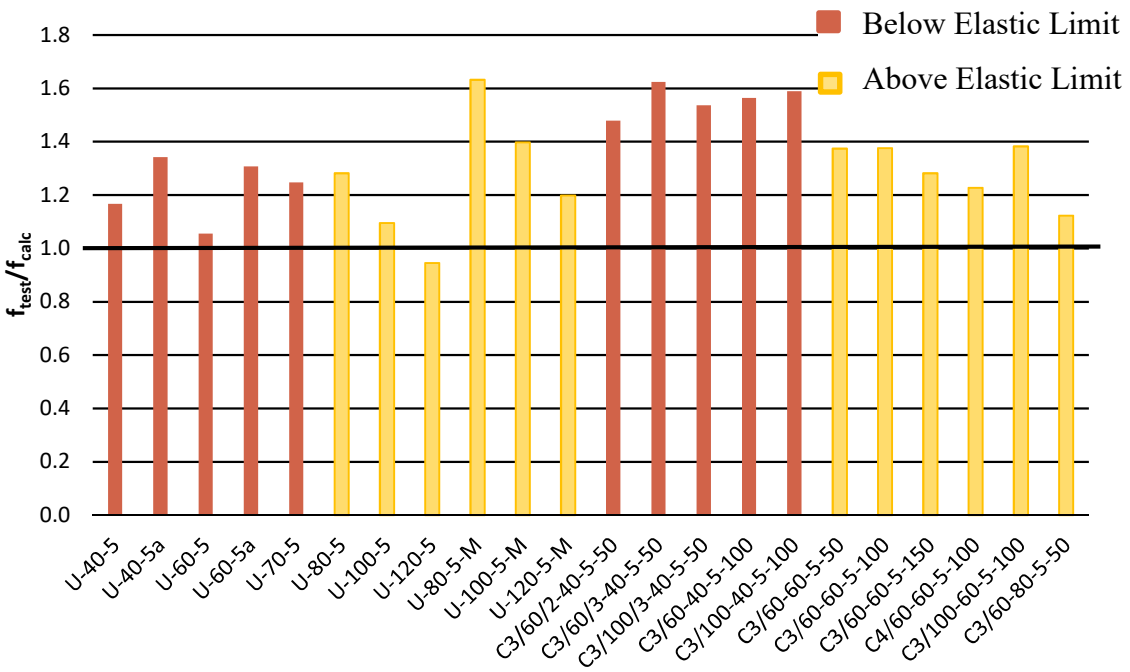

Figure 4.4: Comparison of Strength Calculations for Equation 4-10

As seen from Figure 4.4, most of the specimens were conservatively predicted using Equation 4-10. Specimen U-80-5-M was conservative, although it reached its elastic limit. Proposal CB 603 underpredicted the bar stress by 63% compared with the 33% ACI 318-14 underpredicted the bar stress and the 25% ACI 408R-03 (Equation 4-2) underpredicted the stress. Another observation is that Proposal CB 603 underpredicted the bar stress for the confined $40d_b$ specimens by as much as 62%.

4.2.4 Equation Developed by Pay (2005)

Observations of the effect of axial stiffness and splice length provided the basis for the development of an equation developed by Pay (2005). It was noticed that as the axial stiffness of reinforcing bar increased, the bar stress at failure also increased. Additionally, the effect of splice length on the ultimate stress achieved by the bar is ultimately controlled by the axial

stiffness of the reinforcement. Observing the impact of these factors, a variable L_{eq}, was established to normalize different bar sizes or reinforcement types. L_{eq} represents the splice length required for the reference reinforcement to reach the same bar force as reinforcement having a splice length l_s, cross-sectional area A_b, and modulus of elasticity E_b (Equation 4-11).

$$L_{eq} = l_s \frac{E_b A_b}{E_{ref} A_{ref}} \quad (4\text{-}11)$$

where:

A_b = *area of spliced reinforcement, in.*^{2}

A_{ref} = *area of reference reinforcement, in.*^{2}

E_b = *modulus of elasticity of the spliced reinforcement, ksi*

E_{ref} =*modulus of elasticity of reference reinforcement, ksi*

L_{eq} = *equivalent splice length of reference reinforcement, in.*

l_s =*splice length, in.*

Although the reference reinforcement can be anything, Pay used #5 wrapped, sand coated glass FRP bar.

$A_{ref} = 0.31\ in.^2$ *(area of #5 bar)*

$E_{ref} = 5{,}800\ ksi$ *(modulus of elasticity of wrapped, sand coated Glass FRP)*

A trendline based on data from a combined FRP and steel reinforcing bar database was developed using regression analysis. The resulting equation from the best fit curve is shown in Equation 4-12.

$$F_b \sqrt[4]{4000/f'_c} = 2.1 L_{eq}^{0.50} M \quad (4\text{-}12)$$

Cover and bar spacing dimensions were used to modify the best fit curve as the effect of splice length was already accounted for in the equivalent lap splice length, L_{eq}. Specimens were grouped based on their failure mechanism (face or side splitting). Again, the trend was plotted with a best fit curve. Based on this analysis, modification factors, M, were derived to

incorporate the effects of cover and bar spacing on bond strength. A general equation that can be used for both face and side splitting failures is given in Equation 4-13.

$$M = 0.20\left(\frac{c}{d_b}\right) + 0.75 \tag{4-13}$$

where:

c= minimum of c_{si} or c_b, in. (see Figure 1.3)

After substituting the bar force for the bar stress multiplied by the bar area, Equation 4-12 can be rearranged to solve for l_s as shown in Equation 4-14. This equation is used for analysis purposes as it provides a best predictor.

$$\frac{l_s}{d_b} = \frac{20{,}280}{E_b}\frac{f_b^2 d_b}{\sqrt{f'_c}}\left(\frac{1}{\left(0.20\left(\frac{c}{d_b}\right) + 0.75\right)}\right)^2 \tag{4-14}$$

The cover modification factor can be approximated as 1 to simplify the expression even further. This simplifies Equation 4-14 to Equation 4-15.

$$\frac{l_s}{d_b} = \frac{20{,}280}{E_b}\frac{f_b^2 d_b}{\sqrt{f'_c}} \tag{4-15}$$

Because the cover to bar diameter ratio was limited to 3.0 in the database, the cover to bar diameter ratio should not be taken as larger than 3.0. After adding a bar stress factor of 1.19, to yield conservative results 97.5% of the time, Equation 4-14 becomes Equation 4-16 for use in design.

$$\frac{l_s}{d_b} = \frac{29{,}000}{E_b}\frac{f_b^2 d_b}{\sqrt{f'_c}}\left(\frac{1}{\left(0.20\left(\frac{c}{d_b}\right) + 0.75\right)}\right)^2 \tag{4-16}$$
$$where\ \frac{c}{d_b} \leq 3.0$$

where:

c= minimum of c_{si} or c_b, in.

c_b = *bottom cover, in.*

c_{si} = *half of the bar clear spacing, in.*

d_b = *bar diameter, in.*

E_b = *modulus of elasticity of the spliced reinforcement, ksi*

f_b = *bar stress at failure, ksi*

f_c' = *specified compressive strength of concrete, psi*

l_s = *development length in tension of deformed bar, in.*

If the cover modification factor is approximated as 1, Equation 4-16 simplifies to Equation 4-17.

$$\frac{l_s}{d_b} = \frac{29{,}000}{E_b}\frac{f_b^2 d_b}{\sqrt{f'_c}} \qquad (4\text{-}17)$$

Figure 4.5 compares the bar stress calculated according to Equation 4-15 developed by Pay (2005) (f_{calc}) to the bar stress determined from the maximum average load (f_{test}). It should be noted that f_{calc} represents the stress calculated based on the analysis equation developed by Pay (2005), using the factor 20,280 and no cover modification factor. Figure 4.5 only compares the results from the unconfined beams since Pay did not develop an equation to characterize the additional strength provided by transverse reinforcement. Although some of the results are unconservative, this equation is meant for analysis. Calculations for specimens that did not reach their elastic limit were within 8% of the bar stress measured from testing.

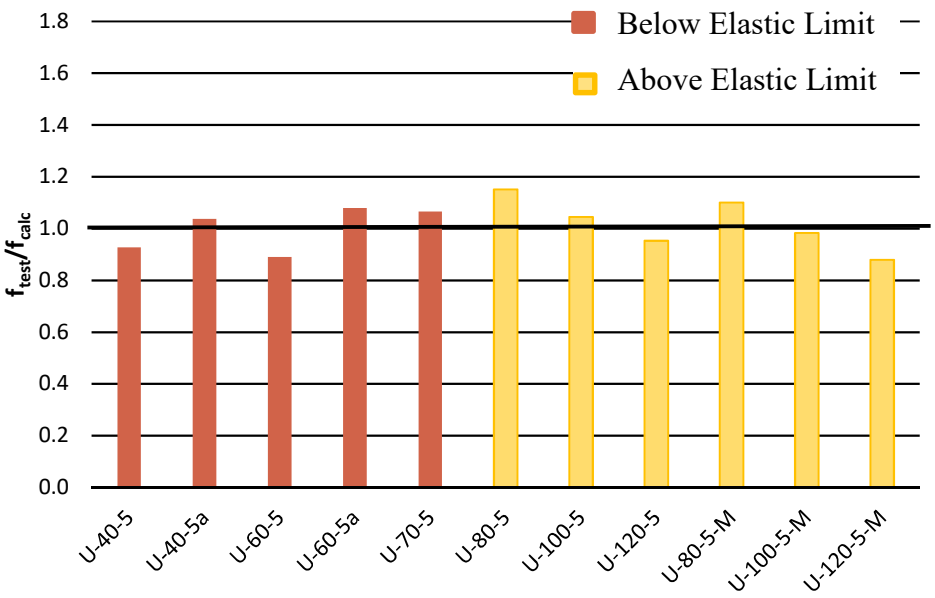

Figure 4.5: Comparison of Strength Calculations for Equation 4-15

Figure 4.6 compares the bar stress calculated according to Equation 4-17 developed by Pay (2005) (f_{calc}) to the bar stress determined from the maximum average load (f_{test}). It should be noted that f_{calc} represents the stress calculated based on the design equation developed by Pay (2005), using the factor 29,000 and no cover modification factor. The design equation developed by Pay does not yield any unconservative results unlike both the ACI 318-14 and ACI 408R-03 equations. Additionally, the specimens that did not reach their inelastic limit had bar stresses that were reliably predicted within 29% of the test results.

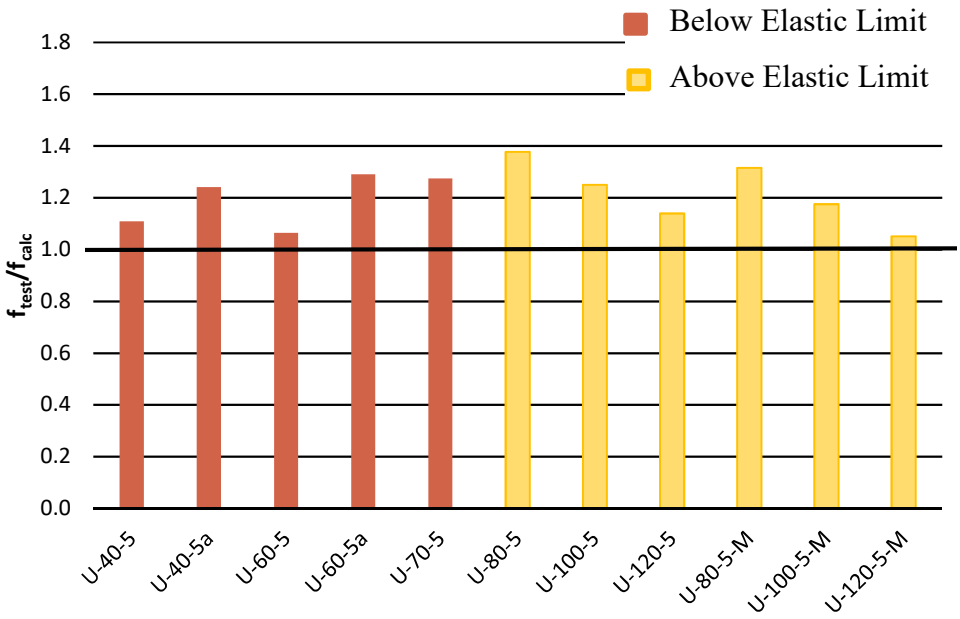

Figure 4.6: Comparison of Strength Calculations for Equation 4-17

4.2.5 Equation Developed by Sim (2014)

An equation for determining the splice length was found by normalizing variables of interest into dimensionless groups (Sim 2014). The Buckingham Π theorem was applied to determine the number of meaningful equations involved. The Buckingham Π theorem states that a meaningful equation involving n variables and k fundamental dimensions can be equivalently rewritten as an equation on n-k dimensionless parameters. Sim determined seven variables of interest (f_b, f'_c, l_s, d_b, c_{min}, F_{tr}, AE) and two dimensions (force and length). Based on the Buckingham Π theorem, five dimensionless ratios were developed. By substituting f_b for the relationship in terms of concrete strength, $k_b(f'_c)^b$, and $A_{ref}E_{ref}$ to represent the axial rigidity of the reference reinforcing bar, the five dimensionless ratios become:

$$\Pi_1 = \frac{F_b}{\pi d_b l_s f_b} \tag{4-18}$$

$$\Pi_2 = \frac{l_s}{d_b} \tag{4-19}$$

$$\Pi_3 = \frac{c_{min}}{d_b} \tag{4-20}$$

$$\Pi_4 = \frac{F_{tr}}{\pi d_b l_s f_b} \tag{4-21}$$

$$\Pi_5 = \frac{AE}{A_{ref}E_{ref}} \tag{4-22}$$

The dimensionless ratio, Π_5 (Equation 4-22), can be neglected because the steel reinforced concrete database only contains specimens with steel reinforcing bars with equivalent moduli of elasticity.

To find a relationship between the dimensionless ratios for spliced beam tests without confinement, the fourth dimensionless ratio (Equation 4-21) for confinement was also neglected. The resulting dimensionless equation becomes Equation 4-23. The constants, k, b_1, b_2, and b_3, were determined from a regression analysis of 252 unconfined beams.

$$\frac{F_b}{\pi d_b l_s} = k(f'_c)^{b_1}\left(\frac{l_s}{d_b}\right)^{b_2}\left(\frac{c_{min}}{d_b}\right)^{b_3} \tag{4-23}$$

where:

c_b = *bottom clear cover of reinforcing bars, in.*

c_{min} = *minimum(c_{so}, c_{si}, c_b), in.*

c_{si} = *half of clear spacing between bars, in.*

c_{so} = *side clear cover of reinforcing bars, in.*

d_b = *nominal diameter of bar, in.*

f_b = *bar stresses at failure, psi*

F_b = *bar force at failure, psi*

f'_c = *specified compressive strength of concrete, psi*

l_s = *splice or development length, in.*

After noticing that the side cover to bar diameter ratio (c_{so}/d_b) has a larger influence than the minimum cover to bar diameter ratio (c_{min}/d_b), the ratio of the minimum cover to bar diameter (c_{min}/d_b) was replaced with the ratio of side cover to bar diameter ratio (c_{so}/d_b) in Equation 4-24. Again, the constants were determined from regression analysis.

$$\frac{F_b}{\pi d_b l_s} = 0.25\sqrt[4]{f'_c}\sqrt{\frac{d_b}{l_s}}\sqrt[4]{\frac{c_{so}}{d_b}} \tag{4-24}$$

Equation 4-24 was transformed into a logarithmic form to preserve the linear model, while investigating the nonlinear relationship between bond stress and splice length as given by Equation 4-25.

$$\frac{l_s}{d_b} = \frac{f_b^2}{\sqrt{f'_c}} \frac{1}{\sqrt{\frac{c_{so}}{d_b}}} \tag{4-25}$$

where:

c_{so} = *side clear cover of reinforcing bars, in.*

d_b = *nominal diameter of bar, in.*

f_b = *bar stresses at failure, psi*

f'_c = *specified compressive strength of concrete, psi*

l_s =*splice or development length, in.*

As with the equation developed by Pay, the cover modification factor can be approximated as 1 to further simplify the expression. Equation 4-25 then becomes Equation 4-26.

$$\frac{l_s}{d_b} = \frac{f_b^2}{\sqrt{f'_c}} \tag{4-26}$$

Figure 4.7 compares the bar stress calculated according to Equation 4-26 developed by Sim (2014) (f_{calc}) to the bar stress determined from the maximum average load (f_{test}). All the predictions using the unconfined term developed by Sim produced conservative results. For the case of specimens reinforced with #8 steel bars (d_b=1.0), the equation Sim developed for unconfined specimens (Equation 4-26) is the same as the design equation developed by Pay (Equation 4-17). Therefore, Figure 4.7 is identical to Figure 4.6.

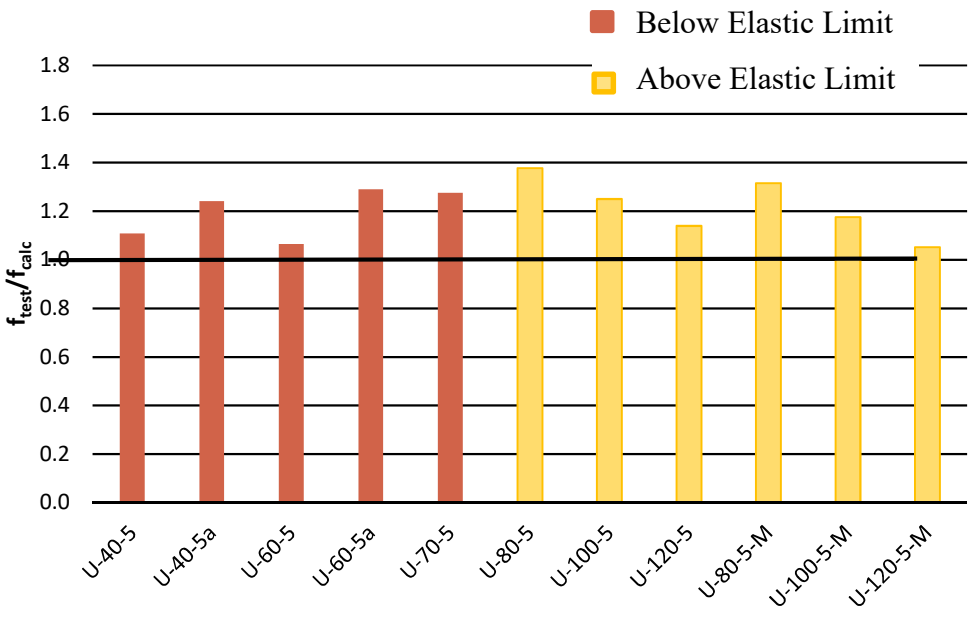

Figure 4.7: Comparison of Strength Calculations for Equation 4-26

To determine the effects of confinement, identical specimens with varying amounts of transverse reinforcement were compared by Sim. The contribution of confinement, F_{tr}, was calculated by subtracting the bar force obtained from an identical unconfined specimen. To develop an equation that calculates the confining force on one spliced bar, the force of all stirrups was divided by the number of spliced bars, N_b. A contribution factor, k, was solved for from each test. The contribution factor is designed to represent the actual contribution of the transverse reinforcement as past studies have shown that transverse reinforcement may not reach yield. It has also been shown that only a certain number of stirrups at the splice ends will be effective in contributing to the splice strength. The range of k values was spread wider when the splice length was less than $20d_b$. Ignoring beams with splice lengths less than $20d_b$, the average value of the contribution factor was found to be 0.5. The resulting equation used to characterize the additional force provided by transverse reinforcement is expressed by Equation 4-27.

$$F_{tr} = k\frac{A_{tr}f_{yt}}{N_b}N_s \qquad (4\text{-}27)$$

where:

A_{tr} = *total area of transverse reinforcement crossing the potential splitting plane* ($A_{tr}=A_{tr,1bar}N_l$), *in.*^{2}

$A_{tr,1bar}$ = *area of one leg of transverse reinforcement, in.*^{2}

f_{yt} = *yield strength of transverse reinforcement, kips*

F_{tr} = *contribution of transverse reinforcement in splice region, kips*

k = *contribution factor, ½*

N_b = *number of spliced or developed bars*

N_l = *number of legs of transverse reinforcement that cross the splitting plane*

N_s = *number of stirrups*

The two terms, F_b and F_{tr} can be added to produce an equation for the determination of the bar strength (Equation 4-28).

$$f_s = \sqrt[4]{f'_c}\sqrt{\frac{l_s}{d_b}}\sqrt[4]{\frac{c_{so}}{d_b}} + \frac{1}{2}\frac{A_{tr}f_{yt}}{N_b A_b}N_s \qquad (4\text{-}28)$$

As with the equation developed by Pay, the cover modification factor can be approximated as 1 for simplicity. Equation 4-28 becomes Equation 4-29.

$$f_s = \sqrt[4]{f'_c}\sqrt{\frac{l_s}{d_b}} + \frac{1}{2}\frac{A_{tr}f_{yt}}{N_b A_b}N_s \qquad (4\text{-}29)$$

Rearranging Equation 4-28, the equation for the determination of splice length with confinement becomes Equation 4-30.

$$l_s = \left[\frac{(f_s - f_{tr})^2}{\sqrt{f'_c}}\frac{1}{\sqrt{\frac{c_{so}}{d_b}}}\right]d_b\Psi_b \qquad (4\text{-}30)$$

where:

A_b = *area of spliced bar, in.*^{2}

A_{tr} = *total area of transverse reinforcement crossing the potential splitting plane* ($A_{tr}=A_{tr,1bar}N_l$), *in.*^{2}

$A_{tr,1ba}$ = *area of one leg of transverse reinforcement, in.*^{2}

c_{so} = *side clear cover of reinforcing bars, in.*

d_b = *nominal diameter of bar, in.*

f_c' = *specified compressive strength of concrete, psi*

f_s = *bar stresses at failure, psi*

f_{tr} = *bar stress contribution from confinement, ksi,* $\left(\frac{1}{2}\frac{A_{tr}f_{yt}}{A_b N_b}N_s\right)$

f_{yt} = *yield strength of transverse reinforcement, kips*

l_s =*splice or development length, in.*

N_b = *number of spliced or developed bars*

N_l = *number of legs of transverse reinforcement that cross the splitting plane*

N_s = *number of stirrups*

Ψ_b = *modification factor for different bar types*

Figure 4.8 compares the bar stress calculated according to Equation 4-29 developed by Sim (2014) (f_{calc}) to the bar stress determined from the maximum average load for confined specimens (f_{test}). To determine f_{calc}, the yield stress based on the 0.2% offset method was used to calculate f_{yt}.

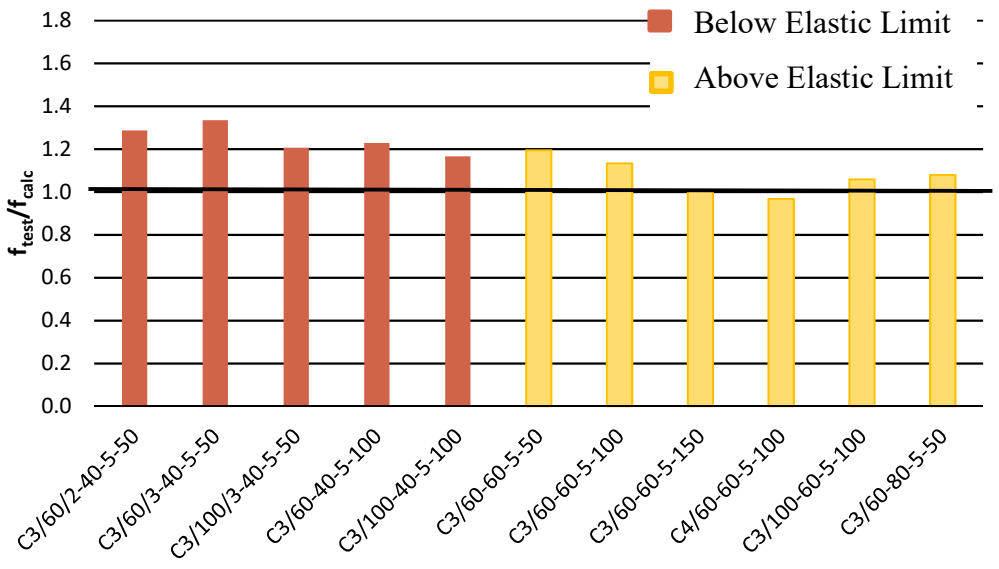

Figure 4.8: Comparison of Strength Calculations for Equation 4-29

The equation developed by Sim conservatively determines the strength of confined specimens that did not reach their elastic limit. All values are predicted within 34% of the testing values.

4.2.6 Unconfined Analysis Term Developed by Pay (2005) and Confined Term Developed by Sim (2014)

While Pay focused on unconfined specimens, Sim's relationship for confinement can be used to provide the additional influence of transverse reinforcement. Therefore, a comparison of the results combining these two approaches was evaluated. Figure 4.9 compares the results of the confined beams. The term f_{calc} represents the stress calculated based on Pay's analysis equation using the analysis factor, 20,280 and no cover modification factor (Equation 4-15), and Sim's confinement term, f_{tr} (second term of Equation 4-29). For steel reinforcing bars, the combined unconfined and confined terms become Equation 4-31.

$$f_s = 1.2\sqrt[4]{f'_c}\frac{\sqrt{l_s}}{d_b} + \frac{1}{2}\frac{A_{tr}f_{yt}}{N_b A_b}N_s \qquad (4\text{-}31)$$

To determine f_{calc}, the yield stress based on the 0.2% offset method was used to calculate f_{yt}. The analysis equation developed by Pay combined with the confinement term developed by Sim conservatively predicts the behavior of the confined specimens. The test results are within 15% of the calculated bar stress. It should be noted that for #8 bars, the equation developed by Sim for unconfined beams is identical to the equation developed by Pay. Based on this analysis, a reduction in the factor used to add conservatism between the analysis and design equation can be used to fine tune the appropriate level of safety. Numerical stress values for each of the different methods are included in Appendix F.

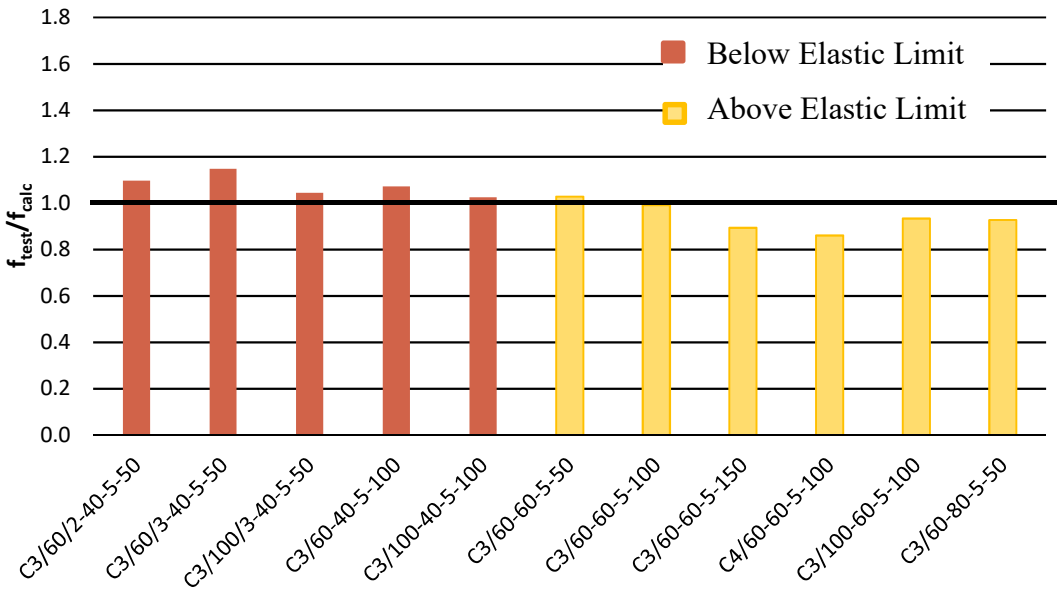

Figure 4.9: Comparison of Strength Calculations for Equation 4-31

5. ANALYSIS AND DESIGN METHODS

5.1 Introduction

In Chapter 4, the methods were evaluated using the data from the beams tested in this experimental program. This chapter evaluates the effects of the parameters investigated in this experimental program to develop a design equation that is appropriate for all grades and splice lengths.

5.2 Influence of Investigated Parameters

The variables investigated in this experimental program are described in depth in Chapter 2. The variables tested in this program include splice length, bar spacing, spacing of transverse reinforcement, and yield strength of transverse reinforcement. All specimens were bottom-cast with similar concrete mixes. The variables are compared using the load-deflection curves and the unnormalized bar stresses in this section.

5.2.1 Splice Length

The effect of splice length on bond strength was investigated in this program. The general trend was a nonlinear increase in bar stress, f_s, as the splice length, l_s, increased. As the splice length increased, the effectiveness per unit length decreased. There was scatter even among specimens that had the same properties.

5.2.1.1 Unconfined

Figure 5.1 shows the relationship between splice length and bond strength. In Figure 5.1, all specimens, except for U-40-5a, exceeded their elastic limits during testing. The bars that reached the elastic limit are noted because of the round house stress-strain curve that is representative of Grade 100 steel (Figure 2.6). As shown in Appendix D, unconfined specimens cannot endure as much bar strain as confined specimens. Because all longitudinal bars in this experimental program are #8 bars, with a diameter of 1 in., the splice length represented in

Figure 5.1(a), in terms of in. is equivalent to the splice length in terms of bar diameter. Figure 5.1(b) shows that with an increase in splice length, there is additional strength added to the splice length up until the longitudinal bars progress beyond their elastic yield. As shown, the behavior is non-linear. The increase in splice strength can be represented by a power or piece-wise function. A trendline with the 0.5 power is plotted in Figure 5.1(b).

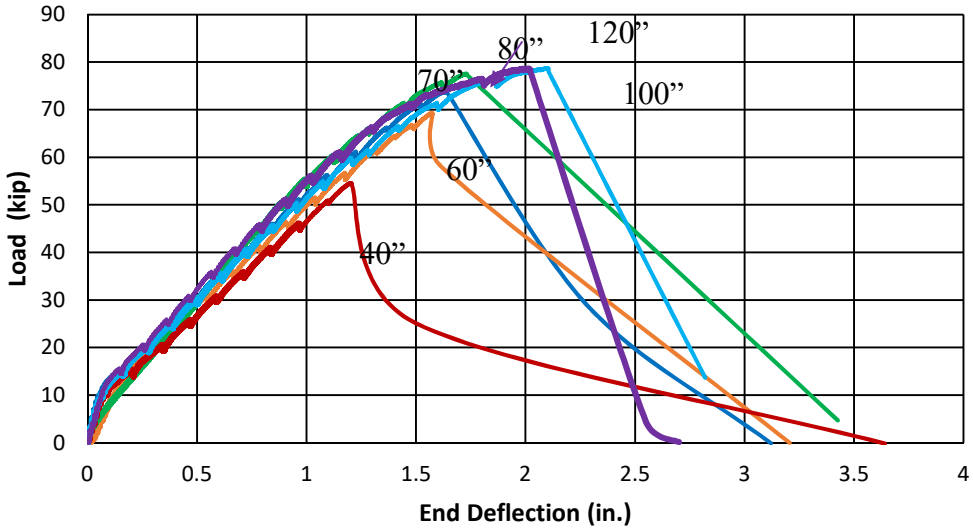

a) Load-Deflection Response

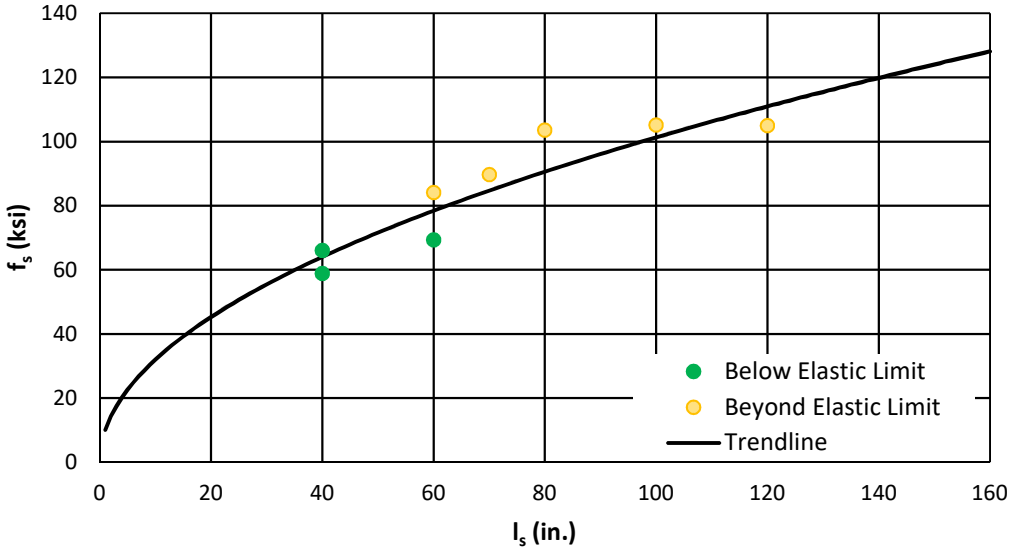

b) Bar Stress

Figure 5.1: Effect of Splice Length on Bond Strength in Unconfined Specimens

5.2.1.2 Confined

Figure 5.2 shows a similar relationship as Figure 5.1. With an increase in splice length, there is also an increase in bond strength. All specimens plotted have an effective pressure of 50 psi so that the effect of splice length can be observed. Specimen C3/60-80-5-50 failed in flexure. As both specimens C3/60-60-5-50 and C3/60-80-5-50 moved past the elastic limit of the longitudinal bars, the difference in splice strength was minimal.

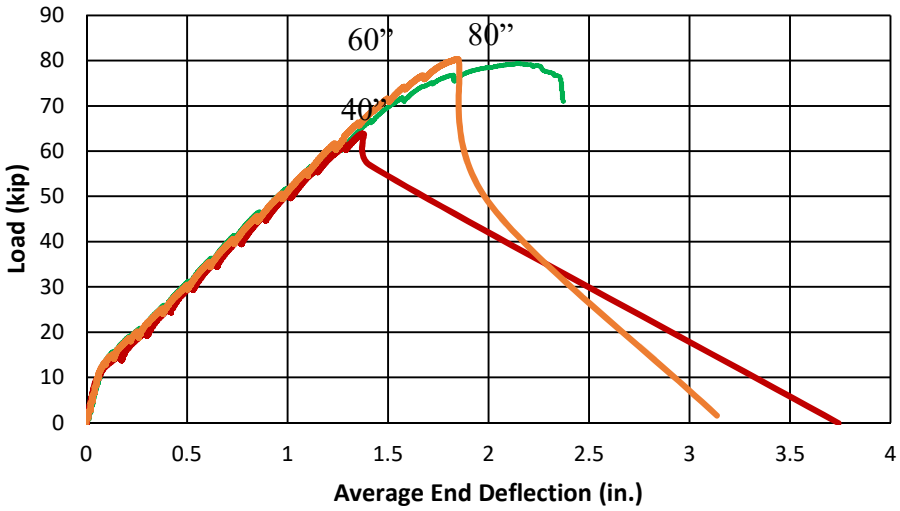

a) Load-Deflection

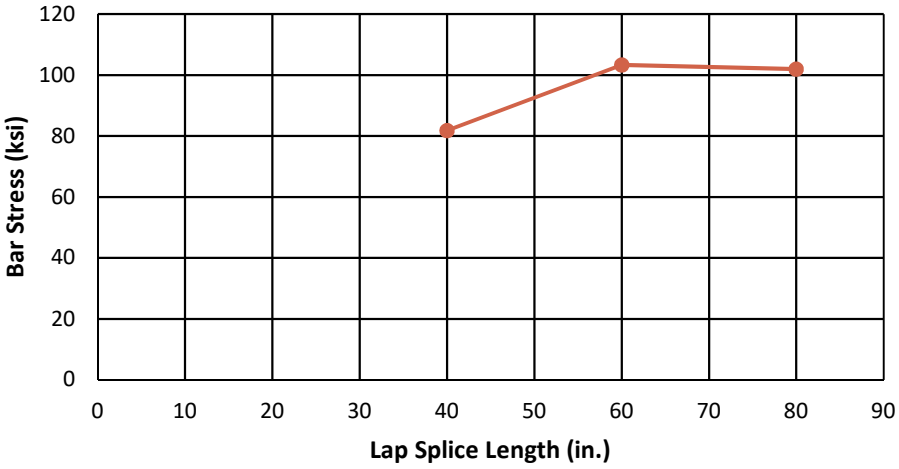

b) Bar Stress

Figure 5.2: Effect of Splice Length on Bond Strength in Confined Specimens (50 psi)

5.2.2 Bar Spacing

The bar spacing in this experimental program was selected based on common design practices. Three specimens were also designed with the minimum bar spacing, d_b, specified in ACI 318-14. Because all three minimum unconfined specimens exceeded the elastic limit of the longitudinal bars (U-80-5-M, U-100-5-M, and U-120-5-M), the impact of bar spacing is difficult to observe (Figure 5.3). The slight increase in bar stress could be a trend observed or typical scatter in the test results.

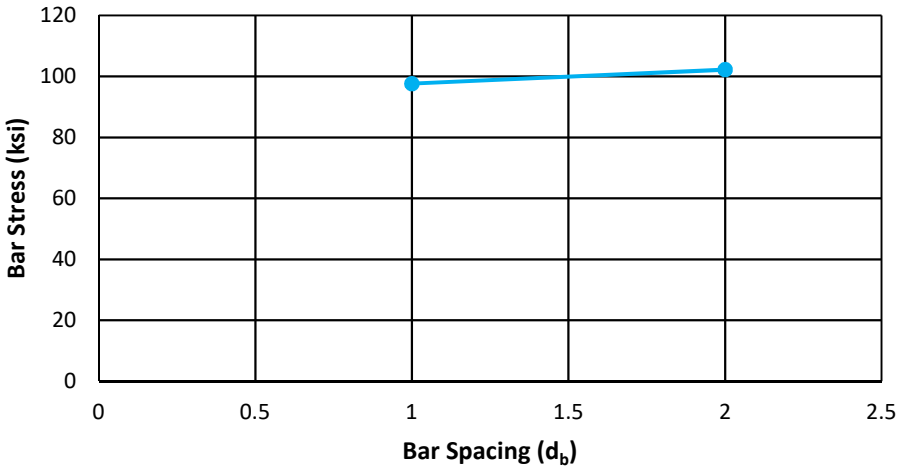

a) 80d_b Splice Length

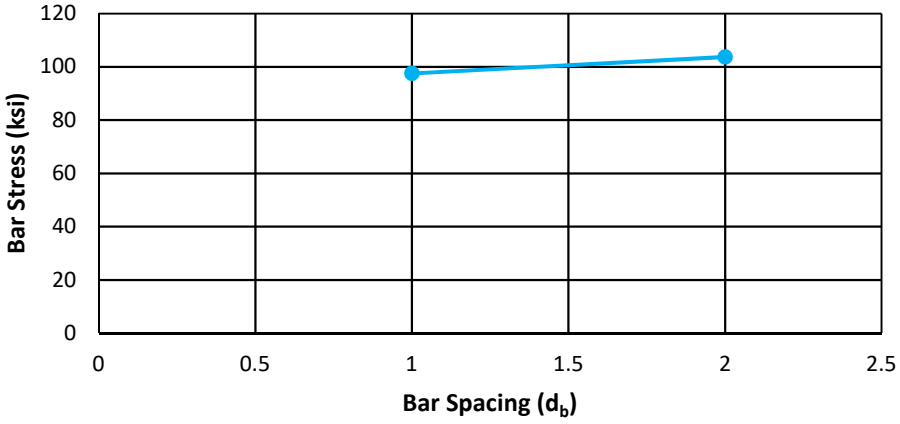

b) 100d_b Splice Length

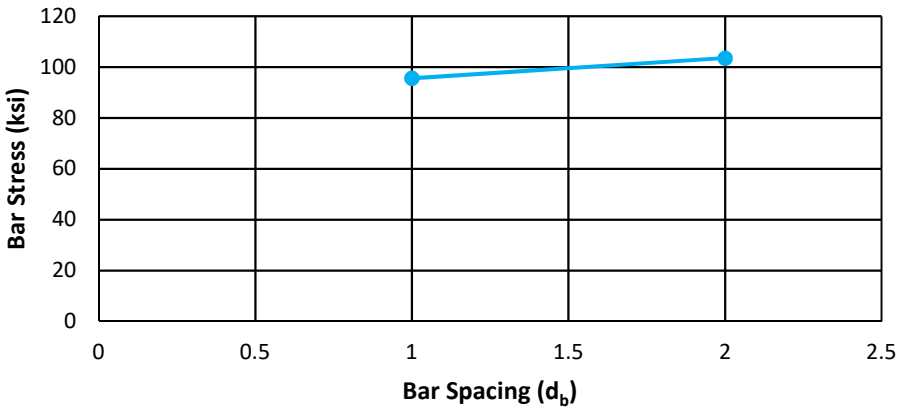

c) 120d_b Splice Length

Figure 5.3: Effect of Bar Spacing on Bond Strength

5.2.3 Confinement

Several variables relating to confinement are investigated in this study: stirrup location, confinement level, and confinement grade.

5.2.3.1 Stirrup Location

Figure 5.4 compares Specimen C3/60/2-40-5-50 (red) to Specimen C3/60/3-40-5-50 (blue). Sim (2014) concluded that stirrups placed closer to the ends of the splice were more effective. Therefore, two identical specimens having the same confinement stress were constructed, except one specimen had two stirrups in the splice region (Specimen C3/60/2-40-5-50) and the other specimen had three (Specimen C3/60/3-40-5-50). The specimen with three stirrups in the splice region (Specimen C3/60/3-40-5-50) performed better than the one with two stirrups (Specimen C3/60/2-40-5-50). Based on Sim's (2014) conclusions, this behavior occurred because the stirrups are placed closer to the end of the splice rather than because of the additional stirrup within the splice region. Elevation views for each of the confined $40d_b$ specimens are shown in Figure 5.5.

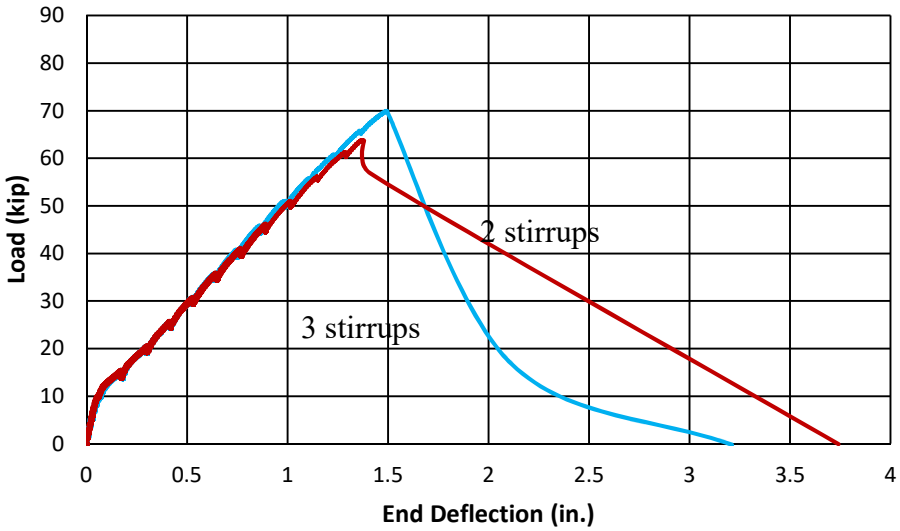

a) Load-Deflection

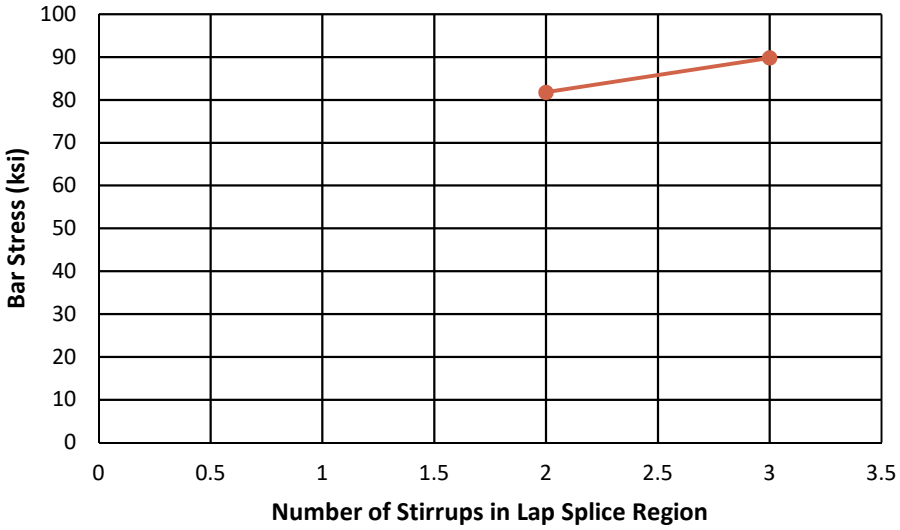

b) Bar Stress

Figure 5.4: Effect of Stirrup Location on Bond Strength

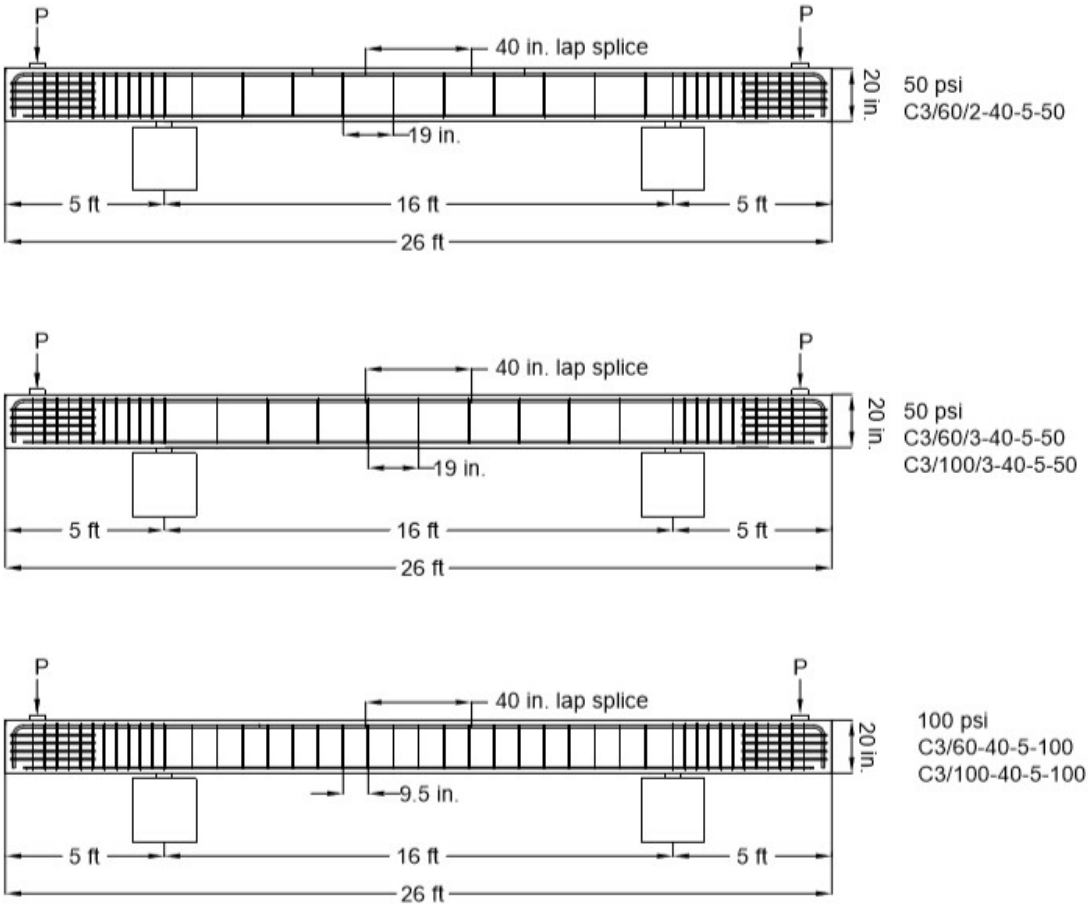

Figure 5.5: Elevations of 40d_b Confined Specimens

5.2.3.2 Confinement Level

As discussed in Section 2.3.4, various transverse reinforcement spacings, corresponding to different effective transverse pressures were investigated. In Figure 5.6, Specimen C3/60/2-40-5-50 (red) was compared with Specimen C3/60-40-5-100 (blue). The only difference in specimens was that Specimen C3/60/2-40-5-50 had a 19 in. center-to-center spacing of transverse reinforcement (50 psi), while Specimen C3/60-40-5-100 had a 9-$^1/_2$ in. center-to-center spacing (100 psi). A 12% increase in strength was observed in the 40d_b specimens (Figure 5.6). The same trends are also observed in the 60d_b specimens (Figure 5.7). The increase cannot be quantified in the case of the 60d_b specimens because the specimens with 100 psi and 150 psi of effective pressure failed in flexure, indicating that the splice strength was sufficient. It is interesting, however, that the increase in bar stress with increasing effective

pressure from 50 psi to 100 psi is approximately the same (10 ksi), regardless of splice length (Figure 5.7(b)).

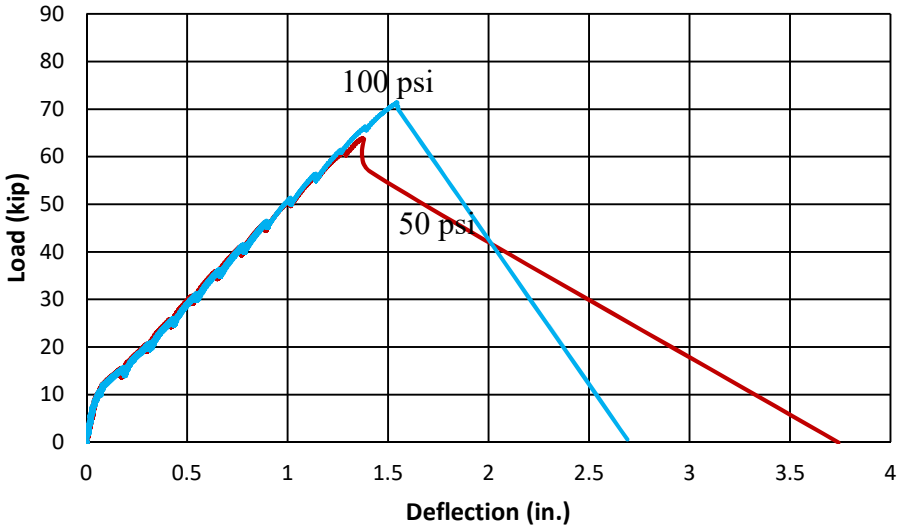

a) Load-Deflection

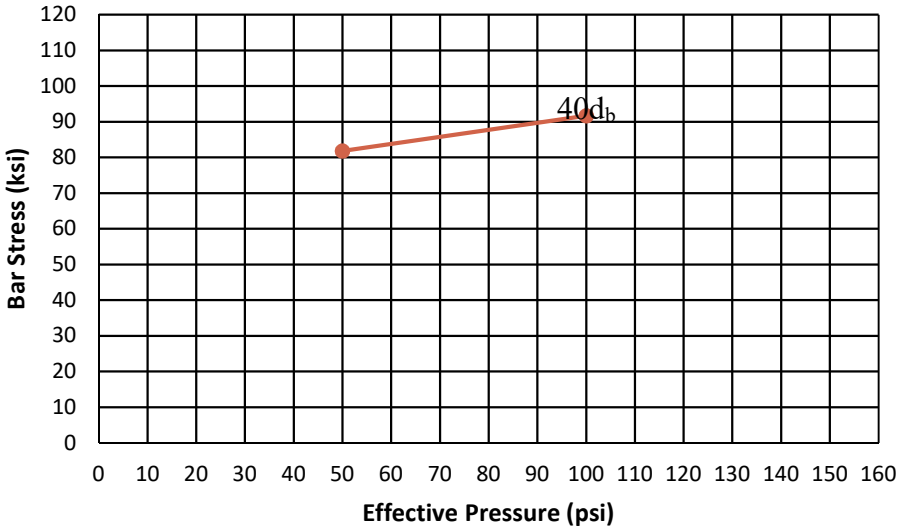

b) Bar Stress

Figure 5.6: Effect of Confinement Level on Bond Strength ($40d_b$ Specimens)

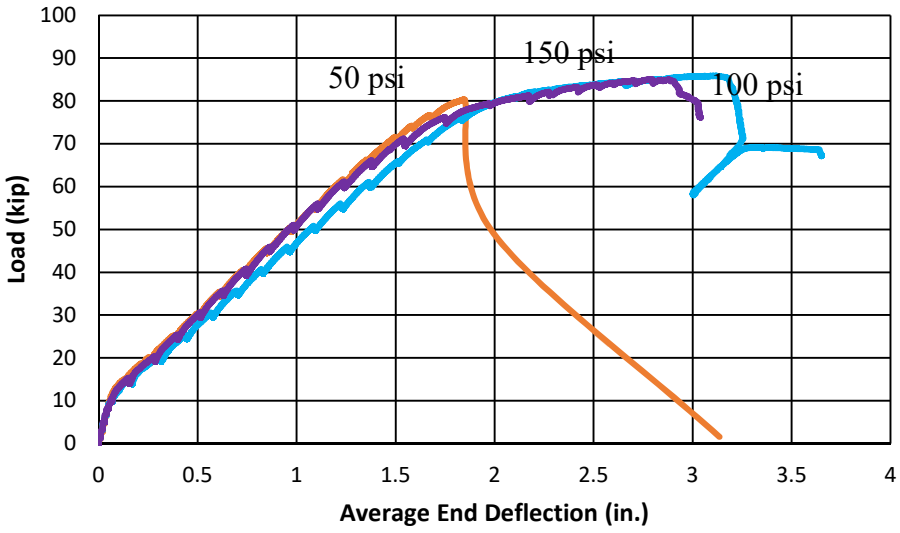

a) Load-Deflection

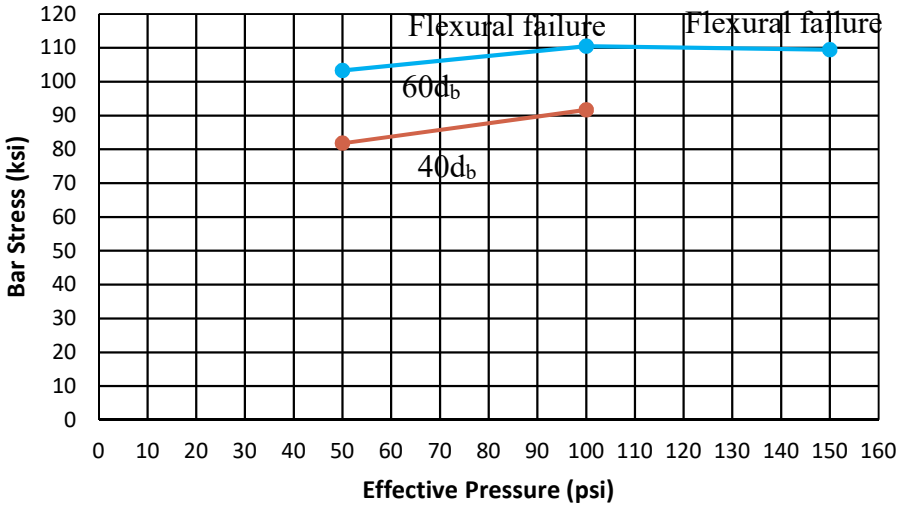

b) Bar Stress

Figure 5.7: Effect of Confinement Level on Bond Strength ($60d_b$ Specimens)

5.2.3.3 Confinement Grade

The effect of Grade 100 transverse reinforcement was also investigated. According to older studies conducted by Maeda et al. (1991), Sakurada et al. (1993), and Azizinamini et al. (1993), transverse reinforcement rarely yields during a bond failure. More recent studies by Azizinamini

et al. (1999) showed that the strain in stirrups, specifically stirrups located at the ends of the splice region, can reach their yield strength.

This experimental program attempted to determine if using Grade 100 transverse reinforcement would be useful. Grade 100 stirrups were used in $40d_b$ (Figure 5.8) and $60d_b$ (Figure 5.9) specimens. As shown in Figure 5.8(b), for both 50 psi and 100 psi confinement levels, the longitudinal bar stresses achieved were independent of the transverse reinforcement grade. The $60d_b$ specimens yielded before experiencing a flexural failure. Even in this case, the longitudinal bar stress achieved remained the same, which was expected for this failure mode (Figure 5.9(b)). The results from tests in this study show that the use of Grade 100 transverse reinforcement provides no increase in bond strength compared with the use of Grade 60 transverse reinforcement.

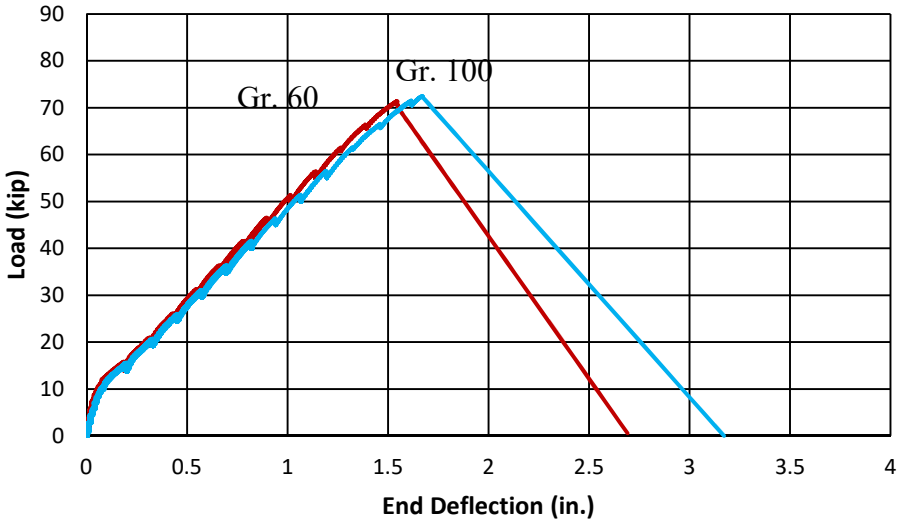

a) Load-Deflection

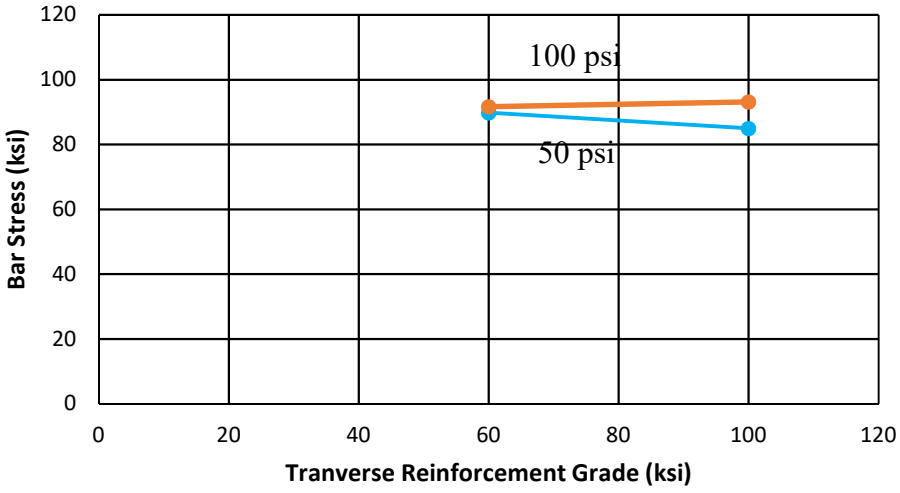

b) Bar Stress

Figure 5.8: Effect of Transverse Reinforcement Grade on Bond Strength ($40d_b$ Specimens)

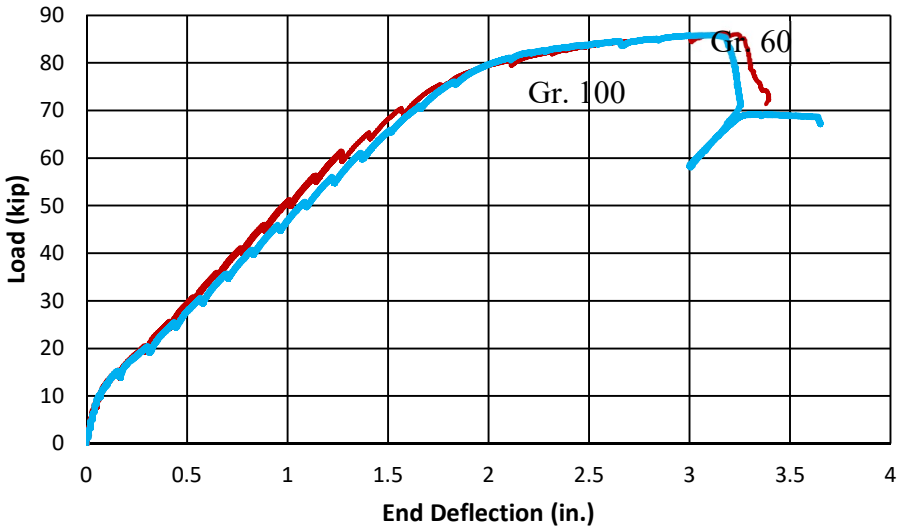

a) Load-Deflection

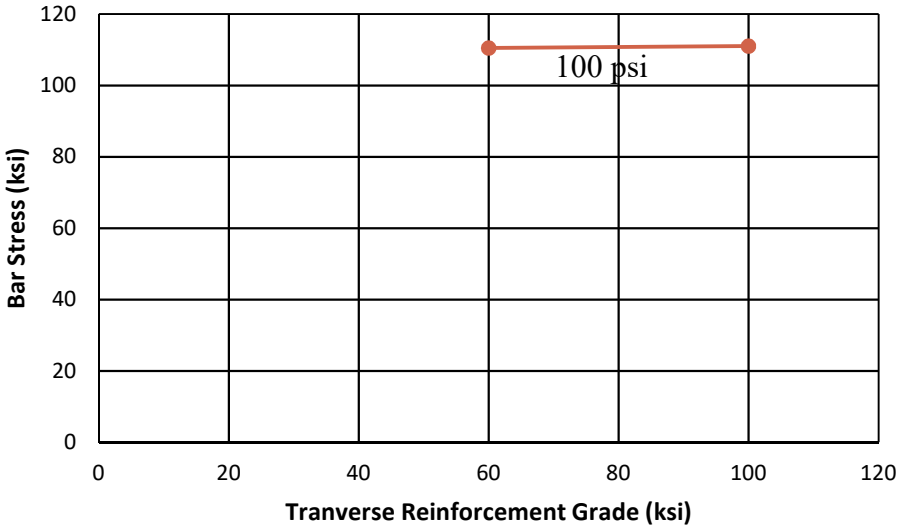

b) Bar Stress

Figure 5.9: Effect of Transverse Reinforcement Grade on Bond Strength ($60d_b$ Specimens)

5.3 Analysis Method for Bond Strength

An analysis method which can be used effectively with confinement, high-strength reinforcement, and various splice lengths was developed in this section. The reliability of the equation will be assessed using the data presented in this experimental program along with past

results from other splice tests. A steel reinforced concrete beam database was compiled by Canbay and Frosch (2005) and amended by Sim (2014). This database was expanded from the ACI 408 Database 10-2001 (ACI 408R-03). All data points represent bottom-cast beams with black bars that experienced a bond failure.

5.3.1 Beams Reinforced with Steel Bars Database

The data points used to develop an appropriate equation include 632 bottom-cast beams (including the specimens from this experimental program). All specimens have uncoated bars and experienced a splitting failure. All beams were loaded with two concentrated loads in a four-point bending test to create a region of constant moment within the splice length. Specimens that did not meet these criteria were removed. Additionally, specimens with concrete strengths less than 2,500 psi or splice lengths less than 12 in. or $16d_b$ were also excluded.

The references, the number of tests considered, and the range of variables are outlined in Table 5.1.

Table 5.1: Summary of Beams Reinforced with Steel Bars Database

Reference	Num. of Tests	d_b (in.)	l_s/d_b	f'_c (ksi)	f_y (ksi)	c_{so} (in.)	c_{si} (in.)	c_b (in.)
Chinn, Ferguson, and Thompson 1955	12	0.75	16.67 to 32	3.58 to 7.48	57	1.06 to 2.94	0.50	0.75 to 1.7
Ferguson and Breen 1965	33	1.00 to 1.41	18.00 to 80.00	2.61 to 5.62	64 to 99	1.42 to 4.59	1.43 to 4.70	1.31 to 2.06
Thompson, Jirsa, Breen, and Meinheit 1975	12	0.75 to 1.69	16.00 to 35.44	2.87 to 4.71	58 to 66	2.00 to 4.000	2.00 to 3.00	1.00 to 3.00
Ferguson and Thompson 1965	4	1.41	35.04 to 44.89	2.73 to 3.41	89	4.64 to 4.65	6.05 to 10.15	1.50 to 3.00
Mathey and Watstein 1961	7	0.50 to 1.00	21.00 to 34.00	3.50 to 4.49	97 to 115	3.500 to 3.750	-	1.50 to 1.75
Cleary, Ramirez 1991	3	0.75	16.00 to 21.33	3.99 to 5.62	65	3.25	3.25	2.00
Hester, Salamizavaregh, Darwin, and McCabe 1991, 1993	17	1.00	16.00 to 22.75	5.24 to 6.45	64 to 71	2.00	1.50 to 4.00	1.83 to 2.17
Choi, Hadje-Ghaffari, Darwin, and McCabe 1990, 1991	8	0.63 to 1.41	16.00 to 19.20	5.36 to 6.01	64 to 71	2.00	2.00	1.00 to 2.00
Rezansoff, Konkankar and Fu 1991	31	0.77 to 1.41	16.47 to 28.93	3.22 to 5.74	61 to 72	1.00 to 2.02	1.67 to 2.98	1.00 to 2.30
DeVries, Moehle, and Hester 1991	1	1.13	19.50	7.46	66	1.50	1.74	1.125
Rezansoff, Akanni, and Sparling 1993	13	0.99 to 1.18	18.73 to 37.63	3.63 to 4.09	65 to 69	1.82 to 1.83	0.50 to 1.18	2.01
Hamad, Mansour 1996	1	0.79	17.51	2.90	69	0.79	4.33	0.79
Darwin, Tholen, Idun, and Zuo 1995	61	0.63 to 1.41	16.00 to 36.00	3.83 to 5.25	60 to 81	1.47 to 3.09	0.40 to 4.50	1.21 to 2.94
Zuo and Darwin 1998	91	0.63 to 1.41	16.00 to 40.00	4.25 to 15.65	63 to 81	1.45 to 4.03	0.39 to 4.05	1.30 to 3.06
Kadoriku 1994	34	0.75	20.00 to 50.00	3.07 to 10.98	64 to 122	1.14 to 3.54	2.20 to 4.80	1.12 to 2.62
Azizinamini, Stark, Roller, Ghosh 1993	12	1.00 to 1.38	17.45 to 58.17	4.82 to 15.10	71 to 78	1.00 to 1.37	1.50 to 1.81	1.00 to 1.37
Azizinamini, Chisala, Ghosh 1995	7	1.38	29.09 to 41.81	14.80 to 16.50	71 to 74	1.37	1.38	1.37
Azizinamini, Pavel, Hatfield and Ghosh,1997	48	1.00 to 1.41	17.02 to 56.74	5.08 to 16.00	71 to 78	1.00 to 3.00	1.00 to 3.18	1.00 to 3.00
El-Hacha, Hossam El-Agroudy, and Sami H. Rizkalla, 2006	7	0.75 to 1.00	16.00 to 80.00	5.71 to 6.87	120	2.13 to 4.87	2.13 to 2.76	1.38 to 1.50
Seliem, Hosny, Rizkalla, Zia, Briggs, Miller, Darwin, Browning, Glass, Hoyt, Donnelly, and Jirsa, 2009	64	0.63 to 1.41	24.00 to 70.40	4.06 to 10.20	120	0.96 to 3.80	1.00 to 7.52	0.70 to 3.00
Richter, Pujol, Sozen, and McCain, 2012	13	1.41	28.37 to 85.11	4.18 to 5.49	80	3.00	3.00	5.00

Table 5.1: Summary of Beams Reinforced with Steel Bars Database (continued)

Reference	Num. of Tests	d_b (in.)	l_s/d_b	f'_c (ksi)	f_y (ksi)	c_{so} (in.)	c_{si} (in.)	c_b (in.)
Eligehausen 1979	7	0.79	30.00 to 30.60	4.03 to 4.52	80	1.57	1.18 to 3.15	1.57 to 5.51
Hegger, Burkhardt 1998	6	0.79	37.50 to 42.50	11.60 to 14.50	83 to 85	0.79 to 1.57	0.79	0.79 to 1.57
Olsen 1990	4	0.63	20.00 to 30.00	3.76 to 10.30	94	1.02	1.65	1.02
Rehm, Eligehausen 1977	9	0.55 to 1.10	22.86 to 72.86	2.76 to 7.07	60 to 81	0.55 to 3.39	0.55 to 3.39	0.59 to 1.10
Tepfers 1973	90	0.32 to 1.26	16.25 to 82.50	2.61 to 14.20	60 to 132	0.12 to 6.57	0.31 to 2.64	0.04 to 3.27
Sim and Frosch 2013	20	0.63 to 1.41	17.02 to 76.80	3.99 to 5.40	65 to 98	1.50 to 2.38	0.50 to 2.38	0.75 to 1.50
Glucksman and Frosch 2018	17	1.00	40.00 to 120.00	4.70 to 7.36	87	1.50 to 1.88	0.50 to 1.00	1.50 to 1.88
Totals	**632**	**0.32 to 1.69**	**16.00 to 120.00**	**2.61 to 16.50**	**57 to 132**	**0.12 to 6.57**	**0.31 to 10.15**	**0.04 to 5.51**

The characteristics of the database were examined by evaluating the distribution of the available data because the applicability of the conclusions derived from using the database depends on the frequency of the variables that occurred. The frequency distribution of f_c', d_b, l_s/d_b and f_y are shown in Figures 5.10 through 5.13, respectively. The histograms show the concentrations of data for all three plots. The majority, 68%, of the specimens previously tested have concrete strengths, f_c', below 7,000 psi (Figure 5.10). Beams have been tested with concrete strengths up to 17,000 psi. The majority, 44%, of beams used #8 bars (Figure 5.11). Splices have been tested with reinforcing bars sizes #3 to #14. There is more data for beams tested with shorter splices (Figure 5.12). The majority, 84%, of the splice beams have splice lengths, in terms of bar diameter, less than $50d_b$. Because most of the data has been conducted on shorter splice lengths, it was important for this study to test beams with longer splices that would be required for high-strength reinforcement. It is important for an analysis equation to work equally well for short splice lengths as well as long splice lengths. The majority, 57%, of specimens in the database have yield strengths less than 80 ksi. This shows a gap in the data for the use of reinforcement with a yield strength greater than 80 ksi.

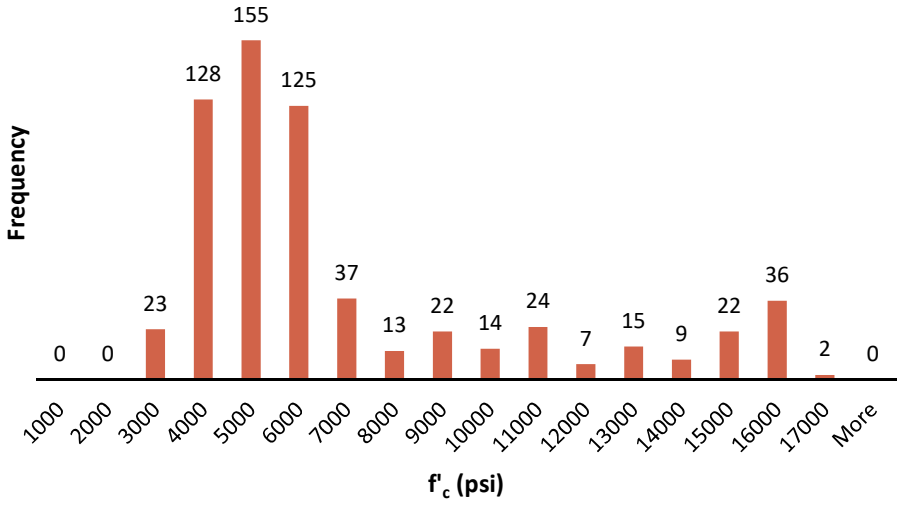

Figure 5.10: Frequency Distribution of Concrete Strength

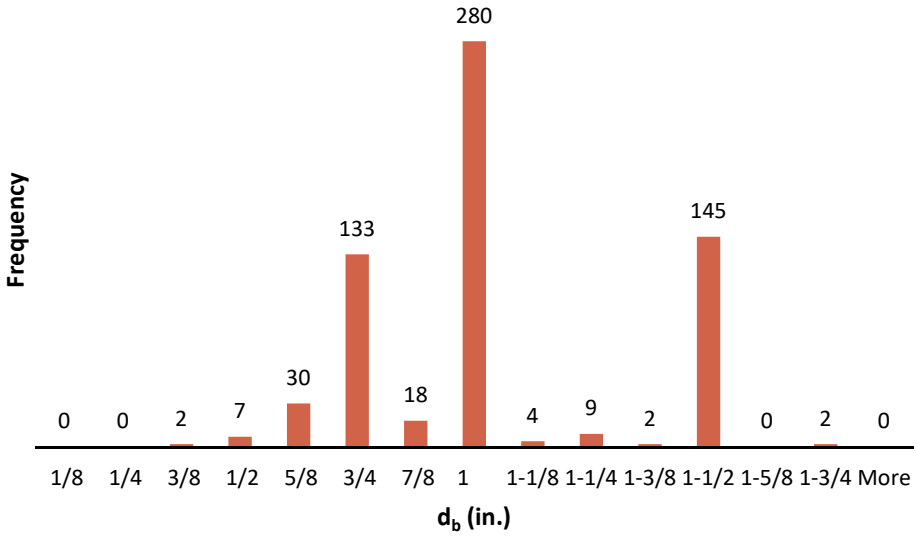

Figure 5.11: Frequency Distribution of Bar Diameter

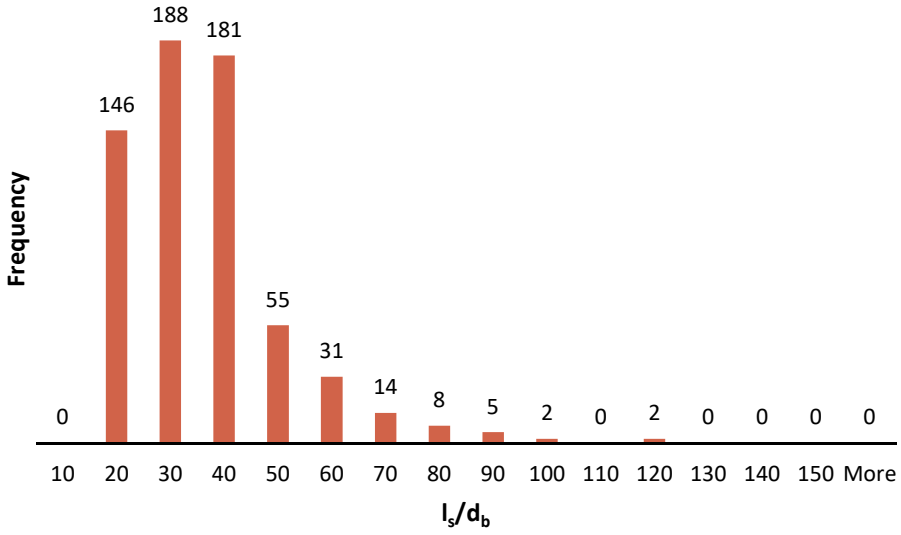

Figure 5.12: Frequency Distribution of Splice Length in Terms of Bar Diameter

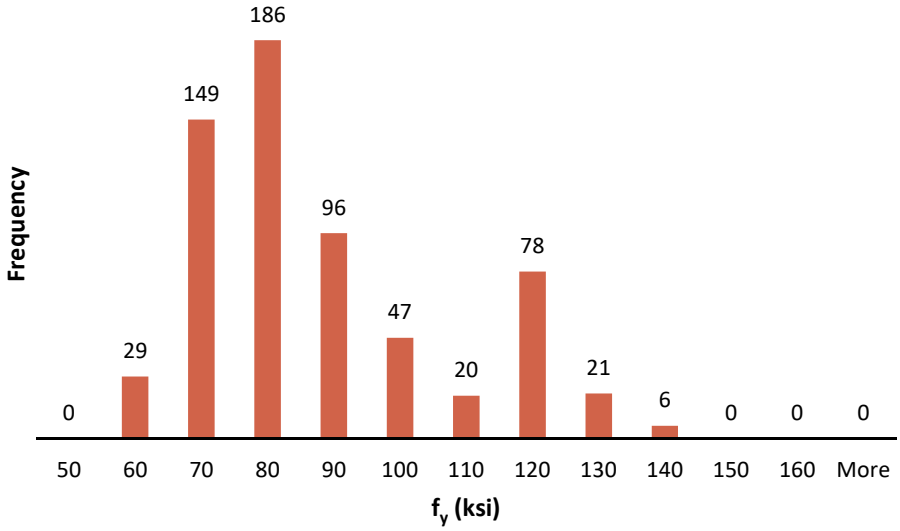

Figure 5.13: Frequency Distribution of Yield Stress of Reinforcing Bars

5.3.2 Analysis

Several observations were made that provide the basis for the development of a simple, yet reliable equation.

1. As the splice length increases, the unit length effectiveness decreases. The general trend between bar stress and splice length seems to fit a power equation. For splice lengths less than $50d_b$, a linear equation could be sufficient.
2. Confinement can be considered as a separate term that is added to an "unconfined" term.
3. Grade 100 transverse reinforcement does not provide any additional benefit to the bond strength compared with the use of Grade 60 transverse reinforcement. Therefore, f_{yt} should not be a variable included in the confinement term of a design equation.

Table 5.2 provides a summary of the beams of the Grade 100 test program along with the normalized bar stress and normalized bar force. Since concrete strength influences the bond strength, stresses and forces were calculated for each specimen in terms of a 5,000 psi specimen. Normalization in this way helps for comparison purposes.

It has been observed by both Canbay and Frosch (2005) and ACI 408R-03 that the effect of concrete strength on bond strength is best described by the fourth root of the compressive strength, $\sqrt[4]{f_c'}$, the results of the different series were compared by normalizing the calculated bar stress or force by the fourth root of the compressive strength. The stresses and forces presented in this section were normalized to 5,000 psi concrete as follows:

$$f_{test(f_c'=5000psi)} = f_{test(f_c')}\sqrt[4]{5000/f_c'} \quad (5\text{-}1)$$

$$F_{test(f_c'=5000psi)} = F_{test(f_c')}\sqrt[4]{5000/f_c'} \quad (5\text{-}2)$$

where:

f_c' = *concrete cylinder strength, psi*

F_{test} = *bar force at failure,* f_{test}*A_b, kips*

f_{test} = *bar stress at failure, ksi*

Table 5.2: Summary of Specimens

Specimen	Failure Mechanism	f_s (ksi)		F_{test} (kip)	
		Test	Normalized to 5000 psi Concrete	Test	Normalized to 5000 psi Concrete
U-40-5	Bond	58.2	59.1	45.9	46.7
U-40-5a	Bond	69.8	65.9	55.1	52.0
U-60-5	Bond	68.4	69.5	54.0	54.9
U-60-5a	Bond	88.9*	83.9	70.2	66.3
U-70-5	Bond	94.9*	89.5	74.9	70.7
U-80-5	Bond	102.2*	103.8	80.7	82.0
U-100-5	Bond	103.7*	105.3	81.9	83.2
U-120-5	Bond	103.6*	105.2	81.8	83.1
U-80-5-M	Bond	97.7*	99.2	77.1	78.3
U-100-5-M	Bond	97.5*	99.0	77.0	78.2
U-120-5-M	Bond	95.6*	97.1	75.5	76.7
C3/60/2-40-5-50	Bond	81.8	77.2	64.6	61.0
C3/60/3-40-5-50	Bond	89.8*	84.8	71.0	67.0
C3/100/3-40-5-50	Bond	85.0	80.2	67.2	63.4
C3/60-40-5-100	Bond	91.7*	86.5	72.4	68.4
C3/100-40-5-100	Bond	93.1*	87.9	73.6	69.4
C3/60-60-5-50	Bond	103.3*	93.8	81.6	74.1
C3/60-60-5-100	Flexure	110.5**	100.4	87.3	79.3
C3/60-60-5-150	Flexure	109.4**	99.4	86.4	78.5
C4/60-60-5-100	Flexure	108.9**	98.9	86.0	78.1
C3/100-60-5-100	Flexure	111.0**	100.8	87.7	79.7
C3/60-80-5-50	Flexure	101.9*	96.2	80.5	76.0

**bar stress reached elastic limit*

***bar stress reached yield stress*

5.3.2.1 Unconfined Splice Strength

Several trendlines that describe the general behavior of the relationship between splice length and bar stress are presented in this section. To determine which trendline characterizes the relationship most reliably, unconfined data were plotted for L_{eq} v. F_{test} (Equations 5-3 and 5-4, respectively). L_{eq} is the normalized splice length. For this evaluation, the splice length was normalized to splice lengths for #8 bars (A_s=0.79 in.^{2}). F_{test} is the normalized splice failure force. Additionally, a term was added to normalize to a concrete strength of 5,000 psi.

Only unyielded specimens with black bars, normalweight concrete, tested in four-point bending, that failed in bond are considered in this analysis. Additionally, specimens with concrete strengths less than 2,500 psi or splice lengths less than 12 in. or $16d_b$ were also excluded.

$$L_{eq} = l_s \frac{A_b}{0.79\ in.^2} \tag{5-3}$$

$$F_{test} = f_s A_b \left(\frac{5000\ psi}{f_c'}\right)^{0.25} \tag{5-4}$$

where:

A_b = *area of bar, in.2*

f_c' =*specified compressive strength of concrete, psi*

f_s = *bar stress, ksi*

F_{test} = *bar force at failure, normalized to a concrete strength of 5,000 psi, kips*

l_s = *splice length, in.*

Using plots of L_{eq} v. F_{test} allowed specimens with different bar sizes and concrete strengths to be compared. Different trendlines were developed (Equations 5-5 through 5-8) and plotted in Figures 5.14 to 5.17. Unconfined historical data is represented in Figures 5.14 to 5.17 with blue points, while the unconfined data from this study is represented with yellow. Statistical analysis, based on F_{test}/F_{calc} ratios, were conducted to determine the effectiveness of the expressions. These results are presented in Table 5.3. Based on reliability as well as simplicity, Equation 5-6, defined by the 0.5 power of L_{eq}, was selected to describe the behavior of the unconfined specimens.

Power Approximations:

$$F_{calc} = 5.7{L_{eq}}^{0.6} \quad (5\text{-}5)$$

$$F_{calc} = 8{L_{eq}}^{0.5} \quad (5\text{-}6)$$

Piece-wise Approximations:

$$\begin{matrix} if\ L_{eq} \leq 50\ in., F_{calc} = 1.5L_{eq} \\ if\ L_{eq} > 50\ in., F_{calc} = 10.5{L_{eq}}^{0.5} \end{matrix} \quad (5\text{-}7)$$

$$\begin{matrix} if\ L_{eq} \leq 50\ in., F_{calc} = 1.5L_{eq} \\ if\ L_{eq} > 50\ in., F_{calc} = 0.5(L_{eq} - 50) + 75 \end{matrix} \quad (5\text{-}8)$$

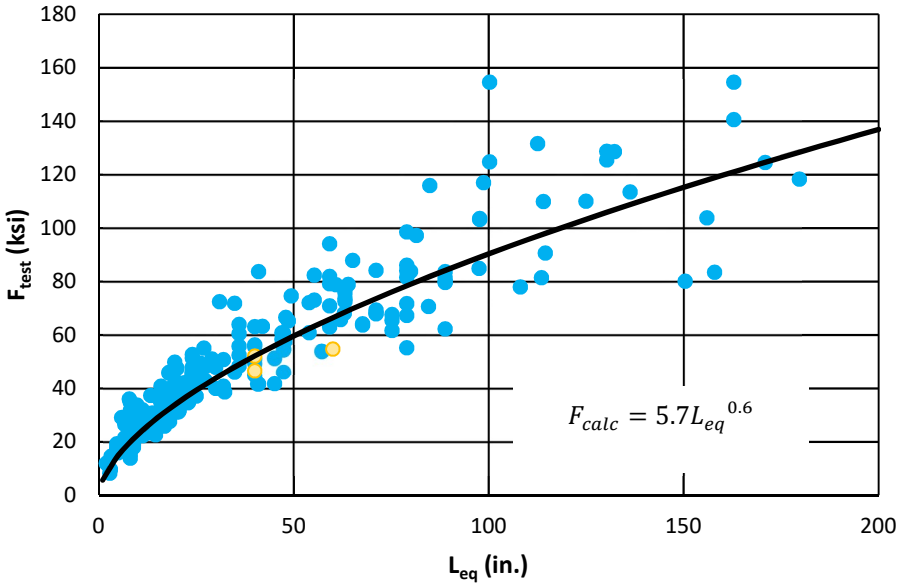

a) General Trend

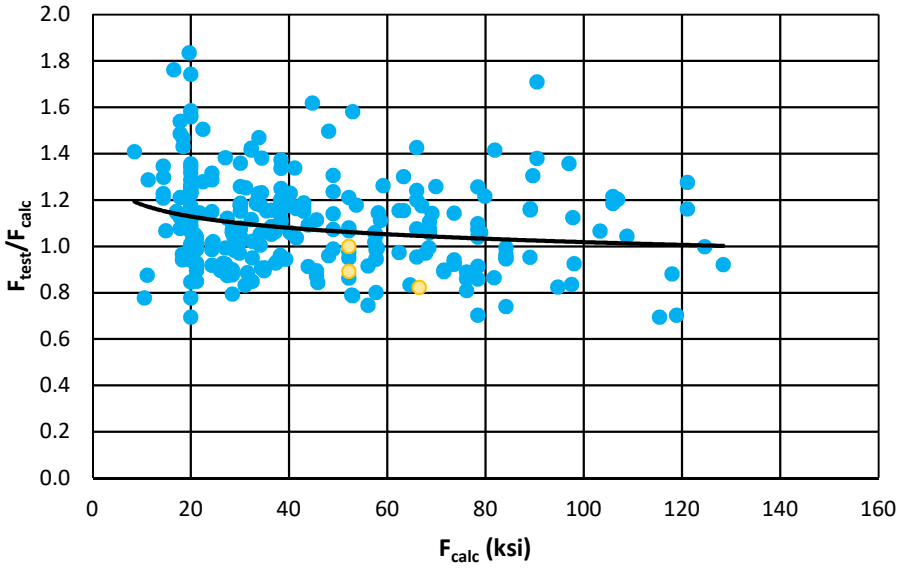

b) Relationship with F_{test}

Figure 5.14: Equation 5-5

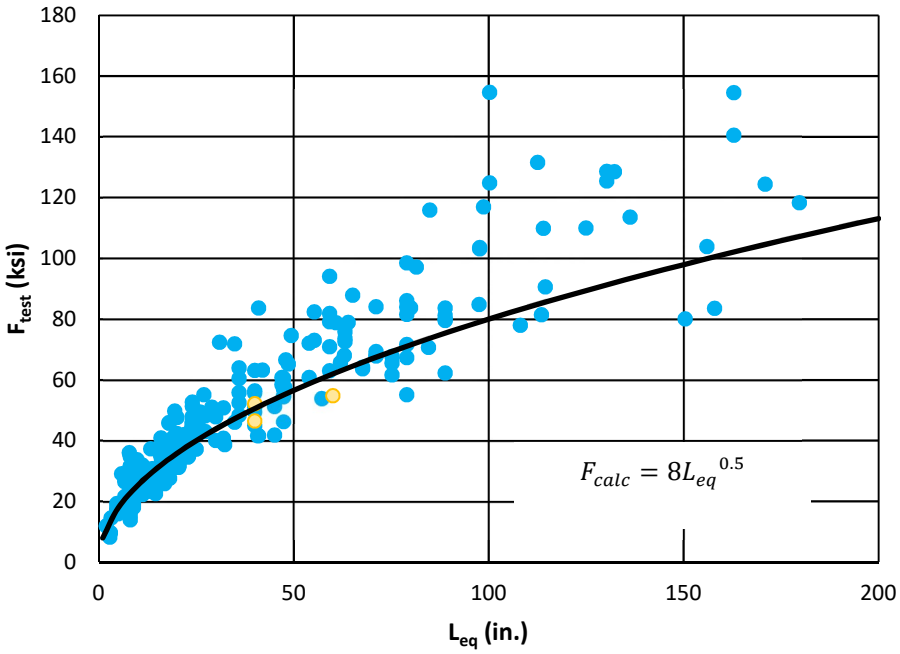

a) General Trend

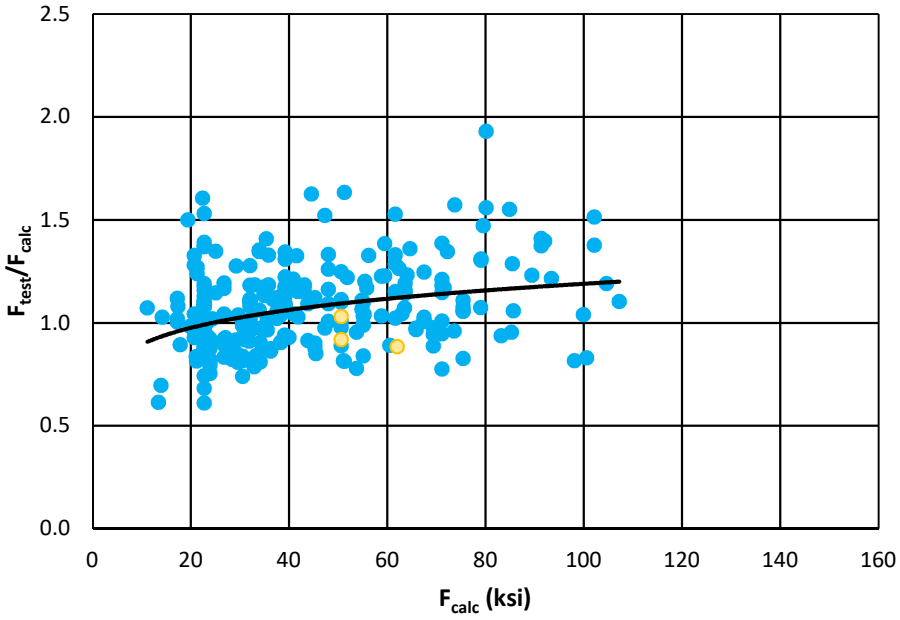

b) Relationship with F_{test}

Figure 5.15: Equation 5-6

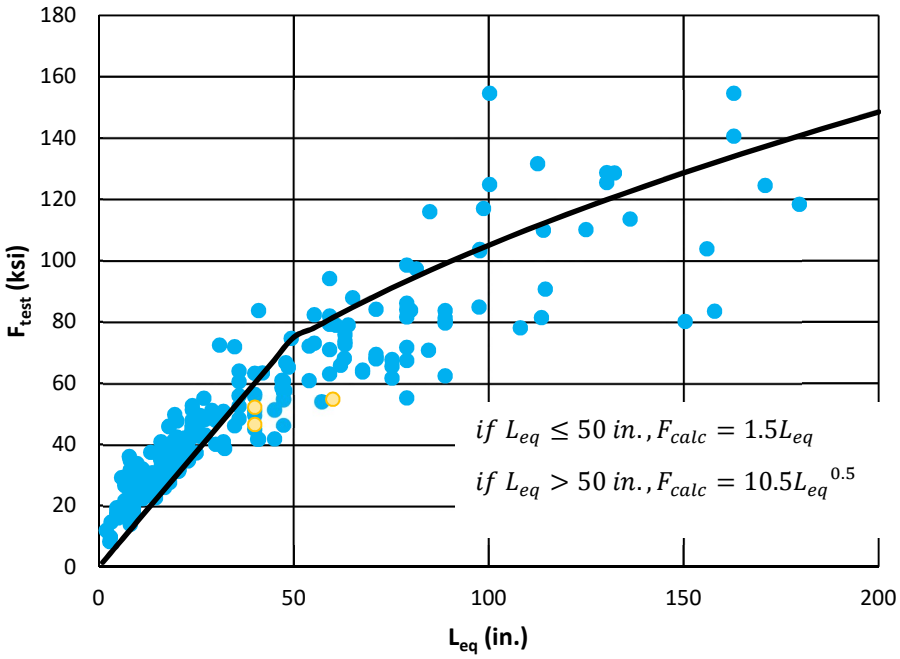

a) General Trend

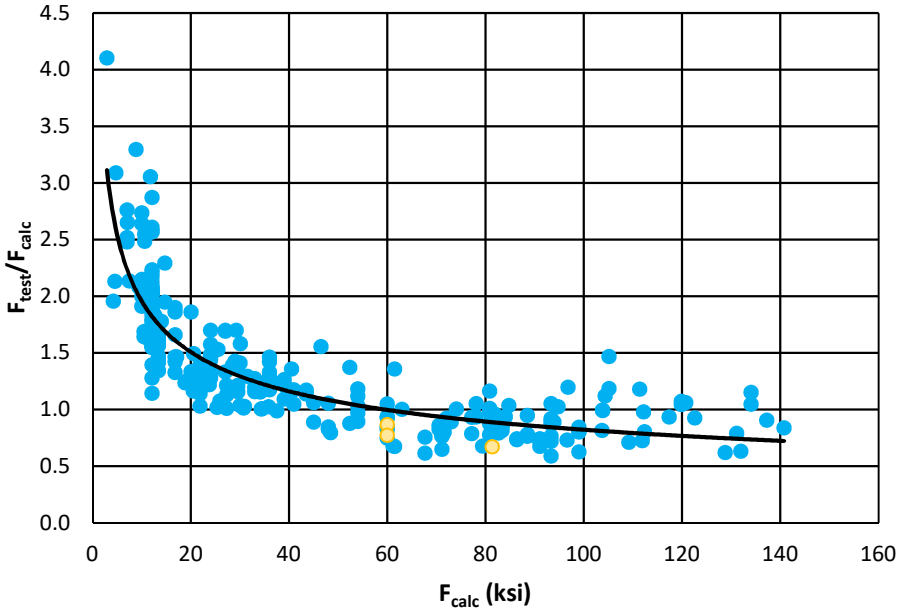

b) Relationship with F_{test}

Figure 5.16: Equation 5-7

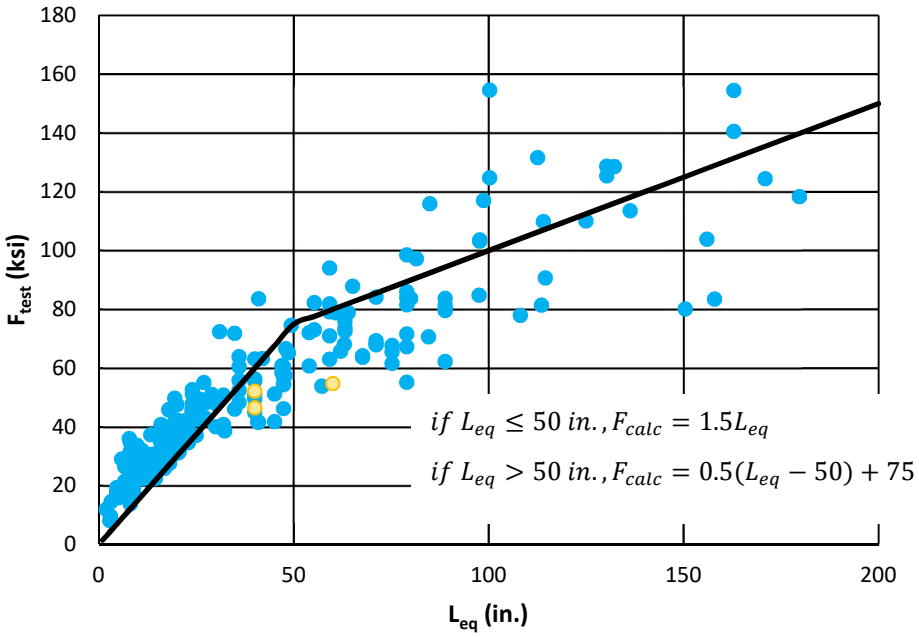

a) General Trend

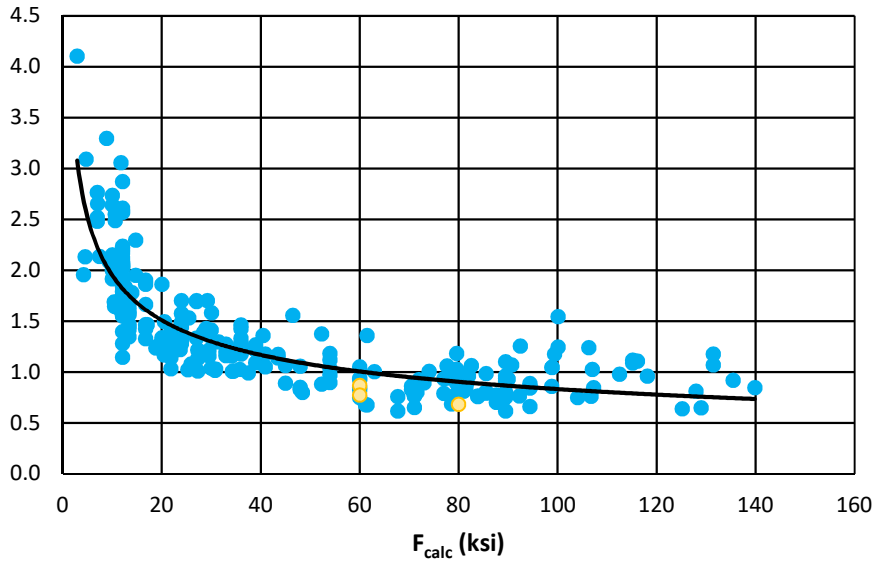

b) Relationship with F_{test}

Figure 5.17: Equation 5-8

Table 5.3: Statistical Analysis of Unconfined Descriptive Equations, F_{test}/F_{calc}

	Eq. 5-5	Eq. 5-6	Eq. 5-7	Eq. 5-8
Mean	1.10	1.07	1.35	1.36
Standard Error	0.01	0.01	0.03	0.03
Standard Deviation	0.20	0.20	0.56	0.55
Minimum	0.69	0.61	0.59	0.62
Maximum	1.83	1.93	4.10	4.10

The proposed unconfined term (Equation 5-6) is evaluated in relation to the bar stress determined from results, f_{test}, as shown in Figure 5.18. Only unconfined data that did not reach yield is plotted. Additionally, specimens with concrete strengths below 2,500 psi and specimens with lap splice lengths less than 12 in. or $16d_b$ were also excluded. The blue data points represent historical data from the database described in Table 5.1. The yellow data points represent unconfined data from this study.

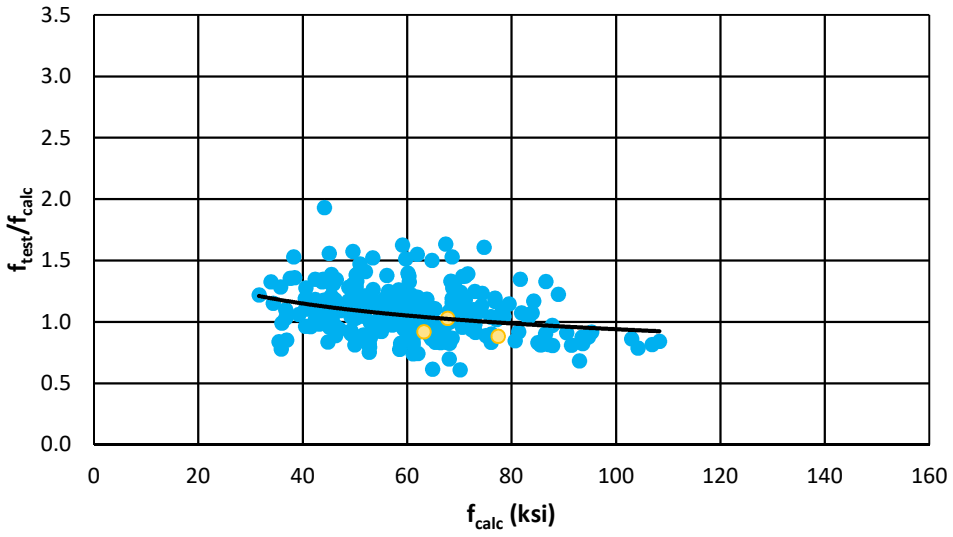

Figure 5.18: Proposed Unconfined Term without Cover Modification Factor (Equation 5-6)

5.3.2.1.1 Cover Modification

The scatter in the unconfined equation can be reduced by adding a cover modification factor. Since cover and bar spacing are shown to have an influence on bond strength, the scatter in the data can be reduced by adding a factor to the unconfined equation to account for variations in

cover or bar spacing. There are three parameters that describe the cover or spacing in specimens: c_b (bottom cover), c_{so} (side cover), and c_{si} (half of the clear spacing between bars). To determine which parameter has the largest influence on bar stress, the value of F_{test}/F_{calc} was plotted against each of the three parameters (Figure 5.19). Equation 5-6, described by the 0.5 power, was used to determine F_{calc}. F_{test} was normalized so that the variation in concrete strength between specimens was not a factor. Only unconfined specimens that did not reach yield are plotted in Figures 5.19 and 5.20.

Both Pay (2005) and Sim (2014) also investigated cover modification factors that could be used to reduce scatter in the data. Sim (2014) found that the side cover to bar diameter (c_{so}/d_b) had the largest influence. Equations 5-9 and 5-10 are the cover modification factors that Pay (2005) and Sim (2014) developed, respectively. The variables that Sim and Pay found to have the largest influence were also investigated.

$$M = 0.20\left(\frac{c}{d_b}\right) + 0.75 \tag{5-9}$$

$$M = \sqrt[4]{\frac{c_{so}}{d_b}} \tag{5-10}$$

where:

c = *minimum of* c_{si} *or* c_b*, in.*

As seen in Figure 5.19, the strongest trend is associated with the side cover, c_{so}. Figure 5.20 investigates the effect of combining multiple variables as considered by Pay.

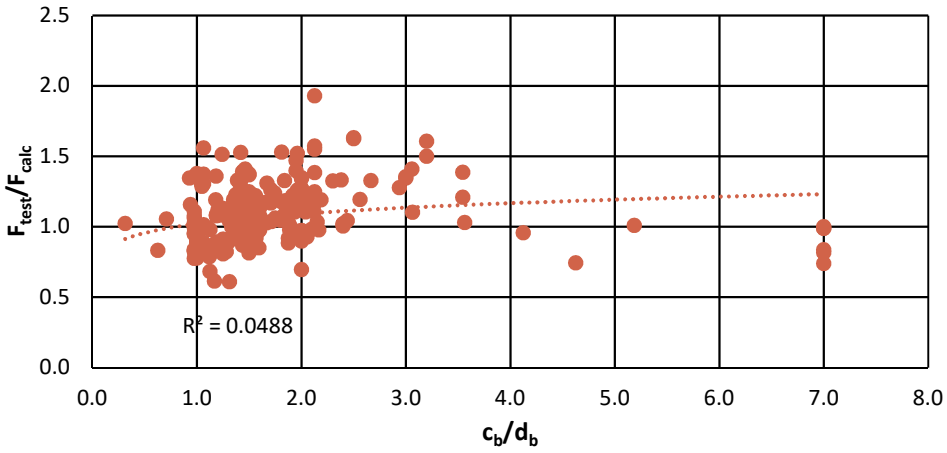

a) Bottom Cover, c_b

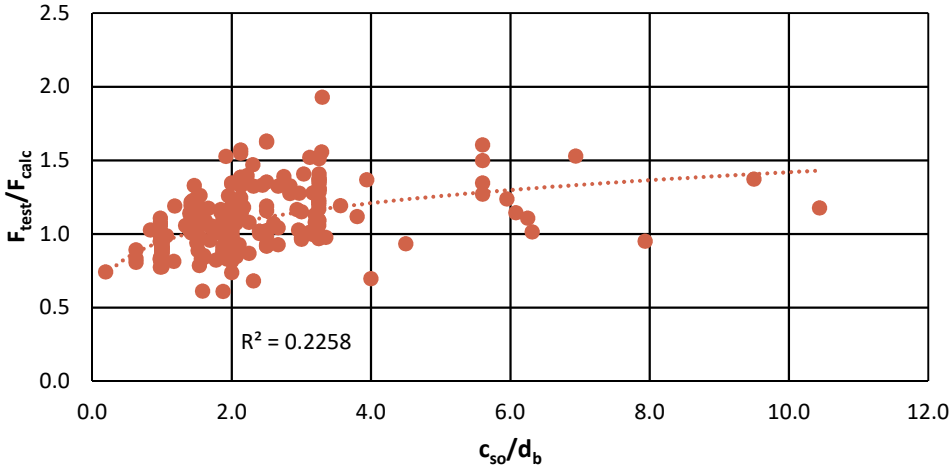

b) Side Cover, c_{so}

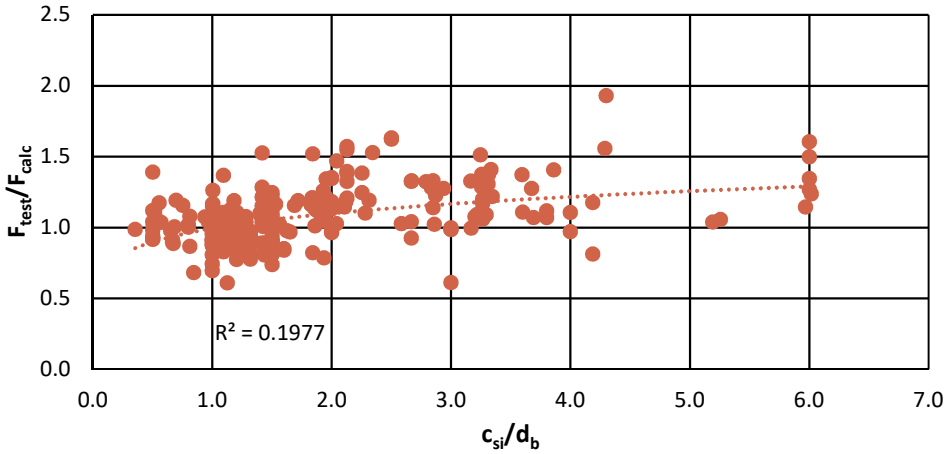

c) Half of Clear Spacing Between Bars, c_{si}

Figure 5.19: Influence of Cover and Bar Spacing on Bar Stress in Terms of Bar Diameter

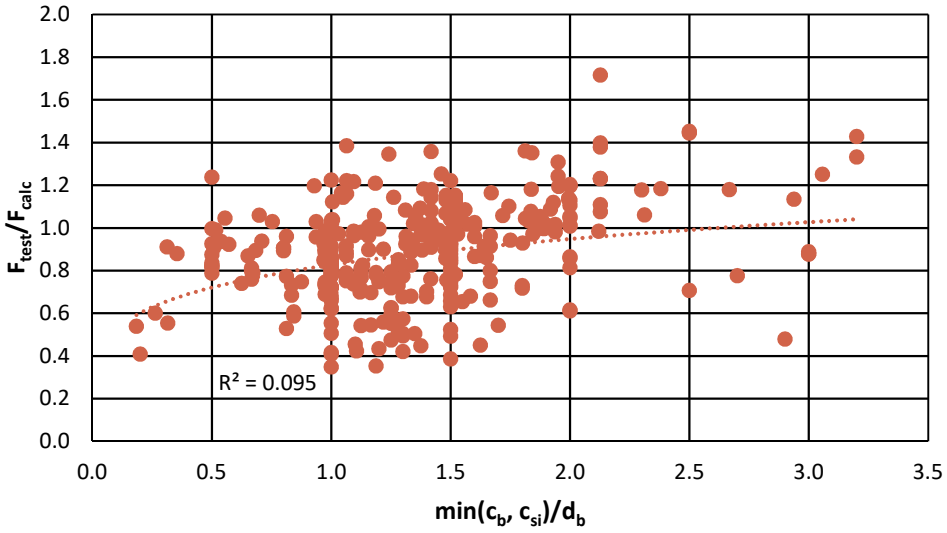

a) Minimum of Two Variables in Terms of Bar Diameter

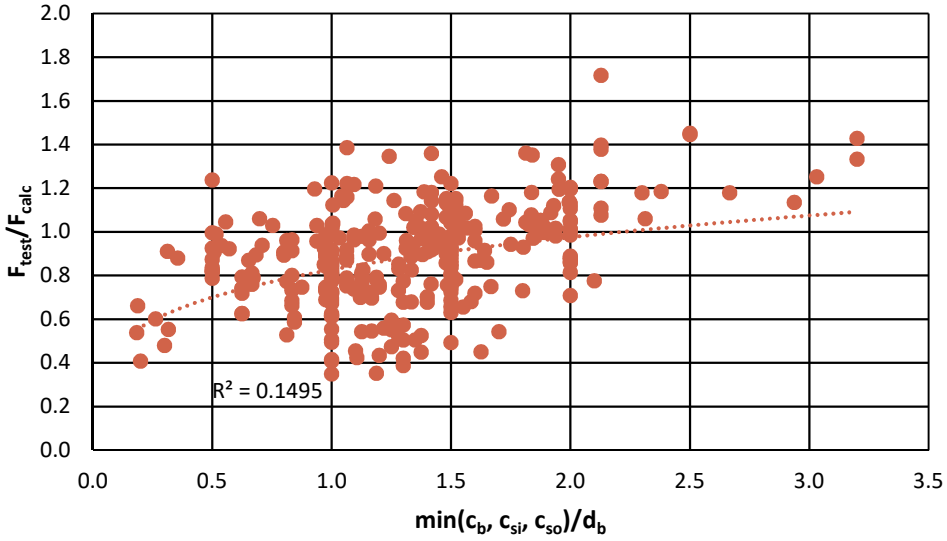

b) Minimum of Three Variables in Terms of Bar Diameter

Figure 5.20: Influence of Minimum of Cover and Bar Spacing on Bar Stress

Since the strongest correlation is found between the value of side cover in terms of bar diameter (c_{so}/d_b) and the proposed unconfined equation (Equation 5-6), the cover modification factor will be represented in terms of c_{so}/d_b to have the largest influence on minimizing the scatter in the data. Based on the power trendline shown in Figure 5.19(b), this variable has a correlation that is best represented by the 0.25 power. As a result, the best cover modification factor for Equation 5-6 is:

$$M = \left(\frac{c_{so}}{d_b}\right)^{0.25} \tag{5-11}$$

For reduced scatter, the unconfined term (Equation 5-6) is multiplied by the cover modification term (Equation 5-11). Using Equations 5-3 and 5-4, bar stress is calculated as:

$$f_s = \frac{8{L_{eq}}^{0.5}}{A_b\left(\frac{5000}{f_c'}\right)^{0.25}}\left(\frac{c_{so}}{d_b}\right)^{0.25} \tag{5-12}$$

The proposed unconfined term (Equation 5-12) is evaluated in relation to the bar stress determined from results, f_{test}, as shown in Figure 5.21. Only unconfined data that did not reach yield is plotted. Additionally, specimens with concrete strengths less than 2,500 psi and splice lengths less than 12 in. or $16d_b$ were also excluded. The blue data points represent historical data from the database described in Table 5.1. The yellow data points represent data obtained from this study.

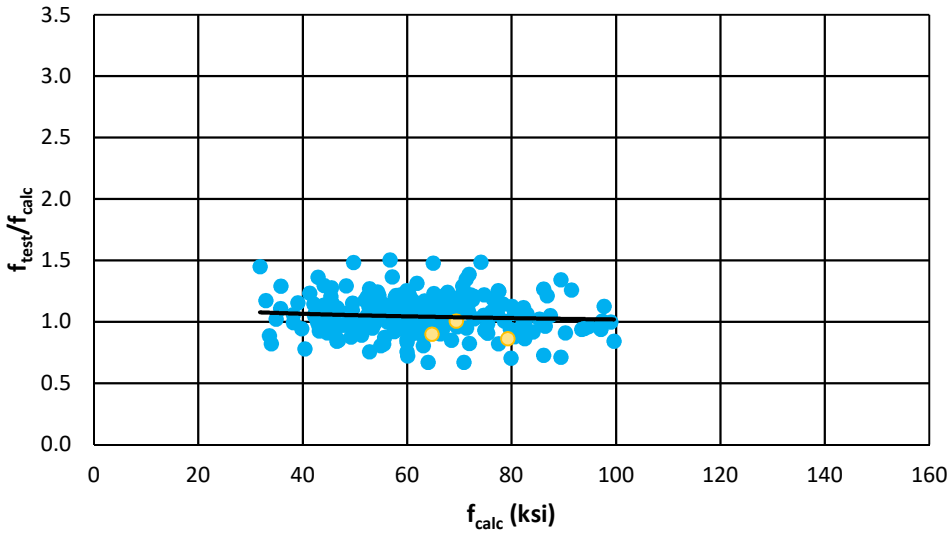

Figure 5.21: Proposed Unconfined Term with Cover Modification Factor (Equation 5-12)

Although the cover modification factor reduces the scatter in the data, it is not necessary as most of the cover modification factors reduce to 1. Additionally, a value of 1 is conservative considering the data and minimum cover requirements. The average F_{test}/F_{calc} of the unconfined data with the modification factor in Equation 5-11 is 1.04 with a standard deviation of 0.17.

5.3.2.2 Confined Splice Strength

To investigate the increase in bar stress because of confinement, unyielded confined specimens with an identical unconfined specimen, with splice lengths longer than $16d_b$ were plotted. The range of splice length included was $16d_b$ to $56d_b$. The lower cutoff was selected because of the limited number of confined tests that did not yield that also had an identical unconfined specimen, the minimum required splice length specified by ACI 318-14, and the increased variation in data below a splice length of $20d_b$ (Sim 2014). Any increase in strength from the confined specimen compared to the identical unconfined specimen was defined as the increase in bar stress because of confinement, f_{tr}.

The increase in bar stress because of confinement was plotted against different variables. Although no trend was observed between the area of one leg of transverse steel and the increase in bar stress because of confinement (Figure 5.22), there was a linear trend found between the total area of transverse steel within the splice length and the bar stress (Figure 5.23).

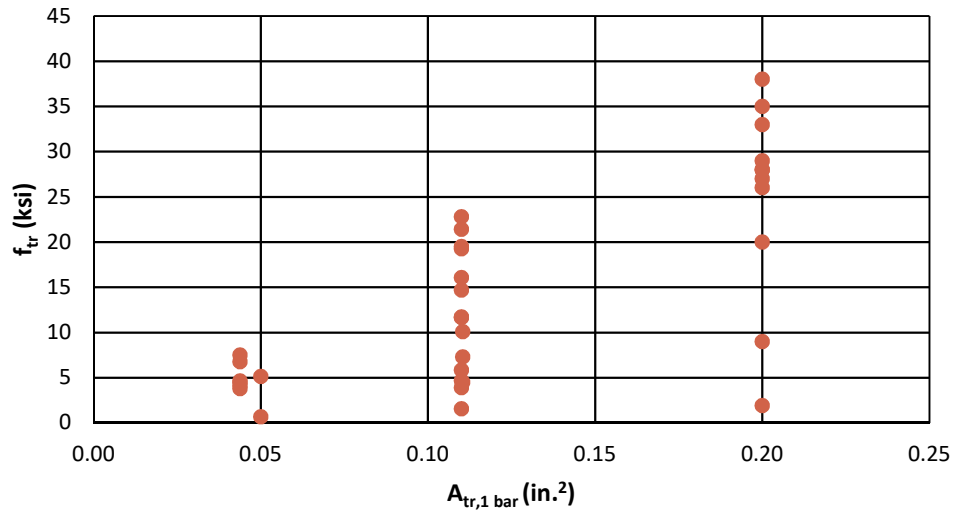

Figure 5.22: Increase in Bar Stress Caused by Area of One Leg of Transverse Steel

To determine if the increase in bar stress is only correlated to the total area of steel in the splice, the total area of steel was plotted against the increase in bar stress for two different bar sizes (#8

and #11 bars) in Figure 5.23. As shown, both #8 and #11 bars are distributed around the trendline.

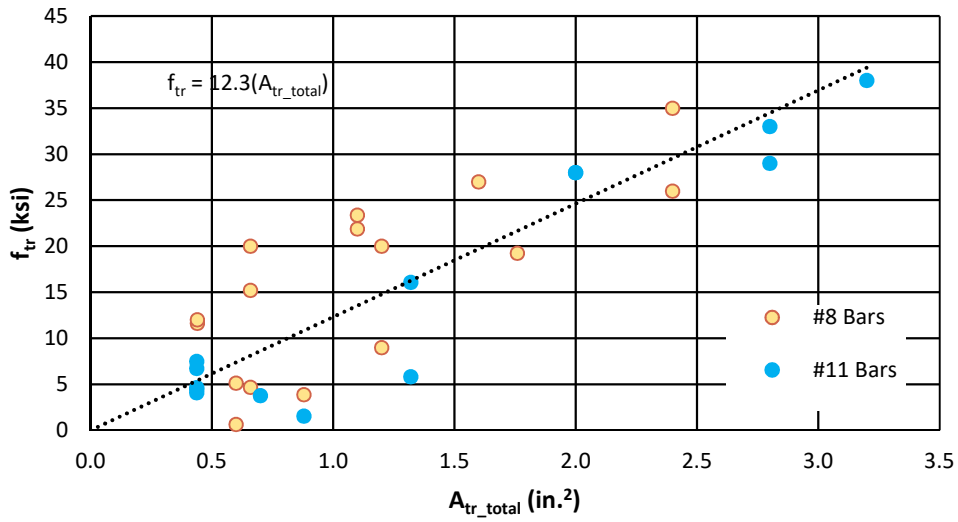

Figure 5.23: Increase in Bar Stress Caused by Total Area of Steel- Linear Trend

While the confinement term in Sim's equation (Equation 4-28) included the yield strength of the transverse reinforcement, f_{yt}, it has been shown that transverse reinforcement rarely reaches its yield strength (Section 1.5.6). As a result, the yield strength was determined not to be important in determining the increase in bar stress that confinement would provide. Other variables that could be considered important to the increase in bar strength because of confinement were also considered: l_s/d_b, N_b, A_b, and f_c'. A trend was not observed between any of these variables and an increase in bar stress because of confinement. The relationship of these variables is plotted in Appendix G.

Based on the trendline in Figure 5.23, a linear relationship with a coefficient of 12 was selected to calculate the increase in bar stress because of confinement (Equation 5-13).

$$f_{tr} = 12A_{tr,1bar}N_lN_s \qquad (5\text{-}13)$$
$$where\ A_{tr\_total} = A_{tr,1bar}N_lN_s$$

where:

A_{tr_total} = *total area of transverse reinforcement within lap splice region, in.*^{2}

$A_{tr,1bar}$ = *area of one leg of transverse reinforcement, in.*^{2}

f_{tr} = *contribution of transverse reinforcement in splice region, ksi*

N_l = *number of legs of transverse reinforcement that cross the splitting plane*

N_s = *number of stirrups*

After plotting the relationship between the total area of steel within the splice region and the ratio of the bar stress determined from testing, f_{test}, and that calculated from Equations 5-12 and 5-13, f_{calc}, a downward trend was observed (Figure 5.24(a)). To correct for this downward trend, a power of 0.5 was applied to the variable A_{tr_total}. The corrected confinement term is shown in Figure 5.24(b), which provides improved results. Figure 5.25 plots both the power trendline (Equation 5-14) and the data used in Figure 5.23.

$$f_{tr} = 12\left(A_{tr,1bar}N_lN_s\right)^{0.5} \quad \text{where } A_{tr\_total} = A_{tr,1bar}N_lN_s \tag{5-14}$$

where:

A_{tr_total} = *total area of transverse reinforcement within lap splice region, in.*^{2}

$A_{tr,1bar}$ = *area of one leg of transverse reinforcement, in.*^{2}

f_{tr} = *contribution of transverse reinforcement in splice region, ksi*

N_l = *number of legs of transverse reinforcement that cross the splitting plane*

N_s = *number of stirrups*

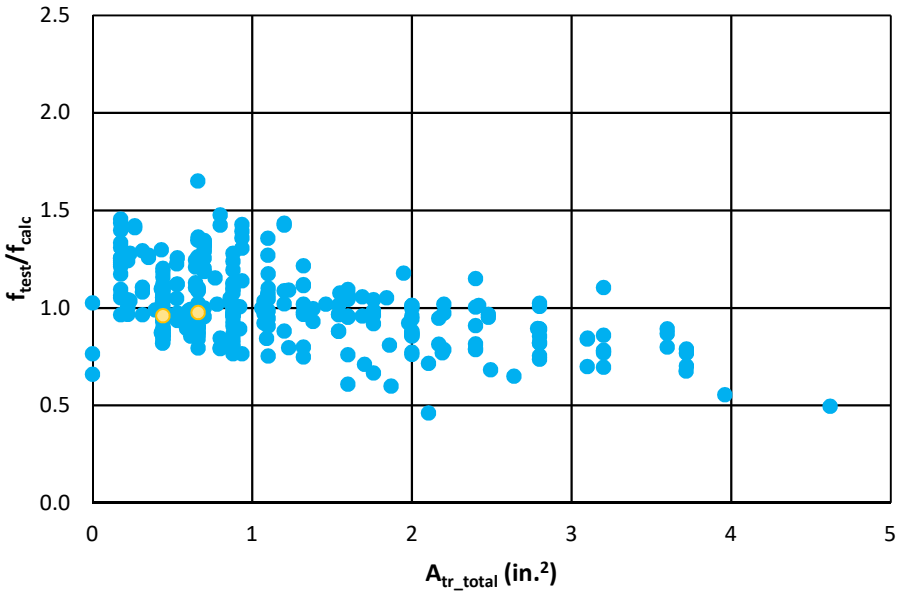

a) Linear Trend (Equation 5-13)

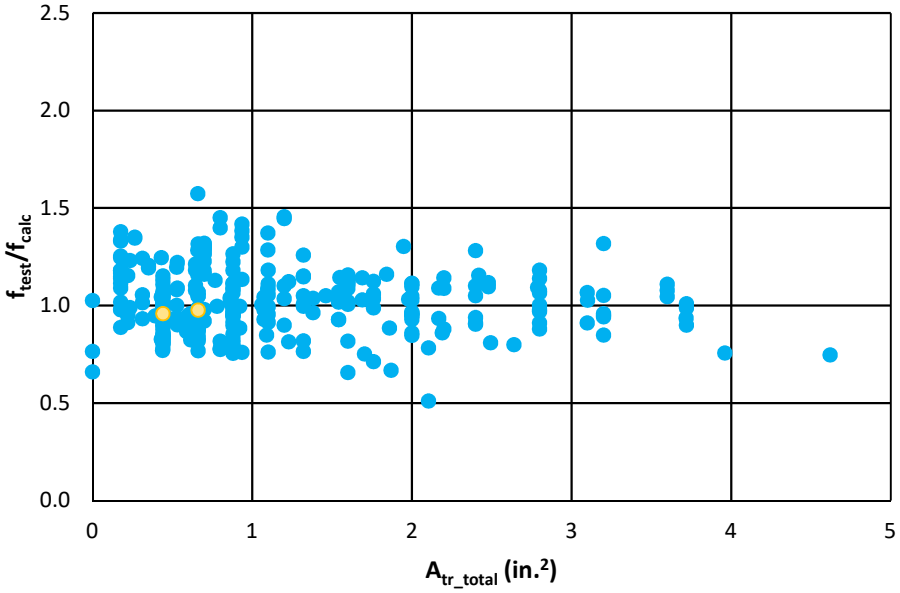

b) Power Trend (Equation 5-14)

Figure 5.24: Confinement Term

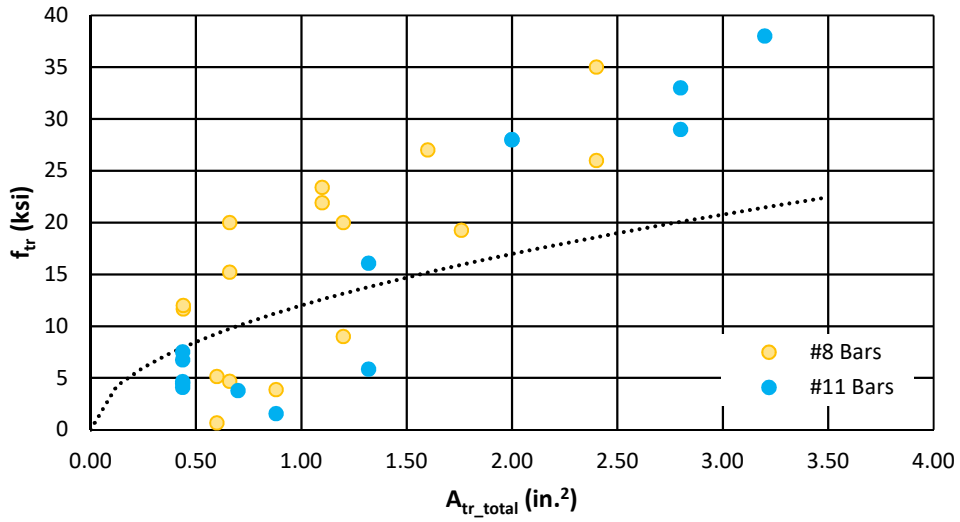

Figure 5.25: Increase in Bar Stress Caused by Total Area of Steel- Power Trend

The increase in bar stress because of confinement ($f_{tr,test}$) was compared with the increase in bar stress calculated with the proposed confinement term ($f_{tr,calc}$, Equation 5-14) in Figure 5.26. The scatter was found to increase for those data points that have a lower total area of steel within the splice length. For low reinforcement amounts, the location of the transverse reinforcement is very important. For higher amounts, this relationship works very well. In Figure 5.26, historical data is represented with blue points, while the data from this study are represented with yellow.

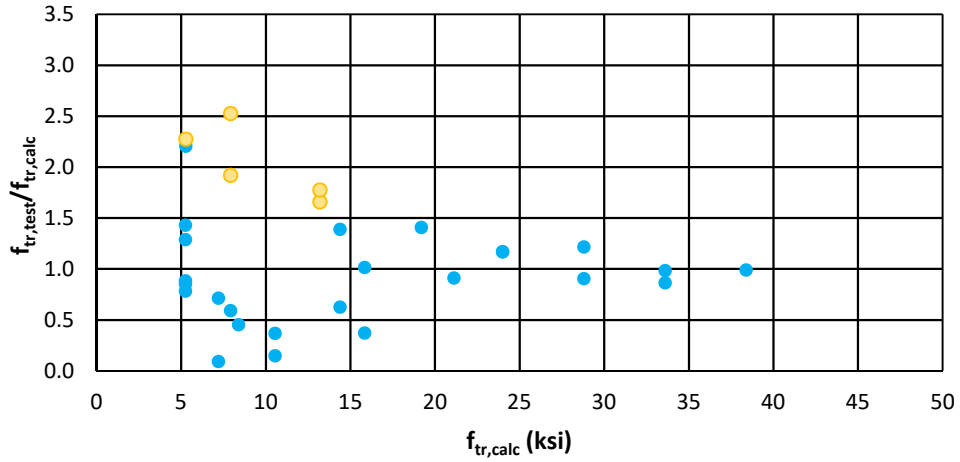

Figure 5.26: Proposed Confined Term (Equation 5-14)

The confinement term developed previously by Sim (Equation 5-15) is included for comparison purposes in Figure 5.27 where f_{test}/f_{calc} is plotted against the increase in bar stress because of confinement.

$$f_{tr} = \frac{1}{2}\frac{A_{tr}f_{yt}}{A_b N_b}N_s \qquad (5\text{-}15)$$

where:

A_{tr}=*total area of transverse reinforcement crossing the potential splitting plane* ($A_{tr}=A_{tr,1bar}N_l$), *in.*^{2}

$A_{tr,1bar}$= *area of one leg of transverse reinforcement, in.*^{2}

f_{yt}= *yield strength of transverse reinforcement, kips*

f_{tr}= *contribution of transverse reinforcement in splice region, ksi*

N_b= *number of spliced or developed bars*

N_l= *number of legs of transverse reinforcement that cross the splitting plane*

N_s= *number of stirrups*

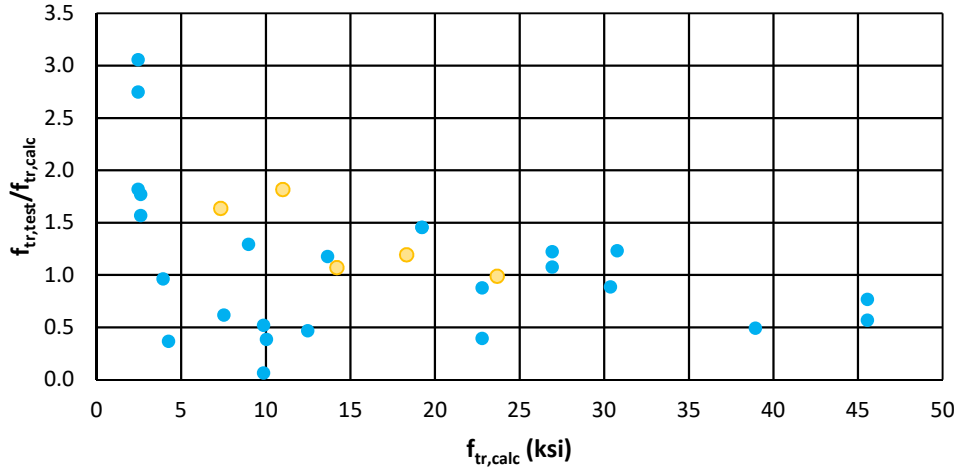

Figure 5.27: Sim Confinement Term (Equation 5-15)

5.3.2.3 Combined Unconfined and Confined Terms

The confinement term (Equation 5-14) can be added to the unconfined term (Equation 5-6). Figure 5.28 plots the unconfined data using Equation 5-16. Figure 5.28 shows how the analysis

equation (f_{calc}) compares to the bar stress values obtained from testing for the unconfined specimens, while Figure 5.29 presents the confined specimens. Figure 5.30 includes all specimens (unconfined and confined) in the database (Table 5.1).

$$f_s = \frac{8{L_{eq}}^{0.5}}{A_b}\left(\frac{c_{so}}{d_b}\right)^{0.25}\left(\frac{f_c'}{5000\ psi}\right)^{0.25} + 12(A_t N_l N_s)^{0.5} \qquad (5\text{-}16)$$

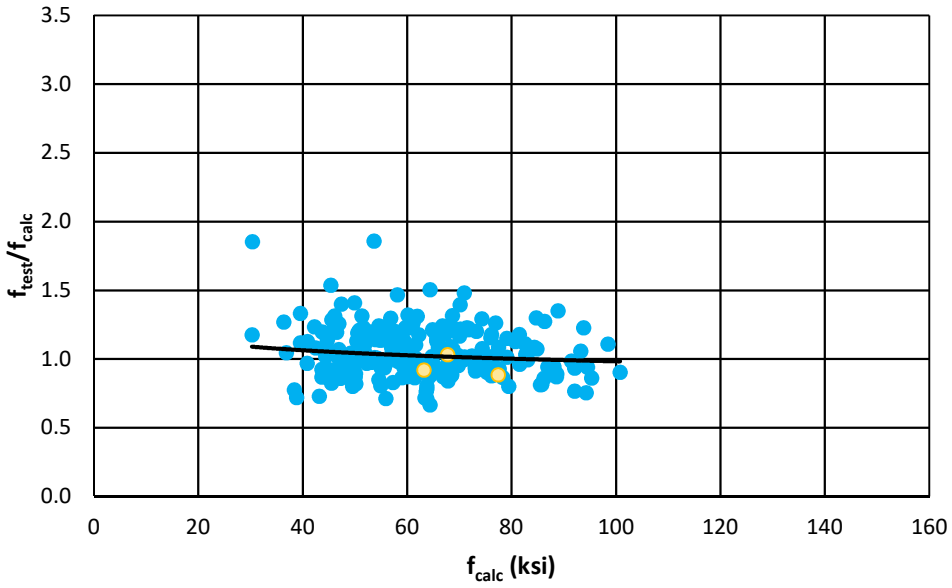

a) Relationship with Calculated Bar Stress

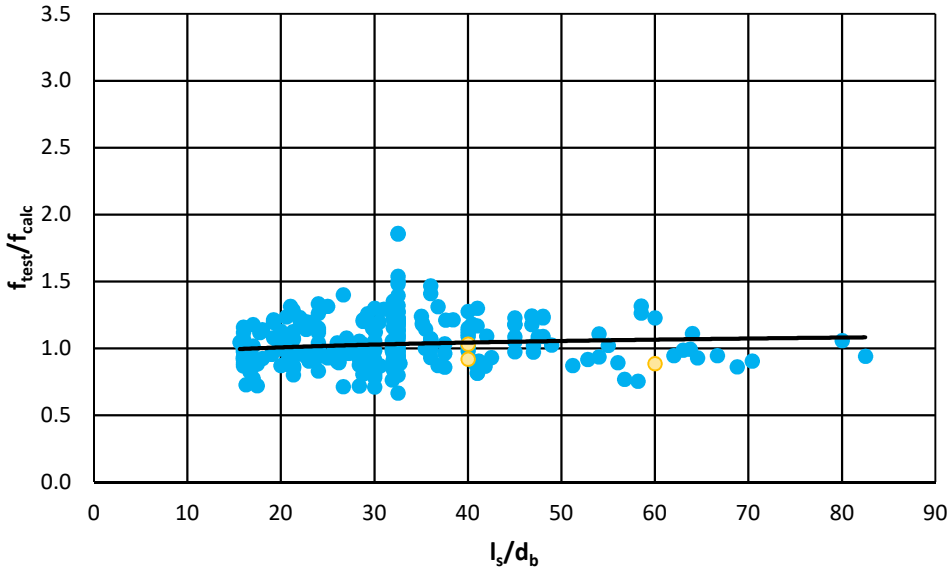

b) Relationship with Splice Length

Figure 5.28: Proposed Analysis Equation- Unconfined Data

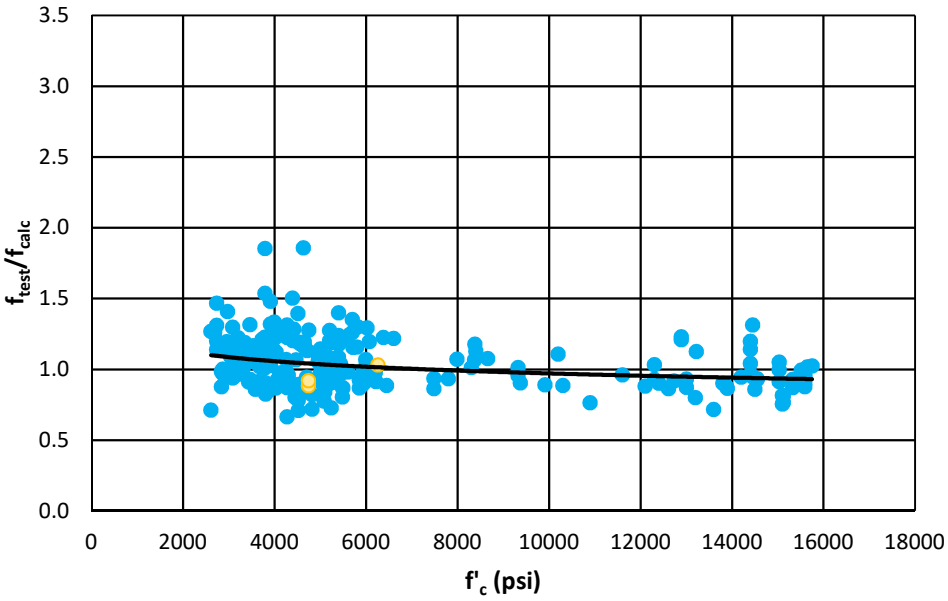

c) Relationship with Concrete Strength

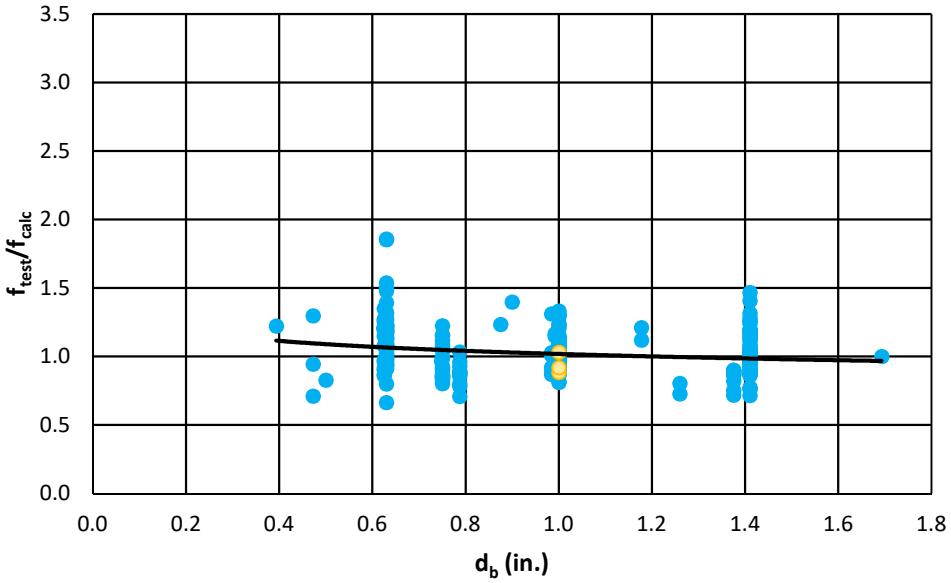

d) Relationship with Bar Diameter

Figure 5.28: Proposed Analysis Equation- Unconfined Data (continued)

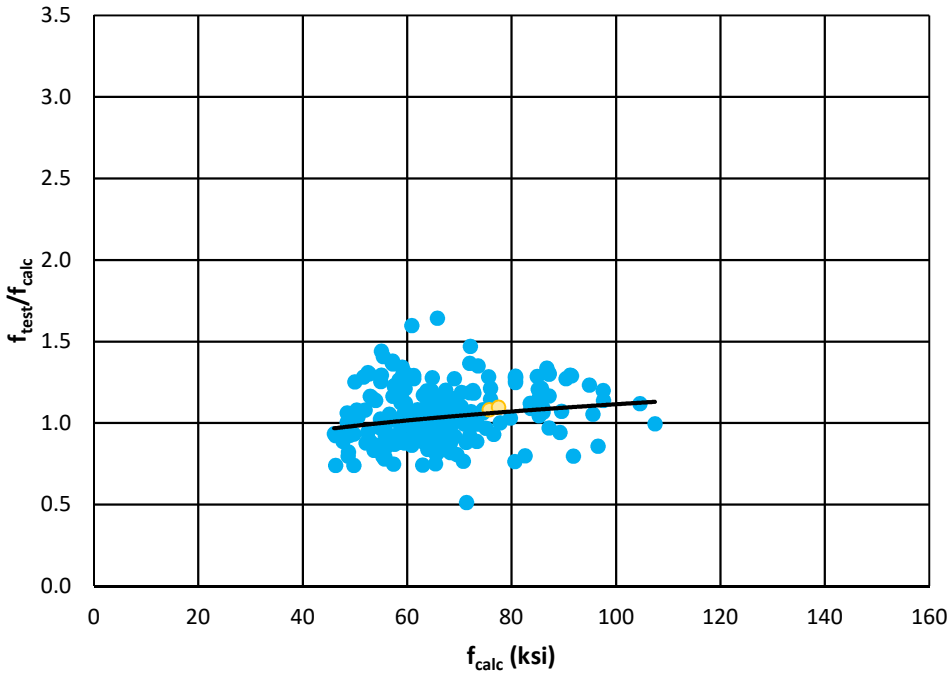

a) Relationship with Calculated Bar Stress

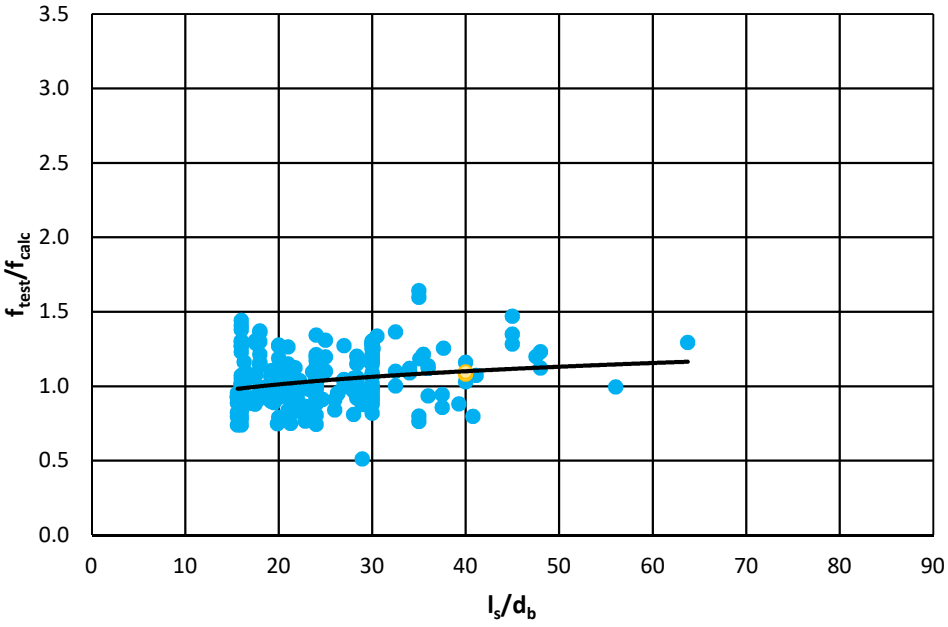

b) Relationship with Splice Length

Figure 5.29: Proposed Analysis Equation- Confined Data

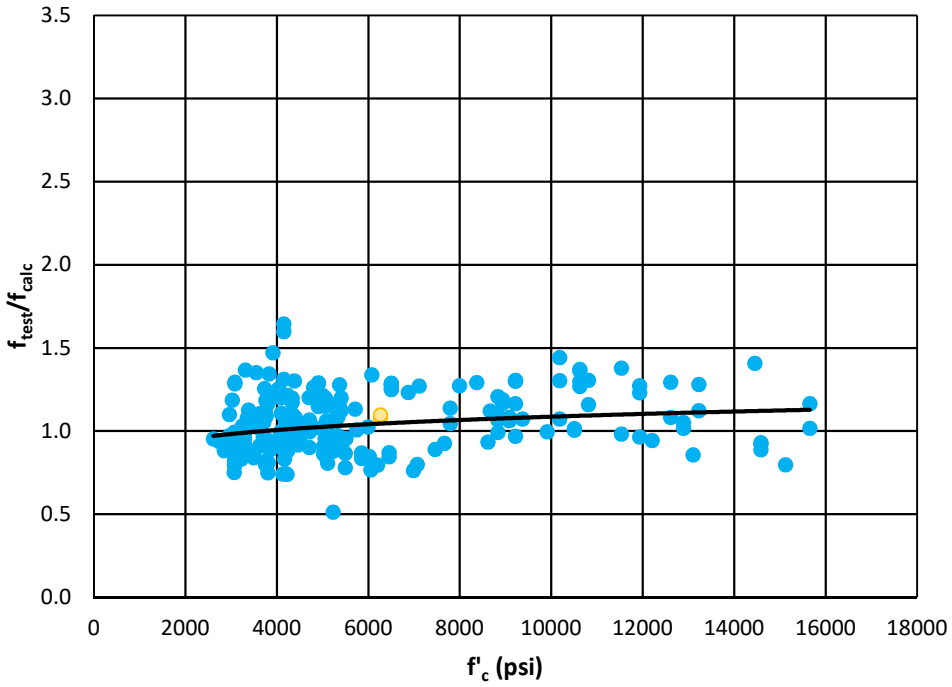

c) Relationship with Concrete Strength

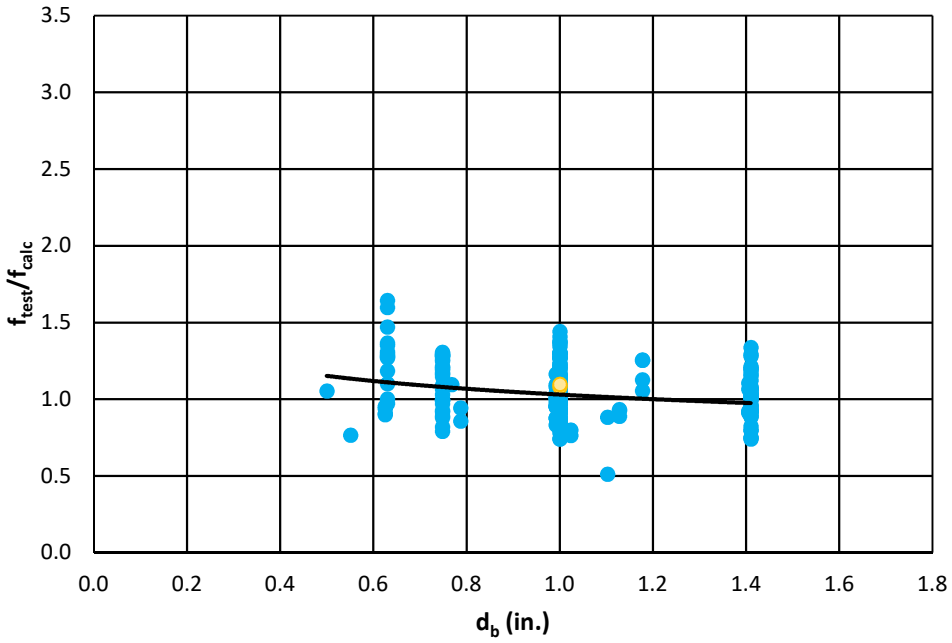

d) Relationship with Bar Diameter

Figure 5.29: Proposed Analysis Equation- Confined Data (continued)

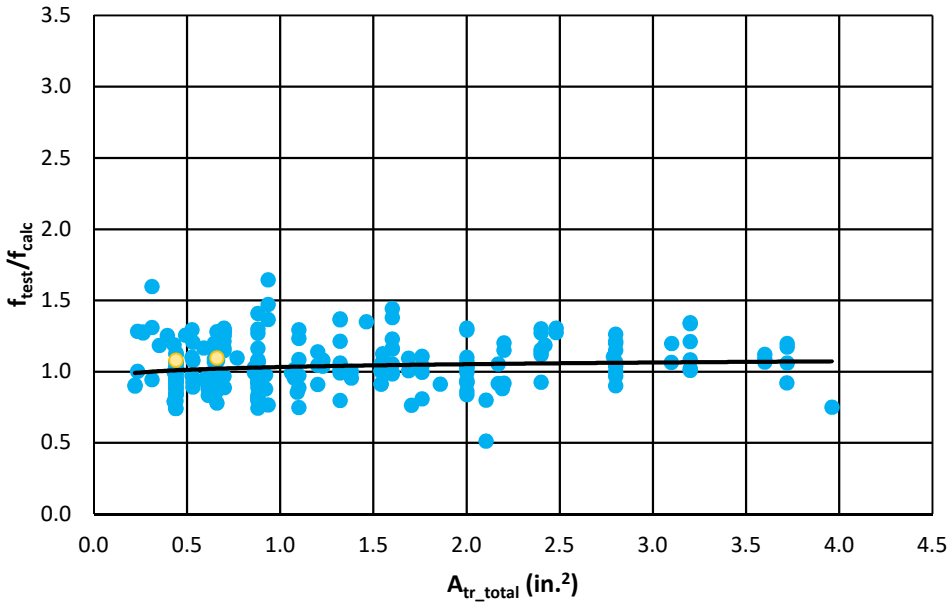

e) Relationship with Total Area of Steel within Splice Region

Figure 5.29: Proposed Analysis Equation- Confined Data (continued)

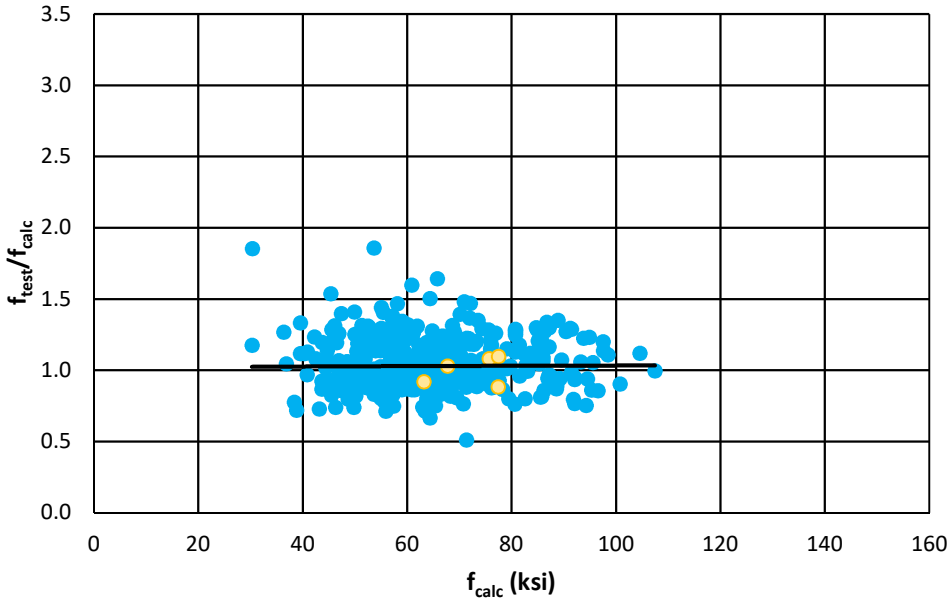

a) Relationship with Calculated Bar Stress

Figure 5.30: Proposed Analysis Equation- All Data

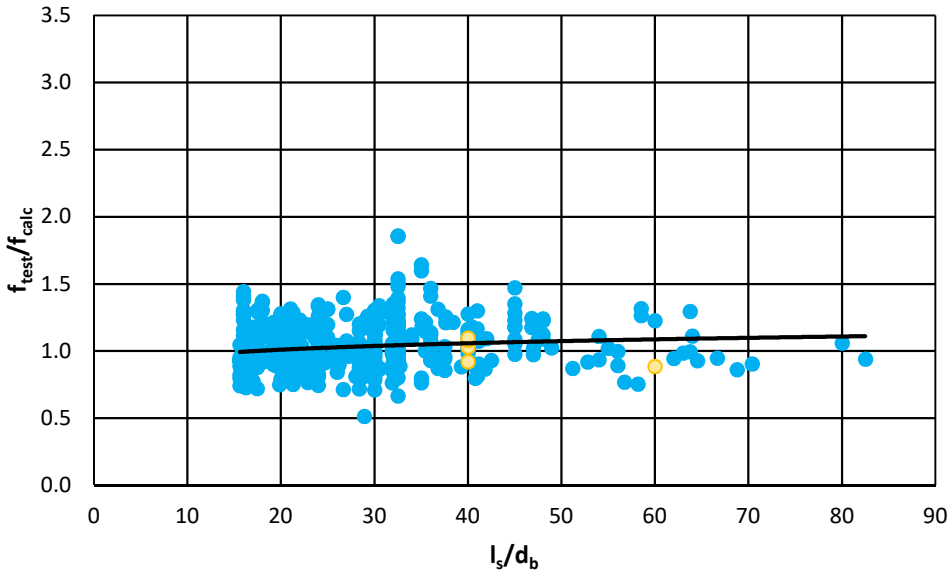

b) Relationship with Splice Length

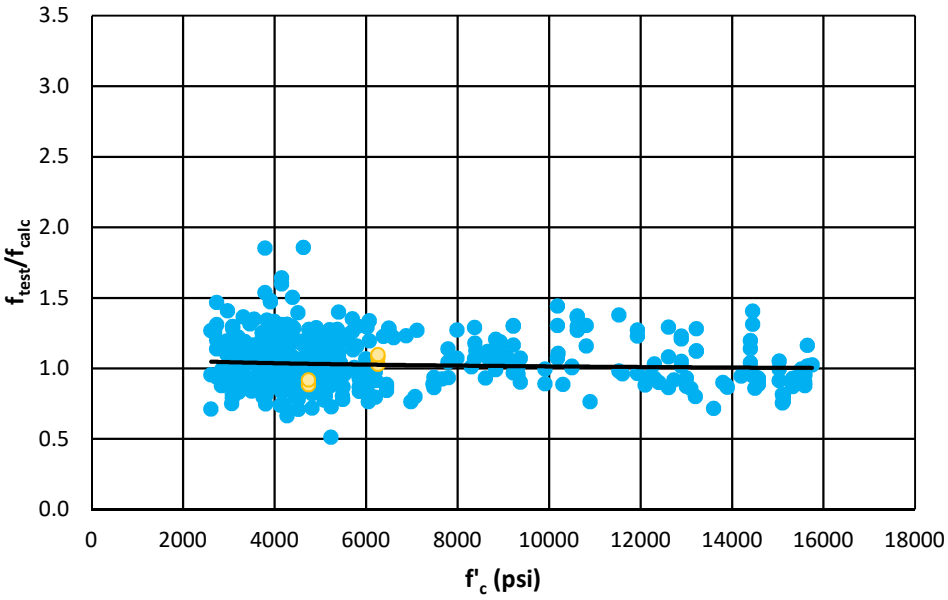

c) Relationship with Concrete Strength

Figure 5.30: Proposed Analysis Equation- All Data (continued)

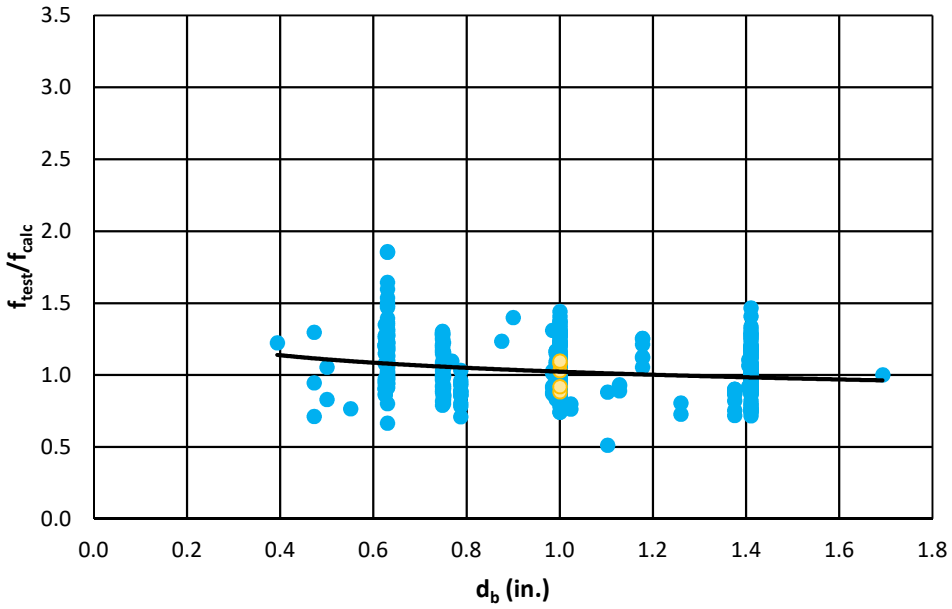

d) Relationship with Bar Diameter

Figure 5.30: Proposed Analysis Equation- All Data (continued)

5.4 Comparison with ACI 318, ACI 408R-03, and CB 603

The equations developed are compared with the code equations presented in Sections 4.2.1 to 4.2.3. While the equation described in Section 5.3 is developed for analysis, a factor of safety can be added for design purposes. A statistical comparison of the various equations is provided in Tables 5.4 to 5.6. The comparison is based on the specimens from the database discussed in Table 5.1. Additionally, histograms of the frequency of the f_{test}/f_{calc} values for each of the various methods are provided in Figures 5.31 to 5.34.

Tables 5.4 to 5.6 show that Equation ACI 318-14 has a larger spread than ACI 408R-03 and the proposed CB 603 equation (larger standard error and standard deviation). The proposed analysis equation has a lower mean than the design equations. This is expected as design equations should be more conservative than an analysis equation. The proposed analysis equation has the least scatter, with the most number of values concentrated around the mean value of 1.0. Change proposal CB 603, has a higher mean and maximum, however, only 2.1% of points are unconservative (Table 5.7).

Table 5.4: Comparison of Equations for Unconfined Data

	ACI 318-14 (Eq. 4-1)	ACI 408 (Eq. 4-2)	CB 603 (Eq. 4-10)	Proposed Analysis (Eq. 5-15)
Mean	1.21	1.27	1.37	1.04
Standard Error	0.02	0.01	0.02	0.01
Standard Deviation	0.40	0.22	0.34	0.17
Minimum	0.59	0.70	0.84	0.67
Maximum	3.00	2.38	3.10	1.86

Table 5.5: Comparison of Equations for Confined Data

	ACI 318-14 (Eq. 4-1)	ACI 408 (Eq. 4-2)	CB 603 (Eq. 4-10)	Proposed Analysis (Eq. 5-15)
Mean	1.22	1.29	1.33	1.05
Standard Error	0.02	0.01	0.02	0.01
Standard Deviation	0.33	0.23	0.25	0.17
Minimum	0.38	0.54	0.74	0.51
Maximum	2.45	2.04	2.37	1.64

Table 5.6: Comparison of Equations for All Data

	ACI 318-14 (Eq. 4-1)	ACI 408 (Eq. 4-2)	CB 603 (Eq. 4-10)	Proposed Analysis (Eq. 5-15)
Mean	1.21	1.28	1.35	1.04
Standard Error	0.01	0.01	0.01	0.01
Standard Deviation	0.36	0.23	0.30	0.17
Minimum	0.38	0.54	0.74	0.51
Maximum	3.00	2.38	3.10	1.86

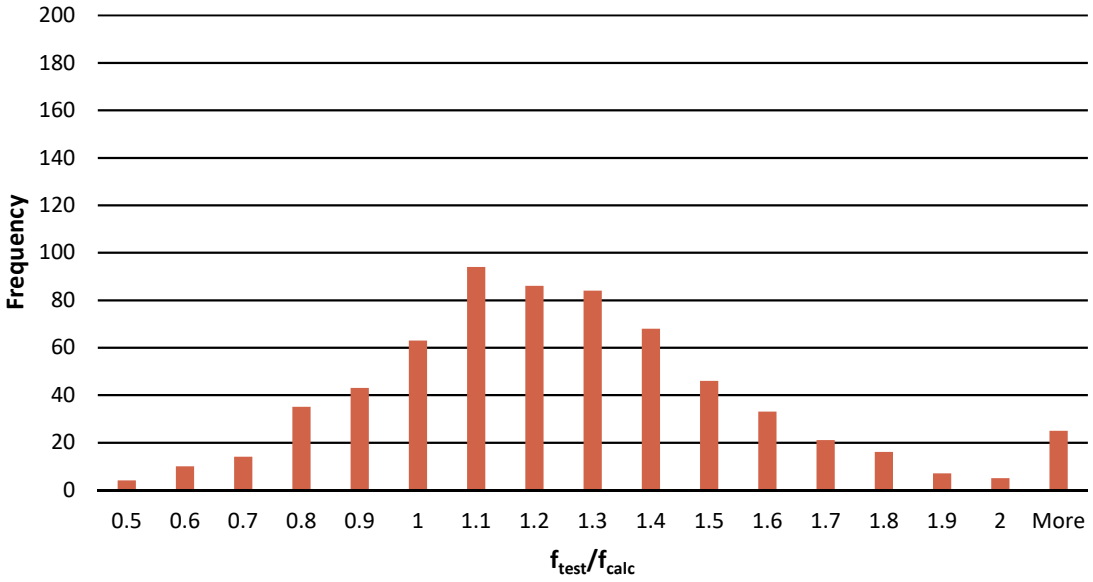

Figure 5.31: Distribution of ACI 318-14

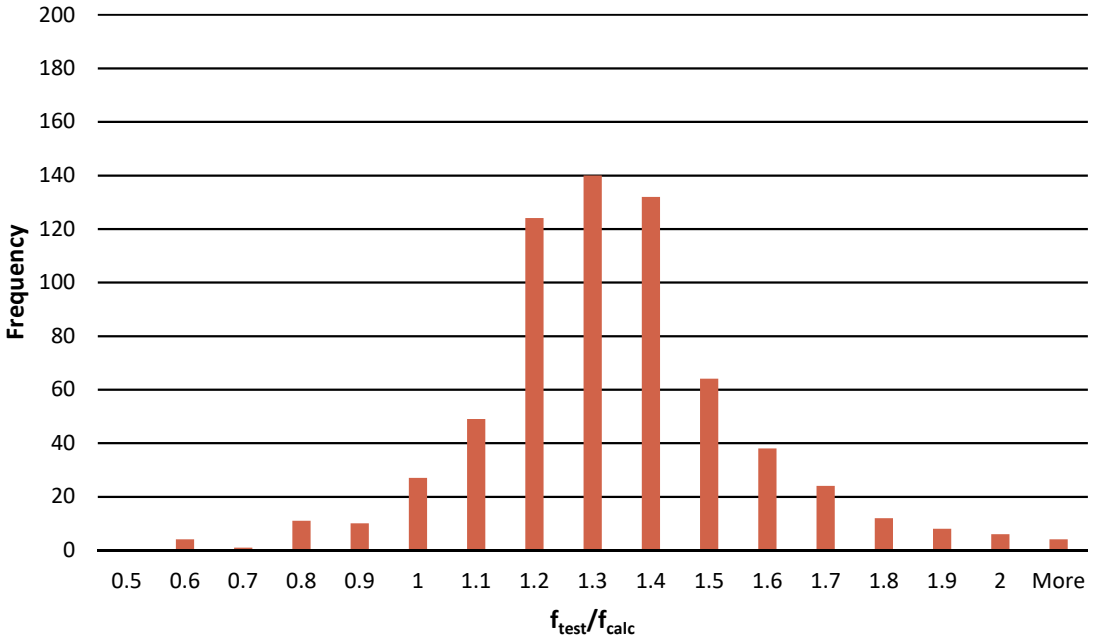

Figure 5.32: Distribution of ACI 408R-03

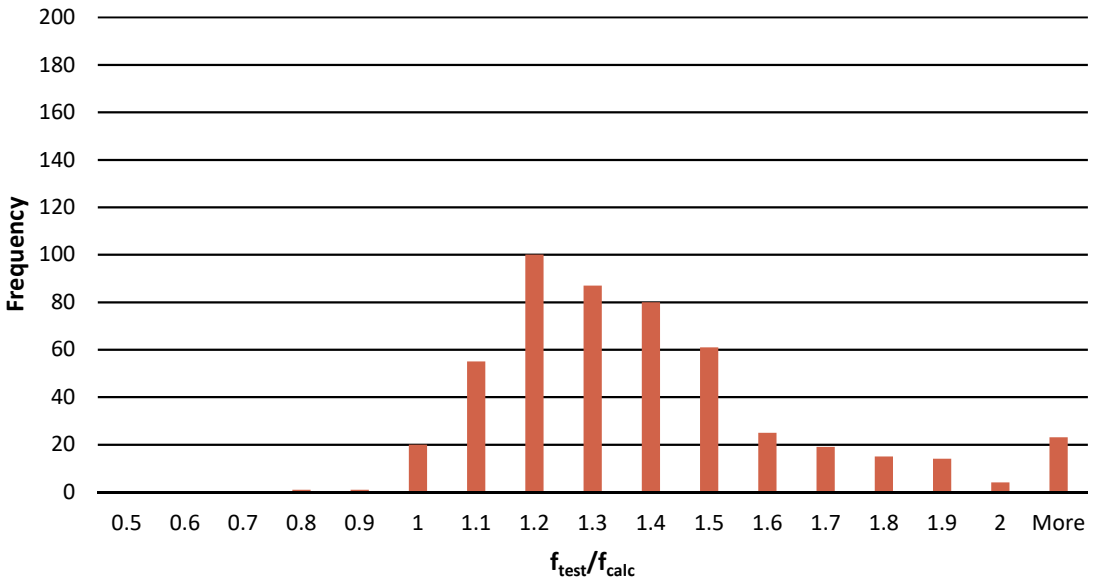

Figure 5.33: Distribution of CB 603

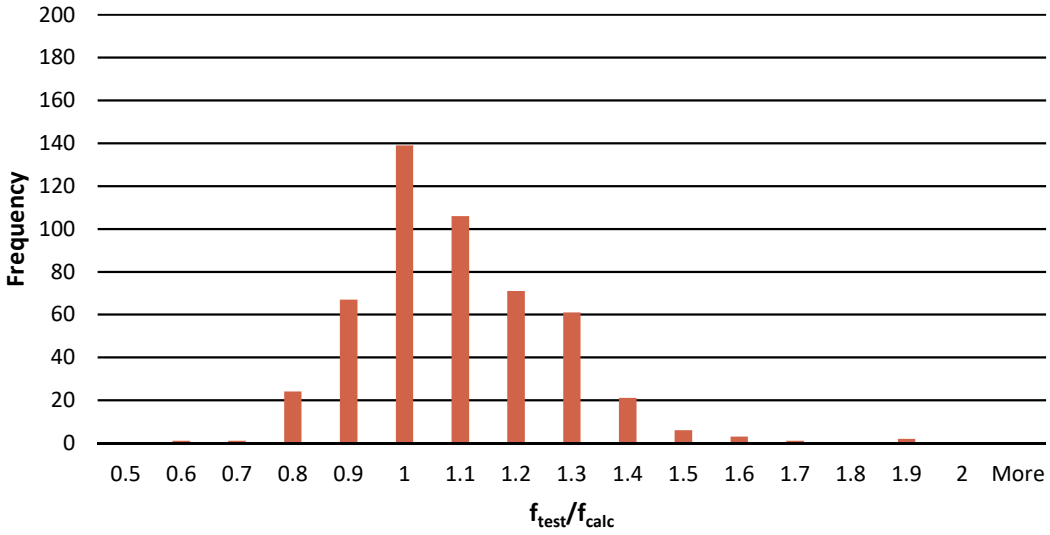

Figure 5.34: Distribution of Proposed Analysis Equation

Table 5.7: Conservatism of Equations

Equation	Percentage of Tests Below f_{test}/f_{calc} Value of 1.0
ACI 318-14	5.2%
ACI 408R-03	4.0%
CB 603	2.1%
Proposed Analysis	18.5%

5.4.1 ACI 318-14

The relationships between the different variables (calculated bar stress, splice length in terms of bar diameter, concrete strength, bar diameter, and total area of steel within the splice region) are plotted versus the ratio of the bar stress determined from testing (f_{test}) over the bar stress determined from ACI 318-14 (f_{calc}) (Figures 5.35 to 5.37). This allows direct comparison of the analysis results presented in Figures 5.28 to 5.30.

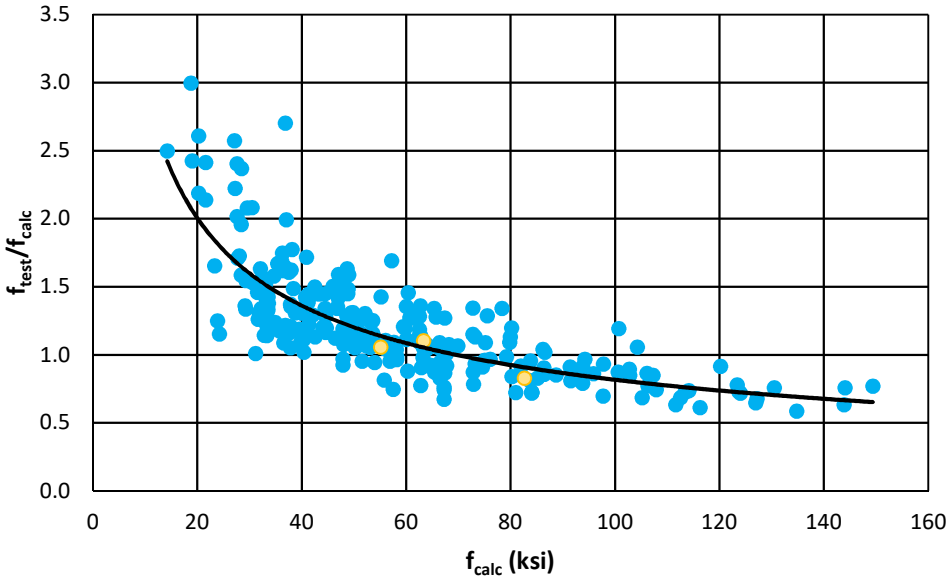

a) Relationship with Calculated Bar Stress

Figure 5.35: ACI 318-14 Equation- Unconfined Data

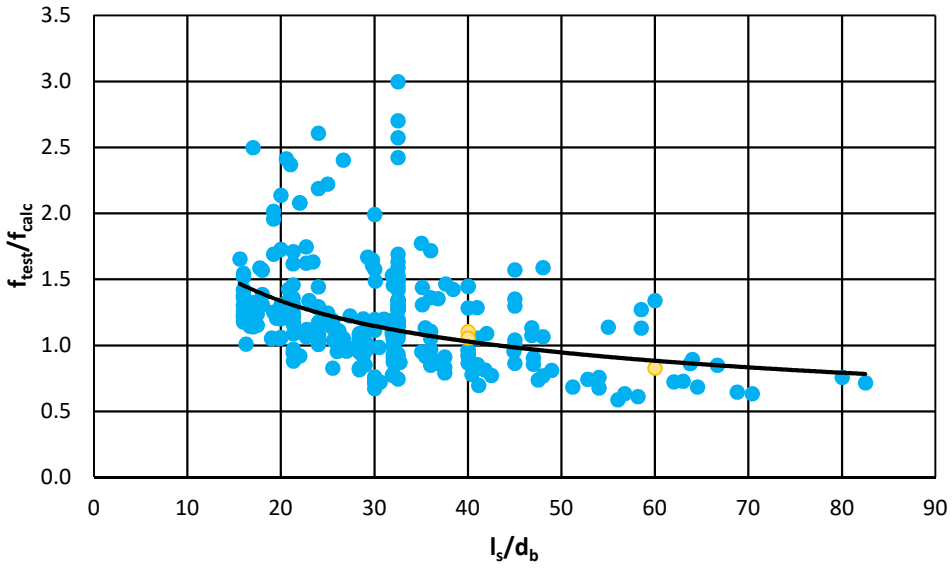

b) Relationship with Splice Length

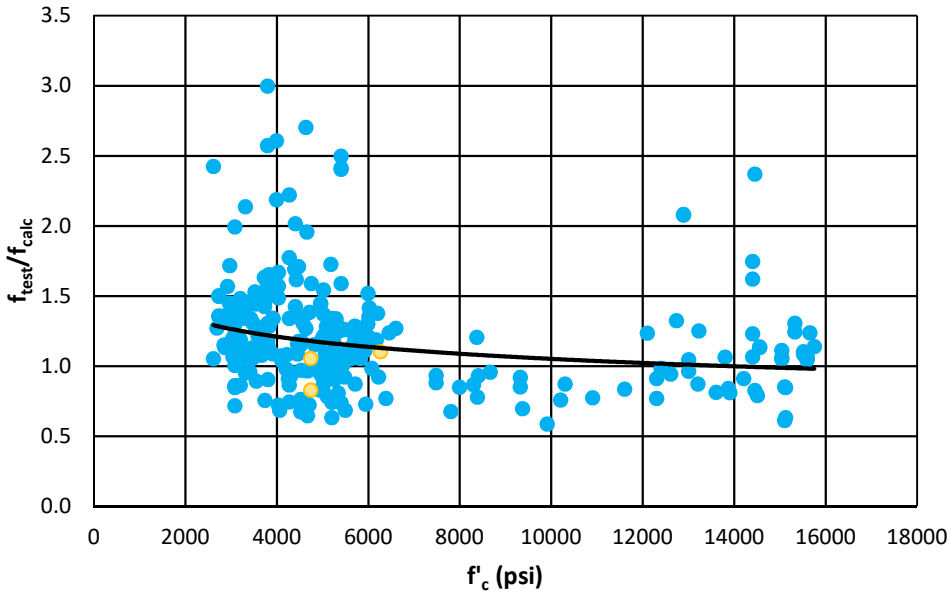

c) Relationship with Concrete Strength

Figure 5.35: ACI 318-14 Equation- Unconfined Data (continued)

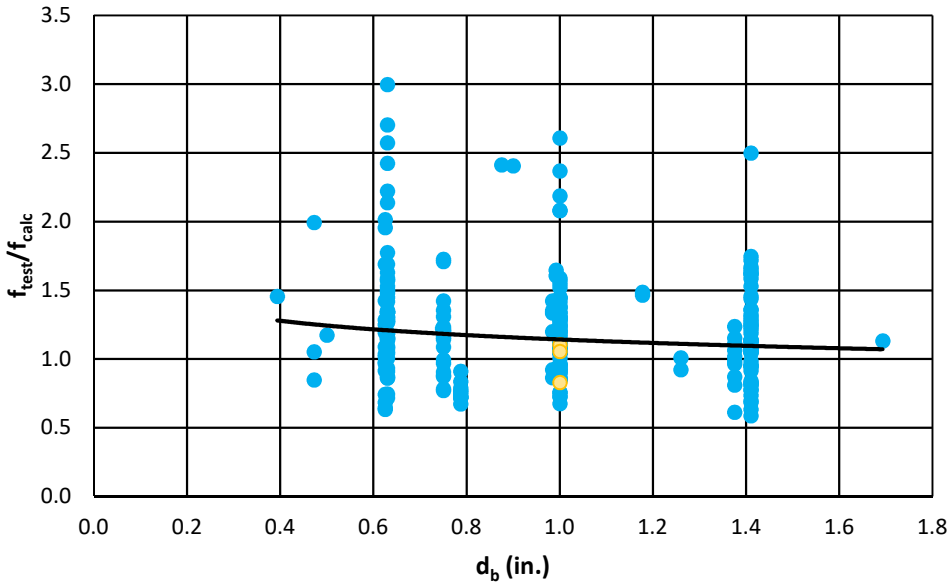

d) Relationship with Bar Diameter

Figure 5.35: ACI 318-14 Equation- Unconfined Data (continued)

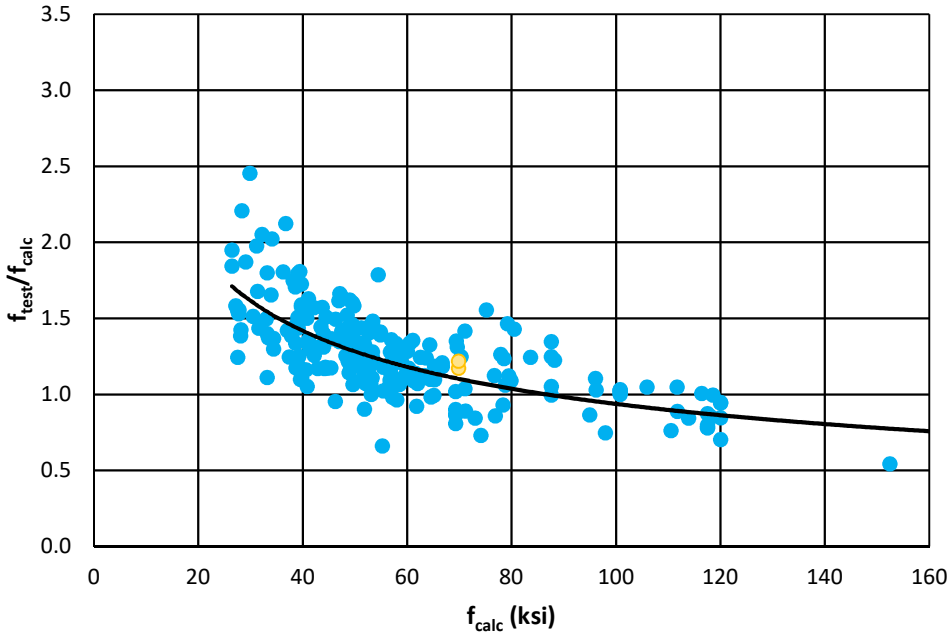

a) Relationship with Calculated Bar Stress

Figure 5.36: ACI 318-14 Equation- Confined Data

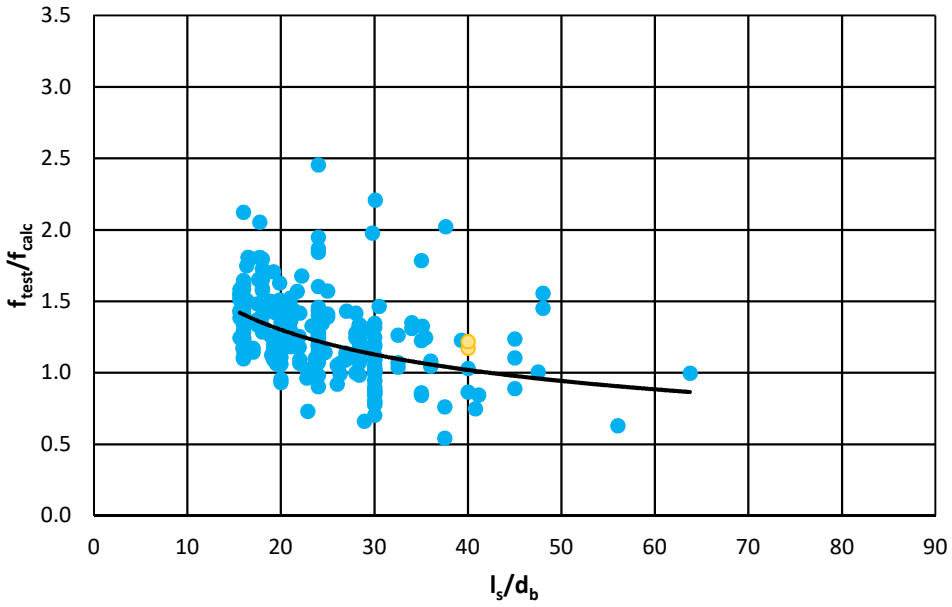

b) Relationship with Splice Length

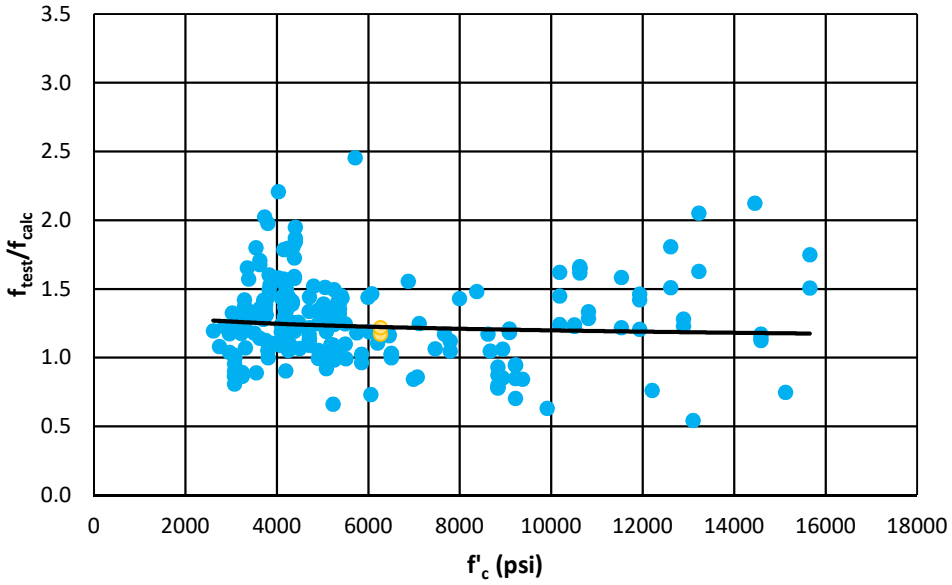

c) Relationship with Concrete Strength

Figure 5.36: ACI 318-14 Equation- Confined Data (continued)

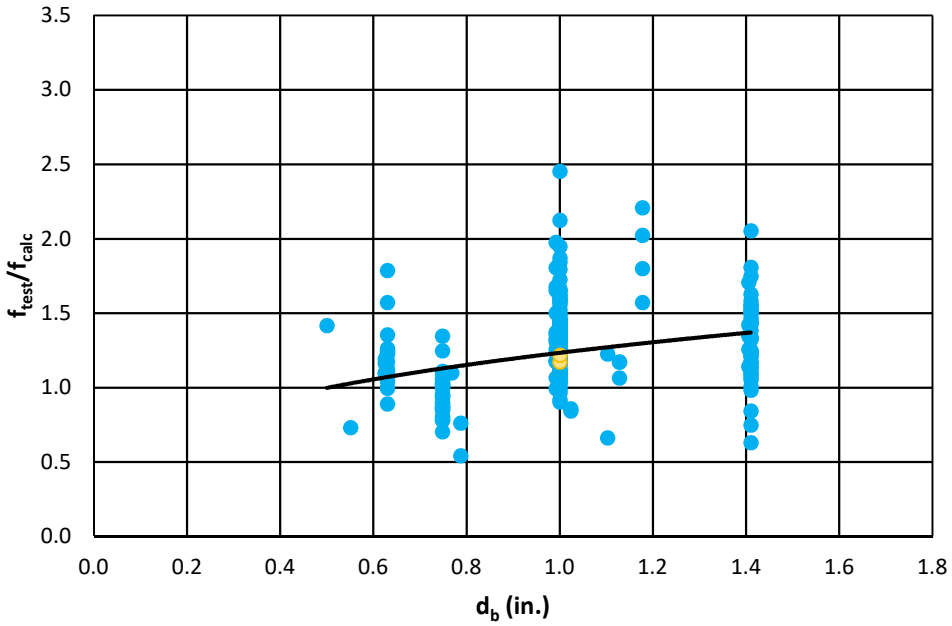

d) Relationship with Bar Diameter

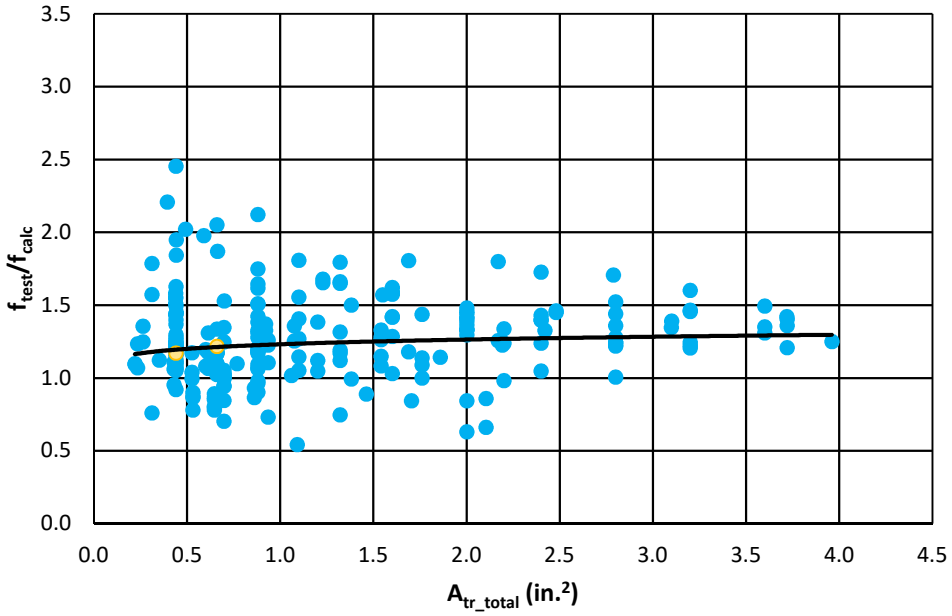

e) Relationship with Total Area of Steel within Splice Region

Figure 5.36: ACI 318-14 Equation- Confined Data (continued)

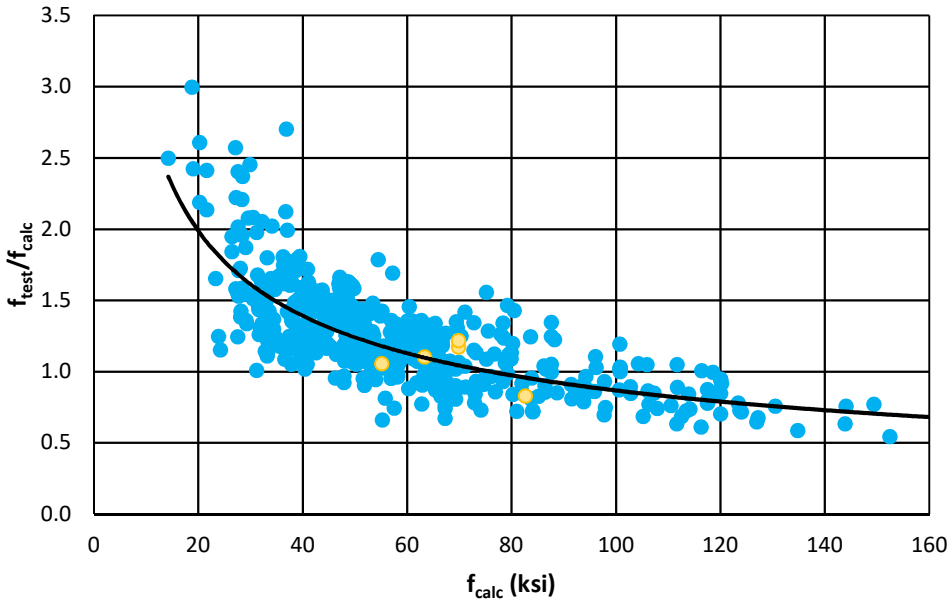

a) Relationship with Calculated Bar Stress

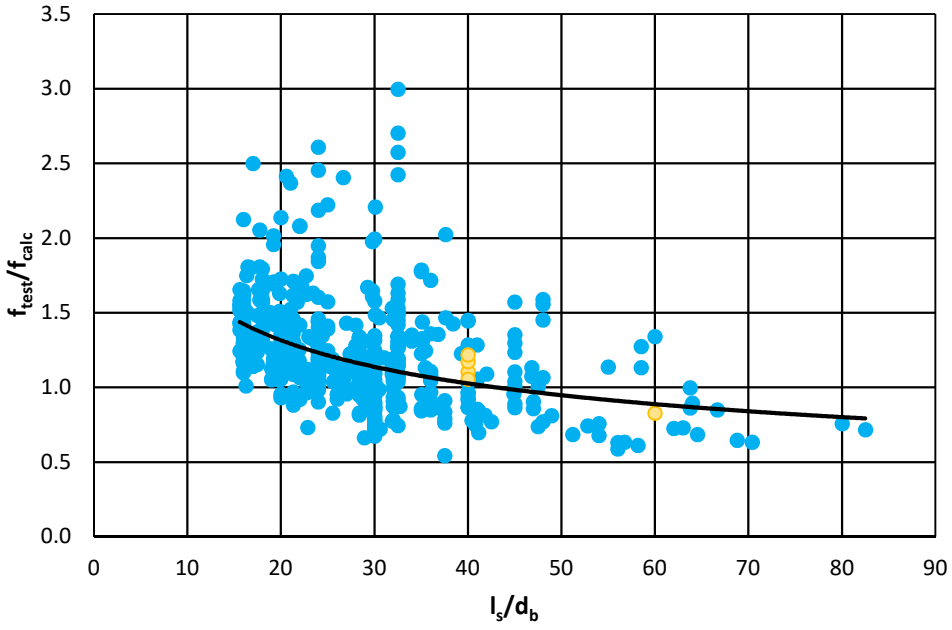

b) Relationship with Splice Length

Figure 5.37: ACI 318-14 Equation- All Data

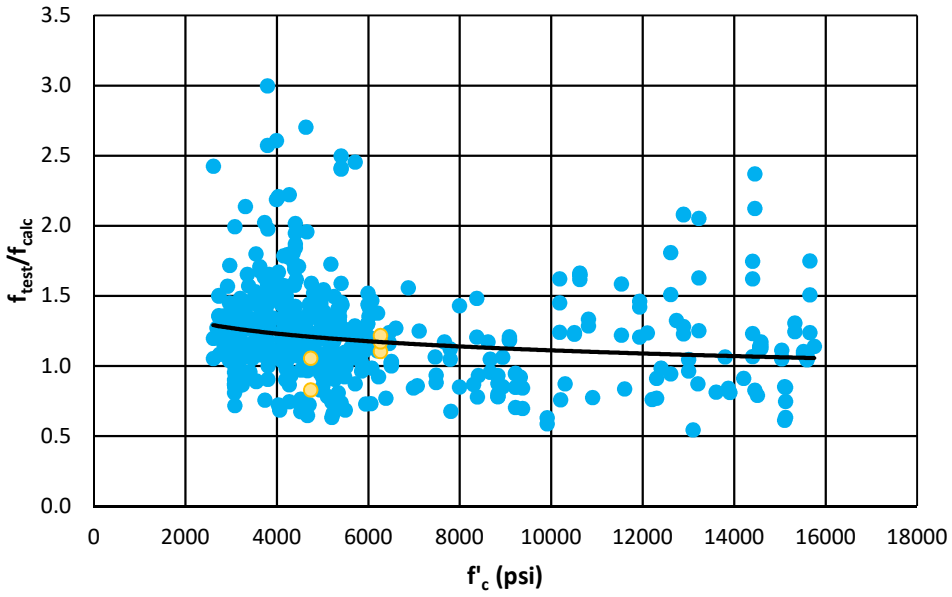

c) Relationship with Concrete Strength

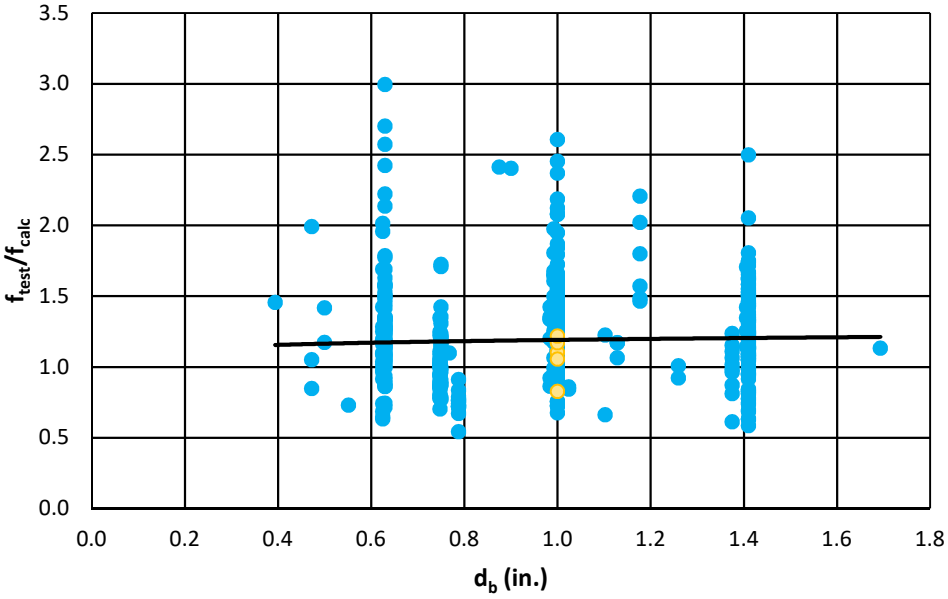

d) Relationship with Bar Diameter

Figure 5.37: ACI 318-14 Equation- All Data (continued)

5.4.2 ACI 408R-03

The relationships between the different variables (calculated bar stress, splice length in terms of bar diameter, concrete strength, bar diameter, and total area of steel within the splice region) are plotted versus the ratio of the bar stress determined from testing (f_{test}) over the bar stress determined from ACI 408R-03 (f_{calc}) (Figures 5.38 to 5.40). This allows direct comparison of the analysis results presented in Figures 5.28 to 5.30.

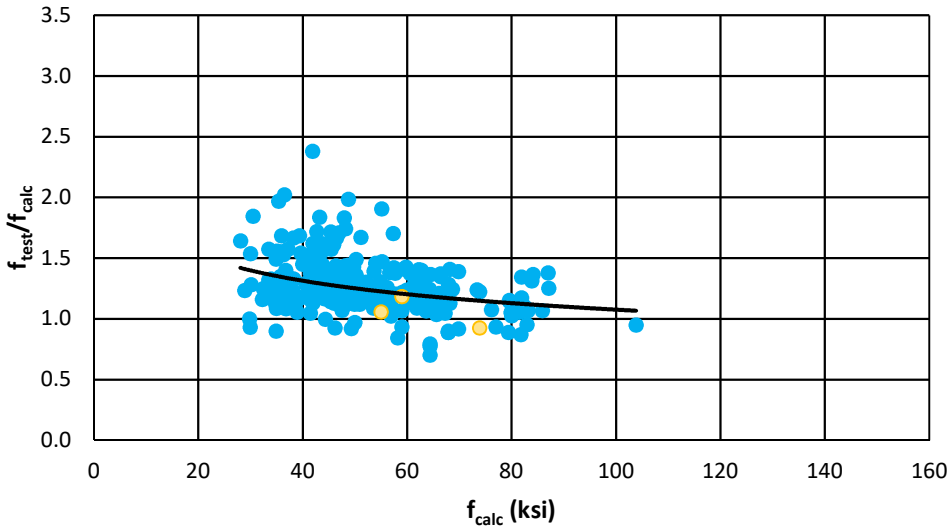

a) Relationship with Calculated Bar Stress

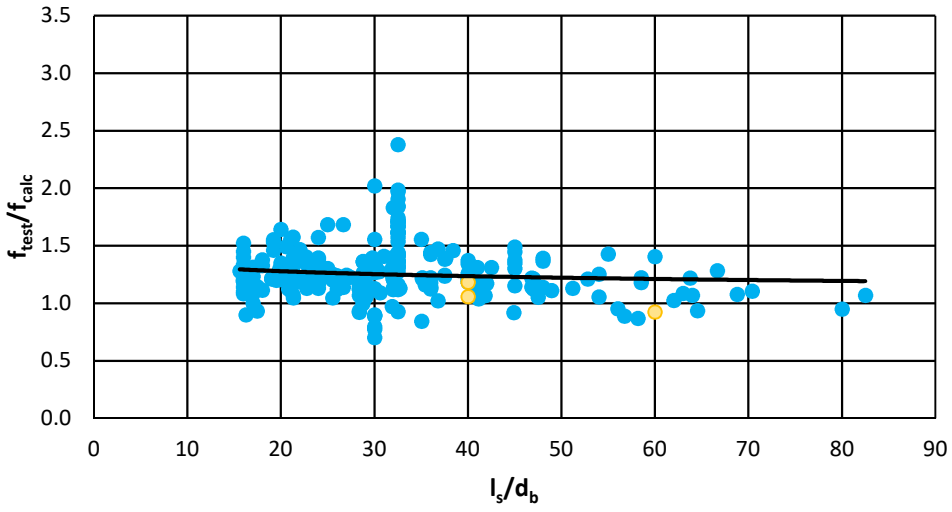

b) Relationship with Splice Length

Figure 5.38: ACI 408R-03 Equation- Unconfined Data

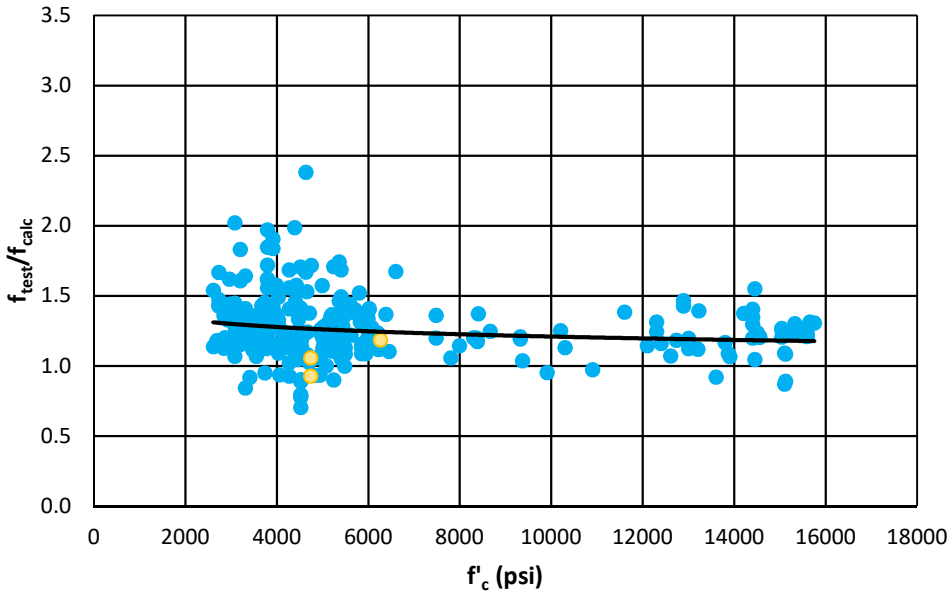

c) Relationship with Concrete Strength

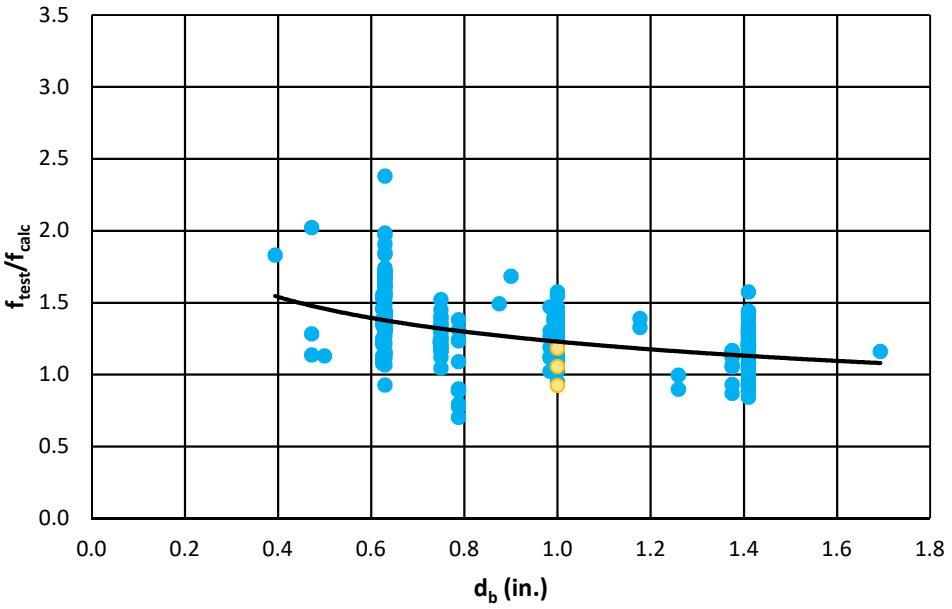

d) Relationship with Bar Diameter

Figure 5.38: ACI 408R-03 Equation- Unconfined Data (continued)

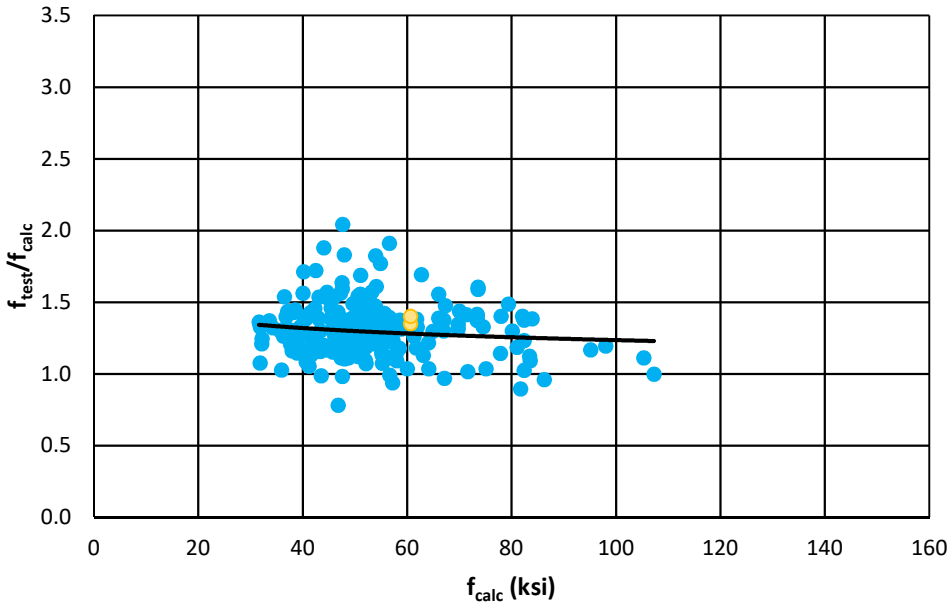

a) Relationship with Calculated Bar Stress

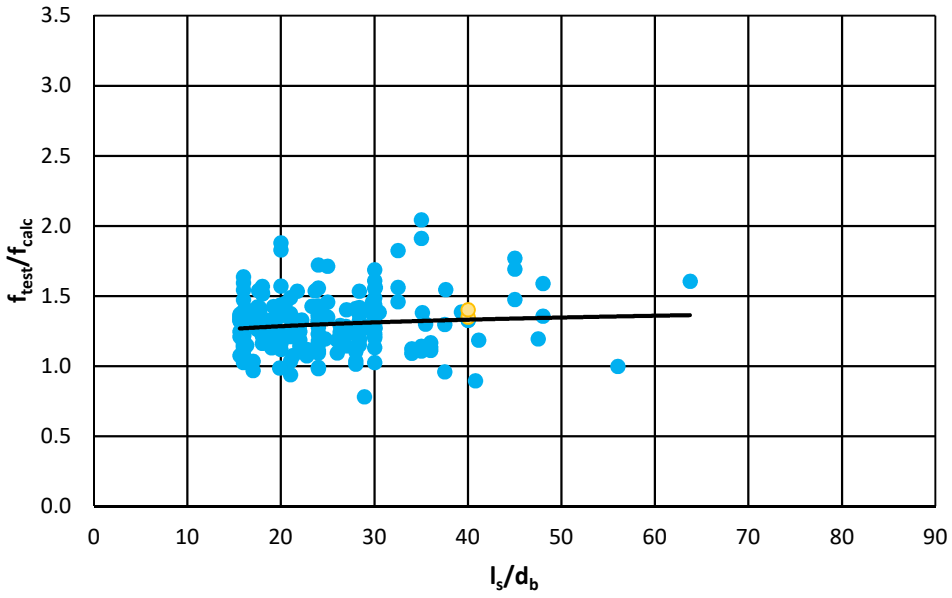

b) Relationship with Splice Length

Figure 5.39: ACI 408R-03 Equation- Confined Data

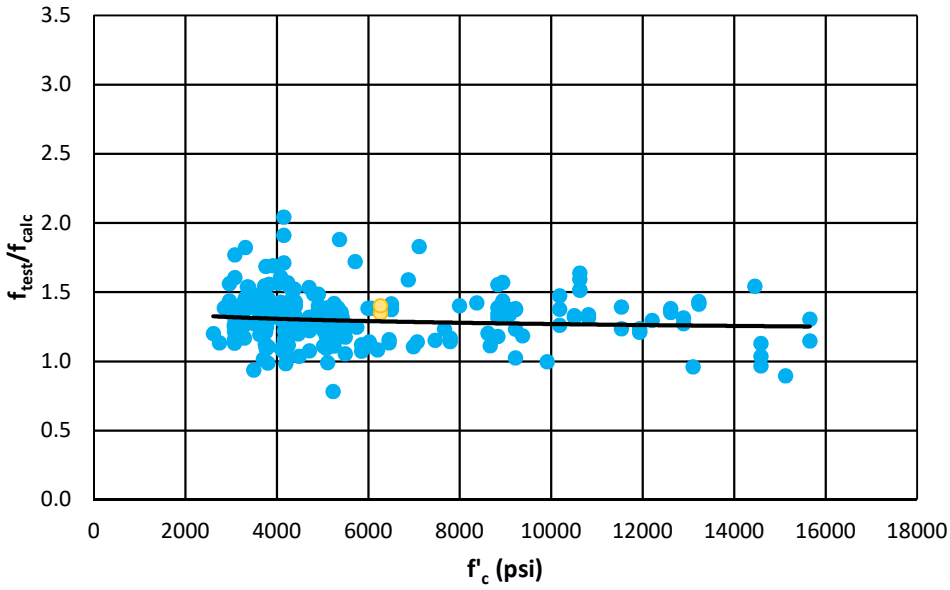

c) Relationship with Concrete Strength

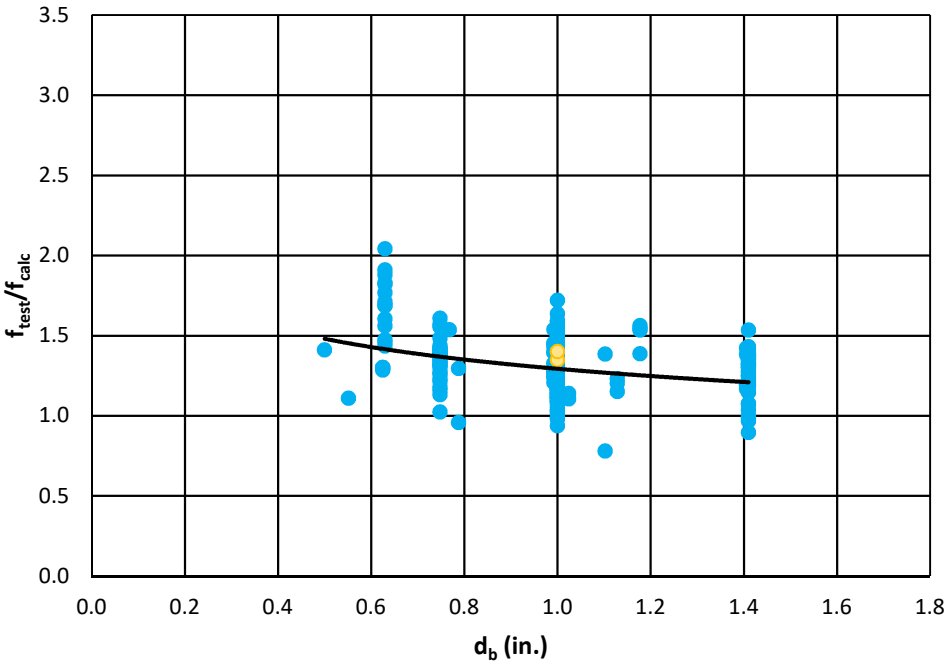

d) Relationship with Bar Diameter

Figure 5.39: ACI 408R-03 Equation- Confined Data (continued)

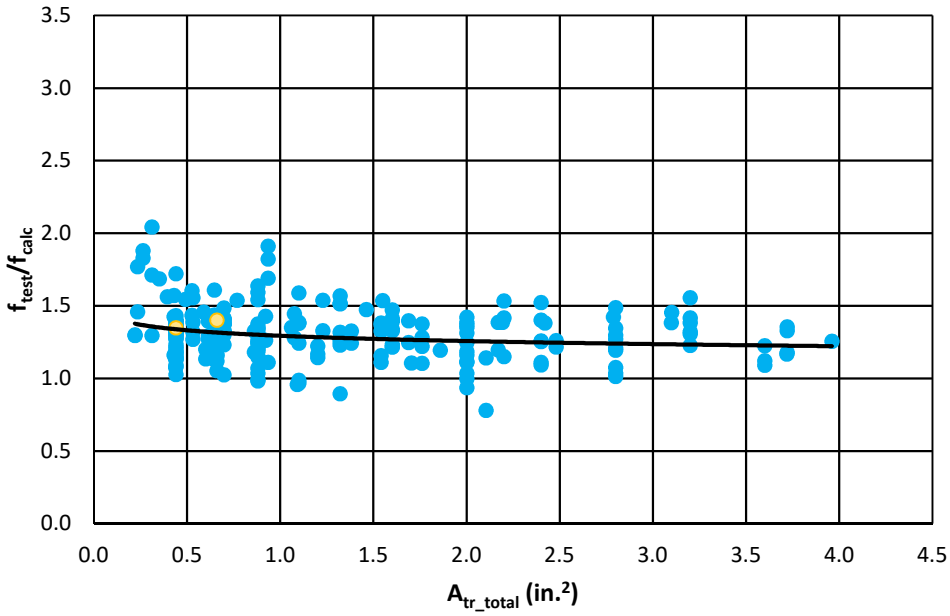

e) Relationship with Total Area of Steel within Splice Region

Figure 5.39: ACI 408R-03 Equation- Confined Data (continued)

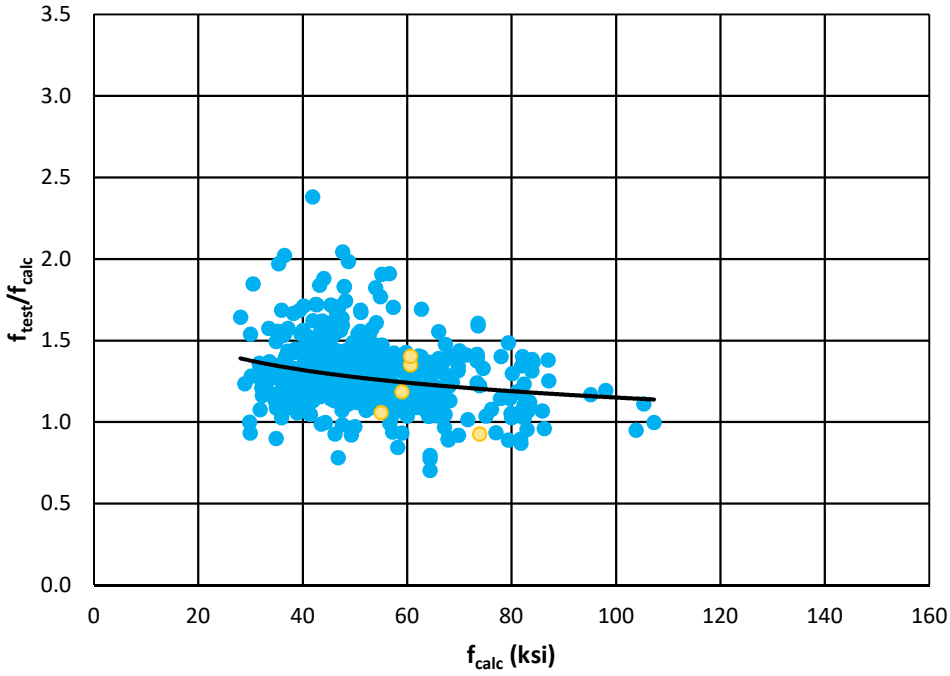

a) Relationship with Calculated Bar Stress

Figure 5.40: ACI 408R-03 Equation- All Data

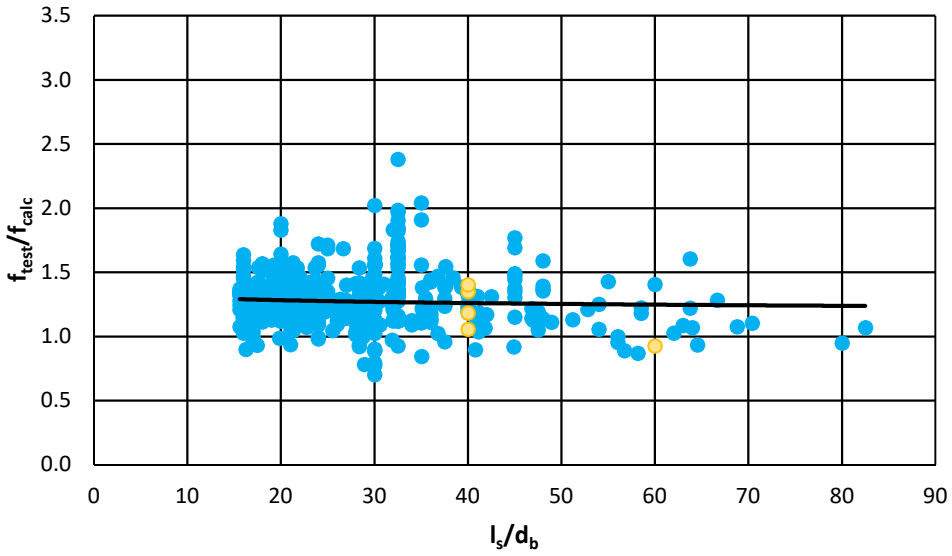

b) Relationship with Splice Length

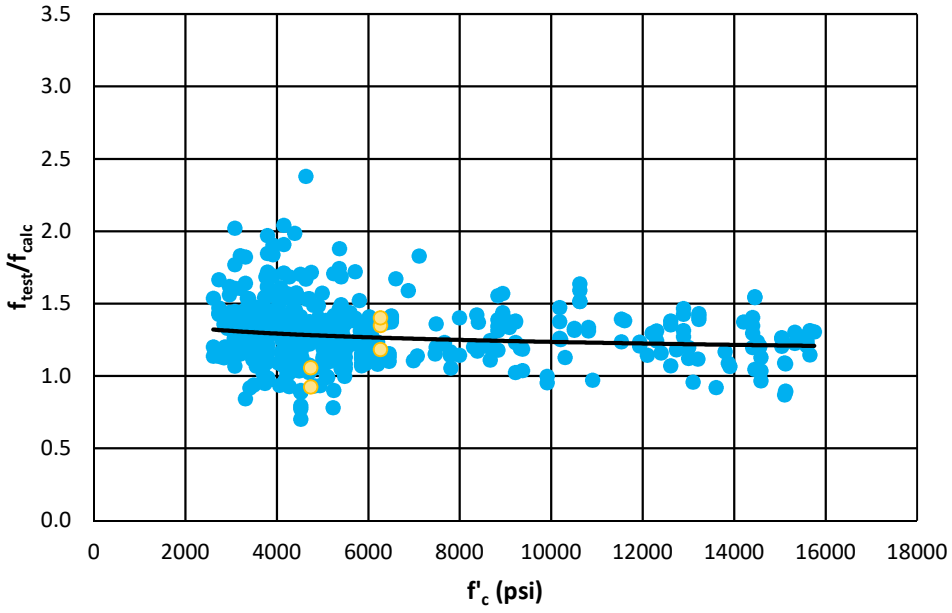

c) Relationship with Concrete Strength

Figure 5.40: ACI 408R-03 Equation- All Data (continued)

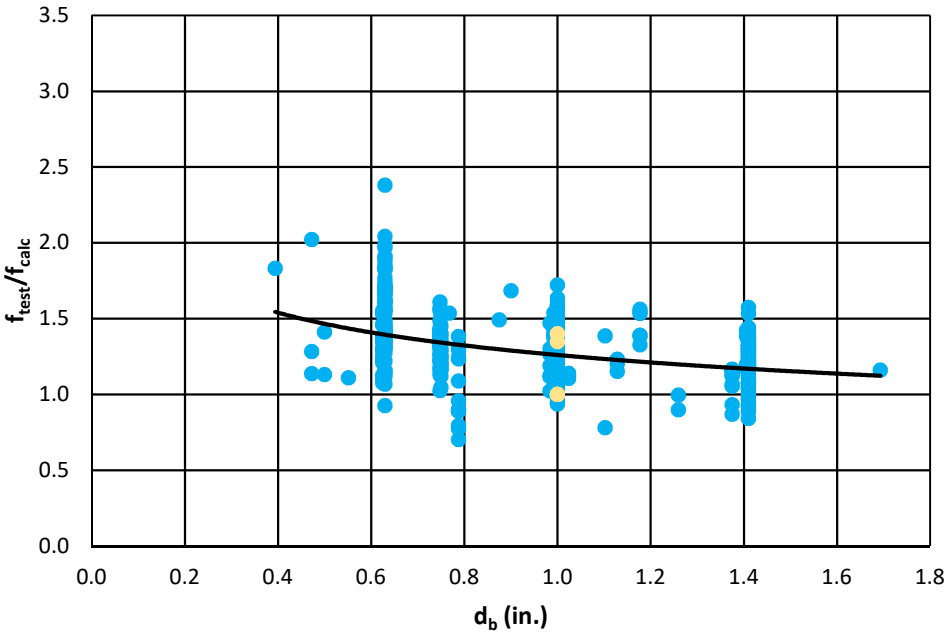

d) Relationship with Bar Diameter

Figure 5.40: ACI 408R-03 Equation- All Data (continued)

5.4.3 CB 603

The relationships between the different variables (calculated bar stress, splice length in terms of bar diameter, concrete strength, bar diameter, and total area of steel within the splice region) are graphed versus the ratio of the bar stress determined from testing (f_{test}) over the bar stress determined from CB 603 (f_{calc}) (Figures 5.41 to 5.43). This allows direct comparison of the analysis results presented in Figures 5.28 to 5.30.

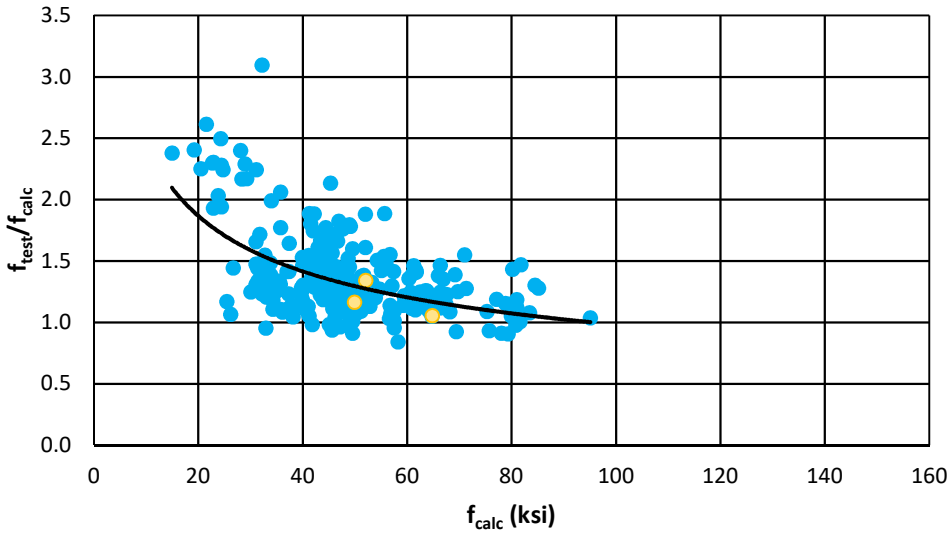

a) Relationship with Calculated Bar Stress

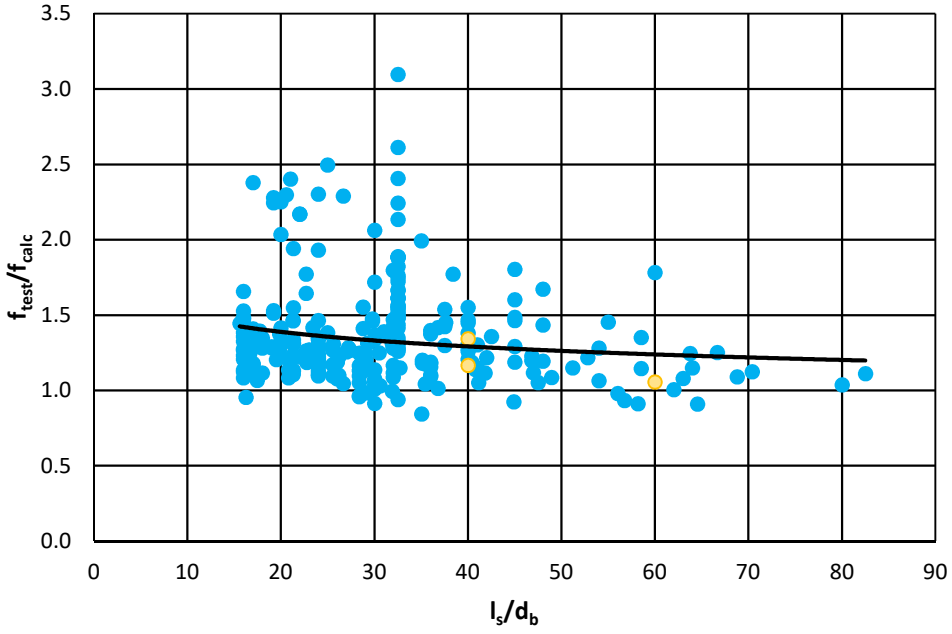

b) Relationship with Splice Length

Figure 5.41: CB 603 Equation- Unconfined Data

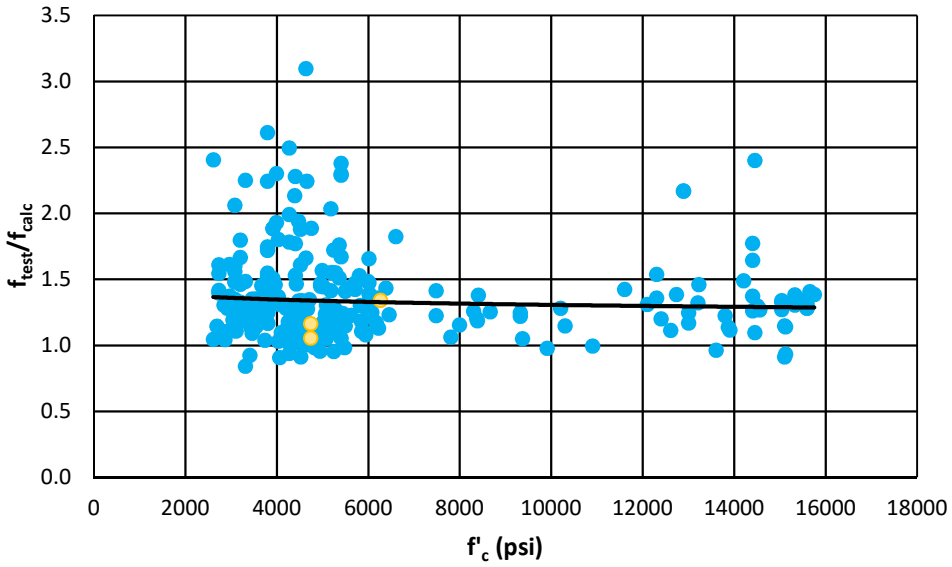

c) Relationship with Concrete Strength

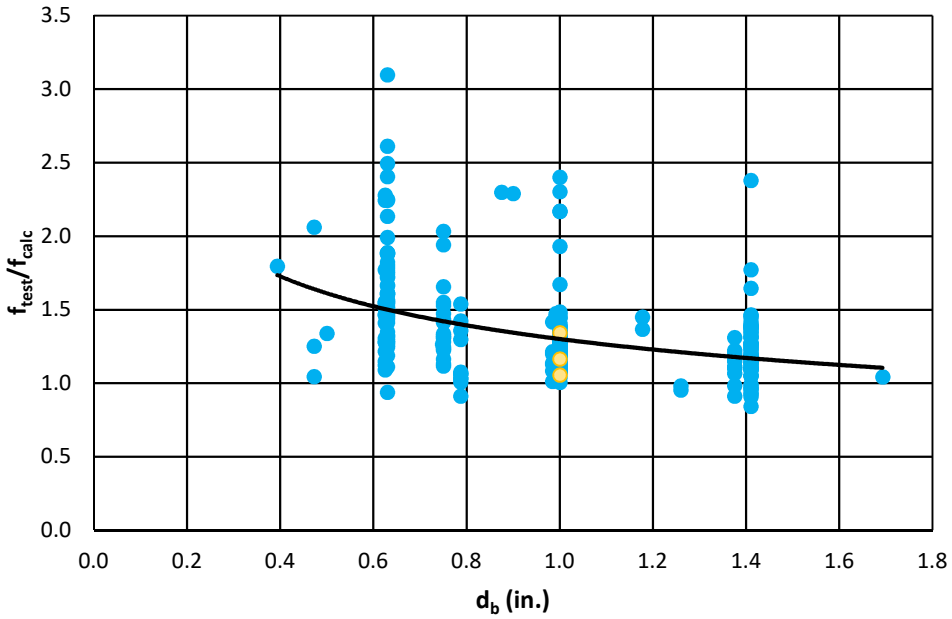

d) Relationship with Bar Diameter

Figure 5.41: CB 603 Equation- Unconfined Data (continued)

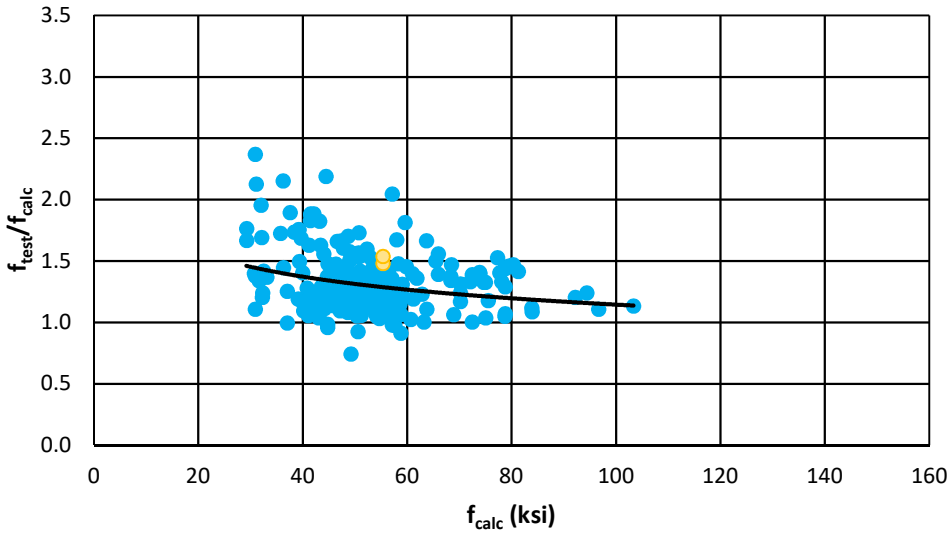

a) Relationship with Calculated Bar Stress

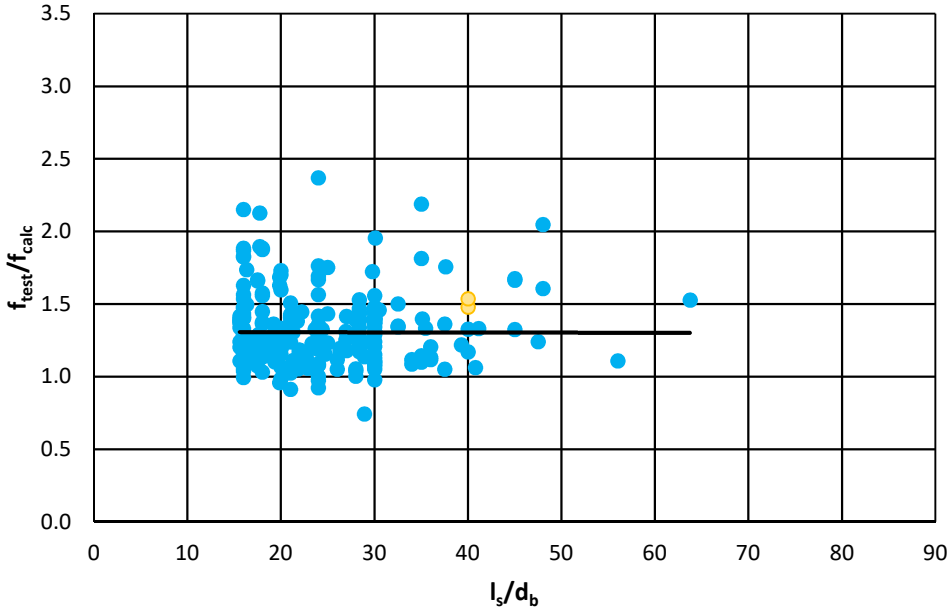

b) Relationship with Splice Length

Figure 5.42: CB 603 Equation- Confined Data

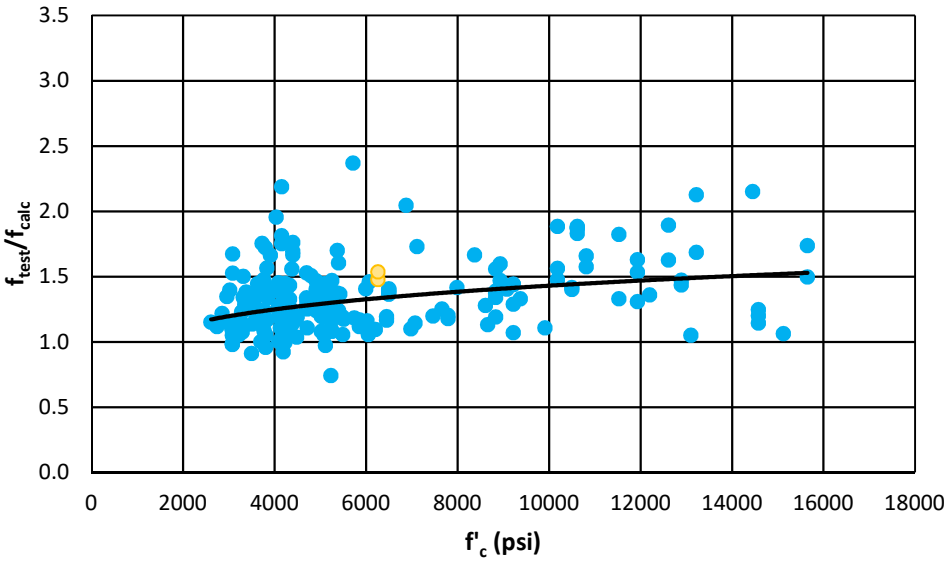

c) Relationship with Concrete Strength

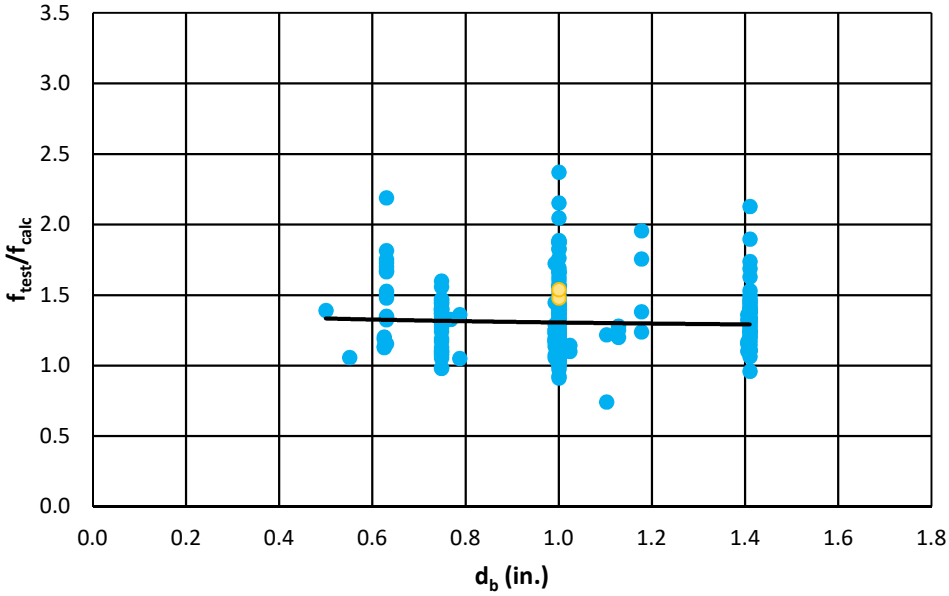

d) Relationship with Bar Diameter

Figure 5.42: CB 603 Equation- Confined Data (continued)

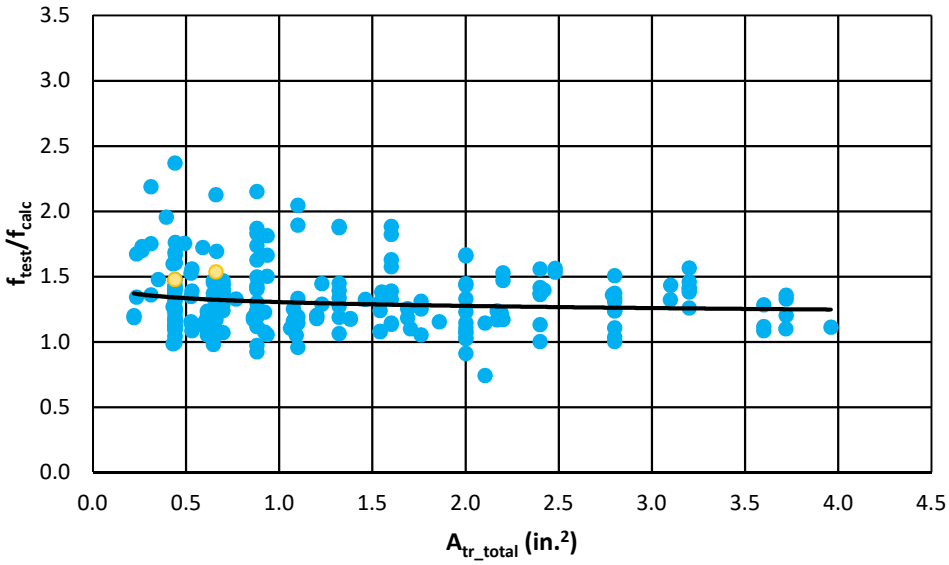

e) Relationship with Total Area of Steel within Splice Region

Figure 5.42: CB 603 Equation- Confined Data (continued)

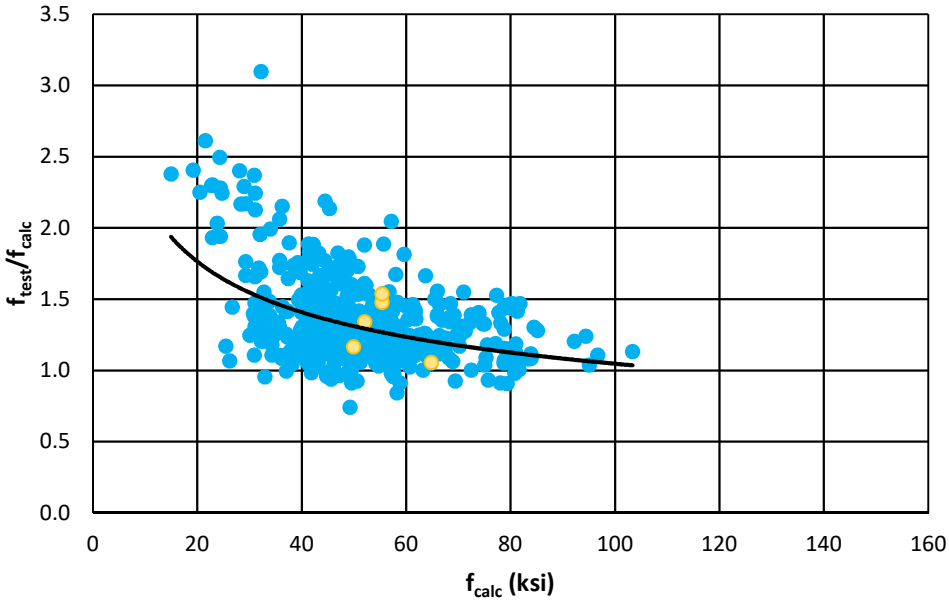

a) Relationship with Calculated Bar Stress

Figure 5.43: CB 603 Equation- All Data

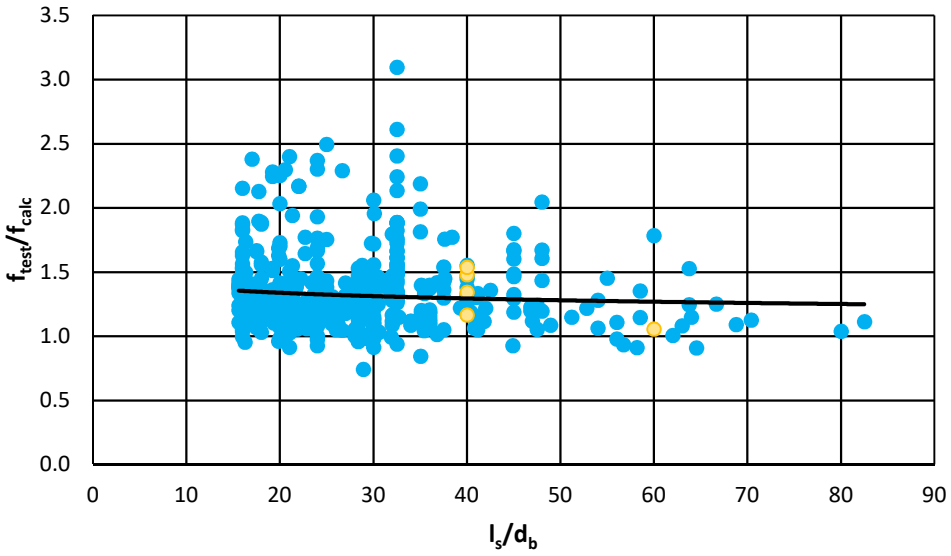

b) Relationship with Splice Length

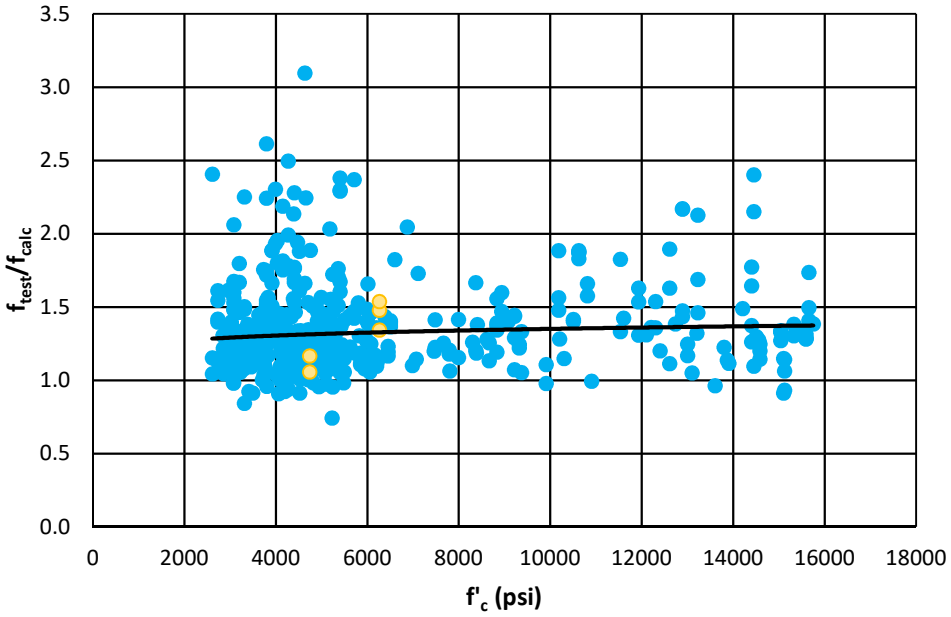

c) Relationship with Concrete Strength

Figure 5.43: CB 603 Equation- All Data (continued)

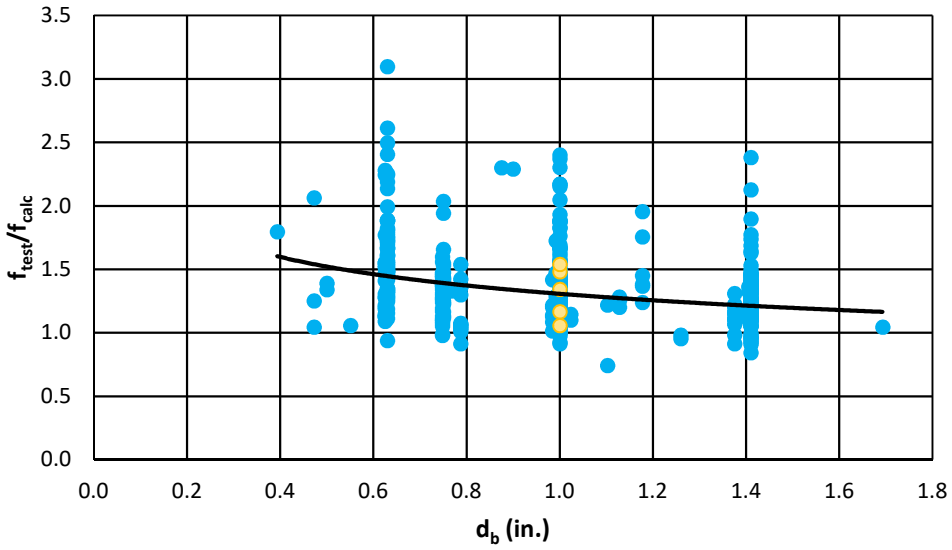

d) Relationship with Bar Diameter

Figure 5.43: CB 603 Equation- All Data (continued)

5.5 Modified ACI 318-14 Equation

As shown in Section 5.4.1, the current ACI 318-14 equation results in unconservative results for calculated strengths greater than 60 ksi. While development of a new design equation can improve accuracy and result in more consistent development lengths, it is possible to modify the current ACI 318-14 equation with a grade modification factor for use with high-strength reinforcement (f_y > 60 ksi).

A modification factor was developed considering the trendline in Figure 5.35(a) for stresses between 60 ksi and 100 ksi. The trendline from 60 ksi to 100 ksi is approximated as linear for simplicity purposes. From the trendline, a Ψ_g factor is calculated (Table 5.8) based on the unconfined data. The values calculated for the unconfined data (Figure 5.44(a)) are less conservative than the values calculated for the confined data (Figure 5.45(a)). This grade modification factor is included in Equation 5-17. The modified results using this factor are plotted in Figures 5.44 to 5.46. As shown, the grade modification factor improves the conservatism for high-strength reinforcement.

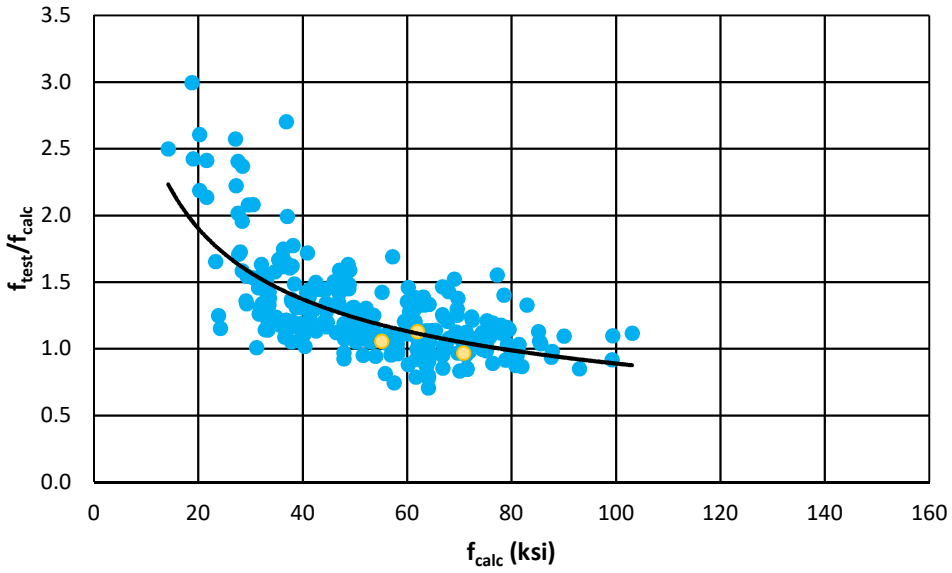

a) Relationship with Calculated Bar Stress

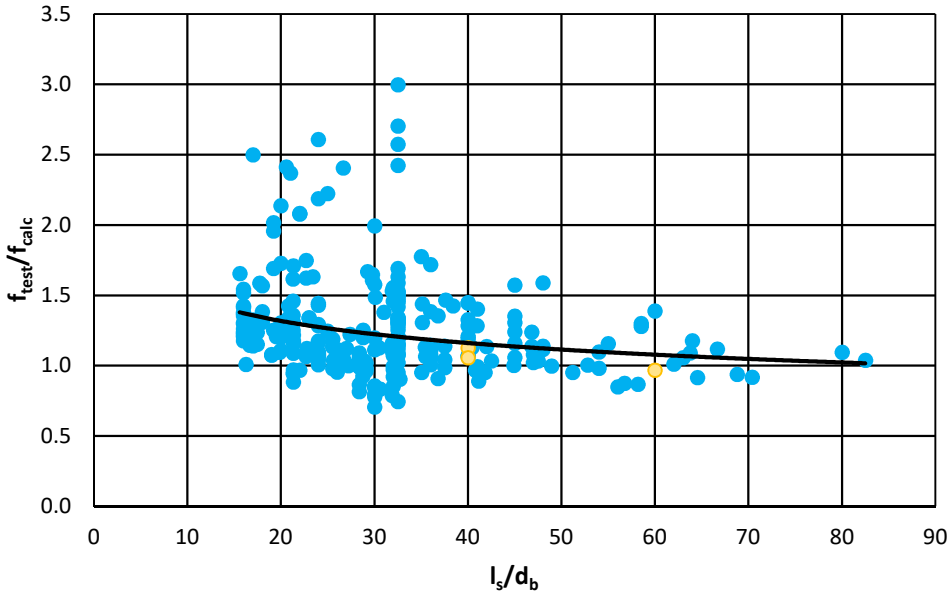

b) Relationship with Splice Length

Figure 5.44: Modified ACI 318-14 Equation- Unconfined Data

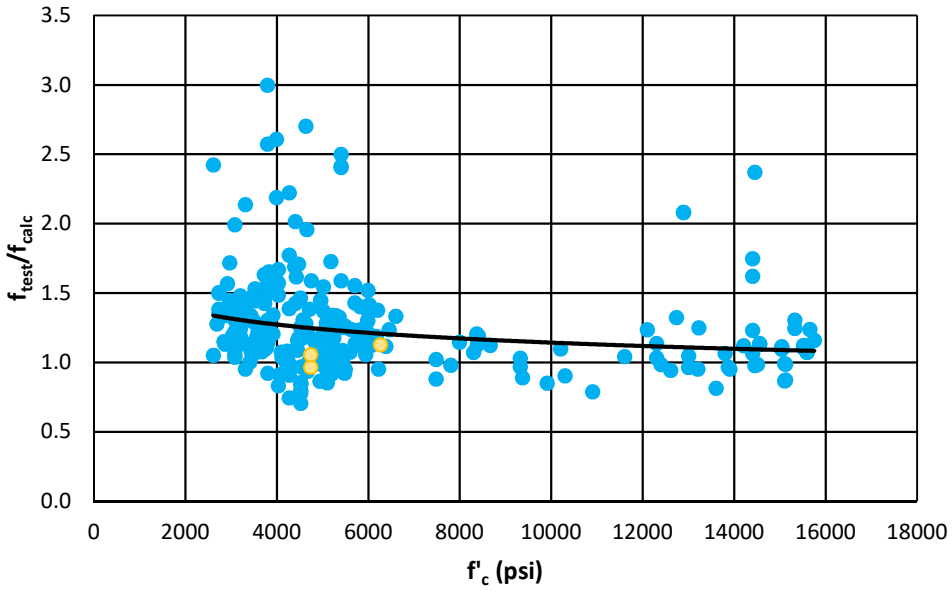

c) Relationship with Concrete Strength

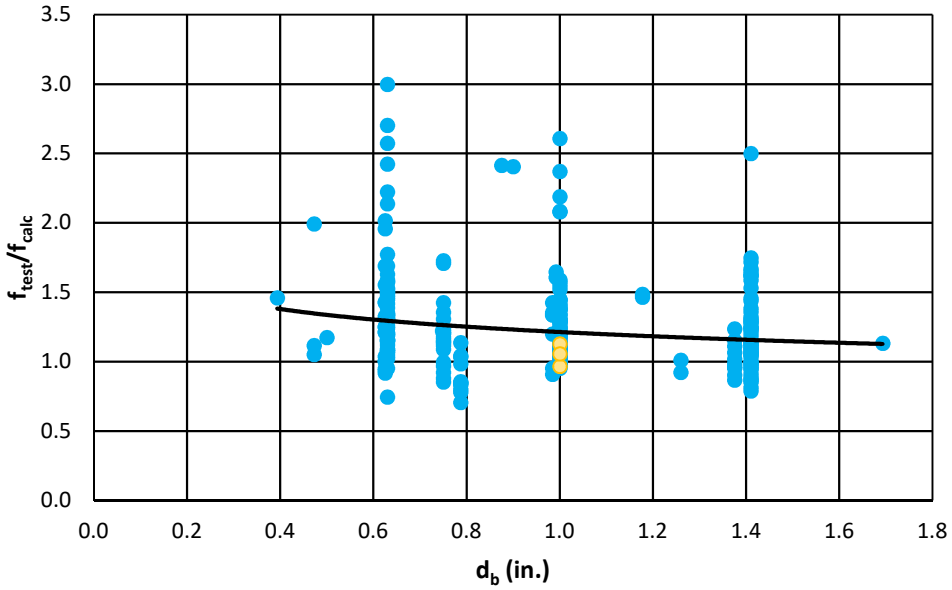

d) Relationship with Bar Diameter

Figure 5.44: Modified ACI 318-14 Equation- Unconfined Data (continued)

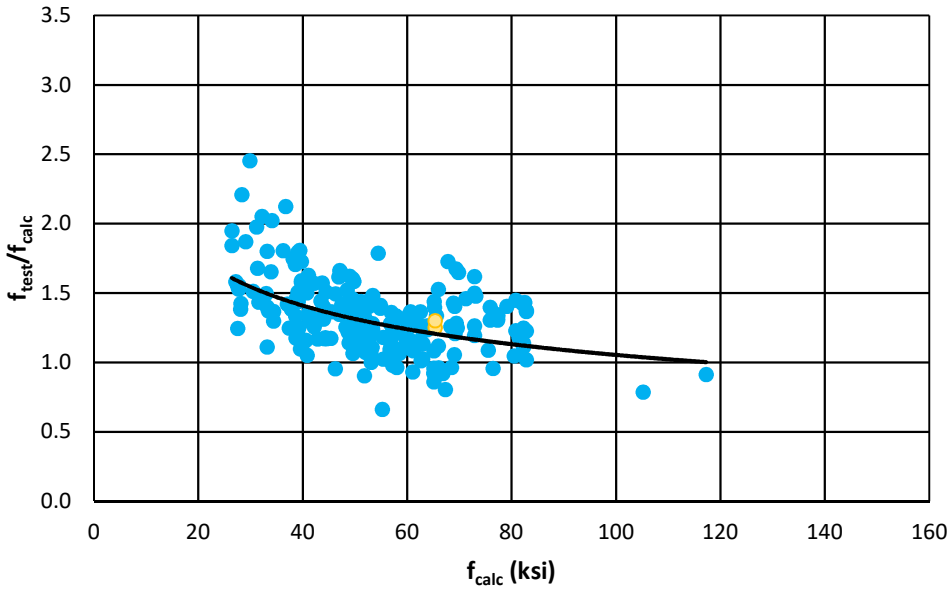

a) Relationship with Calculated Bar Stress

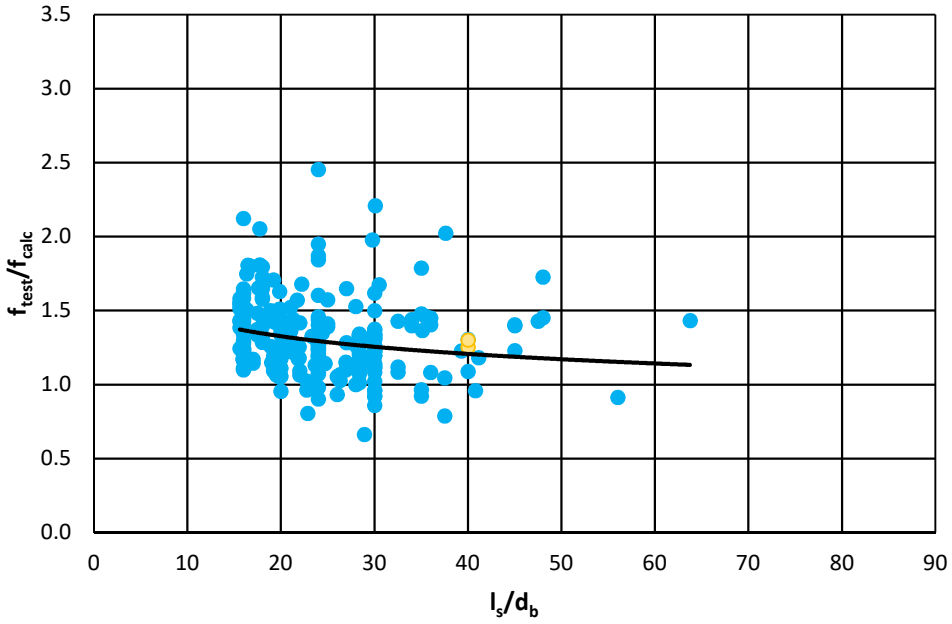

b) Relationship with Splice Length

Figure 5.45: Modified ACI 318-14 Equation- Confined Data

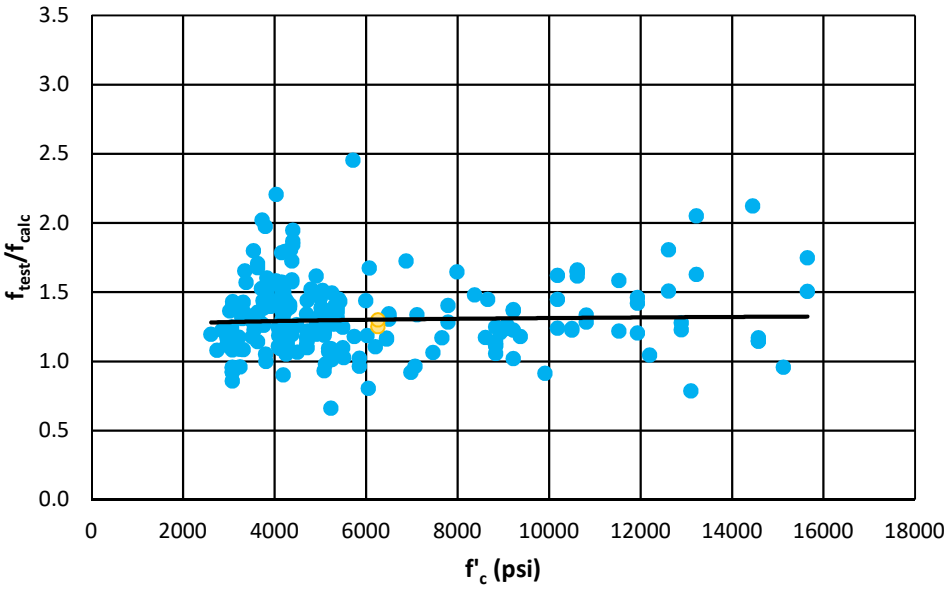

c) Relationship with Concrete Strength

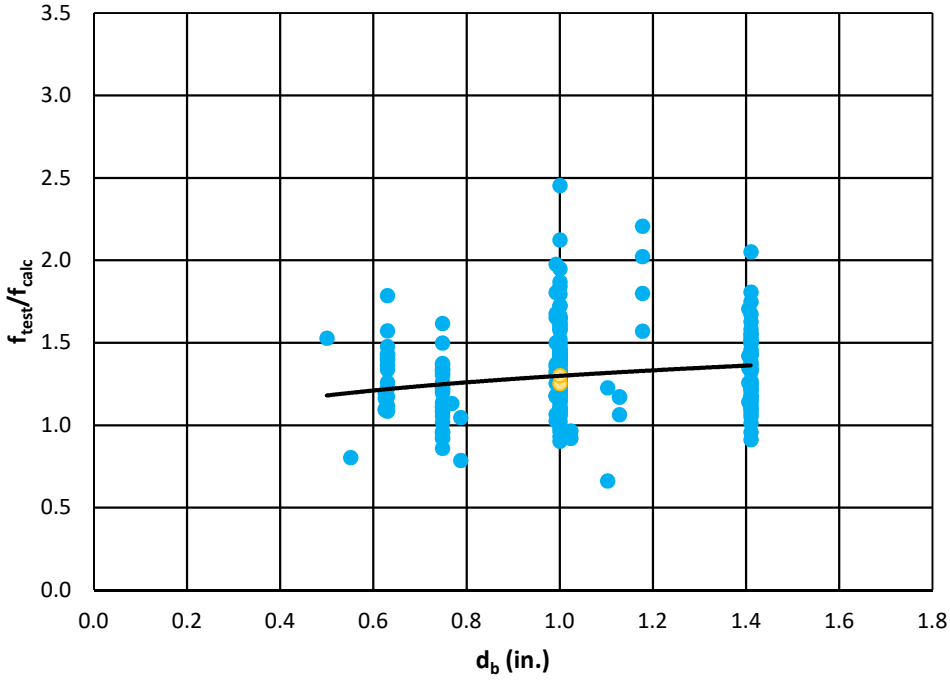

d) Relationship with Bar Diameter

Figure 5.45: Modified ACI 318-14 Equation- Confined Data (continued)

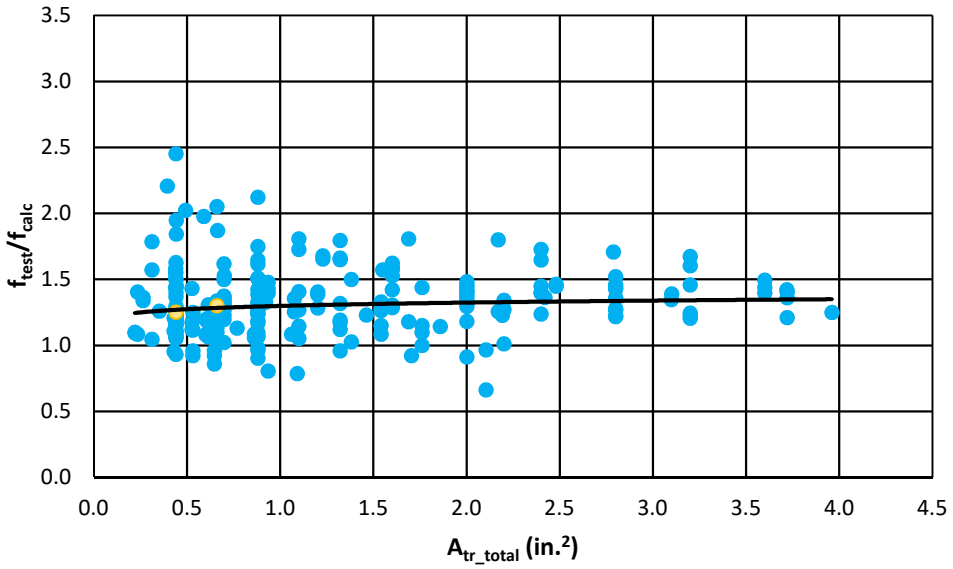

e) Relationship with Total Area of Steel within Splice Region

Figure 5.45: Modified ACI 318-14 Equation- Confined Data (continued)

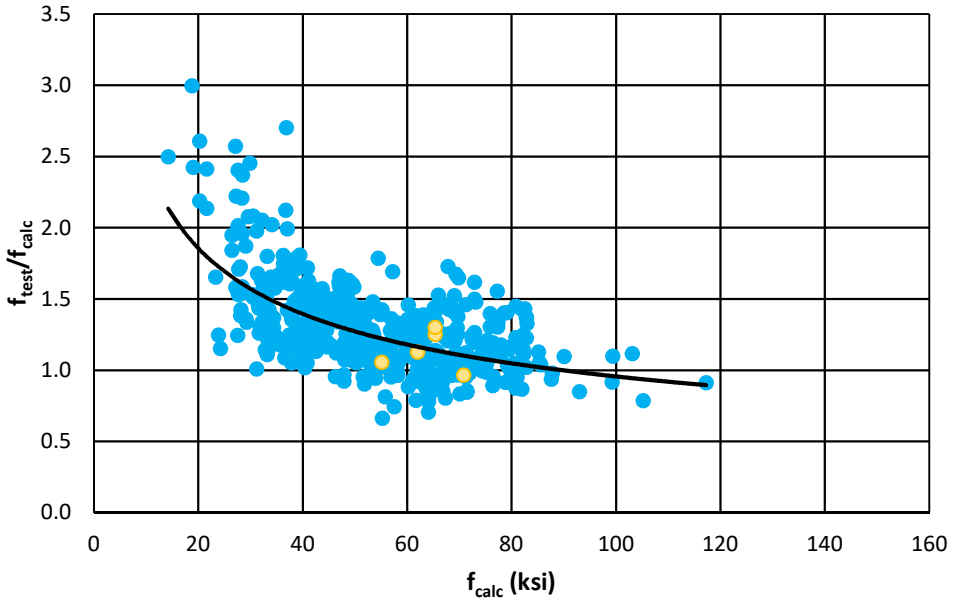

a) Relationship with Calculated Bar Stress

Figure 5.46: Modified ACI 318-14 Equation- All Data

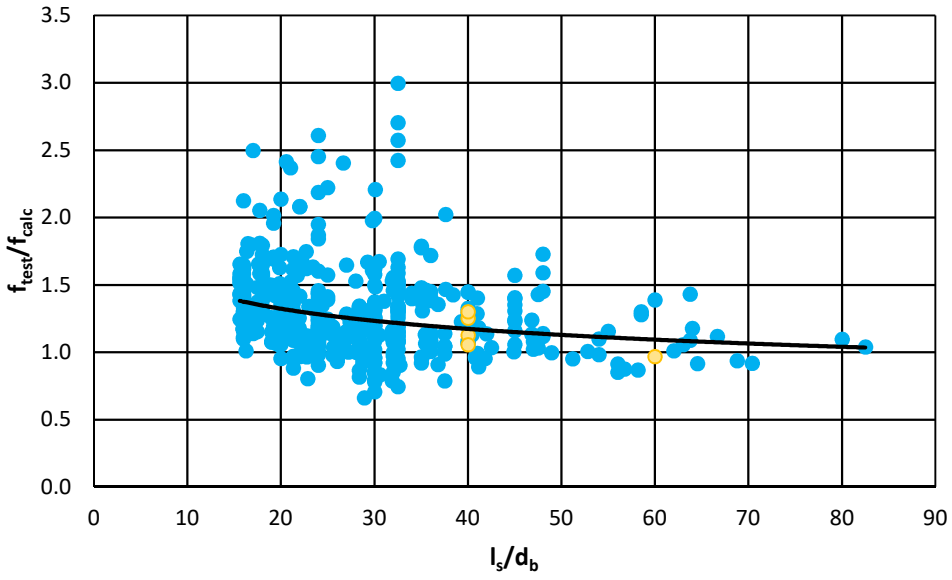

b) Relationship with Splice Length

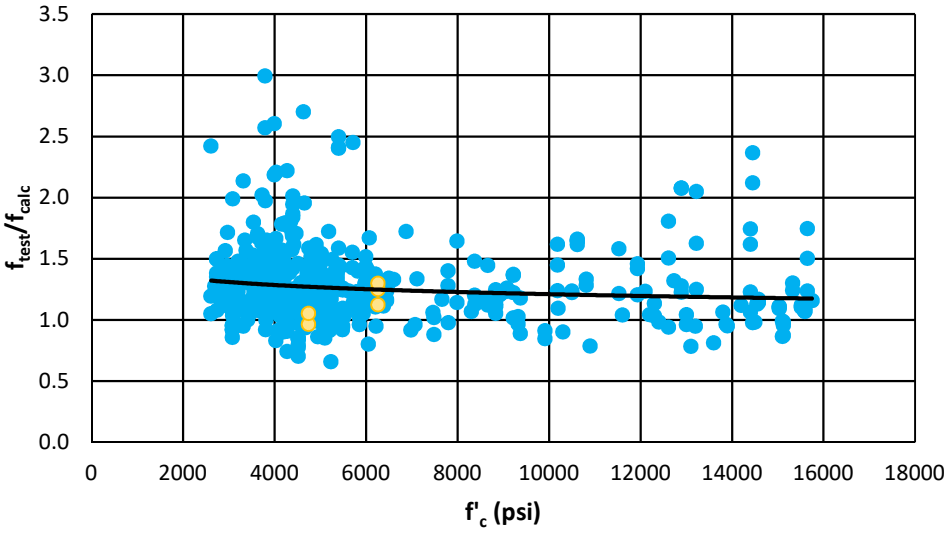

c) Relationship with Concrete Strength

Figure 5.46: Modified ACI 318-14 Equation- All Data (continued)

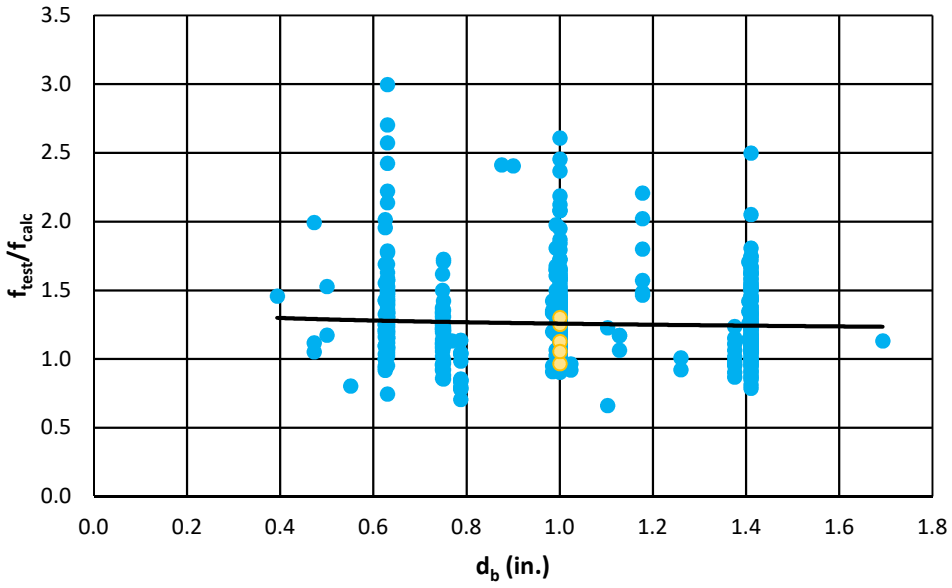

d) Relationship with Bar Diameter

Figure 5.46: Modified ACI 318-14 Equation- All Data (continued)

Table 5.8: Modification Factors

f_{calc}	Ψ_g	Reciprocal
60	1	1
80	1.15	0.87
100	1.3	0.77
120	1.45	0.69

$$l_d = \left(\frac{3}{40} \frac{f_y}{\lambda \sqrt{f_c'}} \frac{\psi_t \psi_e \psi_s \underline{\psi_g}}{\left(\frac{c_b + K_{tr}}{d_b} \right)} \right) d_b \qquad (5\text{-}17)$$

where:

Ψ_g = *factor used to modify development length based on grade of reinforcement*

Table 5.9 provides descriptive statistics for the ACI 318-14 equation with the proposed grade modification factor. Since the grade modification factor does not impact the specimens with a calculated bar stress below 60 ksi, tests with calculated bar stresses below 60 ksi were removed as to not skew the results. Table 5.10 provides descriptive statistics for the ACI 318-14 equation.

Tests with calculated bar stresses below 60 ksi were removed for consistency. The comparison between Tables 5.9 and 5.10 shows with the addition of the proposed modification factor, the current ACI 318-14 equation becomes less unconservative.

Table 5.9: Descriptive Statistics for Modified ACI 318-14 Equation

	Unconfined Data	Confined Data	All Data
Mean	1.27	1.32	1.30
Standard Error	0.02	0.01	0.01
Standard Deviation	0.36	0.28	0.32
Minimum	0.71	0.54	0.54
Maximum	3.00	2.45	3.00

Table 5.10: Descriptive Statistics for ACI 318-14 Equation

	Unconfined Data	Confined Data	All Data
Mean	1.21	1.22	1.21
Standard Error	0.02	0.02	0.01
Standard Deviation	0.40	0.33	0.36
Minimum	0.59	0.38	0.38
Maximum	3.00	2.45	3.00

5.6 Recommendations

Based on the analysis conducted on the steel bar reinforced concrete specimen database and the tests conducted here, the following analysis expression is proposed for the analysis of steel reinforced concrete.

$$f_s = \left(\frac{c_{so}}{d_b}\right)^{0.25} \left(\frac{f_c'}{5000\ psi}\right)^{0.25} \frac{8{L_{eq}}^{0.5}}{A_b} + 12{A_{tr\_total}}^{0.5} \qquad (5\text{-}18)$$

where:

A_b *=area of longitudinal bar, in.*^{2}

A_t *= area of one leg of transverse reinforcement crossing the potential splitting plane, in.*^{2}

A_{tr_total} *= total area of steel within lap splice region* ($A_t N_l N_s$)*, in.*^{2}

c_b *= bottom cover, in.*

d_b *= bar diameter, in.*

f_c' *=specified compressive strength of concrete, psi*

l_s *=splice length of deformed bar, in.*

$$L_{eq} = l_s \frac{A_b}{0.79\ in.^2}$$

N_l *= number of legs of transverse reinforcement that cross the splitting plane*

N_s *= number of stirrups*

A factor of safety can be added to this proposed analysis equation such that any desired level of conservatism can be achieved for design purposes.

6. SUMMARY AND CONCLUSIONS

6.1 Introduction

Research evaluating the development length of high-strength reinforcement ($f_y > 60$ ksi) is limited. Therefore, the objective of this research program is to develop an expression for the development and splicing of high-strength reinforcement. Research focused on the following:

- Evaluating the influence of splice length on bond strength
- Evaluating the influence of confinement on bond strength
- Evaluating the effectiveness of high-strength (100 ksi) transverse reinforcement on bond strength

6.2 Experimental Investigation

The experimental program investigated the bond strength of steel reinforced concrete beams with both unconfined and confined tension lap splices. The study included 22 concrete beams reinforced with deformed steel bars: 11 unconfined and 11 confined specimens. Three reinforcing bars were spliced at the center of the constant moment region of the beam. All beams were rectangular in cross section with a total depth of 20 in. The width of the specimens was controlled by typical spacing and minimum cover requirements. The objective of the experimental program was to evaluate the effect of the splice length, transverse reinforcement spacing, bar spacing, and use of high-strength transverse reinforcement on splice strength.

6.2.1 Behavior of the Specimens

Seventeen of the specimens failed by splitting of the concrete in the splice region, although five specimens failed in flexure (as indicated in Table 3.1). Failures occurring in the splice region were sudden and brittle with no obvious warning signs prior to failure. The use of transverse reinforcement in the splice region allowed the beams to withstand enough bar strain that specimens with sufficient splice lengths could reach yield. As a result, confinement within the splice region was found to be essential for increased beam ductility. Only a minimal amount of

confinement was necessary to sufficiently develop the Grade 100 longitudinal bars: at least 100 psi of confinement for $60d_b$ splice lengths and 50 psi of confinement for $80d_b$ splice lengths.

An increase in bar spacing was found to be inconclusive. The slight increase in bar stress observed could be because of an increase in bar spacing or just attributed to typical scatter. Additionally, Grade 100 transverse reinforcement was found to provide a similar increase in bond strength as Grade 60 transverse reinforcement, as some specimens performed slightly better than those specimens with Grade 60 transverse reinforcement, while others performed slightly worse. This difference was attributed to normal scatter of the test data.

6.2.2 Experimental Findings

The following conclusions were obtained from the experimental program.

1. As the splice length increases, the unit length effectiveness decreases. The relationship between bar stress and splice length can be fit to a power equation ($l_s{}^{0.5}$).
2. The impact of transverse reinforcement on bond strength is primarily affected by the total area of transverse steel within the splice region. This trend can be characterized by the square root ($A_{tr\_total}{}^{0.5}$).
3. Grade 100 transverse reinforcement does not provide an additional increase to the bond strength of a specimen beyond that provided by Grade 60 transverse reinforcement. Therefore, f_{yt} should not be included in expressions used to represent the increase in bond strength provided by transverse reinforcement.
4. Confinement is required within the splice length (100 psi of reinforcement for $60d_b$ splice lengths and 50 psi of transverse reinforcement for $80d_b$ splice lengths) to eliminate bond splitting failure so that the full strength of the splice can be achieved.

6.3 Analytical Investigation

An analysis method which can be used effectively for high-strength reinforcement was developed. Previous test results from steel lap splice tests were evaluated to develop the model. The steel database includes 632 uncoated, bottom-cast, steel reinforced specimens that failed in bond and were tested in four-point bending. Specimens with concrete strengths less than 2,500

psi or a splice length less than 12 in. or $16d_b$ were excluded. Additionally, the tests conducted in this experimental program were considered. The equivalent splice length, L_{eq}, developed by Pay (2005) was used to normalize the test data to an equivalent bar size so test specimens with various size bars could be compared.

6.3.1 Recommendations

Based on the results of this study, the following analysis equation was developed for development length calculations. The first term of the equation provides for the (unconfined) splice length, while the second term provides the additional strength provided by the transverse reinforcement (confinement).

$$f_s = \left(\frac{c_{so}}{d_b}\right)^{0.25} \left(\frac{f_c'}{5000\ psi}\right)^{0.25} \frac{8{L_{eq}}^{0.5}}{A_b} + 12{A_{tr\_total}}^{0.5} \qquad (6\text{-}1)$$

where:

A_b=*area of longitudinal bar, in.*^{2}

A_t= *area of one leg of transverse reinforcement crossing the potential splitting plane, in.*^{2}

A_{tr_total}= *total area of steel within lap splice region* ($A_t N_l N_s$)*, in.*^{2}

c_b= *bottom cover, in.*

d_b= *bar diameter, in.*

f_c'=*specified compressive strength of concrete, psi*

l_s=*splice length of deformed bar, in.*

$L_{eq} = l_s \frac{A_b}{0.79\ in.^2}$

N_l= *number of legs of transverse reinforcement that cross the splitting plane*

N_s= *number of stirrups*

The proposed analysis equation can be adjusted with a factor of safety to provide any desired level of conservatism to be achieved.

6.4 Further Research

The majority of research performed on splice lengths has been on splice lengths less than $40d_b$. Therefore, more research needs to be conducted on tests with longer splice lengths. Additional results shall investigate:

- Slabs. Slabs typically use small covers (0.75 in.) and do not have transverse reinforcement. These members often utilize larger bar spacings, which may be beneficial. Limited test results are available for these members.
- Bond strength of high-strength longitudinal reinforcement with the use of high-strength concrete.
- A range of high-strength bars with different post-elastic stress-strain relationships.
- Location of transverse reinforcement within lap splice region. A study quantifying the strength provided by transverse reinforcement at different locations along the splice length would be extremely valuable to more fully understand this behavior.

REFERENCES

ACI Committee 318 (2014), "Building Code Requirements for Structural Concrete and Commentary (ACI 318-14/ACI318 R-14)," American Concrete Institute, Detroit.

ACI Committee 318, Subcommittee B (2018), "Development Length for Deformed Bars and Deformed Wires in Tension (CB 603)," *Ballot LB18-03*, American Concrete Institute, Detroit.

ACI Committee 408 (2003), "Suggested Development, Splice, and Standard Hook Provisions for Deformed Bars in Tension," (ACI 408.1R-03), American Concrete Institute, Farmington Hills, MI., 49 pp.

Ansley, M. H. (2002), "Investigation into the Structural Performance of MMFX Reinforcing," Florida Department of Transportation.

ATC 115 (2014), "Roadmap for the Use of High-Strength Reinforcement in Reinforced Concrete Design," Applied Technology Council, Red City, CA.

ASTM A1035 (2016), "Standard Specification for Deformed and Plain, Low-carbon, Chromium, Steel Bars for Concrete Reinforcement, Surface Texture (Surface Roughness, Waviness, and Lay)," American Society for Testing and Materials, West Conshohocken, PA., 6 pp.

ASTM A615 (2016), "Standard Specification for Deformed and Plain Carbon-Steel Bars for Concrete Reinforcement," American Society for Testing and Materials, West Conshohocken, PA., 6 pp.

ASTM C192 (2016), "Standard Practice for Making and Curing Concrete Test Specimens in the Laboratory," American Society for Testing and Materials, West Conshohocken, PA., 8 pp.

ASTM C39 (2017), "Standard Test Method for Compressive Strength of Cylindrical Concrete Specimens," American Society for Testing and Materials, West Conshohocken, PA., 7 pp.

ASTM C496 (2014), "Standard Test Method for Splitting Tensile Strength of Cylindrical Concrete Specimens," American Society for Testing and Materials, West Conshohocken, PA., 5 pp.

ASTM E8 (2016), "Standard Test Methods for Tension Testing of Metallic Materials, West Conshohocken, PA. 30 pp.

Azizinamini, A., Stark, M., Roller, J. J., and Ghosh, S. K. (1993), "Bond Performance of Reinforcing Bars Embedded in High-Strength Concrete," *ACI Structural Journal*, Vol. 90, No. 5, pp. 554-561.

Azizinamini, A., Pavel, R., Hatfield, E., and Ghosh, S. K. (1999), "Behavior of Spliced Reinforcing Bars Embedded in High-Strength Concrete," *ACI Structural Journal*, Vol. 96, No. 5, pp. 826-835.

Briggs, M. G. (2008), "Bond Strength of ASTM A1035 Grade 100 Reinforcing Steel," *M.S. Thesis*, School of Civil Engineering, University of Kansas, Lawrence, KS.

Canbay, E., and Frosch, R. J. (2005), "Bond Strength of Lap-Spliced Bars," *ACI Structural Journal*, Vol. 102, No. 4, pp. 605-614.

Chamberlin, S. J. (1956), "Spacing of Reinforcement in Beams," ACI Journal, *Proceedings*, Vol. 53, No. 1, pp. 113-134.

Chinn, J., Ferguson, P. M., and Thompson, J. N. (1955), "Lapped Splices in Reinforced Concrete Beams," ACI Journal, *Proceedings*, Vol. 52, No. 10, Oct., pp. 201-213

El-Hacha, R., El-Agroudy, H., and Rizkalla, S. H. (2006), "Bond Characteristics of High-Strength Steel Reinforcement." *ACI Structural Journal,* Vol. 103, No. 6, pp. 771-782.

Esfahani, M. R., and Rangan, B. V. (1998), "Bond between Normal Strength and High-Strength Concrete (HSC) and Reinforcing Bars in Splices in Beams." *ACI Structural Journal,* Vol. 102, No. 1, pp. 22-30.

Ferguson, P. M., and Krishnaswamy, C. N. (1971), "Tensile Lap Splices Part 2: Design Recommendations for Retaining Wall Splices and Large Bar Splices," *Rep. No. 113-3*. TX: The Texas Highway Department.

Ferguson, P. M., and Thompson, J. N. (1962), "Development Length for Large High-Strength Reinforcing Bars in Bond," ACI Journal, *Proceedings*, Vol. 59, No. 7, July, pp. 887-922.

Goto, Y. (1971), "Cracks Formed in Concrete Around Deformed Tension Bars," ACI Journal, Vol. 68, No. 26, April, pp. 244-251.

Hadje-Ghaffari, H., Choi, O. C., Darwin, D., and McCabe, S. L. (1994), "Bond of Epoxy-Coated Reinforcement: Cover, Casting Position, Slump, and Consolidation." *ACI Structural Journal,* Vol. 91, No. 1, pp. 59-68.

Hwang, H., Park, H., and Yi, W. (2017). "Nonuniform Bond Stress Distribution Model for Evaluation of Bar Development Length." *ACI Structural Journal,* Vol. 114, No. 4, pp. 839-849.

Kluge, R. W., and Tuma, E. C. (1945), "Lapped Bar Splices in Concrete Beams," ACI Journal, *Proceedings*, Vol. 42, Sept., pp. 13-33.

Maeda, M., Otani, S., and Aoyama H., "Bond Splitting Strength in Reinforced Concrete Members," *Transactions*, Japan Concrete Institute, Vol. 13 (1991), pp. 581-588.

Mathey, R., and Watstein, D. (1961), "Investigation of Bond in Beam and Pull-Out Specimens with High-Yield-Strength Deformed Bars," ACI Journal, *Proceedings*, Vol. 57, No. 3, Mar., pp. 1071-1090.

NIST (2014), "Use of High-Strength Reinforcement in Earthquake-Resistant Concrete Structures," *Research Report NIST GCR 14-917-30*, NEHRP Consultants, Red City, CA.

Orangun, C. O., Jirsa, J. O., and Breen, J. E. (1975), "The Strength of Anchored Bars: A Reevaluation of Test Data on Development Length and Splices," *Research Report No. 154-3F*, Center for Highway Research, The University of Texas, Austin, TX, Jan.

Orangun, C. O., Jirsa, J. O., and Breen, J. E. (1977), "Reevaluation of Test Data on Development Length and Splices," *ACI Journal*, Proceedings, Vol. 74, No. 3, pp. 114-122.

Pay, A. C. (2005), "Bond Behavior of Unconfined Steel and Fiber Reinforced Polymer (FRP) Bar Splices in Concrete Beams," *Ph.D. Dissertation*, School of Civil Engineering, Purdue University, West Lafayette, IN.

Pay, A. C., Canbay, E., and Frosch, R. J. (2014), "Bond Strength of Spliced Fiber-Reinforced Polymer Reinforcement." *ACI Structural Journal*, Vol. 111, No. 2, Mar.-April.

Sakurada, T., Morohashi, N. and Tanaka, R. (1993), "Effect of Transverse Reinforcement on Bond Splitting Strength of Lap Splices." *Transactions*, Japan Concrete Institute, Vol. 15, pp. 572-580.

Seliem, H. M., Hosny, A., Rizkalla, S., Zia, P., Briggs, M., Miller, S., Darwin, D., Browning, J., Glass, G. M., Hoyt, K., Donnelly, K., and Jirsa, J. O. (2007), "Bond Behavior of MMFX (ASTM A1035) Reinforcing Steel," *Rep*. Irvine, CA: MMFX Technologies Corporation.

Seliem, H. M., Hosny, A., Rizkalla, S., Zia, P., Briggs, M., Miller, S., Darwin, D., Browning, J., Glass, G. M., Hoyt, K., Donnelly, K., and Jirsa, J. O. (2009), "Bond Characteristics of

ASTM A1035 Steel Reinforcing Bars," *ACI Structural Journal*, V. 106, No. 4, July-Aug., pp. 530-539.

Sim, C. (2014), "Structural and Corrosion Performance of Concrete Bridge Decks Reinforced with Corrosion-Resistant Reinforcing Steel," *Ph.D. Dissertation*, School of Civil Engineering, Purdue University, West Lafayette, IN.

Tepfers, R. (2009), "Bond Characteristics of ASTM A1035 Steel Reinforcing Bars," *ACI Structural Journal*, V. 106, No. 4, July-Aug., pp. 530-539.

Thompson, M. A., Jirsa, J. O., Breen, J. E., and Meinheit, D. F. (1975), "The Behavior of Multiple Lap Splices in Wide Sections," *Research Report No. 154-1*, Center for Highway Research, The University of Texas, Austin, TX.

Zekany, A. J., Neumann, S., Jirsa, J. O., and Breen, J. E. (1981), "The Influence of Shear on Lapped Splices in Reinforced Concrete," *Tech. No. FHWA/TX-81/20+242-2*. Austin, TX: Texas State Department of Highways and Public Transportation; Transportation Planning Division.

Zsutty, T. C. (1968), "Beam Shear Strength Prediction by Analysis of Existing Data," ACI Journal, Proceedings, Vol. 65, No. 11, Nov., pp. 943-951.

Zuo, J., and Darwin, D. (1998), "Bond Strength of High Relative Rib Area Reinforcing Bars," *SM Report No. 46*, University of Kansas Center for Research, Lawrence, KS.

Zuo, J., and Darwin, D. (2000), "Splice Strength of Conventional and High Relative Rib Area Bars in Normal and High-Strength Concrete," *ACI Structural Journal*, Vol. 97, No. 4., pp. 630-641.

APPENDIX A: AS-BUILT DIMENSIONS

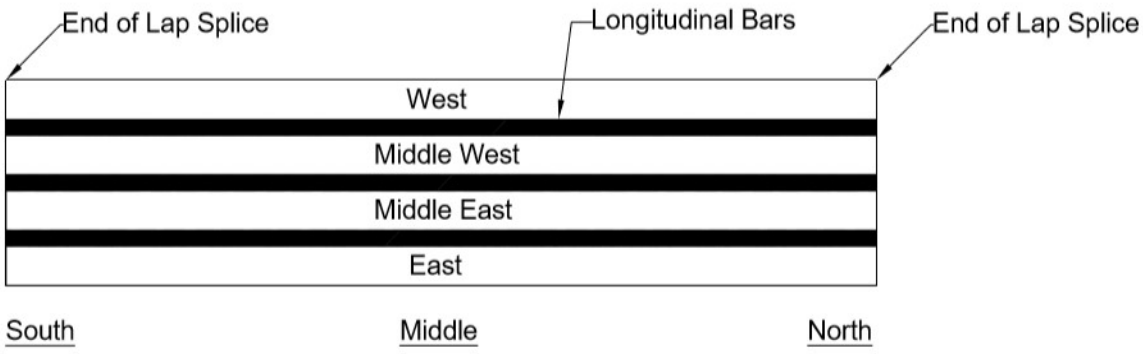

Figure A.1: Nomenclature for As-Built Dimensions

Table A.1: U-40-5

	South (in.)	Middle (in.)	North (in.)
West	1.7630	1.9000	2.0220
Middle West	2.0870	2.1870	2.2205
Middle East	1.7520	1.8870	2.0620
East	1.8940	1.9885	2.2115
Total	13.4960	13.9625	14.5160

Table A.2: U-40-5a

	South (in.)	Middle (in.)	North (in.)
West	2.3140	2.2860	2.1140
Middle West	1.7940	1.9930	2.0800
Middle East	1.9440	1.7420	1.6840
East	2.2120	2.1050	2.1640
Total	14.2640	14.1260	14.0420

Table A.3: U-60-5

	South (in.)	Middle (in.)	North (in.)
West	2.0800	1.9740	1.8180
Middle West	2.4200	2.2040	2.2910
Middle East	1.8890	1.8730	2.1530
East	1.7260	1.7830	1.8430
Total	14.1150	13.8340	14.1050

Table A.4: U-60-5a

	South (in.)	Middle (in.)	North (in.)
West	2.3960	2.1210	2.1230
Middle West	1.7990	1.7850	1.6020
Middle East	1.8410	1.8670	1.7850
East	1.8660	2.1600	2.4380
Total	13.9020	13.9330	13.9480

Table A.5: U-70-5

	South (in.)	Middle (in.)	North (in.)
West	2.3010	1.8580	1.7855
Middle West	1.8450	1.8875	1.8980
Middle East	1.8700	1.8365	1.9985
East	2.0280	2.1405	2.2685
Total	14.0440	13.7225	13.9505

Table A.6: U-80-5

	South (in.)	Middle (in.)	North (in.)
West	2.0020	1.7270	1.8020
Middle West	2.1400	2.1690	2.1280
Middle East	1.8720	1.8420	1.8890
East	1.8240	1.9070	1.9440
Total	13.8380	13.6450	13.7630

Table A.7: U-100-5

	South (in.)	Middle (in.)	North (in.)
West	1.9640	2.0080	2.0140
Middle West	1.7760	2.0900	1.9660
Middle East	1.8590	1.9390	1.8790
East	1.9370	1.7680	1.9910
Total	13.5360	13.8050	13.8500

Table A.8: U-120-5

	South (in.)	Middle (in.)	North (in.)
West	2.0290	1.8690	2.1280
Middle West	2.1110	1.8710	1.6480
Middle East	1.5600	1.7000	1.5880
East	1.8640	2.1870	2.5140
Total	13.5640	13.6270	13.8780

Table A.9: U-80-5-M

	South (in.)	Middle (in.)	North (in.)
West	2.3390	2.2620	2.2730
Middle West	0.7350	0.7170	0.6150
Middle East	0.9320	1.1030	1.1040
East	1.9065	1.9280	1.9530
Total	11.9125	12.0100	11.9450

Table A.10: U-100-5-M

	South (in.)	Middle (in.)	North (in.)
West	2.2210	2.1805	1.9430
Middle West	0.9735	0.9860	1.0700
Middle East	0.8925	0.8820	0.7400
East	1.5020	1.6445	1.9105
Total	11.5890	11.6930	11.6635

Table A.11: U-120-5-M

	South (in.)	Middle (in.)	North (in.)
West	2.0020	1.9830	2.2310
Middle West	0.8970	0.9590	0.7420
Middle East	0.7140	0.9240	0.8390
East	2.1130	2.1460	2.0780
Total	11.7260	12.0120	11.8900

Table A.12: C3/60/2-40-5-50

	South (in.)	Middle (in.)	North (in.)
West	2.7430	2.6350	2.7270
Middle West	1.5290	1.3410	1.2320
Middle East	1.2860	1.3270	1.4760
East	2.4100	2.5880	2.6420
Total	13.9680	13.8910	14.0770

Table A.13: C3/60/3-40-5-50

	South (in.)	Middle (in.)	North (in.)
West	2.6720	2.5980	2.5220
Middle West	1.7110	1.8470	1.8760
Middle East	1.1040	1.0800	1.1400
East	2.2960	2.4800	2.4880
Total	13.7830	14.0050	14.0260

Table A.14: C3/100/3-40-5-50

	South (in.)	Middle (in.)	North (in.)
West	2.0985	2.1240	2.1505
Middle West	1.8445	1.6340	1.6215
Middle East	1.3540	1.4360	1.4825
East	2.4065	2.6055	2.5585
Total	13.7035	13.7995	13.8130

Table A.15: C3/60-40-5-100

	South (in.)	Middle (in.)	North (in.)
West	2.3285	2.2900	2.0955
Middle West	1.5185	1.5510	1.2825
Middle East	1.6755	1.7025	1.8225
East	2.2985	2.4935	2.5620
Total	13.8210	14.0370	13.7625

Table A.16: C3/100-40-5-100

	South (in.)	Middle (in.)	North (in.)
West	2.4020	2.1890	1.9970
Middle West	1.4700	1.5490	1.5110
Middle East	1.8440	1.7990	1.8420
East	2.2680	2.3630	2.5770
Total	13.9840	13.9000	13.9270

Table A.17: C3/60-60-5-50

	South (in.)	Middle (in.)	North (in.)
West	1.9805	2.1025	2.1365
Middle West	2.0155	1.9635	1.9810
Middle East	1.7935	1.8090	1.7955
East	2.1390	2.1345	2.1295
Total	13.9285	14.0095	14.0425

Table A.18: C3/60-60-5-100

	South (in.)	Middle (in.)	North (in.)
West	2.0050	2.1370	2.1865
Middle West	1.9170	2.0180	2.1670
Middle East	1.6885	1.5430	1.4960
East	2.0805	2.1770	2.0235
Total	13.6910	13.8750	13.8730

Table A.19: C3/60-60-5-150

	South (in.)	Middle (in.)	North (in.)
West	2.3095	2.1850	2.0905
Middle West	1.8305	1.8160	1.8280
Middle East	1.8345	1.8225	1.8165
East	2.0965	2.0165	2.0985
Total	14.0710	13.8400	13.8335

Table A.20: C4/60-60-5-100

	South (in.)	Middle (in.)	North (in.)
West	2.3605	1.9935	2.1650
Middle West	1.5035	1.6470	1.6025
Middle East	1.5880	1.5890	1.5940
East	2.4230	2.3490	2.3905
Total	13.8750	13.5785	13.7520

Table A.21: C3/100-60-5-100

	South (in.)	Middle (in.)	North (in.)
West	2.3805	2.3070	2.0835
Middle West	1.6000	1.8490	2.0770
Middle East	1.3860	1.3510	1.2225
East	2.4475	2.3770	2.4140
Total	13.8140	13.8840	13.7970

Table A.22: C3/60-80-5-50

	South (in.)	Middle (in.)	North (in.)
West	1.7800	2.0265	2.1805
Middle West	1.7365	1.6475	1.7965
Middle East	1.3550	1.3130	1.3610
East	2.8740	2.8305	2.6305
Total	13.7455	13.8175	13.9685

APPENDIX B. STRESS-STRAIN CURVES

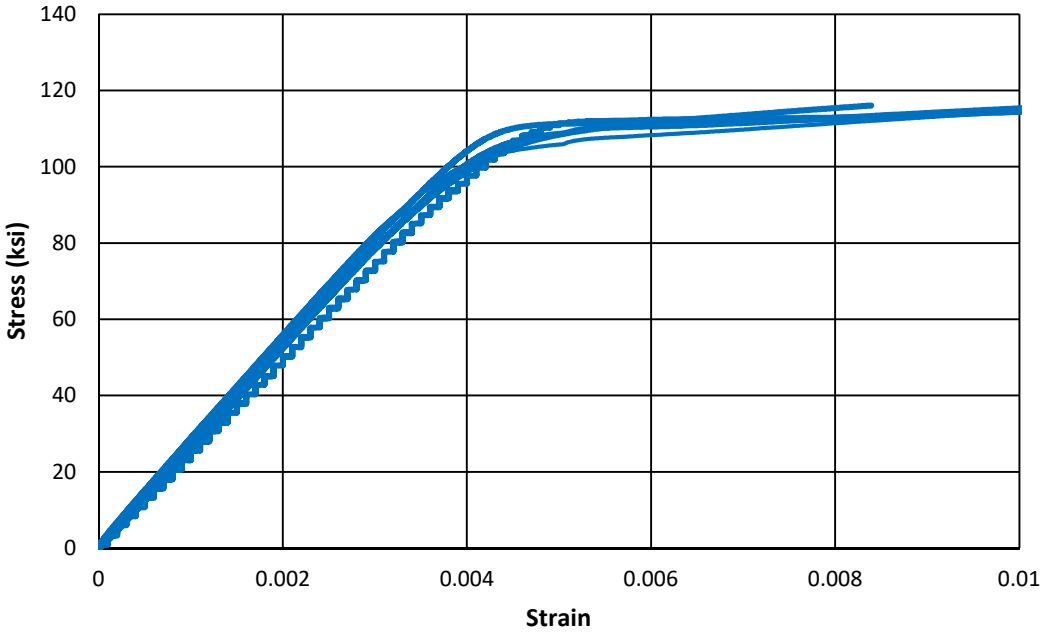

a) Partial Curve

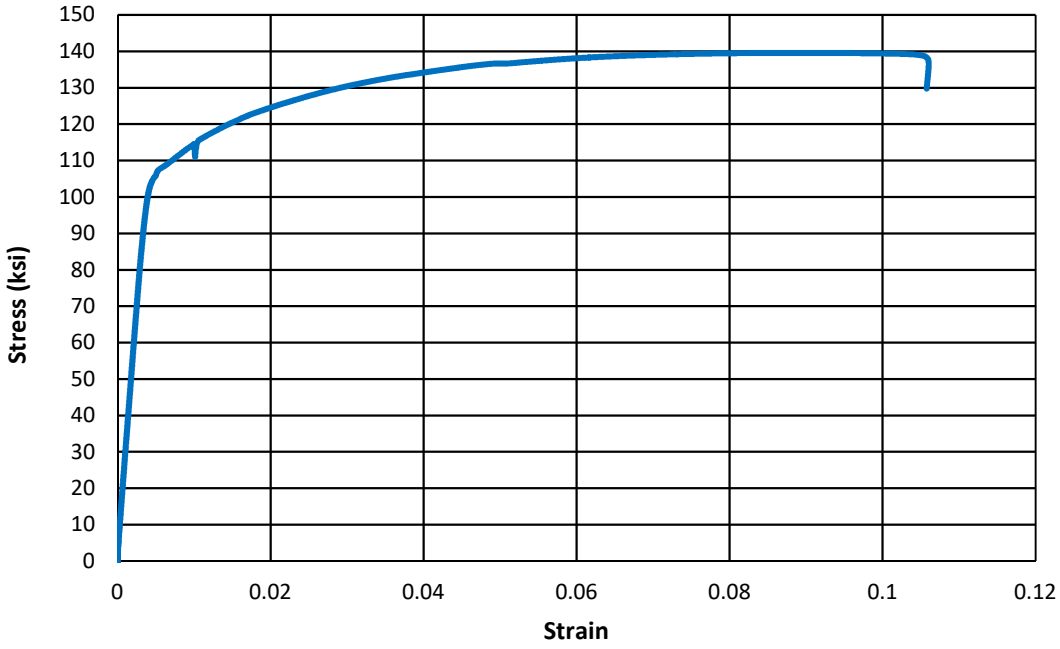

b) Complete Curve

Figure B.1: Stress-Strain Curve for #8 Grade 100 Longitudinal Bar

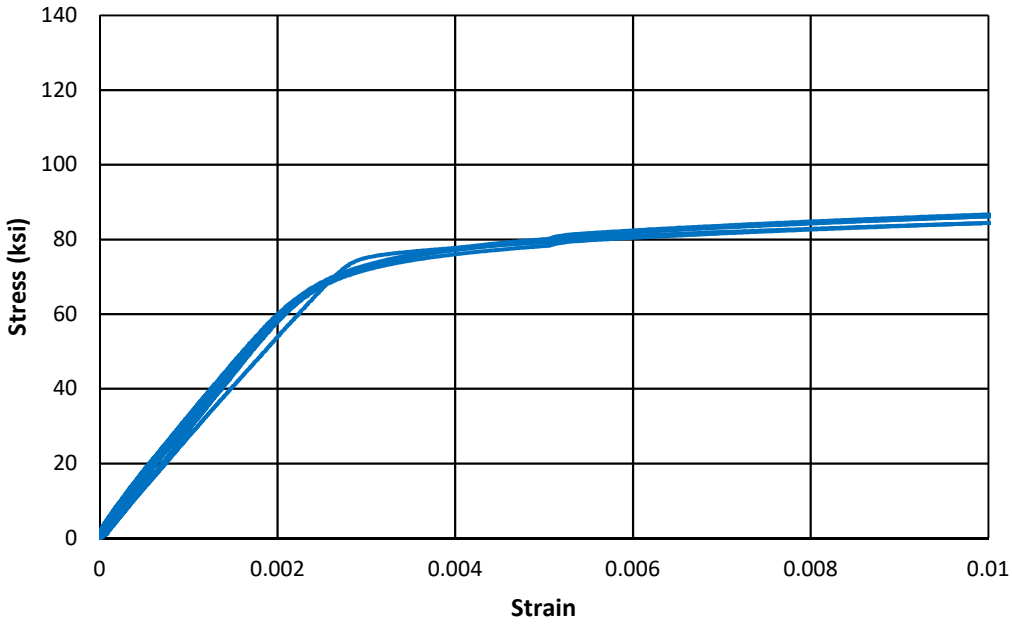

a) Partial Curve

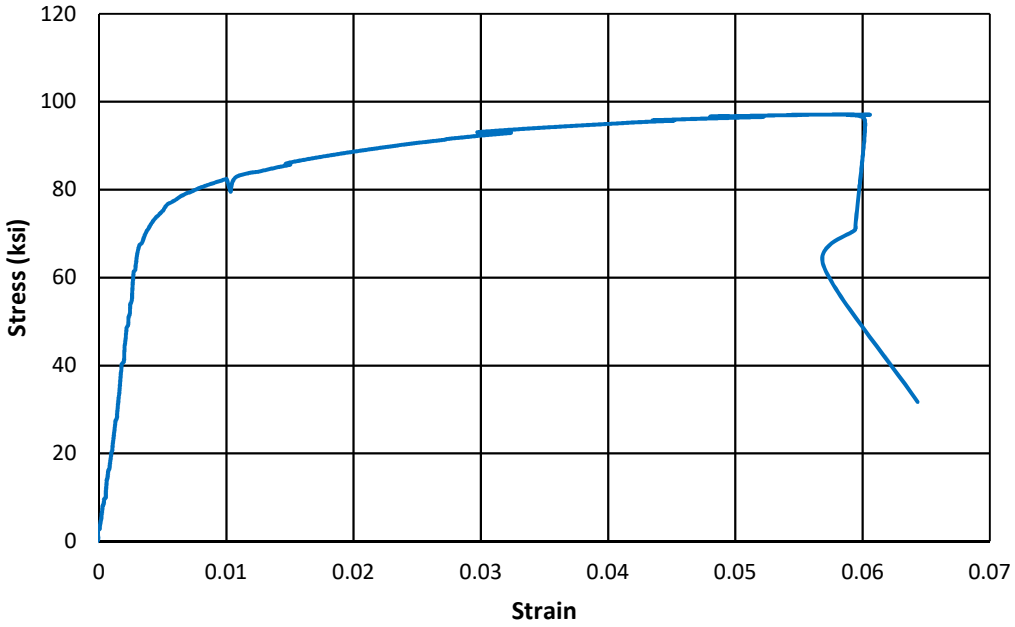

b) Complete Curve

Figure B.2: Stress-Strain Curve for #3 Grade 60 Stirrups

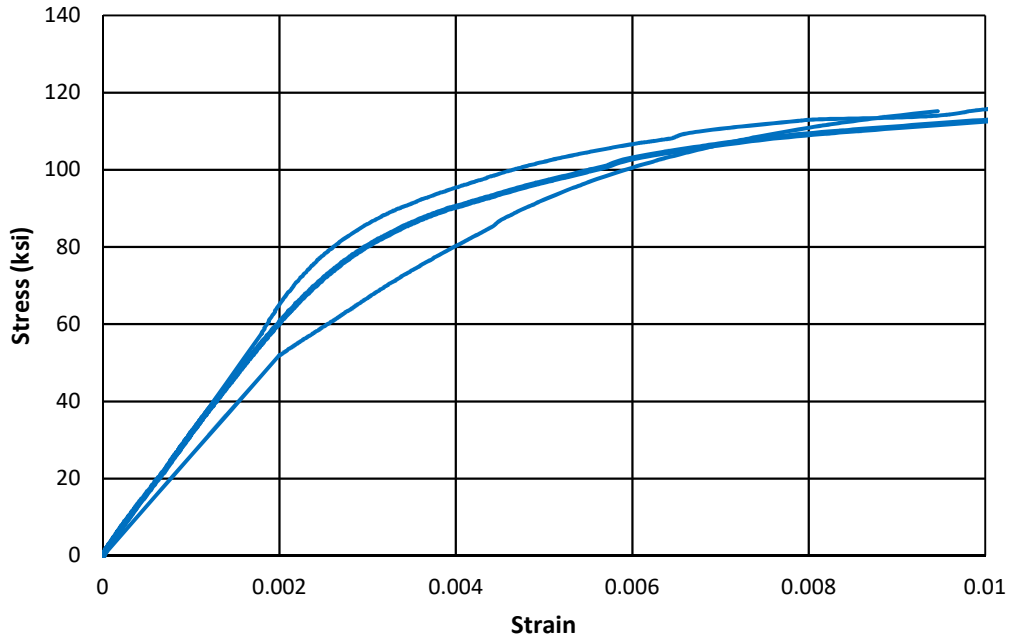

a) Partial Curve

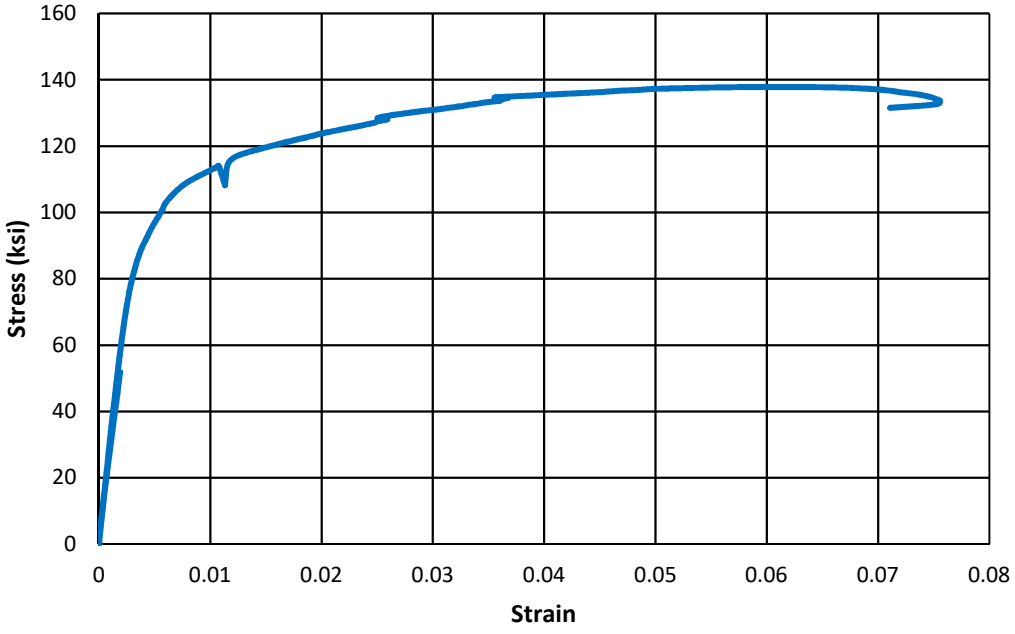

b) Complete Curve

Figure B.3: Complete Stress-Strain Curve for #3 Grade 100 Stirrups

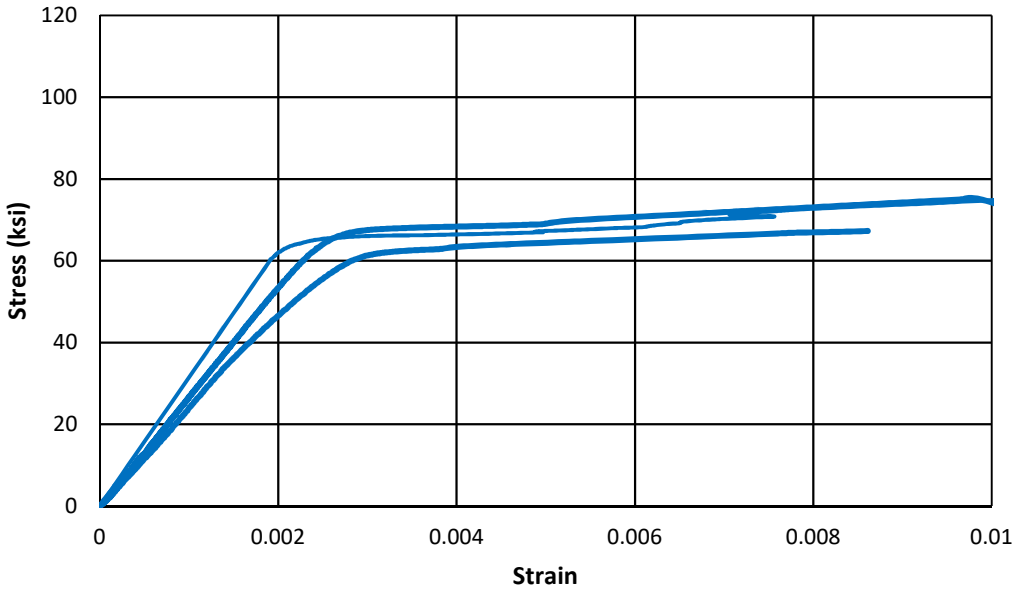

a) Partial Curve

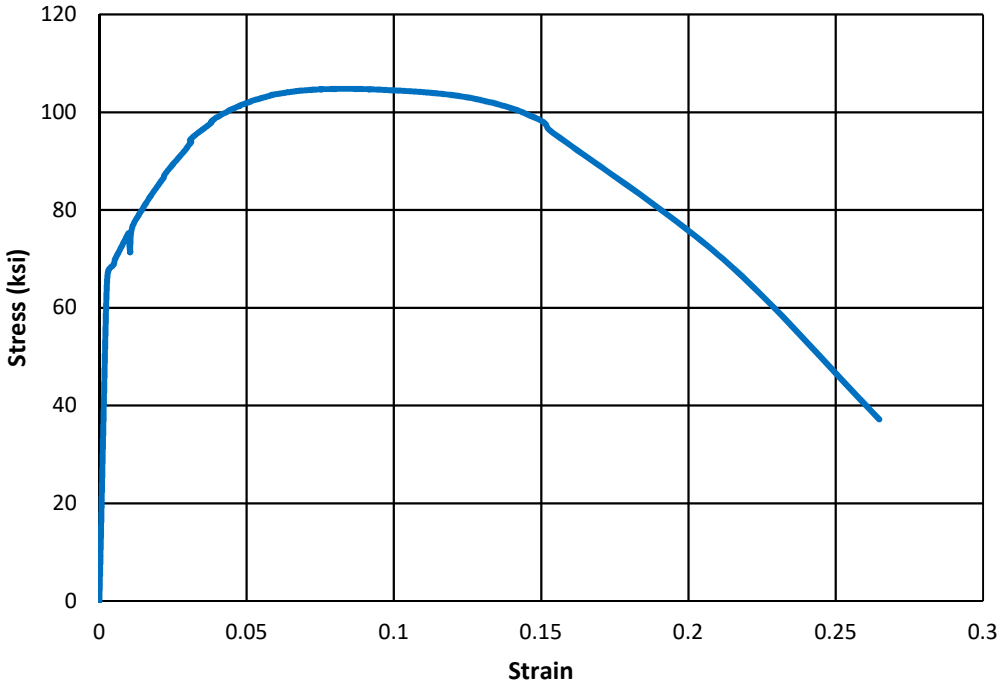

b) Complete Curve

Figure B.4: Complete Stress-Strain Curve for #4 Grade 60 Stirrups

APPENDIX C. CONCRETE MIX INFORMATION

Table C.1: Concrete Mixes as Supplied

Series	1		2		3		4	
Truck	1	2	1	2	1	2	1	2
Mix Code	4101CC		4601CC		4101CC		4101CC	
Nominal Strength (psi)	4000		4500		4000		4000	
Type I Cement (lb/cy)	515.3	519.4	561.7	561.7	518.4	515.3	515.3	520
#8 Limestone (lb/cy)	1865.8	1861.8	1841.8	1846.3	1872.4	1864.1	1868.2	1865.8
Fine Aggregate (lb/cy)	1471.1	1471.3	1444.8	1447.0	1472.4	1471.3	1470.3	1468.8
Water (lb/cy)	242.3	243.3	243.3	243.3	249.3	257.4	234.2	232.2
Water Added (lb/cy)	11.1	4.9	4.6	-	4.4	-	4.4	11.1
Mid-Range Water Reducer (oz/cy)	20.8	20.6	11.2	11.2	20.7	20.6	20.5	20.7
Slump (in.)	7.5	6	4	6	7	6.5	5.5	6.5

Table C.2: Concrete Used in Each Specimen

Series	Specimen	Truck
I	U-40-5	2
	U-60-5	
	U-80-5	
	U-100-5	
	U-120-5	1
	U-80-5-M	
	U-100-5-M	
	U-120-5-M	
II	C3/60-60-5-50	1
	C3/60-60-5-100	
	C3/60-60-5-150	
	C3/60-60-5-200	
	C4/60-60-5-100	2
	C4/60-60-5-150	
	C3/100-60-5-100	
	C3/100-60-5-150	
III	C3/60-80-5-50	1
	C3/60-80-5-100	
	C3/60-80-5-150	
	C3/60-80-5-200	
	C4/60-80-5-100	2
	C4/60-80-5-150	
	C3/100-80-5-100	
	C3/100-80-5-150	
IV	U-40-5a	1
	U-60-5a	
	U-70-5	
	C3/60/2-40-5-50	
	C3/60/3-40-5-50	
	C3/100/3-40-5-50	2
	C3/60-40-5-100	
	C3/100-40-5-100	

APPENDIX D: LOAD-DEFLECTION RESPONSE

Accurate deflection measurements could not be exported.

a) Load-Deflection

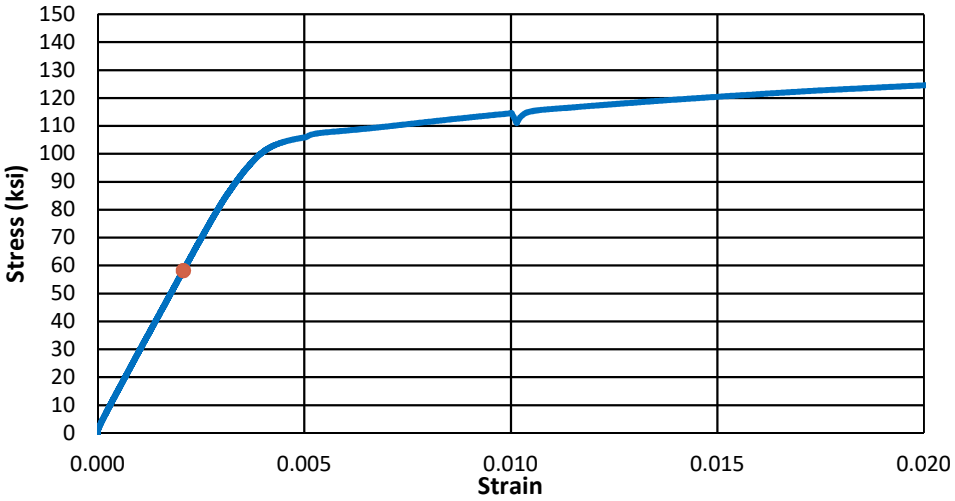

b) Stress-Strain

Figure D.1: U-40-5

Accurate deflection measurements could not be exported.

a) Load-Deflection

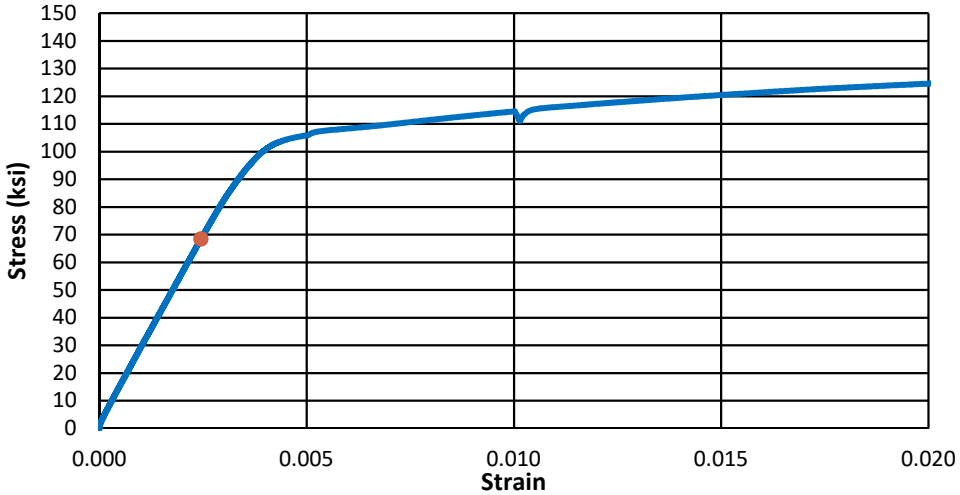

b) Stress-Strain

Figure D.2: U-60-5

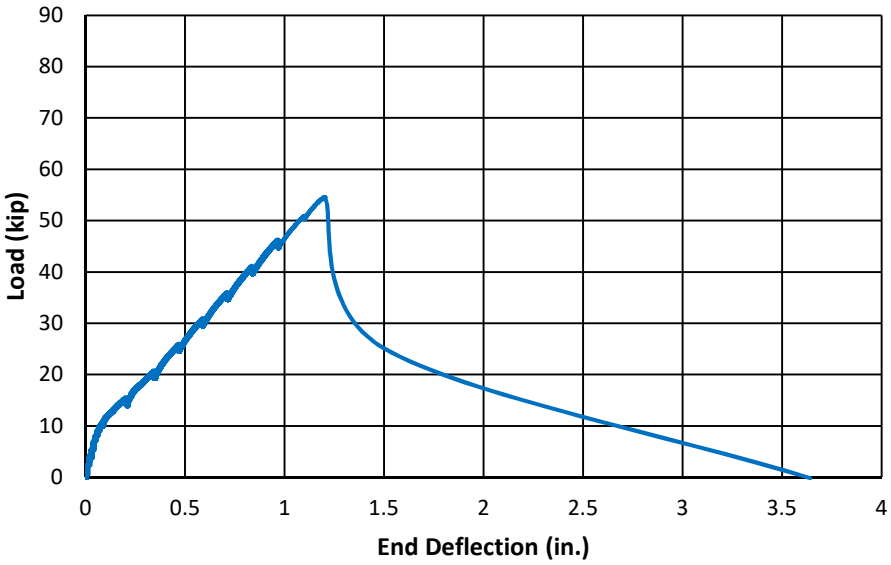

a) Load-Deflection

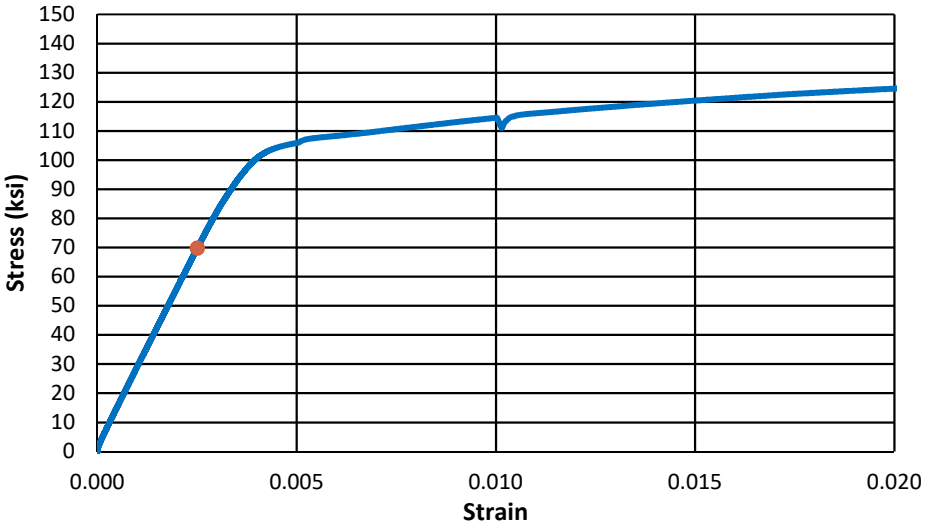

b) Stress-Strain

Figure D.3: U-40-5a

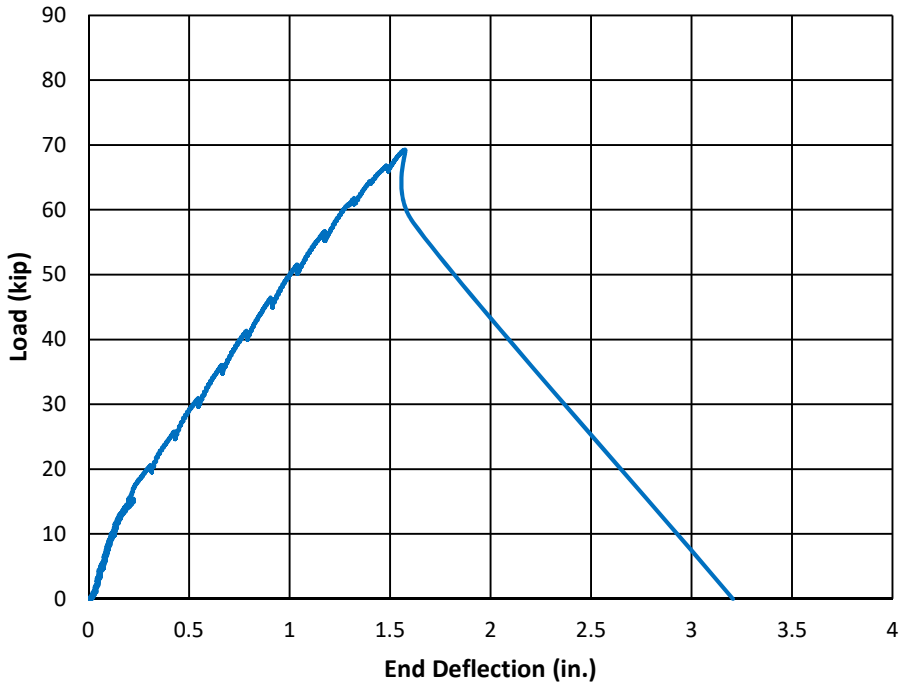

a) Load-Deflection

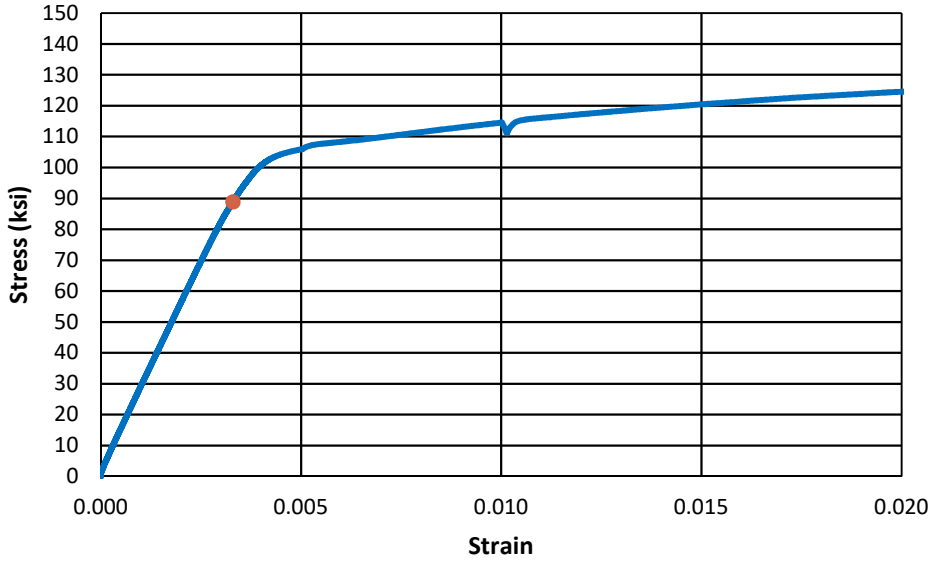

b) Stress-Strain

Figure D.4: U-60-5a

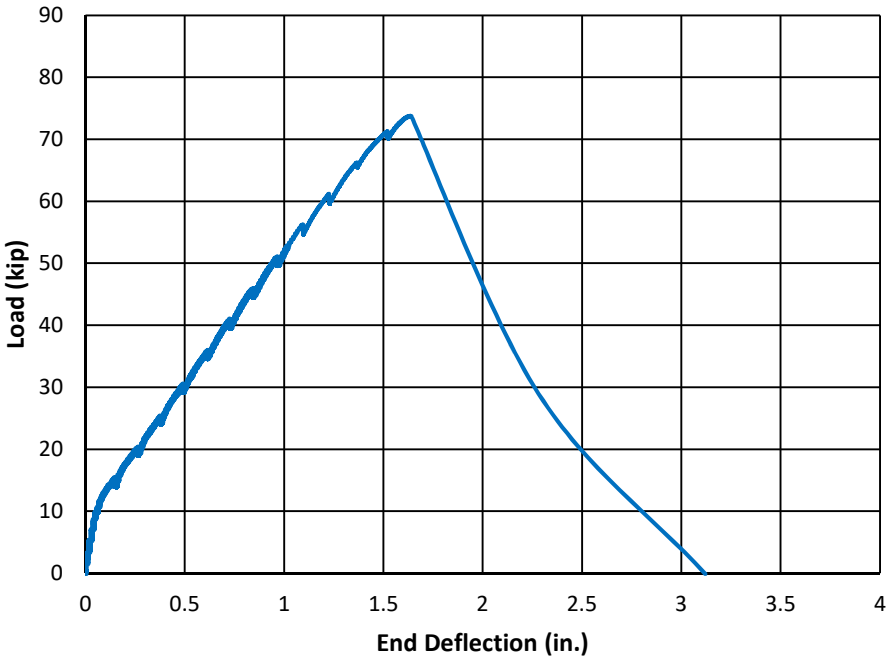

a) Load-Deflection

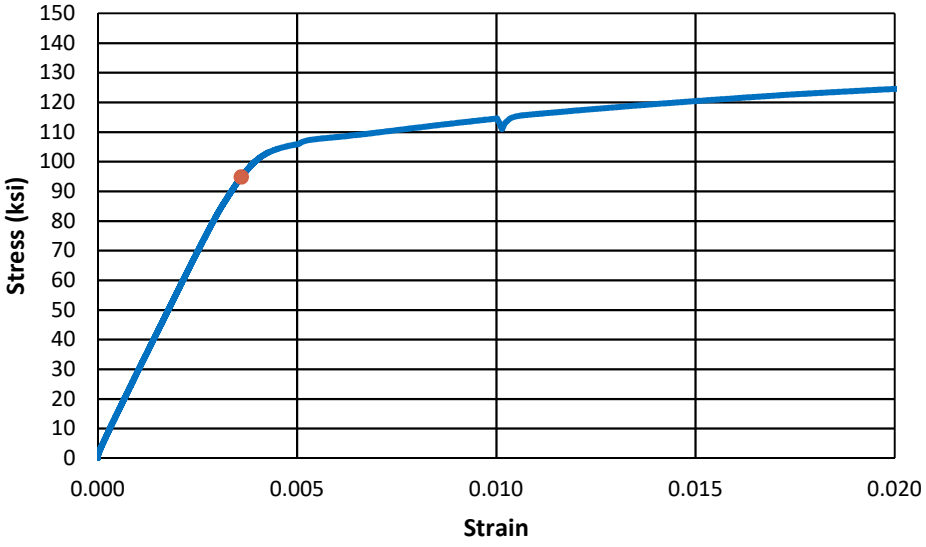

b) Stress-Strain

Figure D.5: U-70-5

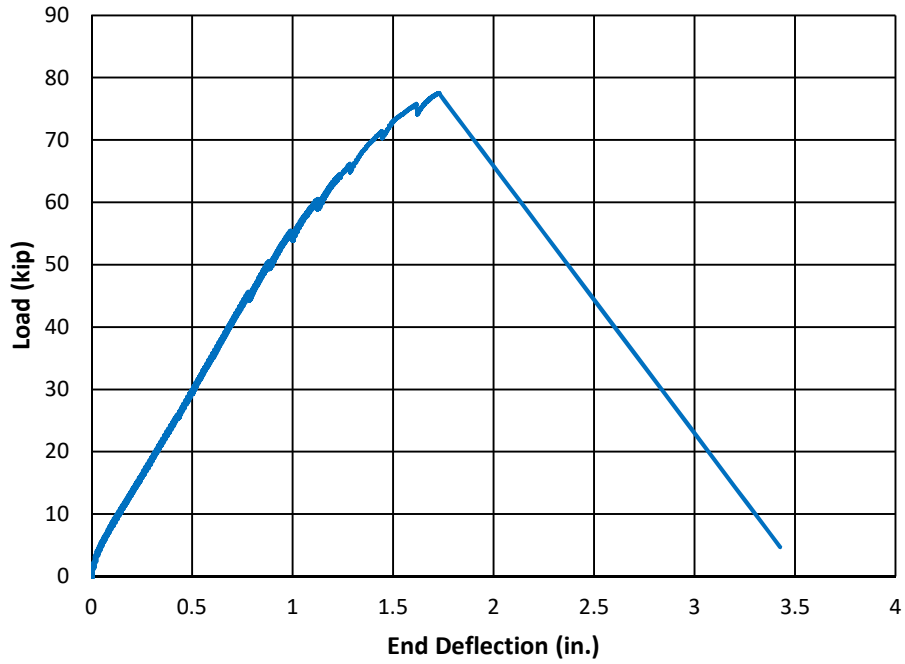

a) Load-Deflection

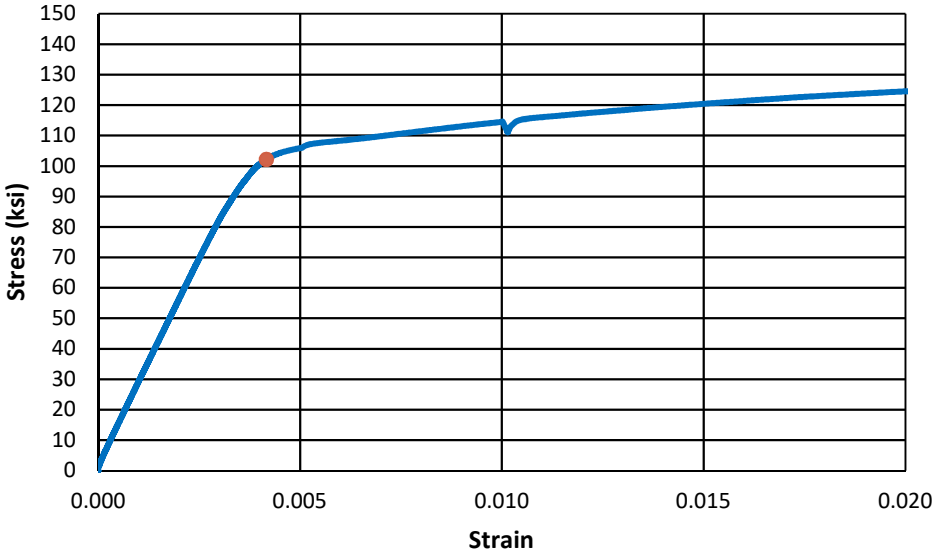

Stress-Strain

Figure D.6: U-80-5

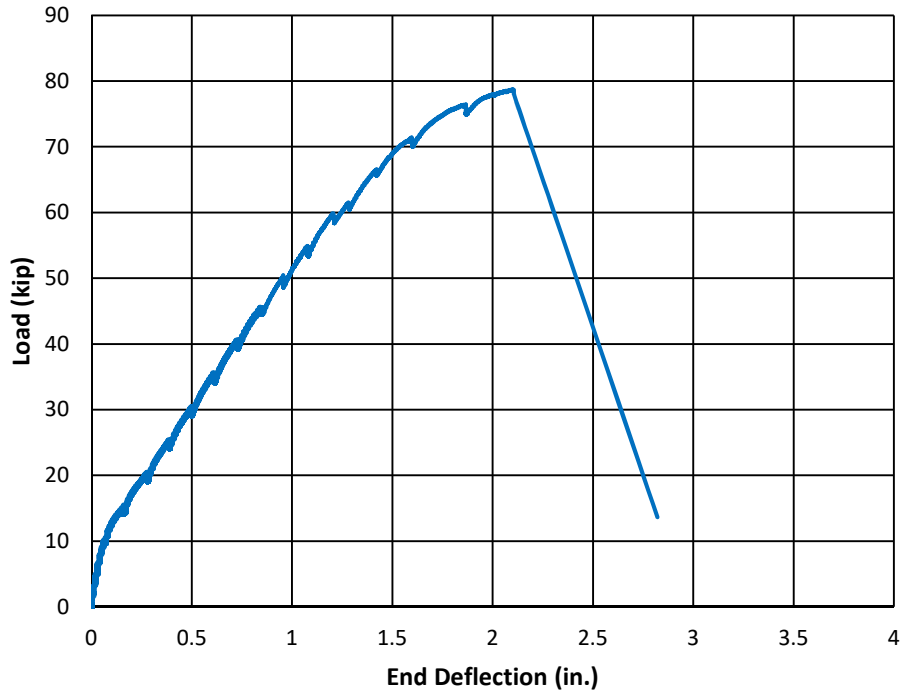

a) Load-Deflection

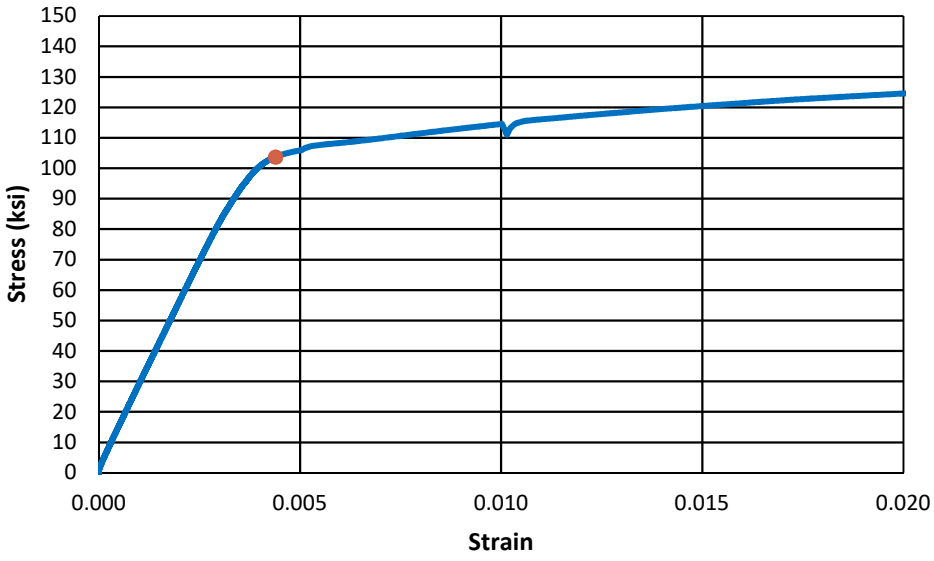

b) Stress-Strain

Figure D.7: U-100-5

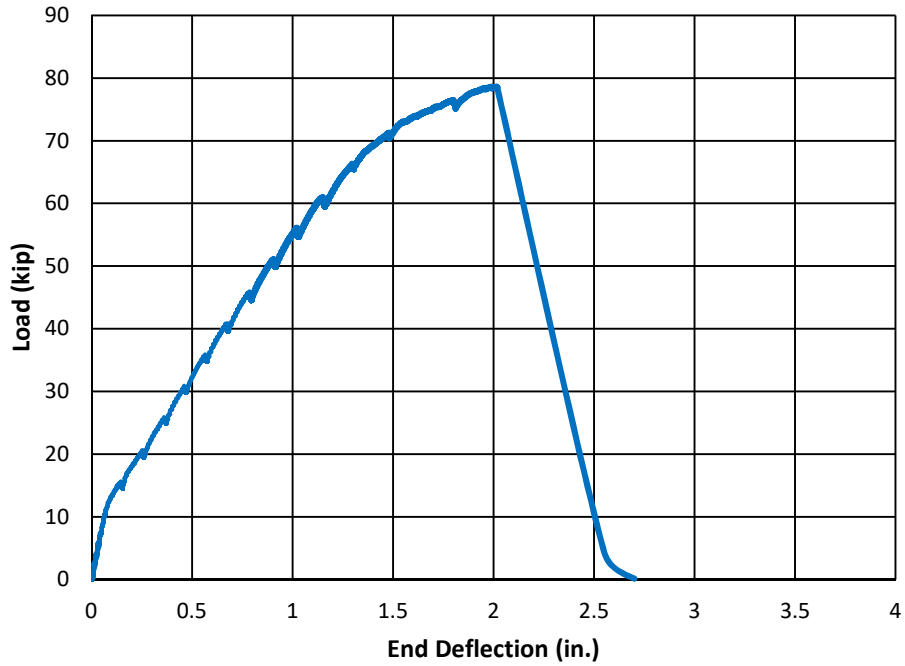

a) Load-Deflection

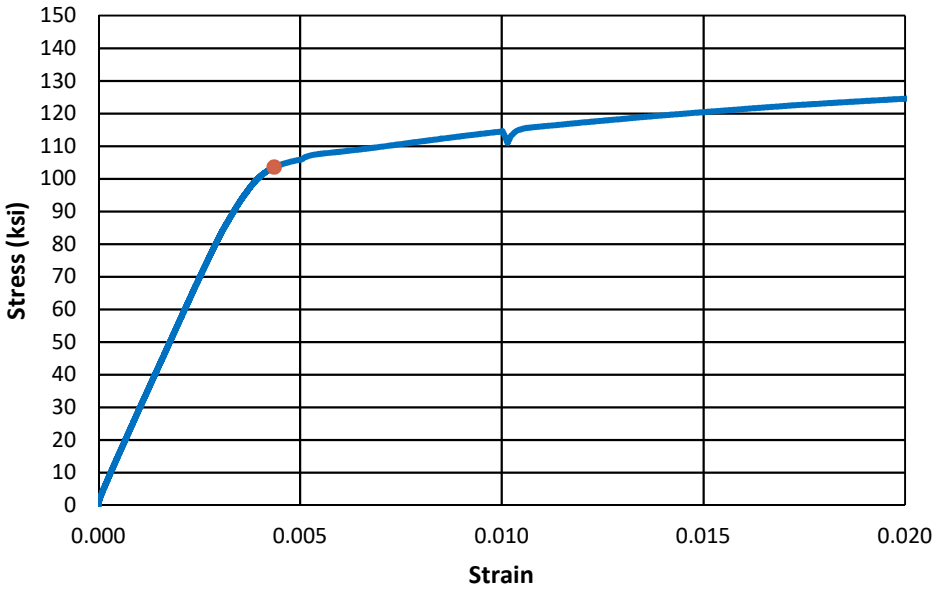

b) Stress-Strain

Figure D.8: U-120-5

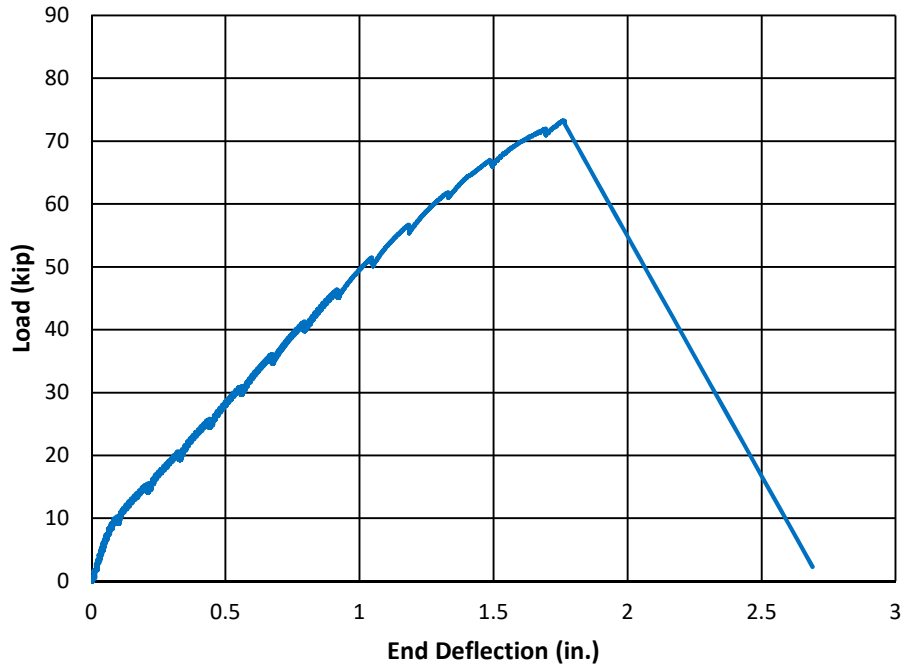

a) Load-Deflection

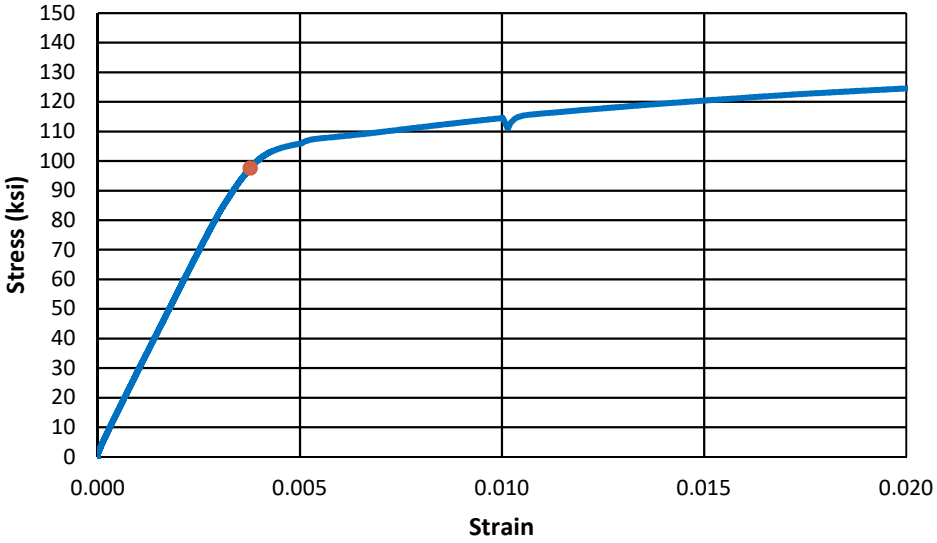

b) Stress-Strain

Figure D.9: U-80-5-M

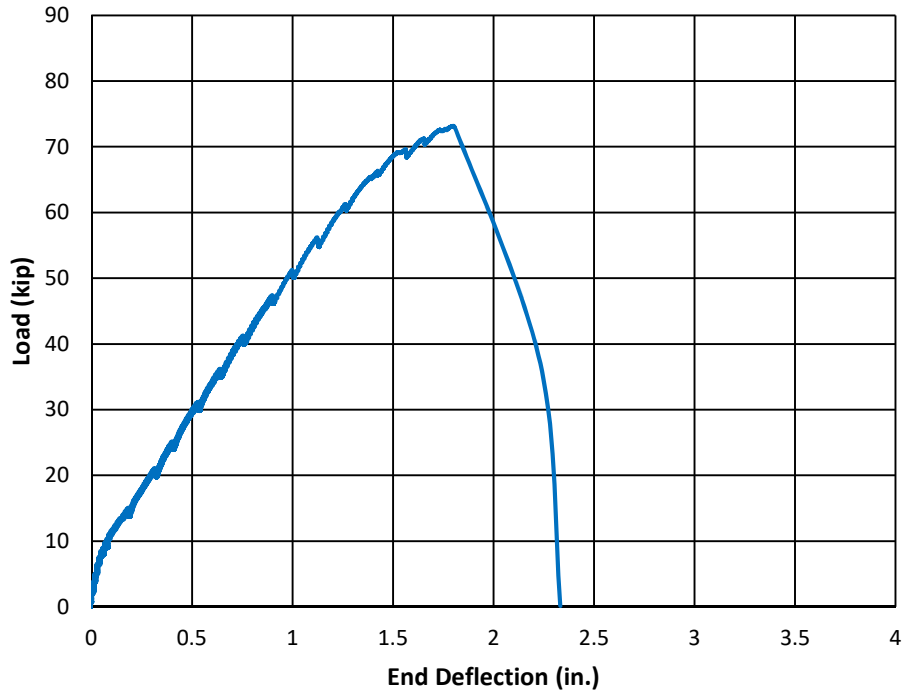

a) Load-Deflection

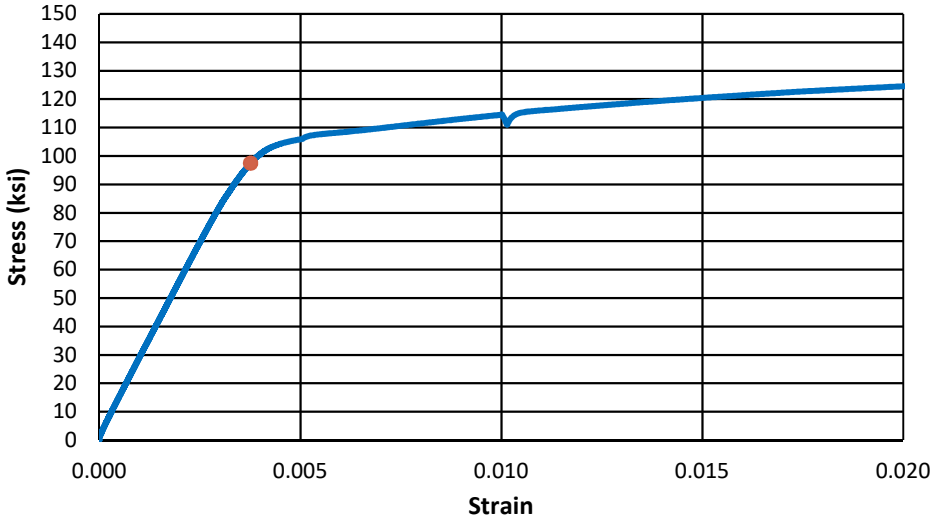

b) Stress-Strain

Figure D.10: U-100-5-M

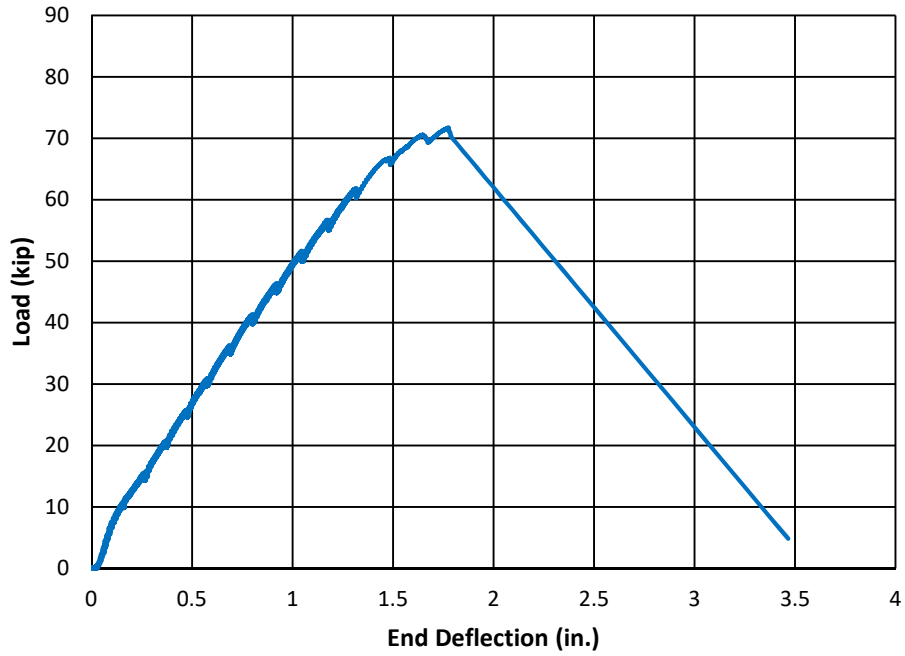

a) Load-Deflection

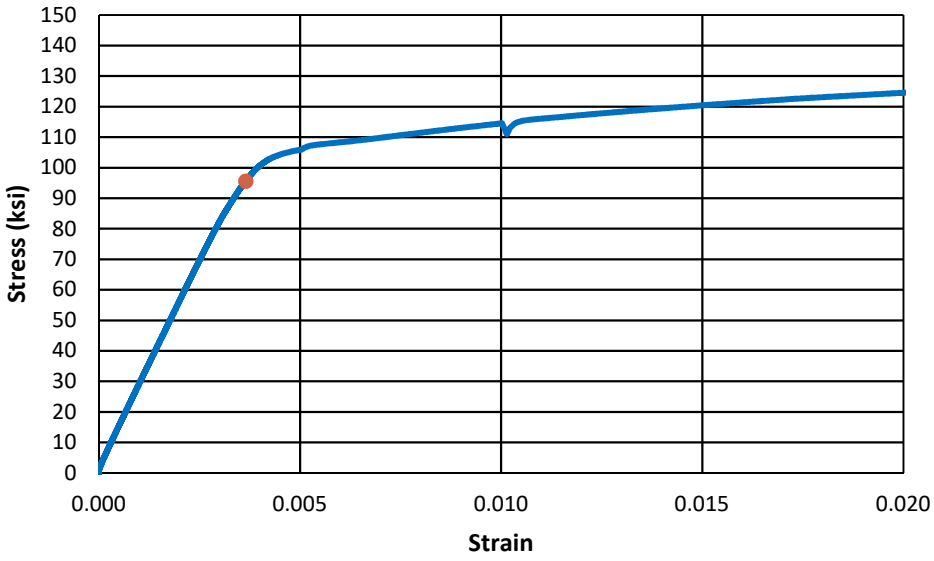

b) Stress-Strain

Figure D.11: U-120-5-M

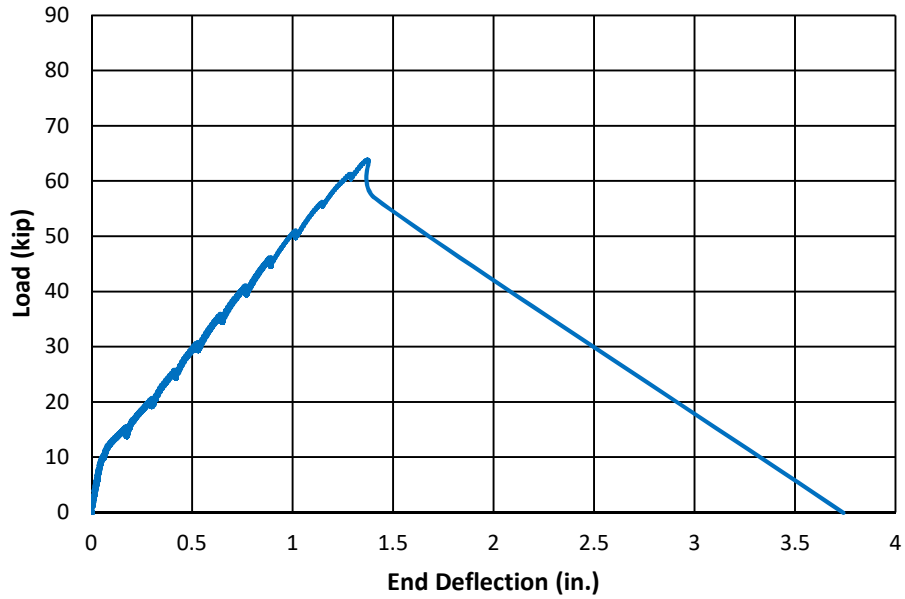

a) Load-Deflection

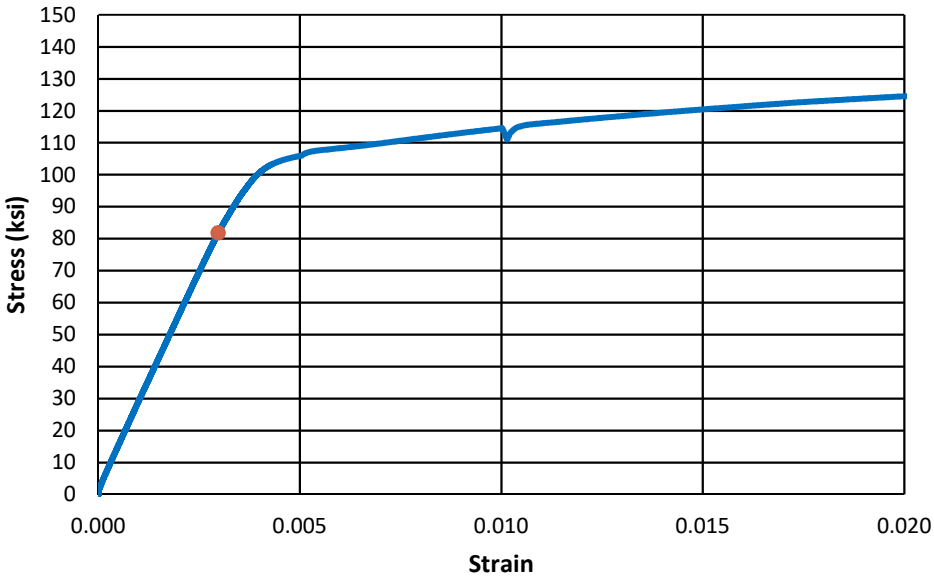

b) Stress-Strain

Figure D.12: C3/60/2-40-5-50

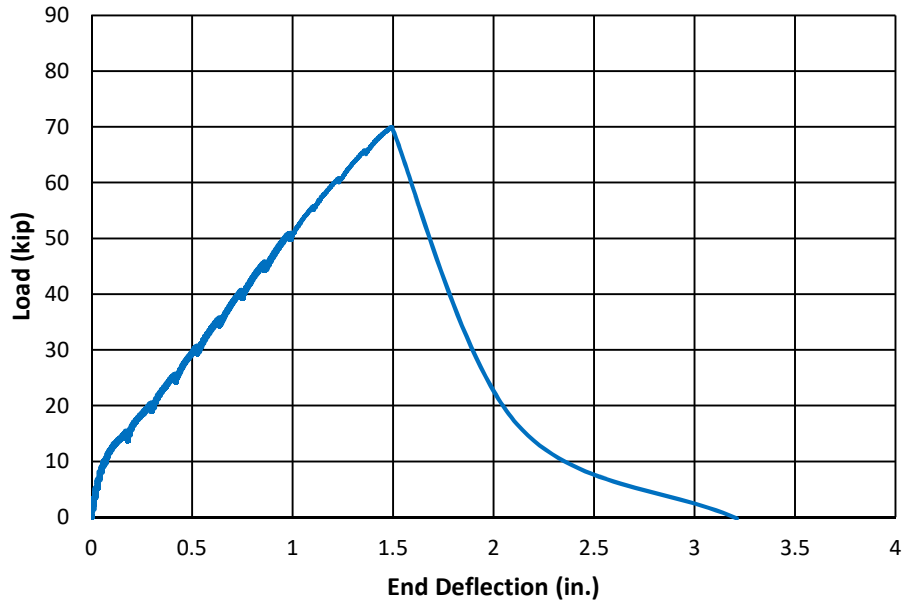

a) Load-Deflection

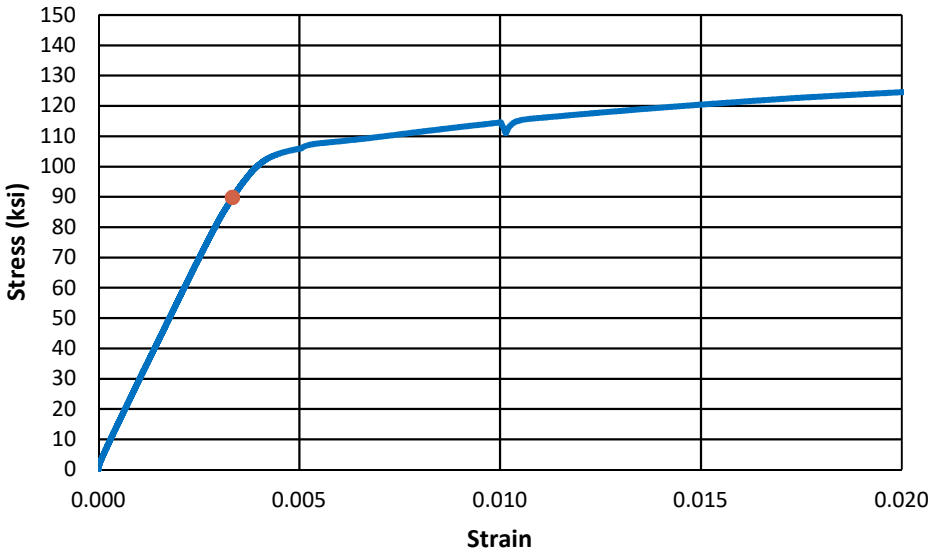

b) Stress-Strain

Figure D.13: C3/60/3-40-5-50

Accurate deflection measurements could not be exported.

a) Load-Deflection

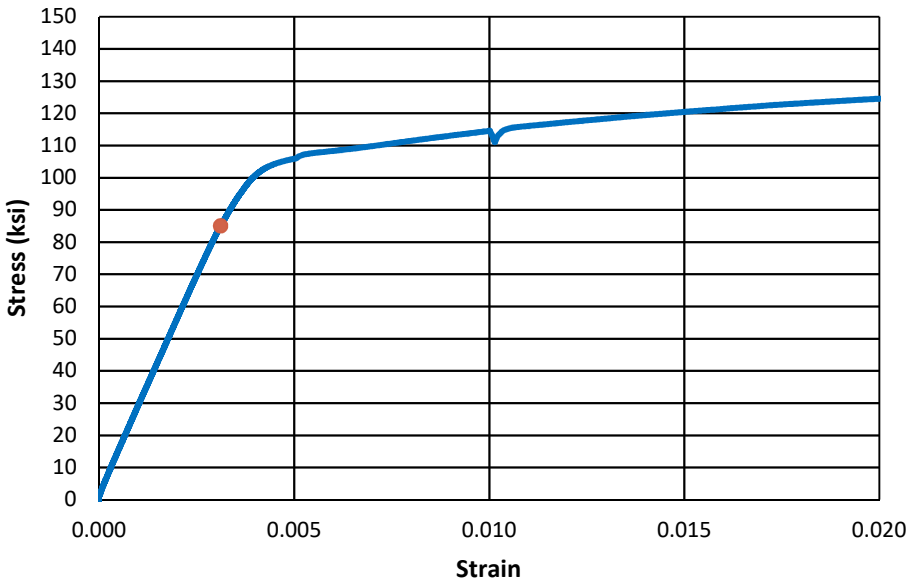

b) Stress-Strain

Figure D.14: C3/100/3-40-5-50

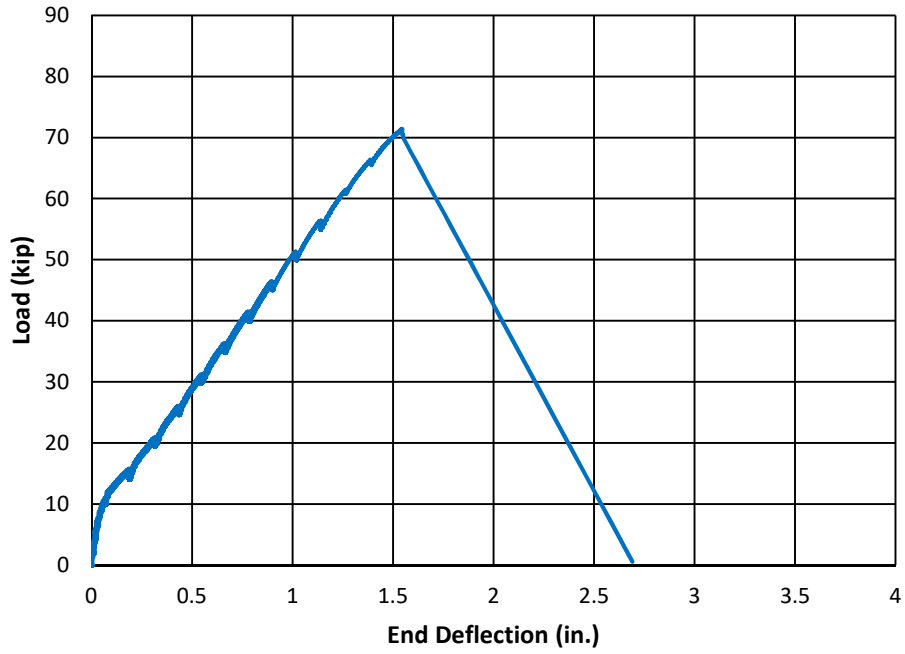

a) Load-Deflection

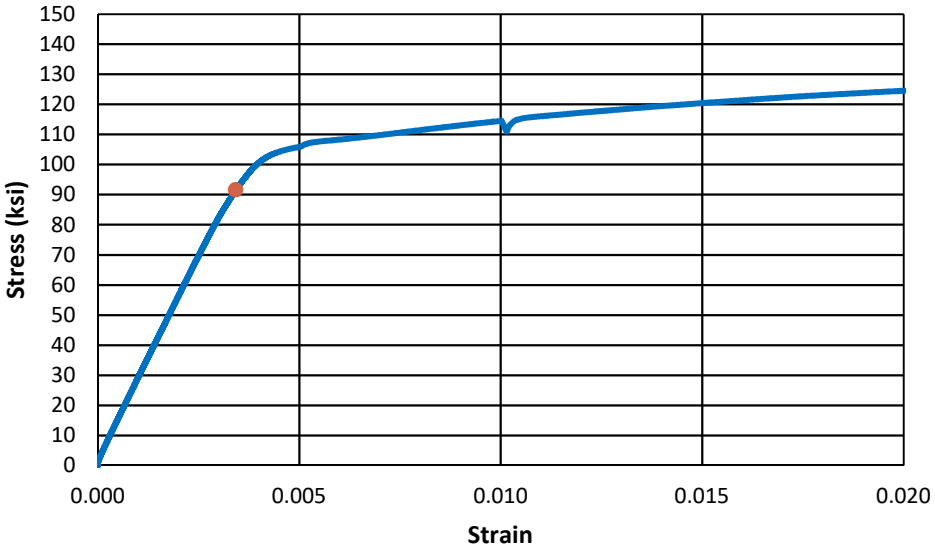

b) Stress-Strain

Figure D.15: C3/60-40-5-100

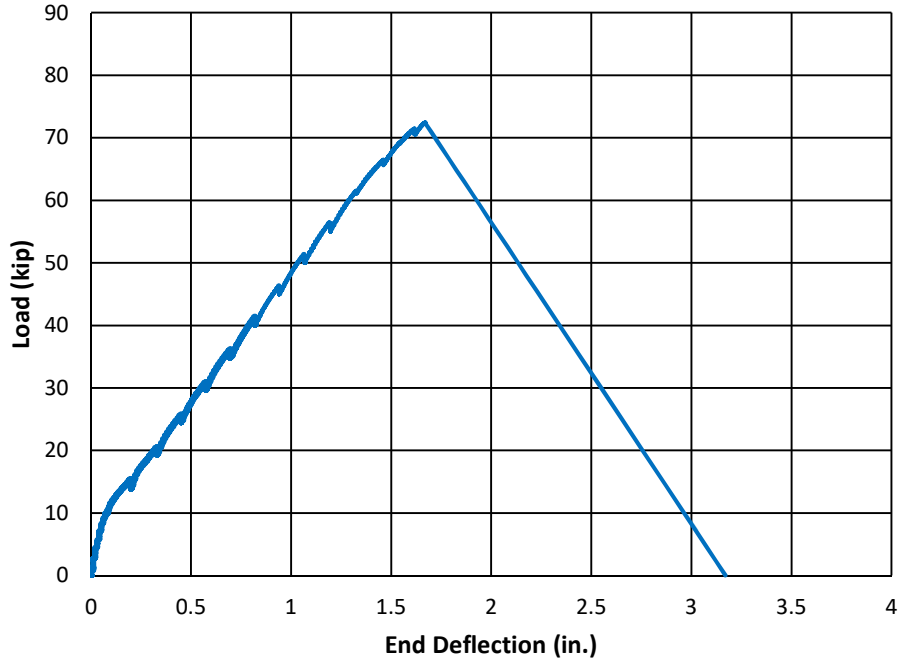

a) Load-Deflection

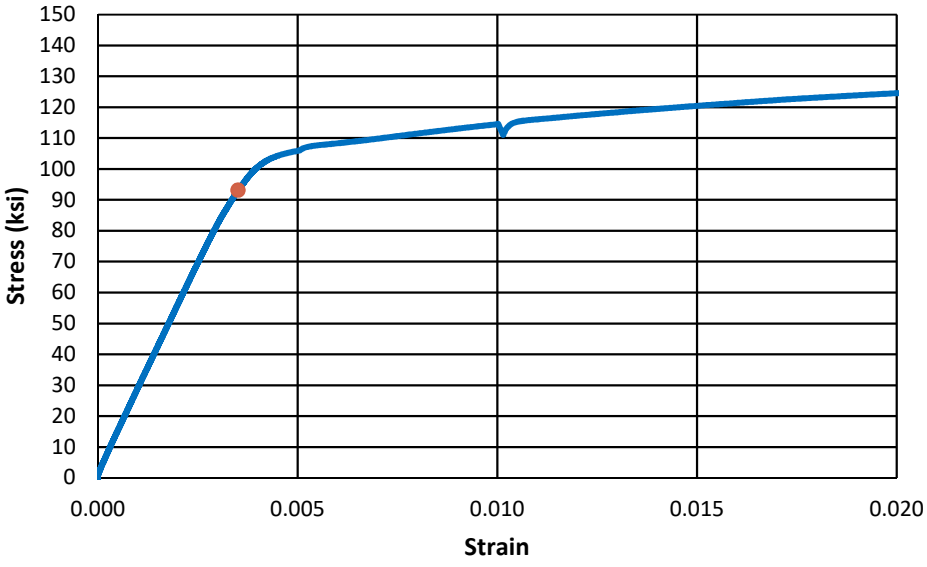

b) Stress-Strain

Figure D.16: C3/100-40-5-100

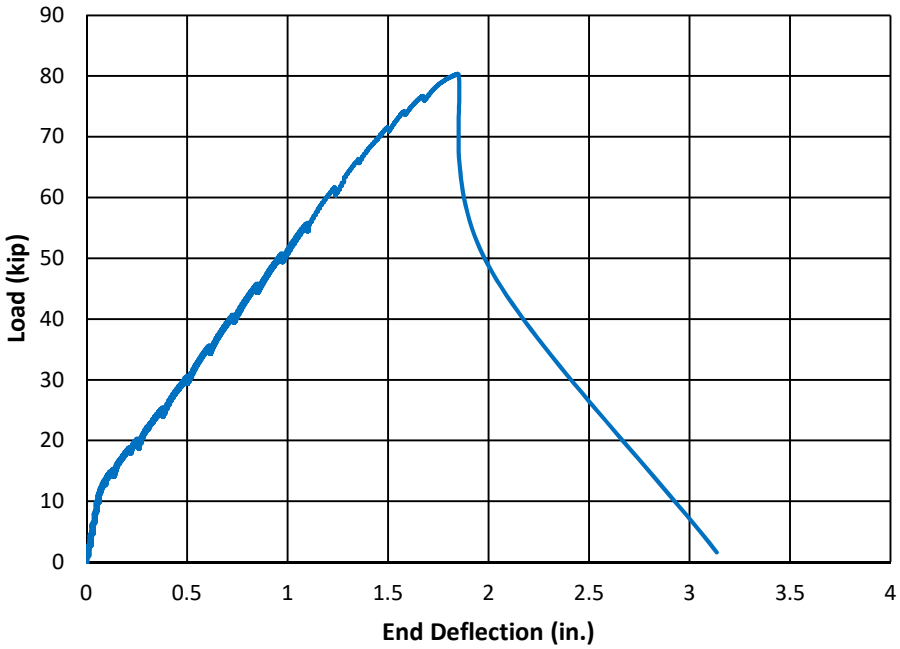

a) Load-Deflection

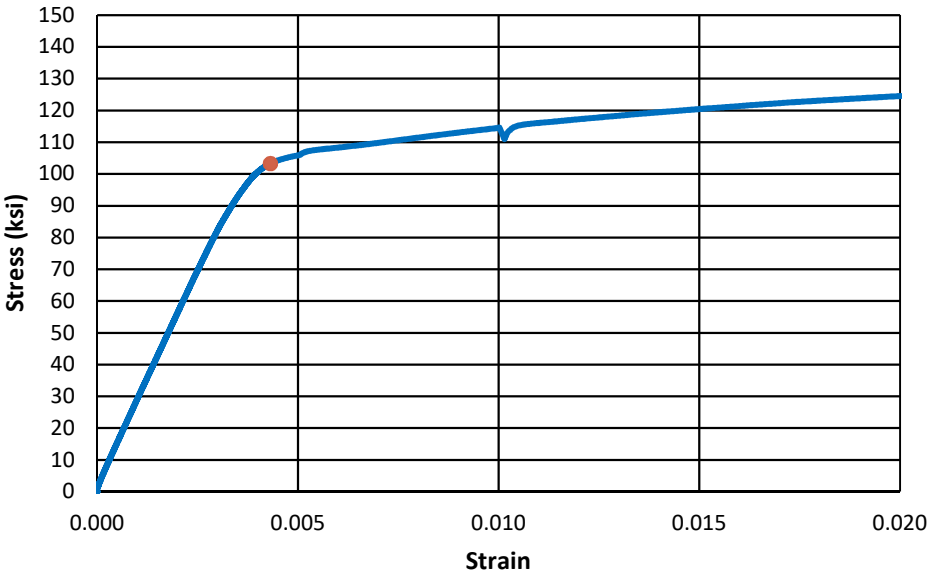

b) Stress-Strain

Figure D.17: C3/60-60-5-50

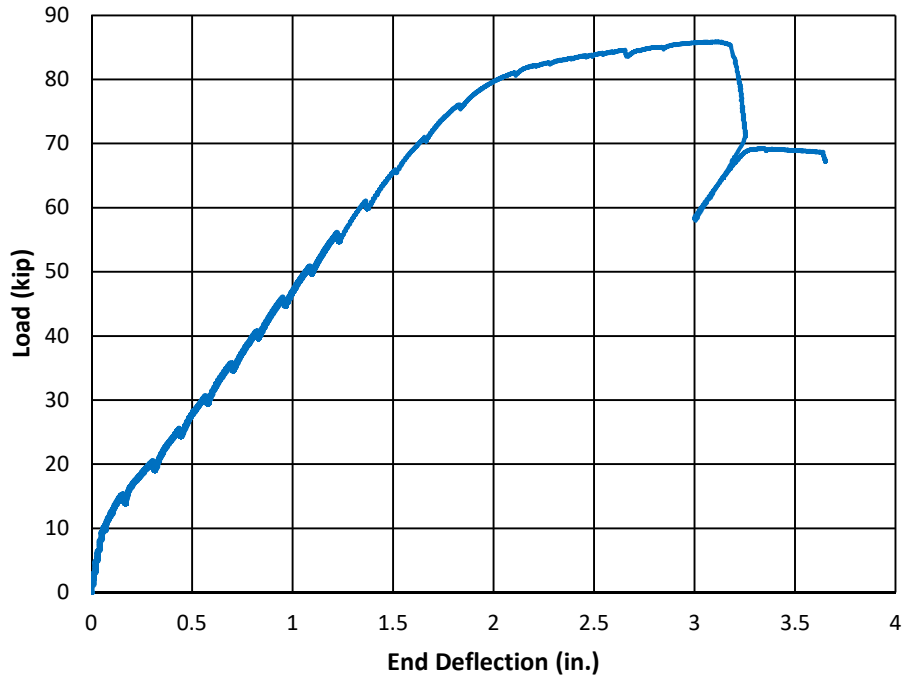

a) Load-Deflection

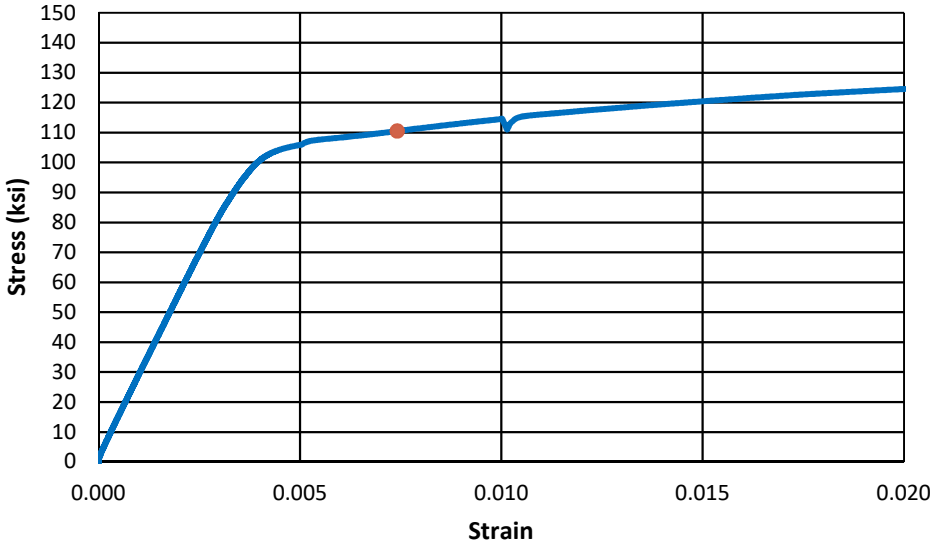

b) Stress-Strain

Figure D.18: C3/60-60-5-100

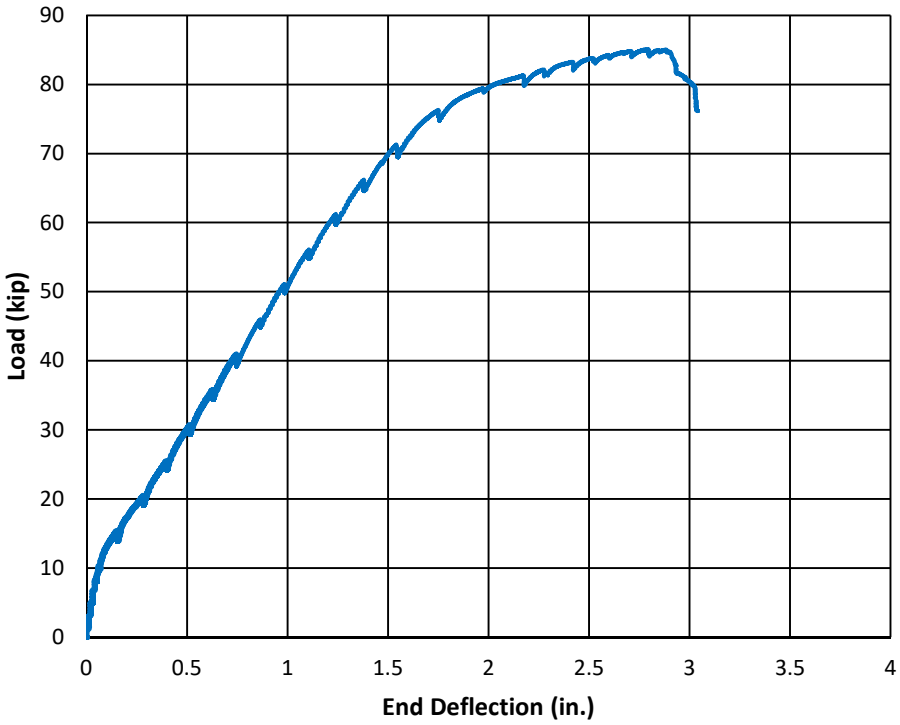

a) Load-Deflection

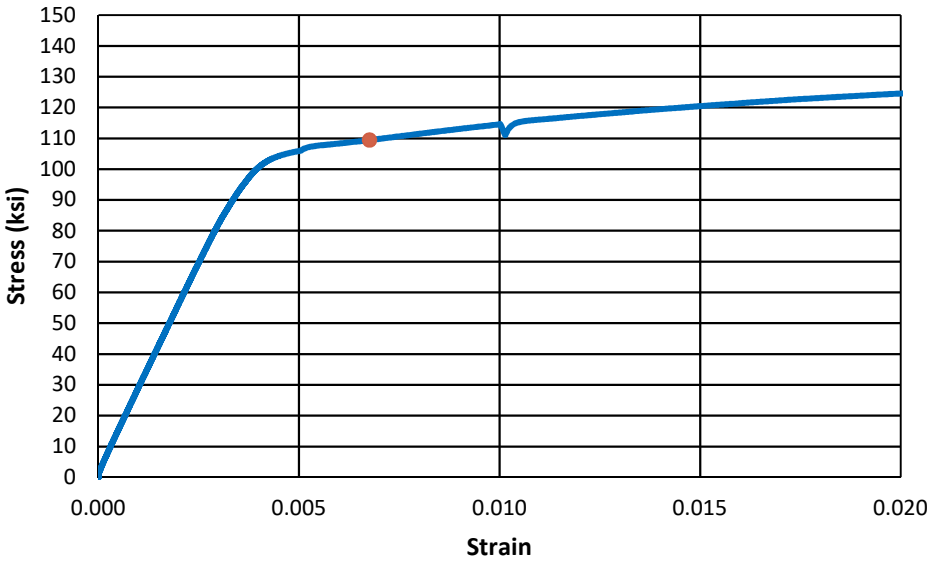

b) Stress-Strain

Figure D.19: C3/60-60-5-150

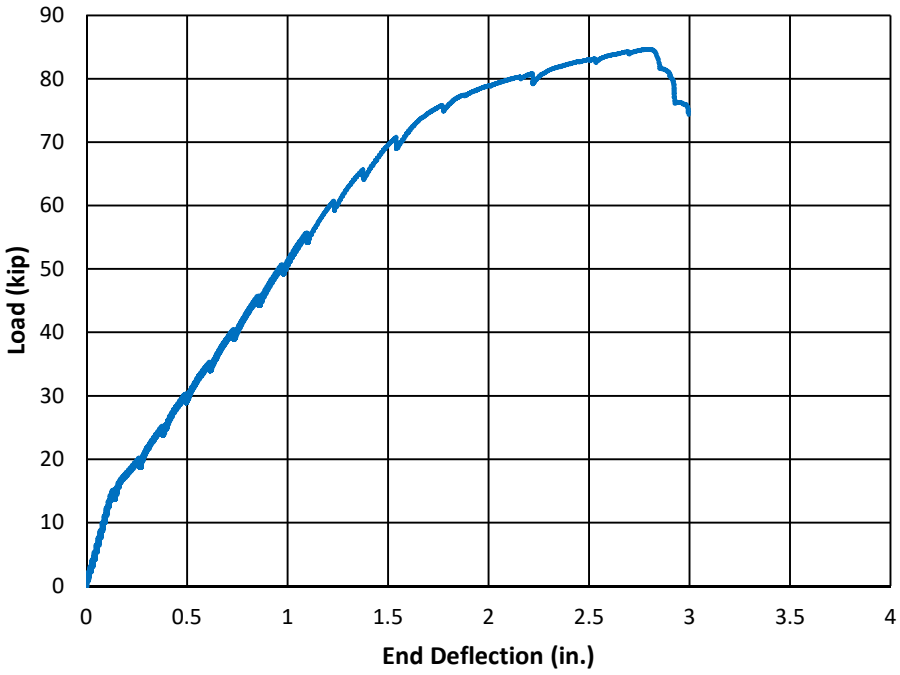

a) Load-Deflection

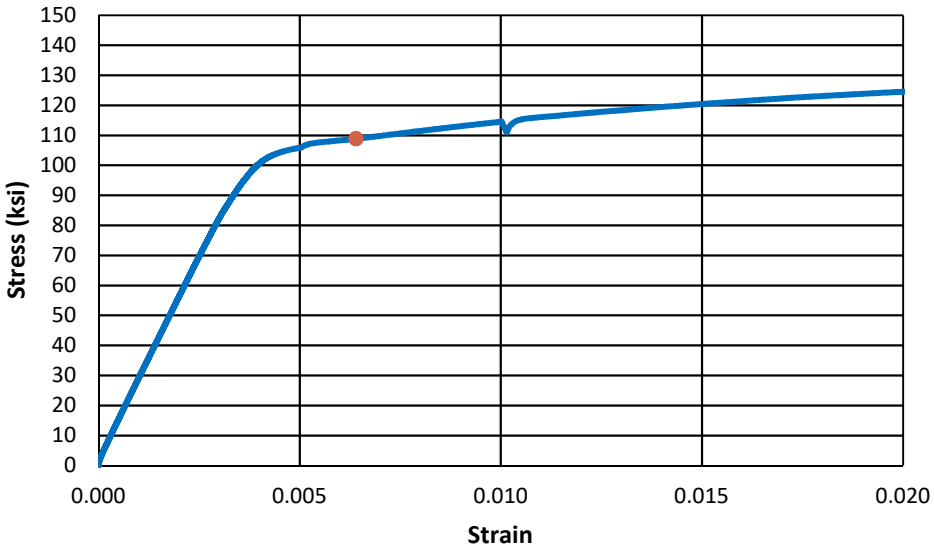

b) Stress-Strain

Figure D.20: C4/60-60-5-100

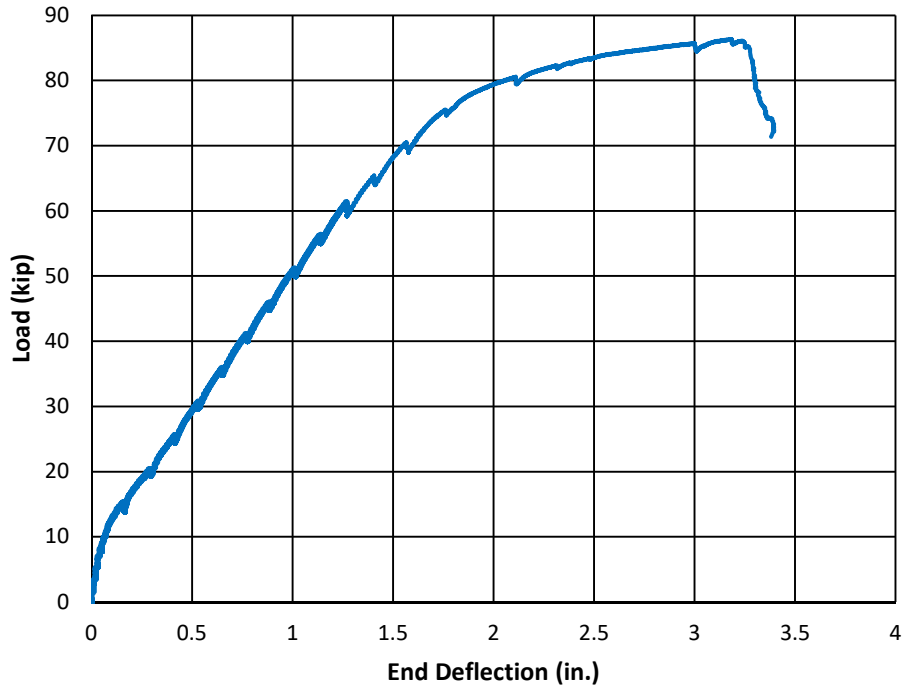

a) Load-Deflection

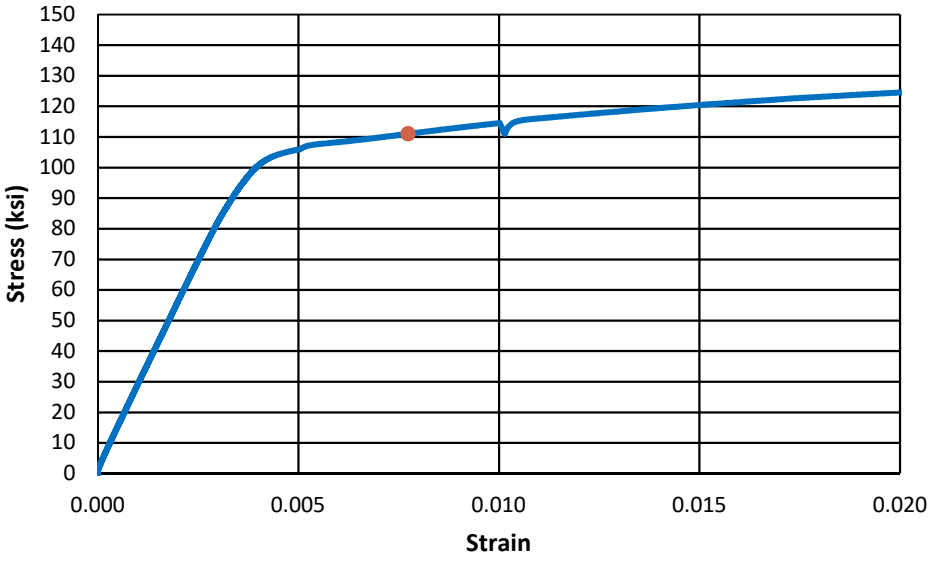

b) Stress-Strain

Figure D.21: C3/100-60-5-100

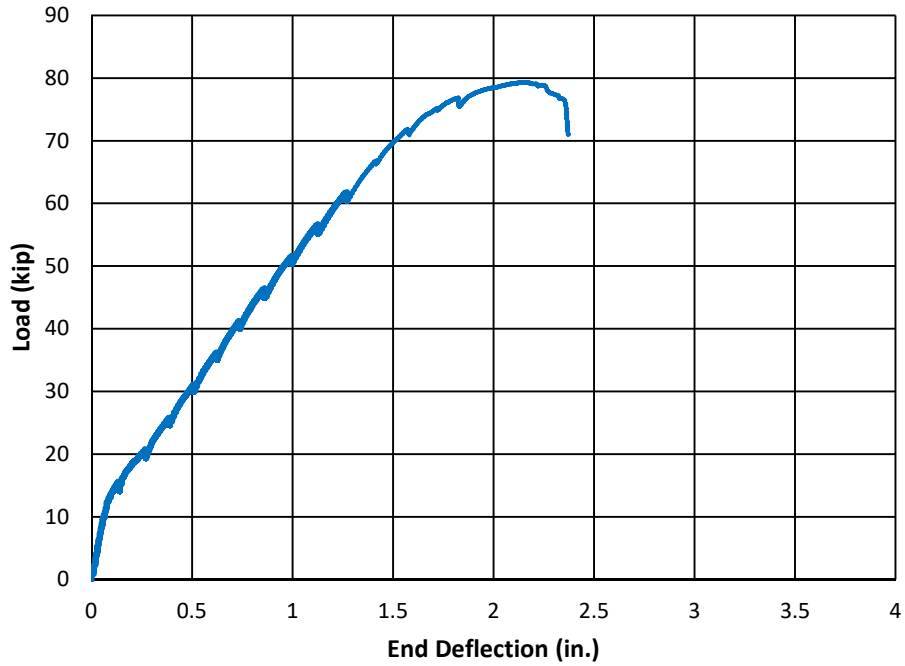

a) Load-Deflection

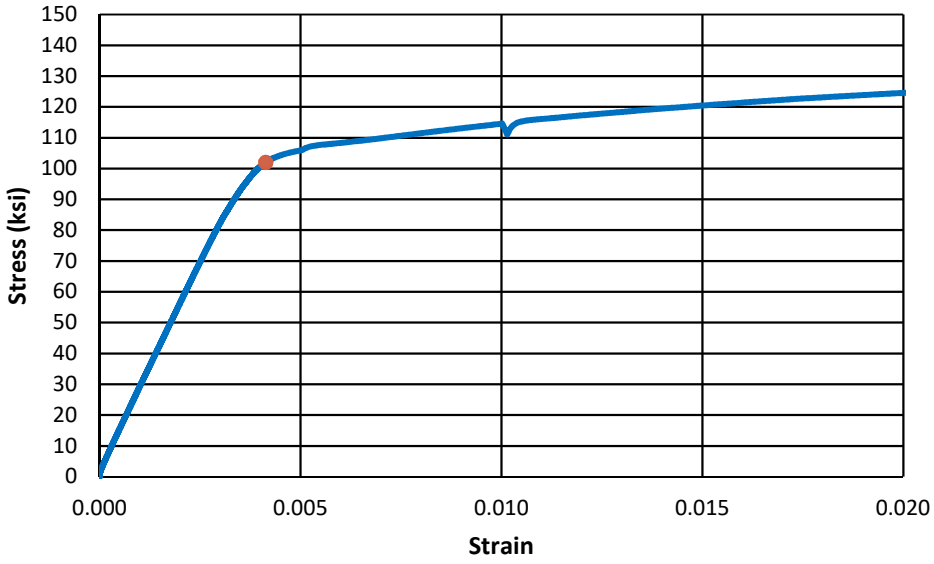

b) Stress-Strain

Figure D.22: C3/60-80-5-50

APPENDIX E: CRACK WIDTH MEASUREMENTS

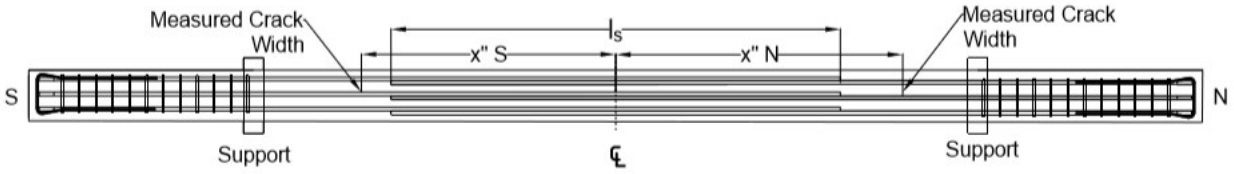

Figure E.1: Description of Nomenclature

Crack widths were not recorded for Specimens U-40-5 and C3/100/3-40-5-50.

Table E.1: U-40-5a

Load (kip)	Bar Stress (ksi)	Crack Widths (in.)				
		56.5" N	26.5" N	36" S	53" S	Average
15	19.0	0.004	0.003	0.003	0.003	0.0033
20	25.3	0.008	0.005	0.005	0.005	0.0058
25	31.7	0.009	0.007	0.006	0.007	0.0073
30	38.1	0.011	0.009	0.007	0.009	0.0090
35	44.5	0.011	0.012	0.009	0.011	0.0108
40	50.9	0.012	0.014	0.010	0.013	0.0123
45	57.3	0.012	0.016	0.013	0.015	0.0140

Table E.2: U-60-5

Load (kip)	Bar Stress (ksi)	Crack Widths (in.)				
		Crack 1	Crack 2	Crack 3	Crack 4	Average
20	25.7	0.005	0.010	0.005	0.005	0.0063
25	32.1	0.005	0.010	0.005	0.005	0.0063
30	38.6	0.010	0.020	0.010	0.010	0.0125
35	45.1	0.015	0.025	0.010	0.020	0.0175
40	51.6	0.020	0.025	0.010	0.020	0.0188
45	58.2	0.020	0.030	0.015	0.020	0.0213
50	64.8	0.020	0.030	0.015	0.025	0.0225

*Crack location not measured

Table E.3: U-60-5a

Load (kip)	Bar Stress (ksi)	Crack Widths (in.)				
		77" N	53" N	44" S	59" S	Average
15	19.0	0.002	0.002	0.003	0.002	0.0023
20	25.3	0.006	0.003	0.003	0.004	0.0040
25	31.7	0.008	0.005	0.006	0.006	0.0063
30	38.1	0.013	0.007	0.008	0.007	0.0088
35	44.5	0.015	0.009	0.011	0.009	0.0110
40	50.9	0.018	0.011	0.014	0.012	0.0138
45	57.3	0.021	0.013	0.016	0.013	0.0158
50	63.7	0.021	0.014	0.021	0.016	0.0180
55	70.2	0.025	0.016	0.022	0.018	0.0203

Table E.4: U-70-5

Load (kip)	Bar Stress (ksi)	Crack Widths (in.)				
		63.5" N	43" N	47" S	63.5" S	Average
15	19.0	0.002	0.002	0.002	0.002	0.0020
20	25.3	0.003	0.004	0.003	0.002	0.0030
25	31.7	0.004	0.006	0.003	0.003	0.0040
30	38.1	0.006	0.006	0.004	0.004	0.0050
35	44.5	0.007	0.009	0.006	0.005	0.0068
40	50.9	0.009	0.009	0.008	0.009	0.0088
45	57.3	0.010	0.012	0.009	0.010	0.0103
50	63.7	0.012	0.017	0.009	0.012	0.0125
55	70.2	0.014	0.018	0.011	0.013	0.0140
60	76.7	0.019	0.021	0.012	0.019	0.0178

Table E.5: U-80-5

Load (kip)	Bar Stress (ksi)	Crack Widths (in.)				
		Crack 1	Crack 2	Crack 3	Crack 4	Average
15	19.2	0.004	0.006	0.004	0.005	0.0048
20	25.7	0.004	0.007	0.005	0.005	0.0053
25	32.1	0.005	0.009	0.005	0.005	0.0060
30	38.6	0.007	0.010	0.006	0.011	0.0085
35	45.1	0.011	0.012	0.013	0.013	0.0123
40	51.6	0.014	0.013	0.014	0.013	0.0135
45	58.2	0.012	0.011	0.014	0.016	0.0133
50	64.8	0.013	0.013	0.016	0.020	0.0155
55	71.4	0.015	0.013	0.018	0.020	0.0165
60	78.1	0.017	0.013	0.019	0.022	0.0178

*Crack location not measured

Table E.6: U-100-5

Load (kip)	Bar Stress (ksi)	Crack Widths (in.)				
		74" N	66" N	64" S	85" S	Average
15	19.2	0.002	0.004	0.003	0.003	0.0030
20	25.7	0.005	0.007	0.004	0.005	0.0053
25	32.1	0.005	0.008	0.004	0.006	0.0058
30	38.6	0.007	0.009	0.004	0.011	0.0078
35	45.1	0.008	0.014	0.005	0.016	0.0108
40	51.6	0.010	0.017	0.008	0.017	0.0130
45	58.2	0.010	0.020	0.010	0.017	0.0143
50	64.8	0.012	0.023	0.010	0.019	0.0160
55	71.4	0.015	0.023	0.012	0.025	0.0188
60	78.1	0.016	0.030	0.012	0.028	0.0215

Table E.7: U-120-5

Load (kip)	Bar Stress (ksi)	Crack Widths (in.)				
		90" N	78" N	70" S	79" S	Average
20	25.7	0.005	0.006	0.007	0.007	0.0063
25	32.1	0.007	0.009	0.007	0.017	0.0100
30	38.6	0.009	0.011	0.009	0.019	0.0120
35	45.1	0.010	0.011	0.009	0.024	0.0135
40	51.6	0.013	0.015	0.010	0.024	0.0155
45	58.2	0.014	0.018	0.012	0.025	0.0173
50	64.8	0.016	0.018	0.018	0.025	0.0193
55	71.4	0.016	0.019	0.018	0.030	0.0208
60	78.1	0.019	0.025	0.018	0.035	0.0243

Table E.8: U-80-5-M

Load (kip)	Bar Stress (ksi)	Crack Widths (in.)				
		78.5" N	48.5" N	56.5" S	68" S	Average
15	19.4	0.005	0.004	0.004	0.003	0.0040
20	25.9	0.007	0.006	0.006	0.005	0.0060
25	32.4	0.010	0.011	0.008	0.007	0.0090
30	39.0	0.012	0.012	0.010	0.007	0.0103
35	45.5	0.013	0.012	0.013	0.008	0.0115
40	52.2	0.016	0.015	0.014	0.011	0.0140
45	58.8	0.018	0.017	0.015	0.011	0.0153
50	65.5	0.021	0.024	0.018	0.012	0.0188

Table E.9: U-100-5-M

Load (kip)	Bar Stress (ksi)	Crack Widths (in.)				
		87.5" N	72" N	66.5" S	72.5" S	Average
20	25.9	0.006	0.007	0.006	0.005	0.0060
25	32.4	0.007	0.009	0.010	0.007	0.0083
30	39.0	0.015	0.012	0.011	0.011	0.0123
35	45.5	0.017	0.013	0.014	0.014	0.0145
40	52.2	0.019	0.020	0.015	0.015	0.0173
45	58.8	0.021	0.022	0.018	0.017	0.0195
50	65.5	0.022	0.025	0.022	0.017	0.0215
55	72.3	0.028	0.025	0.027	0.021	0.0253

Table E.10: U-120-5-M

Load (kip)	Bar Stress (ksi)	Crack Widths (in.)				
		80" N	71" N	64" S	78" S	Average
15	19.4	0.003	0.004	0.004	0.006	0.0043
20	25.9	0.008	0.007	0.007	0.009	0.0078
25	32.4	0.011	0.010	0.014	0.010	0.0113
30	39.0	0.015	0.011	0.015	0.013	0.0135
35	45.5	0.016	0.013	0.018	0.014	0.0153
40	52.2	0.019	0.014	0.022	0.014	0.0173
45	58.8	0.024	0.015	0.025	0.015	0.0198
50	65.5	0.029	0.019	0.027	0.015	0.0225
55	72.3	0.031	0.021	0.028	0.015	0.0238
60	79.1	0.033	0.025	0.028	0.016	0.0255

Table E.11: C3/60/2-40-5-50

Load (kip)	Bar Stress (ksi)	Crack Widths (in.)				
		68" N	29" N	28" S	55" S	Average
15	19.0	0.005	0.005	0.003	0.004	0.0043
20	25.3	0.007	0.007	0.005	0.006	0.0063
25	31.7	0.010	0.010	0.006	0.008	0.0085
30	38.1	0.012	0.013	0.007	0.011	0.0108
35	44.5	0.013	0.014	0.010	0.015	0.0130
40	50.9	0.016	0.015	0.010	0.017	0.0145
45	57.3	0.018	0.015	0.013	0.019	0.0163
50	63.7	0.019	0.016	0.014	0.019	0.0170

Table E.12: C3/60/3-40-5-50

Load (kip)	Bar Stress (ksi)	Crack Widths (in.)				
		37" N	27" N	37" S	56" S	Average
15	19.0	0.003	0.002	0.003	0.003	0.0028
20	25.3	0.004	0.003	0.006	0.004	0.0043
25	31.7	0.008	0.005	0.006	0.006	0.0063
30	38.1	0.010	0.006	0.007	0.010	0.0083
35	44.5	0.012	0.006	0.009	0.011	0.0095
40	50.9	0.013	0.007	0.010	0.013	0.0108
45	57.3	0.014	0.007	0.011	0.015	0.0118
50	63.7	0.014	0.010	0.015	0.017	0.0140

Table E.13: C3/60-40-5-100

Load (kip)	Bar Stress (ksi)	Crack Widths (in.)				
		73" N	29" N	37" S	56" S	Average
15	19.0	0.003	0.003	0.004	0.002	0.0030
20	25.3	0.003	0.006	0.005	0.005	0.0048
25	31.7	0.003	0.007	0.009	0.007	0.0065
30	38.1	0.004	0.007	0.010	0.009	0.0075
35	44.5	0.004	0.010	0.012	0.011	0.0093
40	50.9	0.006	0.014	0.014	0.012	0.0115
45	57.3	0.006	0.015	0.015	0.014	0.0125
50	63.7	0.009	0.017	0.016	0.017	0.0148
55	70.2	0.009	0.018	0.020	0.019	0.0165

Table E.14: C3/100-40-5-100

Load (kip)	Bar Stress (ksi)	Crack Widths (in.)				
		73" N	29" N	37" S	56" S	Average
15	19.0	0.004	0.005	0.003	0.005	0.0043
20	25.3	0.005	0.006	0.006	0.005	0.0055
25	31.7	0.008	0.006	0.007	0.007	0.0070
30	38.1	0.010	0.006	0.009	0.009	0.0085
35	44.5	0.011	0.013	0.011	0.009	0.0110
40	50.9	0.013	0.014	0.014	0.012	0.0133
45	57.3	0.017	0.017	0.016	0.013	0.0158
50	63.7	0.019	0.020	0.017	0.015	0.0178
55	70.2	0.024	0.023	0.019	0.017	0.0208

Table E.15: C3/60-60-5-50

Load (kip)	Bar Stress (ksi)	Crack Widths (in.)				
		70" N	49" N	71" S	87" S	Average
20	25.4	0.006	0.004	0.008	0.006	0.0060
25	31.7	0.010	0.005	0.011	0.009	0.0088
30	38.1	0.012	0.007	0.014	0.012	0.0113
35	44.5	0.013	0.009	0.016	0.013	0.0128
40	50.9	0.017	0.013	0.019	0.017	0.0165
45	57.3	0.020	0.015	0.021	0.018	0.0185
50	63.7	0.020	0.017	0.025	0.022	0.0210
55	70.2	0.025	0.021	0.027	0.022	0.0238
60	76.7	0.030	0.022	0.031	0.026	0.0273

Table E.16: C3/60-60-5-100

Load (kip)	Bar Stress (ksi)	Crack Widths (in.)				
		71" N	55.5" N	41" S	57" S	Average
15	19.0	0.004	0.005	0.003	0.003	0.0038
20	25.4	0.005	0.006	0.005	0.004	0.0050
25	31.7	0.010	0.011	0.008	0.005	0.0085
30	38.1	0.011	0.014	0.011	0.006	0.0105
35	44.5	0.014	0.016	0.014	0.009	0.0133
40	50.9	0.016	0.021	0.017	0.009	0.0158
45	57.3	0.018	0.022	0.018	0.009	0.0168
50	63.7	0.020	0.024	0.021	0.011	0.0190
55	70.2	0.025	0.027	0.023	0.012	0.0218
60	76.7	0.026	0.032	0.025	0.012	0.0238

Table E.17: C3/60-60-5-150

Load (kip)	Bar Stress (ksi)	Crack Widths (in.)				
		54.5" N	42.5" N	40.25" S	65" S	Average
15	19.0	0.003	0.002	0.002	0.003	0.0025
20	25.4	0.004	0.004	0.008	0.006	0.0055
25	31.7	0.005	0.005	0.013	0.006	0.0073
30	38.1	0.008	0.006	0.014	0.009	0.0093
35	44.5	0.009	0.007	0.015	0.012	0.0108
40	50.9	0.010	0.010	0.020	0.012	0.0130
45	57.3	0.010	0.010	0.020	0.016	0.0140
50	63.7	0.015	0.010	0.022	0.017	0.0160
55	70.2	0.016	0.010	0.030	0.019	0.0188
60	76.7	0.016	0.014	0.030	0.019	0.0198
65	83.1	0.016	0.014	0.032	0.020	0.0205
70	89.6	0.016	0.018	0.033	0.021	0.0220

Table E.18: C3/100-60-5-100

Load (kip)	Bar Stress (ksi)	Crack Widths (in.)				
		80.25" N	55.25" N	55.25" S	74.75" S	Average
15	19.0	0.005	0.004	0.003	0.005	0.0043
20	25.4	0.007	0.007	0.006	0.009	0.0073
25	31.7	0.010	0.009	0.007	0.010	0.0090
30	38.1	0.010	0.009	0.011	0.011	0.0103
35	44.5	0.012	0.010	0.012	0.018	0.0130
40	50.9	0.014	0.011	0.018	0.020	0.0158
45	57.3	0.019	0.013	0.018	0.020	0.0175
50	63.7	0.019	0.014	0.019	0.028	0.0200
55	70.2	0.019	0.018	0.021	0.028	0.0215
60	76.7	0.023	0.020	0.025	0.032	0.0250
65	83.1	0.029	0.023	0.025	0.033	0.0275
70	89.6	0.029	0.024	0.031	0.036	0.0300

Table E.19: C4/60-60-5-100

Load (kip)	Bar Stress (ksi)	Crack Widths (in.)				
		85" N	60.5" N	58" S	81" S	Average
15	19.0	0.005	0.005	0.004	0.006	0.0050
20	25.4	0.007	0.005	0.006	0.007	0.0063
25	31.7	0.010	0.006	0.011	0.011	0.0095
30	38.1	0.010	0.007	0.011	0.012	0.0100
35	44.5	0.012	0.009	0.013	0.013	0.0118
40	50.9	0.014	0.011	0.017	0.017	0.0148
45	57.3	0.015	0.011	0.018	0.019	0.0158
50	63.7	0.018	0.013	0.019	0.023	0.0183
55	70.2	0.018	0.015	0.023	0.026	0.0205
60	76.7	0.020	0.017	0.026	0.029	0.0230
65	83.1	0.025	0.018	0.028	0.030	0.0253
70	89.6	0.026	0.020	0.030	0.034	0.0275

Table E.20: C3/60-80-5-50

Load (kip)	Bar Stress (ksi)	Crack Widths (in.)				
		73" N	46" N	46" S	67" S	Average
20	25.2	0.007	0.005	0.006	0.005	0.0058
25	31.6	0.010	0.008	0.006	0.006	0.0075
30	37.9	0.014	0.009	0.009	0.010	0.0105
35	44.3	0.015	0.009	0.010	0.012	0.0115
40	50.7	0.017	0.010	0.011	0.015	0.0133
45	57.1	0.021	0.012	0.014	0.014	0.0153
50	63.5	0.022	0.015	0.015	0.020	0.0180
55	70.0	0.024	0.016	0.018	0.020	0.0195
60	76.4	0.029	0.016	0.019	0.025	0.0223

APPENDIX F. COMPARISON OF METHODS

Table F.1: Comparison of Methods

Specimen	f_s (ksi)							
	f_{test}	ACI 318-14	ACI 408R-03 φ=0.82	ACI 408R-03 φ=0.92	CB 603	Analysis Eq. by Pay (2005)	Design Eq. by Pay (2005)	Analysis Eq. by Sim (2014)
U-40-5	58.2	55.1	55.0	62.1	38.8	62.8	52.5	52.5
U-40-5a	69.8	63.3	58.9	66.5	41.6	67.3	56.3	56.3
U-60-5	68.4	82.6	73.9	83.5	58.2	76.9	64.3	64.3
U-60-5a	88.9	94.9	79.2	89.5	62.4	82.4	68.9	68.9
U-70-5	94.9	110.8	89.3	101.0	72.8	89.0	74.4	74.4
U-80-5	102.2	110.2	92.8	104.9	77.6	88.7	74.2	74.2
U-100-5	103.7	137.7	111.7	126.3	97.0	99.2	83.0	83.0
U-120-5	103.6	165.2	130.6	147.7	116.4	108.7	90.9	90.9
U-80-5-M	97.7	73.4	78.0	88.1	51.7	88.7	74.2	74.2
U-100-5-M	97.5	91.8	92.7	104.8	64.6	99.2	83.0	83.0
U-120-5-M	95.6	110.2	107.5	121.6	77.6	108.7	90.9	90.9
C3/60/2-40-5-50	81.8	69.8	62.4	70.4	45.9	74.6	63.6	63.6
C3/60/3-40-5-50	89.8	69.8	62.4	70.4	45.9	78.3	67.3	67.3
C3/100/3-40-5-50	85.0	69.8	62.4	70.4	45.9	81.5	70.5	70.5
C3/60-40-5-100	91.7	76.3	65.8	74.3	50.1	85.6	74.6	74.6
C3/100-40-5-100	93.1	76.3	65.8	74.3	50.1	90.9	79.9	79.9
C3/60-60-5-50	103.3	113.5	88.3	99.7	71.6	100.5	86.4	86.4
C3/60-60-5-100	110.5	124.1	94.1	106.3	78.3	111.5	97.4	97.4
C3/60-60-5-150	109.4	134.5	99.8	112.8	84.9	122.5	108.4	108.4
C4/60-60-5-100	108.9	141.5	103.6	117.1	89.3	126.6	112.5	112.5
C3/100-60-5-100	111.0	124.1	94.1	106.3	78.3	118.9	104.9	104.9
C3/60-80-5-50	101.9	140.2	106.6	120.5	91.9	110.0	94.4	94.4

APPENDIX G. RELATIONSHIP BETWEEN INCREASE IN STRESS CAUSED BY CONFINEMENT AND DIFFERENT VARIABLES

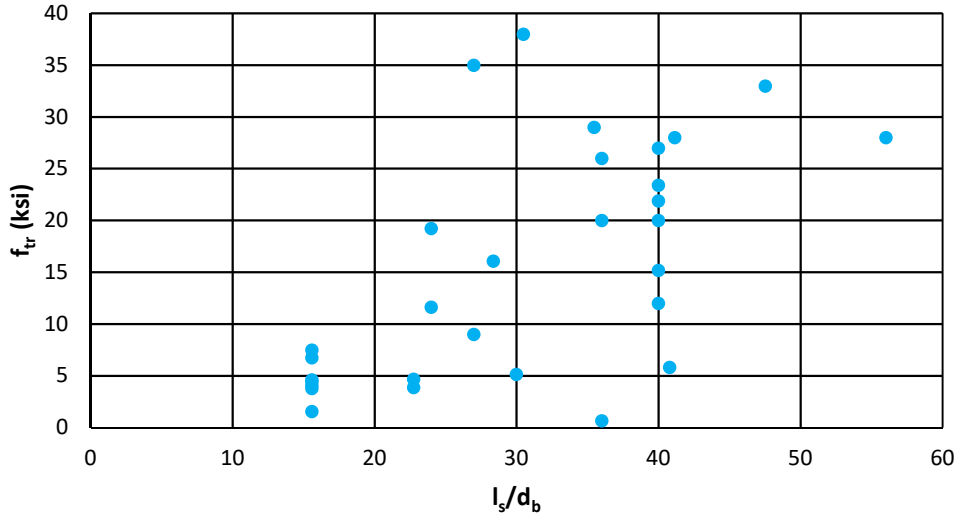

Figure G.1: Relationship between Increase in Stress Caused by Confinement and Splice Length in Terms of Bar Diameter

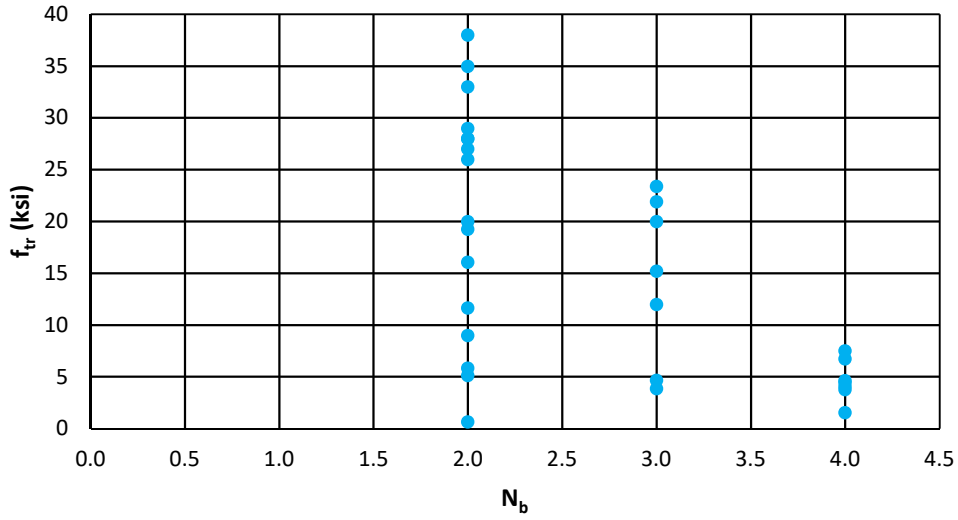

Figure G.2: Relationship between Increase in Stress Caused by Confinement and Number of Bars

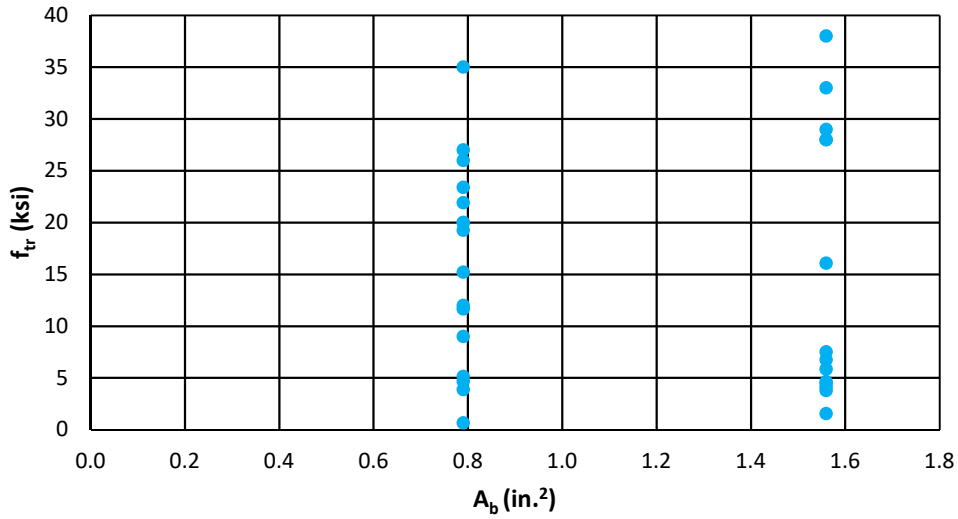

Figure G.3: Relationship between Increase in Stress Caused by Confinement and Bar Area

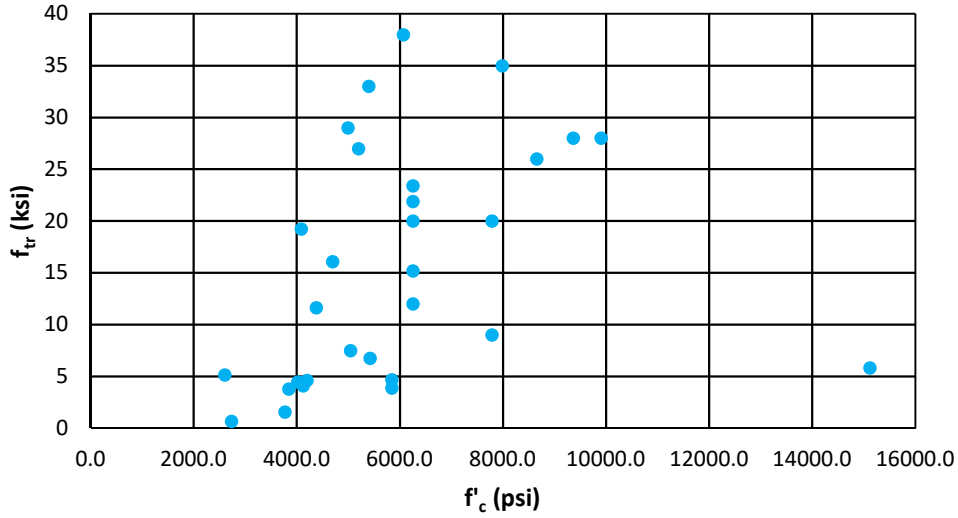

Figure G.4: Relationship between Increase in Stress Caused by Confinement and Concrete Strength